THE UNIVERSITY OF CHICAGO

VISUALIZING PROTEIN SORTING IN THE GOLGI APPARATUS

A DISSERTATION SUBMITTED TO
THE FACULTY OF THE DIVISION OF THE BIOLOGICAL SCIENCES
AND THE PRITZKER SCHOOL OF MEDICINE
IN CANDIDACY FOR THE DEGREE OF
DOCTOR OF PHILOSOPHY

GRADUATE PROGRAM IN CELL AND MOLECULAR BIOLOGY

BY
JASON C. CASLER

CHICAGO, ILLINOIS
AUGUST 2020

Somewhere, something incredible is waiting to be known.

- Carl Sagan

TABLE OF CONTENTS

LIST OF FIGURES

LIST OF TABLES

LIST OF MOVIES

ACKNOWLEDGMENTS

This work would not have been possible without the support of my mentors, colleagues, friends, and family.

First I would like to thank my excellent boss, Ben Glick. Truly a person who leads by example, Ben has shown me how to write, speak, and think like a scientist and it has been a pleasure to work in his lab. Ben surrounds himself with an excellent team of scientists and I must thank the current and past members of the Glick lab for their support.

I would specifically like to thank Kasey Day, who taught me how to be a bench scientist. Her patience, kindness, and guidance allowed me to develop the essential skills used in this work. She has been a great friend and source of conversation, ideas, dog photos, and two rather nice bookshelves throughout this process.

My thesis committee has been an essential line of critical support. Our discussions strengthened my projects and helped me hone my presentation and critical thinking skills. Christine Labno and Vytas Bindokas at the Light Microscopy Core have been invaluable resources for technical support.

I am also lucky enough to have a massive support network outside the lab. My mother, Eileen Casler, and sister, Sarah Casler, have been my most ardent supporters, and I cannot thank them enough for all the love and encouragement they have given me. My pets, Little Jens, Princess Kiki, and Olive have been essential sources of companionship even though they do not understand what a PhD is or why I need to leave the apartment so often for it. I am eternally grateful to my partner, Erica Price. She has put up with long rants about the Golgi, my inconsistent working hours, and a terrible commute to work all so we can share our lives together. Her support kept me sane and grounded throughout this process. I must also thank the Price and Ginder families, who have always treated me as one of their own, as well as all of my loved ones who have supported me along the way.

ABSTRACT

In this work I investigated the mechanisms governing protein sorting in the Golgi. The cisternal maturation model of Golgi function postulates that anterograde movement of protein cargoes occurs passively during maturation while resident Golgi proteins are recycled via vesicular transport. Despite suggestive evidence, these predictions had not been tested.

Cisternal maturation has been visualized in budding yeast; however, there has not been a tool to enable simultaneous visualization of Golgi cisternae and cargo proteins. Therefore, I first engineered a tool to visualize protein cargoes during Golgi maturation. The tool, Erv29-dependent Secretory Cargo (ESCargo), traps a fluorescent protein in aggregates within the ER. The aggregates are dissolved to release the fluorescent protein for synchronous transport through the secretory pathway. I demonstrated this tool behaves like a *bona fide* secretory cargo by visualizing its sequential localization with early and then late Golgi cisternae, tracking oligosaccharide modifications, and detecting cargo secreted into the medium. With this tool I verified a key prediction of the cisternal maturation model: secretory cargo remains within the lumen of maturing Golgi cisternae. Unexpectedly, I also discovered that secretory cargo can be recycled within the Golgi in a manner dependent on the AP-1 adaptor complex.

Next I dissected how different classes of cargo proteins transit the Golgi. Most models postulate that all cargoes uniformly transit the Golgi to the latest stage of the *trans*-Golgi network (TGN) where they are sorted into vesicles. To test this hypothesis, I modified ESCargo for transport to the vacuole. I found that vacuolar cargoes exit the Golgi at the beginning of the late Golgi stage, significantly earlier than secretory cargoes. The departure was dependent on the Gga adaptors but not the AP-1 adaptor complex. Thus, the sorting of different cargoes is kinetically segregated during Golgi maturation.

ESCargo utilizes evolutionarily conserved machinery and should function in other model organisms. I, along with several collaborators, tested the efficacy of ESCargo in *Saccharomyces cerevisiae*, mammalian tissue culture, *Drosophila melanogaster*, and the ciliate *Tetrahymena thermophila*. In all model organisms tested, ESCargo successfully generated a synchro-

nized cohort of fluorescent secretory cargo - thus permitting comparative studies of secretory cargo trafficking between species.

Finally I aimed to clarify the role of the AP-1 adaptor complex in intra-Golgi recycling. Using ESCargo, I found that secretory cargo recycling requires AP-1 and the mannosyltransferase Mnn1. Further, I demonstrated that inhibiting endocytosis in AP-1 mutants causes the mislocalization of resident Golgi enzymes and a severe defect in cisternal maturation. These results suggest that endocytosis acts as a backup recycling pathway for leaked late Golgi proteins in AP-1 mutants. Thus, AP-1 mediates an intra-Golgi recycling pathway that drives cisternal maturation.

The majority of the data collected in this work is video microscopy. To appreciate the dynamic nature of protein sorting in the Golgi, it is essential to visualize these processes in real time. The movies associated with each chapter are included as supplementary files online. The first frame and a legend are located at the end of each chapter for reference.

CHAPTER 1

INTRODUCTION

A hallmark of eukaryotic cellular life is the partitioning of the cytoplasm into membrane bound organelles. Organelles have distinct functions vital to the survival of the cell. Common organelles across most of Eukaryota include mitochondria, the nucleus, the endoplasmic reticulum (ER), endosomes, the Golgi apparatus, lysosomes (vacuoles in yeast), peroxisomes, and the plasma membrane. These compartments are constantly in flux, exchanging materials with one another and the environment through various mechanisms. To facilitate this exchange, cells have evolved complex mechanisms to maintain organelle identity while permitting the exchange of materials.

Currently, the best characterized mechanism of transport between organelles is via transport intermediates. Various cargoes are selectively packaged into vesicular carriers that bud from one compartment and fuse at another. By electron microscopy these vesicles have been characterized on the range of 60-120 nm and are sometimes accompanied by a protein coat (Bonifacino and Glick, 2004). Recently more methods of transport between organelles have been identified. Direct contact between organelles facilitated by protein tethers has been shown to be important not only for the positioning of organelles within the cytoplasm but for the exchange of lipids and other molecules (reviewed in Prinz et al., 2019). Transient tubule formation between organelles has also been suggested to facilitate the exchange of molecules (Mironov et al., 1997). Many of these contacts are likely transient, which has prevented their detection until recently. All of these mechanisms are likely utilized by the secretory pathway to maintain homeostasis while transporting proteins and lipids throughout the cell.

The Secretory Pathway

The secretory pathway encompasses the network of interactions between the ER, the Golgi apparatus, endosomes, and lysosomes that facilitates the processing and movement of pro-

teins and lipids throughout the cell. The secretory pathway begins at the ER. Most commonly, proteins are directed for translocation into the ER via signal sequences (Ng et al., 1996). Within the ER proteins undergo various processing steps to promote protein maturation. First, signal sequences are cleaved by proteases. Complex protein folding is chaperoned and improperly folded proteins are degraded by robust quality control mechanisms. The first stages of carbohydrate modifications also begin (Barlowe and Miller, 2013). Secretory cargo molecules are concentrated into vesicles at ER exit sites (ERES) and transported to the Golgi (Miller et al., 2003). Within the Golgi many proteins are modified by the addition and trimming of glycans and/or proteolytic processing (Day et al., 2013). At the *trans*-Golgi network (TGN) cargo is packaged into vesicular carriers for transport within the endolysosomal network or directed towards the plasma membrane for secretion (Bard and Malhotra 2006). Resident proteins of these organelles are continuously recycled to their appropriate compartments in vesicular carriers. Thus, maintaining a functional secretory pathway requires a careful balance of anterograde and retrograde cargo movement. The directionality of transport intermediates and their role in maintaining Golgi homeostasis are actively debated.

Membrane Transport Machinery

The existence of functionally unique membrane-bound compartments necessitates mechanisms to differentiate compartments. Cells utilize a range of both lipid and protein molecules to establish organelle identity. While arguments could be made about the relative importance of each component, it is a combination of the mechanisms described below that constitute membrane identity.

Most vesicles are surrounded by protein coats which could contribute to specificity. The most well characterized coats are COPI, COPII, and clathrin. It should be noted, however, that other complexes, such as exomer in yeast, have been proposed to act as coats (Wang et al., 2006). Further, there is evidence of vesicle formation that occurs without traditional

protein coats - for example, clathrin-independent endocytosis (Spang, 2008). While molecularly distinct, coat proteins have many functional and structural similarities. Coats form two distinct layers - an inner layer that binds cargo and an outer layer that forms a cage (Faini et al., 2013). Each coat displays a distinct subcellular localization, but all polymerize in patches on the cytosolic face of their respective membranes. Polymerization likely induces membrane curvature and helps concentrate cargo molecules (Faini et al., 2013). The final stage of vesicle formation is scission from the donor membrane and complete encapsulation of the vesicle by the coat lattice. COPII localizes to small domains of the ER termed ER exit sites (ERES) where it concentrates proteins for transport to the Golgi (Bannykh et al., 1996). COPI is present on Golgi membranes and has been implicated in recycling both resident ER and Golgi proteins (Szul and Sztul, 2011). Interestingly, by electron microscopy separate classes of COPI vesicles were identified by their appearance and location relative to the Golgi stack (Donahoe et al., 2007). Current interpretations lead to the hypothesis that there are two distinct classes of COPI vesicles, COPIa and COPIb, for Golgi-to-ER and intra-Golgi recycling respectively (Donahoe et al., 2007). COPI has also been implicated in the anterograde transport of secretory cargo through the Golgi stack (Lavieu et al., 2013; Dunlop et al., 2017). Clathrin has a much wider intracellular distribution and is found on endosomes, the TGN, and the plasma membrane where it functions in endosome-Golgi transport, intra-Golgi recycling, and endocytosis respectively (Kirchhausen, 2000). These diverse functions are mediated by a series of accessory and adaptor proteins (Kirchhausen, 2000). Thus, different coat complexes have distinct intracellular distributions and cargo clients that serve as one layer of determining the specificity of intracellular trafficking.

SNARE (soluble N-ethylmaleimide-sensitive factor attachment protein receptor) proteins were originally thought to be the primary determinants of molecular specificity within membrane trafficking (Furukawa and Mima, 2014). SNAREs are long coiled-coil proteins that form a four helical bundle to generate the energy necessary to drive fusion of opposing membranes. Most SNAREs are type II transmembrane proteins and some are anchored via lipid

modifications, such as palmitoylation (Malsam et al., 2008). There are at least seven distinct sets of SNARE complexes in yeast and mammals, which act in distinct endomembrane trafficking routes (Jahn and Scheller, 2006). Despite primarily functioning in a specific trafficking pathway, both *in vitro* and *in vivo* experiments have demonstrated that some SNAREs operate in multiple pathways and can compensate for the loss of function of other SNAREs (Tsui and Banfield, 2000). Further, meticulous biochemical studies have demonstrated that SNAREs operate over a very short range, ~25nm, and are thus unlikely to be the first recognition event for an incoming vesicle (Jahn and Scheller, 2006). Regardless, formation of the appropriate SNARE assemblies contributes a layer of specificity to membrane trafficking.

More recently, vesicle tethers have been recognized as components contributing to specificity in membrane trafficking. There are two primary types of vesicle tethers, long coiled-coil proteins and multisubunit tethering complexes (Yu and Hughson, 2010). Tethers operate at significantly longer distances than SNAREs - on the range of 100-600nm (Yu and Hughson, 2010). Many tethers are non-essential, however, and their removal often has little effect on vesicle trafficking. Currently it is appreciated that many tethers likely have overlapping functions, which has hindered assigning specific functions to each tether. Interestingly, relocalization of tethers to mitochondria is sufficient to capture specific vesicle populations, and several tethers are capable of capturing the same types of vesicles (Wong and Munro, 2014). Thus, the localization of a tether to a specific site is likely partially responsible for directing the trafficking of different types of vesicles. The physical link between tethers and vesicles is not well characterized. Many tethers have motifs in their N-terminus that interact with vesicles by unknown mechanisms (Wong et al., 2017). Further, some specific adaptor molecules that link tethers to vesicles have been discovered (Shin et al., 2017). Upon capture of a vesicle, tethers are thought to either collapse in on themselves or bend in order to bring the vesicle closer to the target membrane for fusion (Cheung et al., 2015). The capture of vesicles by tethers may be the first step in directing membrane traffic.

Lipid composition is a key determinant of organelle identity. A well studied functional example is the presence of distinct phosphoinositide species at various organelles. Functional phosphoinositides include PI(3)P (phosphatidylinositol 3-phosphate) at endosomes, PI(4)P (phosphatidylinositol 4-phosphate) at the TGN, and PI(4,5)P2 (Phosphatidylinositol 4,5-bisphosphate) at the plasma membrane (Di Paolo and De Camilli, 2006). These species are generated by the function of kinases and phosphatases. The localization of lipid modifying proteins to specific organelles coupled with the directed transport of lipid molecules can create cycles that generate gradients of various lipid species (de Saint-Jean et al., 2011). Enrichment of lipid species is associated with local protein recruitment and activation (Di Paolo and De Camilli, 2006). Thus, organelle identity is not solely dictated by protein factors, but also the composition of the membrane itself.

Finally, small GTPases play crucial roles in regulating membrane trafficking. These proteins function as molecular switches and can convert between an "on" and an "off" state based on the hydrolysis of bound GTP to GDP, respectively (Hutagalung and Novick, 2011). This process can be exquisitely tuned by the activation of GEFs (guanine nucleotide exchange factors) and GAPs (GTPase activating proteins). Membrane trafficking is primarily controlled by the Arf and Rab GTPase families. Mammalian cells contain over 60 Rabs while yeast only have 11 (Hutagalung and Novick, 2011). Turning a GTPase "on" or "off" leads to recruitment of numerous effector proteins, such as vesicle coat proteins and their adaptors. Thus, controlling the activation and localization of GTPases is a crucial mechanism to bestow membrane identity. For example, maturation of early endosomes to late endosomes is thought to result primarily from the conversion from Rab5 to Rab7 and the downstream recruitment of their effectors (Rink et al., 2005). Similar models have been proposed for the maturation of the Golgi via the conversion from Ypt1 (Rab1) to Ypt31/32 (Rab11) (Rivera-Molina and Novick, 2009; Kim et al., 2016).

Thus, cells utilize robust molecular identifiers consisting of coats, adaptors, SNAREs, tethers, lipids, and GTPases that operate in a coordinated fashion to bestow membrane

identity and provide directionality to membrane traffic. The field is now faced with the challenge of dissecting the networks of interactions generated by these molecules that underlies the circuitry of membrane traffic.

Golgi Organization

Originally discovered through the examination of neurons in 1898 by Camillo Golgi (Golgi C, 1898), the Golgi apparatus has since been recognized as the key sorting hub in the secretory pathway; however, the mechanisms by which the Golgi spatially and temporally segregates its functions are highly debated. Our understanding of these processes is informed by morphological, biochemical, and dynamic studies.

The first attempts to define Golgi organization were guided by the examination of Golgi morphology. Electron micrographs show the Golgi typically consists of a polarized stack of several elongated, flattened sacs with rounded rims (Mogelsvang et al., 2004). Often these stacks are adjacent to the ER (Farquhar and Palade, 1981). The cisternae nearest to the ER comprise the *cis* face of the Golgi. At the *cis*-Golgi cargo from the ER arrives in COPII vesicles and ER resident proteins are recycled via COPI vesicles (Papanikou and Glick, 2014). The cisternae within the center of the Golgi stack are referred to as *medial* and the cisternae furthest from the ER are referred to as *trans*. Within the Golgi stack protein cargoes are modified by the addition and trimming of glycans and some are proteolytically processed. The *trans*-most cisternae and its tubular projections are designated as the *trans*-Golgi network (TGN) (Farquhar and Palade, 1981). At the TGN cargo molecules are packaged into vesicles and transported to the plasma membrane and the endolysosomal system. Despite extensive conservation of Golgi proteins, there is a remarkable diversity in the physical organization of the Golgi between species. Golgi stacks can consist of very few or dozens of cisternae. Some organisms, including the budding yeast *Saccharomyces cerevisaie*, display an unstacked Golgi where cisternae are scattered throughout the cytoplasm (Pruess et al., 1992). In many mammalian cells the Golgi is fused into a ribbon-like structure that localizes to one side

of the nucleus. Some organisms even have no detectable Golgi-like organelle, although it is likely they have a functionally equivalent compartment such as an ER domain (Mowbrey and Dacks, 2009). Simply based on morphology it is not obvious how protein cargo would traverse the Golgi stack.

Extensive efforts have been dedicated to biochemically characterizing Golgi compartments. Golgi cisternae are not homogeneous and are composed of unique sets of enzymes, lipids, and membrane traffic components. Many cargoes moving through the Golgi are post-translationally modified by the addition and trimming of oligosaccharides (Kornfeld and Kornfeld, 1985). These modifications occur sequentially by the action of several enzymes. It is possible that the compartmentalized organization of the Golgi is required to facilitate the accuracy of these modifications. Thus, the distribution of glycosylation enzymes could be used to define unique Golgi compartments. This idea is challenged by the findings that many glycosylation enzymes have overlapping localizations and that the enzymes themselves and the glycan modifications vary widely amongst species (Nilsson et al., 1993; Velasco et al., 1993; Rabouille et al., 1995; Harris and Waters, 1996; Munro, 2001). Aside from protein modifications the Golgi is also a major source of lipid production and itself displays a polarized lipid composition. The Golgi produces sphingolipids and distinct phosphoinositide species which have broad functional roles in cell physiology (D'Angelo et al., 2013). The TGN is enriched in phosphatidylinositol-4-phosphate (PI4P) which has been shown to be functionally involved in the recruitment of adaptor complexes to aid in protein sorting (De Matteis et al., 2013). Membrane trafficking machinery also displays a polarized localization in the Golgi. COPI localizes primarily to the *cis*-Golgi while the *trans*-Golgi and TGN are enriched in clathrin and the Gga and AP-1 clathrin adaptors. The polarized localization of trafficking components is a key determinant of Golgi function, but the overlapping distributions of many of these components makes it difficult to define discrete biochemically unique cisternae.

A recent and crucial insight into Golgi function comes from the study of Golgi dynamics. The discovery of fluorescent protein tags revolutionized our ability to understand the dynamics of protein trafficking. Video microscopy using fluorescently labeled Golgi proteins and lipid probes has permitted real time visualization of Golgi dynamics in living cells (Wooding and Pelham, 1998; Losev et al., 2006; Matsuura-Tokita et al., 2006). While differences exist between organisms, the prevailing observation is that Golgi cisternae are highly dynamic structures that can form *de novo*, fuse homotypically, and terminally mature into secretory carriers. Thus, the dynamic nature of Golgi cisternae makes it difficult to precisely define discrete physical compartments. Further, there is often little consistency with the definitions of Golgi compartments within the field and standard naming conventions can be a hindrance to understanding Golgi function. Despite this, there is an obvious difference in function between Golgi cisternae nearest to the ER and those furthest. For simplicity, in this work the term "early Golgi" is approximately synonymous with the traditional terms *cis* and *medial* Golgi while "late Golgi" is approximately synonymous with the *trans* Golgi and TGN.

Based on these observations, the field has been dominated by two models of Golgi function: the stable compartments model, and the cisternal maturation model (Glick and Luini, 2011). In the stable compartments model, the Golgi is a static organelle that consists of several biochemically distinct cisternae. Newly synthesized cargoes are transported to the Golgi via COPII vesicles and move forward through the stack by continuous vesicular transport in COPI vesicles. Resident Golgi enzymes remain within their respective compartments. This model is strongly challenged by results that demonstrate that COPI vesicles primarily contain resident Golgi enzymes (Adolf et al., 2019), that large cargoes such as algal scales and collagen, which cannot fit into COPI vesicles, also transit the Golgi (Becker et al., 1995; Bonfanti et al., 1998), and that the biochemical composition of an individual cisterna changes over time (Losev et al., 2006; Matsuura-Tokita et al., 2006). In contrast, the cisternal maturation model predicts that cargo-containing COPII vesicles generated at the ER homotypically fuse to form new Golgi cisterna. Maturation occurs as a Golgi cisterna recycles resident ER

and early Golgi proteins in COPI vesicles and receives recycled late Golgi proteins from older Golgi cisternae (Figure 1.1). The final stage of maturation is the dissolution of the cisterna into secretory carriers destined for the plasma membrane. In this model, cargo is passively carried forward within the cisternal lumen during maturation (Figure 1.1). Several key predictions of the cisternal maturation model have been verified. Most strikingly, the biochemical conversion of a Golgi cisterna from early-to-late was directly visualized in the budding yeast *Saccharomyces cerevisae*. Using fluorescently tagged early and late resident Golgi proteins it was possible to directly visualize a new Golgi cisterna form, lose the early Golgi marker while it acquired the late Golgi marker, and then subsequently lose the late Golgi marker (Losev et al., 2006; Matsuura-Tokita et al., 2006). Later studies using conditional COPI depletion demonstrated that COPI mediated protein recycling is essential for cisternal maturation (Papanikou et al., 2015; Ishii et al., 2016). Several key predictions of the cisternal maturation model remain untested, however. First, protein cargo within maturing Golgi cisterna has not been directly observed. The cisternal maturation model predicts that cargoes moving through the Golgi will remain within the cisternal lumen during maturation (Figure 1.1). This has not been tested due to a lack of available tools to visualize Golgi cargoes in a model organism where cisternal maturation can be visualized. Second, a mechanism for the recycling of late Golgi proteins has not been clearly established. The cisternal maturation model predicts that maturation is driven by the continued recycling of Golgi proteins from older to younger cisternae. A large body of work supports that early Golgi proteins are recycled in COPI vesicles, however, recent work has shown that COPI is likely not responsible for the recycling of late Golgi proteins (Papanikou et al., 2015). Thus, for the cisternal maturation model to be valid there must be an additional recycling mechanism for the retention of late Golgi proteins. The most likely candidate is the AP-1 adaptor complex, though the evidence for this is far from definitive (Figure 1.1). Testing these fundamental predictions of the cisternal maturation model serves as the basis of this work.

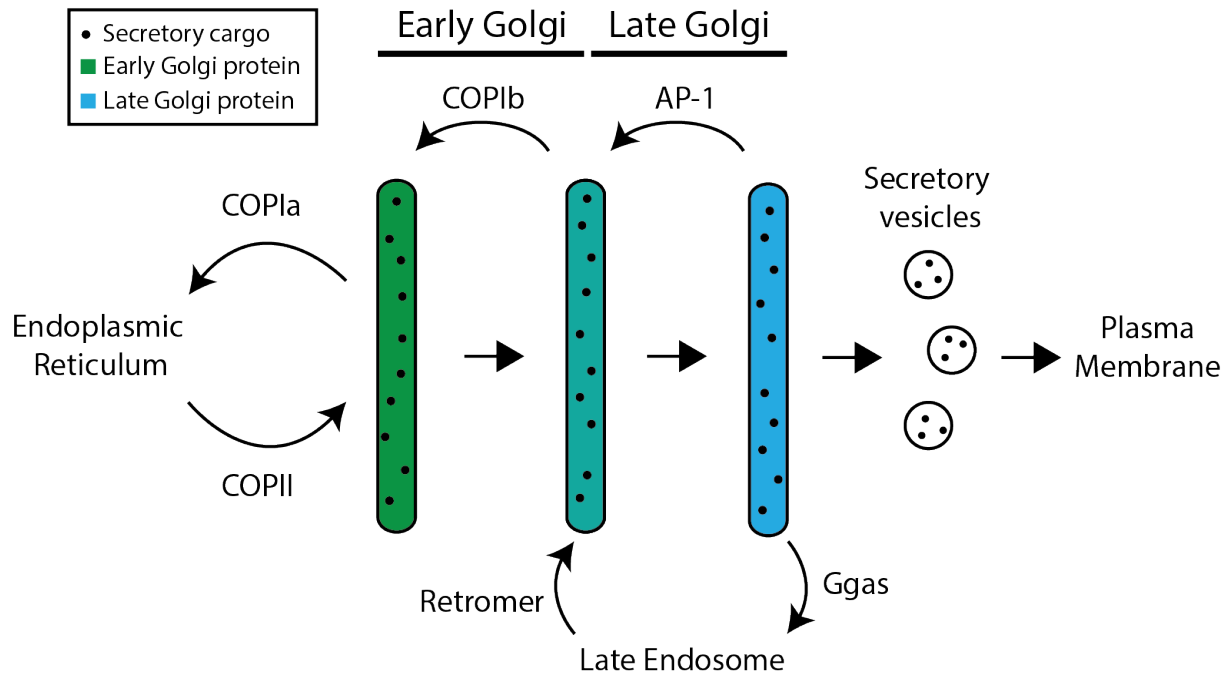

Figure 1.1: **Model of Golgi cisternal maturation.** Newly synthesized cargo molecules (black dots) arrive at the Golgi in COPII vesicles. Resident ER proteins are recycled from the early Golgi via COPIa. As a cisterna matures, it receives COPIb vesicles carrying resident early Golgi enzymes (green color). At the early-to-late transition the cisterna begins to receive AP-1 vesicles carrying resident late Golgi proteins (blue color). Vacuolar proteins are sorted to the late endosome by the Ggas and their receptors are recycled to the Golgi via retromer. The terminal stage of maturation results in the formation of secretory vesicles that fuse with the plasma membrane. Secretory cargo is passively carried forward within the cisternal lumen during maturation.

Protein Sorting in the Secretory Pathway

Resident Golgi Protein Sorting

Resident Golgi protein localization is determined by a balance of anterograde and retrograde transport. Newly synthesized molecules are continuously transported to the Golgi from the ER in COPII vesicles. Within the Golgi movement of cargo through the stack is thought to be primarily driven by cisternal maturation, though anterograde vesicular transport in COPI vesicles has not been completely ruled out (Glick and Luini 2011). Resident Golgi proteins are localized by continuous recycling from maturing cisternae in vesicular carriers. The recycling of early and late Golgi proteins likely involves distinct mechanisms.

Early Golgi protein sorting

COPI

COPI mediates protein recycling at the early Golgi (Figure 1.1). Recycling of resident ER proteins, such as ER export adaptors, from the Golgi has been fairly well characterized. A well understood example is that of The KDEL receptor. The KDEL receptor recognizes a tetrapeptide KDEL motif to incorporate proteins into COPI vesicles that recycle from the early Golgi to the ER (Capitani and Sallese, 2009). Thus, some ER resident proteins and early Golgi proteins continuously cycle through the ER and Golgi to maintain their steady state localization. Addition of a KDEL motif is sufficient to direct proteins for COPI dependent Golgi to ER recycling (Capitani and Sellese, 2009). Other cargo adaptors, such as Vps74, have been implicated in specifically recognizing different sets of resident Golgi proteins and directing them for recycling in COPI vesicles (Wood et al., 2009). Thus, different proteins may be incorporated into COPI vesicles at different times by the action of distinct cargo adaptors. Interestingly, morphological and biochemical analyses have described multiple types of COPI vesicles, referred to as COPIa and COPIb (Malsam et al., 2005; Donohoe et al., 2007). Although untested, an interesting hypothesis is that COPIa and COPIb vesicles mediate recycling from the Golgi to the ER and within the Golgi respectively (Figure 1.1). This model would provide a framework for how different early Golgi enzymes display different kinetics during cisternal maturation and account for the observation that some early Golgi proteins do not seem to recycle through the ER. Currently there is no molecular distinction between COPIa and COPIb vesicles as they seem to utilize identical coat proteins that form the same coat structure (Bykov et al., 2017).

Late Golgi protein sorting

Protein sorting at the late Golgi involves a complicated network with multiple inputs and outputs. The early Golgi receives input via vesicles from the ER and older Golgi cisternae

and generates output via COPI vesicles. In contrast, the late Golgi generates vesicles destined for endosomes, lysosomes/vacuoles, younger Golgi cisternae, and the plasma membrane, and receives vesicles from endosomes, older Golgi cisternae, and, at least in plants and yeast, the plasma membrane via endocytosis. Despite this complexity, some progress has been made in understanding how resident late Golgi proteins are sorted.

Ggas

A well characterized pathway of late Golgi protein sorting is Gga mediated transport from the late Golgi to the late endosome (Figure 1.1). Monomeric Gga clathrin adaptors directly recognize sorting motifs in the cytosolic tails of cargo proteins (Myers and Payne, 2013). Gga vesicles are then trafficked to the late endosome where they fuse to deliver cargo. Retrograde transport of Golgi proteins from the late endosome is mediated by sorting nexins and the retromer complex (Figure 1.1) (Ma and Burd, 2020). Vps10, a receptor for the vacuolar hydrolase carboxypeptidase Y (CPY), has been well characterized to cycle through the Golgi and late endosome for its steady state localization (Cooper and Stevens 1996). Other Golgi proteins, such as the protease Kex2, may utilize this pathway, though a comprehensive analysis of proteins that recycle via the late endosome has not been reported.

AP-1

The AP-1 adaptor complex likely mediates an intra-Golgi recycling pathway at the late Golgi. AP-1 is a heterotetrameric clathrin adaptor complex that localizes exclusively to the late Golgi in yeast (Day et al., 2018). In mammalian cells AP-1 has also been detected on recycling endosomes (Hinners and Tooze, 2003). Recycling endosomes and the TGN are often in close proximity and seem to have partially overlapping functions, however. Like the Ggas, AP-1 recognizes cargo molecules via motifs in their cytosolic tails (Myers and Payne, 2013). In yeast AP-1 has been shown to be essential for the retention of a subset of late Golgi proteins (Valdivia et al., 2002). In mammalian cells, isolated clathrin coated vesicles

contain resident Golgi proteins that are lost when AP-1 function is compromised (Hirst et al., 2012). Interestingly, AP-1 mutants display only mild phenotypes and many late Golgi proteins localize normally in the absence of AP-1 (Valdivia et al., 2002). In contrast, COPI is essential and conditional mutants show severe defects in Golgi morphology and function (Papanikou et al., 2015). One possibility is that removal of AP-1 does not completely block recycling of late Golgi proteins. The epsin-like protein Ent5 has been shown to directly interact with clathrin at the late Golgi and has been shown to suppress some AP-1 mutant phenotypes (Duncan et al., 2003; Costaguta et al., 2006; Copic et al., 2007). Thus, Ent5 and/or other epsin-like proteins may be sufficient to drive intra-Golgi recycling even in the absence of AP-1. A second possibility is that endocytosis acts as a backup retrieval pathway for leaked late Golgi proteins. In plants and yeast endocytic vesicles are targeted directly to the late Golgi (LaMontagne and Heese, 2017; Day et al., 2018). In the absence of AP-1 late Golgi proteins may default into secretory vesicles that are targeted to the plasma membrane. Endocytosis of leaked Golgi proteins could then return them to the late Golgi (See chapter 6, figure 6.9). Further characterization of the mechanism of intra-Golgi recycling at the late Golgi is a crucial next step.

Secretory Cargo Sorting

A primary function of the Golgi is to process and sort secretory cargo. Secretory cargoes comprise a diverse set of proteins. These include small soluble cargoes, such as the yeast mating pheromone α-factor, transmembrane or lipid anchored proteins, and supermolecular cargoes, such as procollagen and algal scale proteins. Despite vast differences in size, all of these cargoes transit through the lumen of the Golgi.

Anterograde transport of small soluble and transmembrane cargoes can readily be explained by the stable compartments or cisternal maturation model. In the stable compartments model, cargo molecules are packaged into COPI vesicles that bud from one Golgi cisterna and fuse with another. This mechanism could explain transport of small cargoes

that can easily be packaged into COPI vesicles but does not explain how large cargoes, such as procollagen, can be transported through the stack. Procollagen is a rigid molecule with a diameter of ~300 nm, far larger than the ~ 80 nm size described for COPI vesicles (Canty and Kadler, 2005). In contrast, the cisternal maturation model predicts cargo molecules are present within the lumen of the cisterna throughout maturation, which could easily encompass large cargoes. At the terminal stage of maturation, cargo is packaged into vesicles for transport to the plasma membrane or endosomal compartments. Algal scales and procollagen have been detected within the lumen of Golgi cisternae (Bonafanti et al., 1998; Donohoe et al., 2012). Thus, it is likely that secretory cargo molecules traverse the Golgi stack primarily via cisternal maturation. This prediction has not been verified experimentally in systems where cisternal maturation can be directly visualized, however.

Anterograde movement of secretory cargo during cisternal maturation is likely more complicated than current models suggest, however. Several observations in mammalian cells challenge the classical cisternal maturation model. In mammalian cells, multiple cargoes traffic through the Golgi with exponential exit kinetics (Patterson et al., 2008). If all cargo molecules were uniformly transported within the lumen of a maturing cisternae, as predicted by the classical cisternal maturation model, then cargo would exit the Golgi with linear kinetics. Exponential transport kinetics could be observed in the cisternal maturation model if a portion of the secretory cargo was being recycled within the Golgi. Currently there is no experimental evidence for the recycling of secretory cargo molecules, however. Another challenge comes from studies in mammalian cells showing intercisternal continuities between Golgi cisternae (Beznoussenko et al., 2014). These tunnels could provide a means for small soluble cargoes to rapidly diffuse through the Golgi while larger cargoes would be excluded. Thus, understanding secretory cargo trafficking through the Golgi will require more rigorous characterization of the movement of different secretory cargoes through the Golgi and their interaction with various trafficking machinery. Current models of Golgi function need to be revisited to explain these observations.

At the latest stages of Golgi maturation, secretory cargo is packaged into secretory vesicles. How cargoes are recognized and sorted at the TGN is poorly understood. High resolution imaging studies have shown that the TGN in mammalian cells consists of distinct domains marked by different adaptor proteins (Huang et al., 2019). How these domains are established and maintained, however, is unknown. Recently, sphingomylein enriched domains have been implicated in the sorting of subsets of cargo molecules into distinct vesicular carriers (Deng et al., 2018). Thus, the packaging of cargo molecules likely involves the coordinated effort of lipids and adaptor proteins. How these processes are spatially and temporally organized is an important question for future research.

Vacuolar Protein Sorting

Aside from secretory cargo the Golgi also processes and sorts cargoes of the endolysosomal system. Early studies revealed that vacuolar proteins are modified by the same glycosylation machinery as secretory cargoes and traffic through the same Golgi compartments (Stevens et al., 1982). Thus, vacuolar proteins are also present within the lumen of maturing Golgi cisternae. Genetic screens in yeast identified two primary pathways for transport from the Golgi to the vacuole (Robinson et al., 1988; Cowles et al., 1997). These were termed the carboxypeptidaseY (CPY) and alkaline phosphatase (ALP) pathways after model cargoes that exclusively follow these routes.

The CPY pathway involves transport to an endosomal compartment prior to arrival at the vacuole. CPY overexpression leads to secretion, which would occur if a Golgi localized receptor was saturated. The receptor was identified as Vps10 (Marcusson et al., 1994). Vps10 is a homolog of mammalian sortilin that recognizes a four amino acid motif in the pro-peptide of CPY (Johnson et al., 1987; Valls et al., 1987; Valls et al., 1990; Marcusson et al., 1994). The receptor and cargo are packaged into Gga vesicles and trafficked to the PVE, the late endosome equivalent in yeast. The low pH within the PVE facilitates the release of CPY from Vps10, likely due to a conformational change in the receptor (Leloup et al., 2017). Vps10

is then recycled to the Golgi for further rounds of CPY transport (Ma and Burd 2020). Similar pathways of receptor mediated transport of endosomal/lysosomal proteins have been described in mammalian cells. Cargo delivery is thought to occur via fusion of endosomes with the vacuole, however this process has not been formally demonstrated in yeast. Full fusion of PVE compartments seems unlikely, as stable PVE structures can be visualized over very long periods of time (Day et al., 2018). Another potential mechanism for cargo delivery from the PVE to the vacuole is "kiss-and-run" fusion. This mechanism hypothesizes that transient pores open between the PVE and vacuole that allow the transfer of cargo via diffusion. Both "kiss-and-run" and full fusion events have been directly visualized in mammalian cells between late endosomes and lysosomes (Bright et al., 2005).

The ALP pathway transports cargo molecules from the Golgi directly to the vacuole without passage through an endosomal intermediate. The AP-3 adaptor complex localizes to the Golgi and is required for transport of ALP to the vacuole (Cowles et al., 1997; Day et al., 2018). ALP is delivered to the vacuole normally in CPY trafficking mutants, implying that AP-3 operates a parallel pathway for direct Golgi-to-vacuole trafficking (Piper et al., 1997). While structurally and functionally similar to other adaptor complexes, AP-3 may not require clathrin for vesicle formation in yeast (Vowles and Payne, 1998).

While the CPY and ALP trafficking pathways are individually well characterized, how these processes are coordinated with other Golgi functions is not. The late Golgi integrates vacuolar, secretory, and resident protein sorting. It is not obvious how such complex sorting could be accomplished. One possibility is that different sorting processes are kinetically offset. Examination of the AP-3 adaptor complex revealed that it arrives at the Golgi earlier than the canonical late Golgi protein Sec7 (Day et al., 2018). Similarly, the Gga and AP-1 adaptors have been shown to assemble at the late Golgi sequentially (Daboussi et al., 2012). Therefore, an attractive hypothesis is that different transport routes are kinetically segregated during Golgi maturation. Vacuolar protein sorting would precede secretory cargo

sorting and resident Golgi protein recycling. These hypotheses are testable in the budding yeast *Saccharomyces cerevisiae*, where cisternal maturation can be directly observed.

Perspective

Over the last several decades the membrane trafficking field has shifted from broad morphological observations of membrane bound compartments to meticulous characterization of the proteins and lipids involved in membrane transport. Now that many of the key molecular players have been identified, the field is faced with the challenge of dissecting the wiring network that underlies their biological behavior. Due to the enormous complexity of membrane trafficking, it is helpful to work in a simple model organism. For this purpose the budding yeast *Saccharomyces cerevisiae* has taken a leading role. One way to probe the molecular circuitry underlying the secretory pathway is to simultaneously observe cargo molecules and Golgi membranes while disrupting different aspects of trafficking. Unfortunately, *S. cerevisiae* has not had a robust tool that permitted visualization of cargo sorting during Golgi transport.

In this study, I developed a method, termed ESCargo, to track a fluorescent protein cargo as it traverses the secretory pathway in *S. cerevisiae*. By tracking cargo molecules during cisternal maturation I demonstrated that secretory cargo persists in the lumen of the Golgi throughout maturation. Further, I identified that some secretory cargo recycles within the Golgi in a manner dependent on the AP-1 adaptor complex. To examine how different classes of cargo molecules traverse the Golgi I modified ESCargo by appending a vacuole targeting motif. The results demonstrated that vacuolar cargoes exit the Golgi near the midpoint of cisternal maturation, significantly earlier than secretory cargoes. Vacuolar cargo transport requires Ggas but not AP-1. Thus, the sorting of different cargoes can be kinetically segregated during Golgi maturation. Further, I provided evidence that AP-1 is specifically involved in intra-Golgi recycling at the late Golgi and that endocytosis can act as a retrieval mechanism for late Golgi proteins in AP-1 mutants. Finally, I demonstrated

that ESCargo functions in other model organisms. These constructs have been made available through Addgene and will facilitate comparative studies of cargo trafficking between different model organisms.

CHAPTER 2

VISUALIZING SECRETORY CARGO TRANSPORT IN BUDDING YEAST

Abstract

Budding yeast is an excellent model organism for studying the dynamics of the Golgi apparatus. To characterize Golgi function, it is important to visualize secretory cargo as it traverses the secretory pathway. We describe a recently developed approach that generates fluorescent protein aggregates in the lumen of the yeast endoplasmic reticulum and allows the fluorescent cargo to be solubilized for transport through the Golgi by addition of a small-molecule ligand. We further describe how to generate a yeast strain expressing the regulatable secretory cargo, and we provide protocols for visualizing the cargo by 4D confocal microscopy and immunoblotting.

Introduction

The budding yeast *Saccharomyces cerevisiae* is ideally suited to analyze the dynamic operation of the secretory pathway for two reasons. First, the versatility of this experimental organism has generated a wide range of strains, plasmids, and methods for studying membrane traffic (Duden and Schekman, 1997). Second, the *S. cerevisiae* Golgi is not stacked, so individual cisternae can be tracked in live cells by fluorescence microscopy (Wooding and Pelham, 1998). These properties allowed for a test of two competing models for Golgi function. The stable compartments model predicted that Golgi compartments would be long-lived, whereas the cisternal maturation model predicted that early Golgi cisternae would undergo biochemical transformation into late Golgi cisternae. 4D confocal microscopy of yeast Golgi

This chapter is a version of a manuscript published in Current Protocols in Cell Biology, 2019, 83, e80; with the same title and the following author list: Jason C. Casler and Bejamin S. Glick. I developed the methodology, performed all experiments, and wrote the manuscript. B.S.G supervised the project and edited the manuscript.

cisternae provided definitive support for cisternal maturation (Losev et al., 2006; Matsuura-Tokita et al., 2006).

A deficient component of the *S. cerevisiae* toolbox has been secretory cargo proteins that could be visualized by microscopy during transport. Ideally, a cohort of fluorescent secretory cargo molecules would be trapped in the endoplasmic reticulum (ER) until a stimulus released them for synchronous transport through the secretory pathway. For mammalian cells, several methods have been developed to trap secretory cargo proteins reversibly in the ER (Boncompain and Perez, 2013). We adapted one such method for yeast. In the original approach, a GFP-tagged monomeric secretory cargo protein was fused to four copies of a dimerizing mutant of the FK506-binding protein (FKBP) to generate aggregates in the ER lumen (Rivera et al., 2000). Addition of a ligand dissolved the aggregates by blocking FKBP dimerization, thereby allowing the solubilized monomers to exit the ER. As shown in Figure 2.1, we modified this approach by fusing the tetrameric red fluorescent protein DsRed-Express2 (Strack et al., 2008) to a single copy of a reversibly dimerizing mutant of FKBP. Our construct forms ER-localized aggregates, which can be dissolved by addition of a ligand to create soluble tetramers that proceed through the secretory pathway. Although this concept is simple, the implementation required significant engineering of the cargo and the yeast strain (Barrero et al., 2016; Casler et al., 2019).

Here we describe protocols for generating a drug-sensitive yeast strain that expresses the regulatable secretory cargo (Basic Protocol 1), for visualizing the secretory cargo in yeast cells by microscopy (Basic Protocol 2), and for detecting the secreted cargo by immunoblotting (Basic Protocol 3).

Strategic Planning

The red fluorescent aggregates generated by our construct can be dissolved by addition of a synthetic ligand of FKBP (SLF; Holt et al., 1993) to create soluble tetramers. Optimization of the FKBP mutant was needed because the original reversibly dimerizing FKBP generated

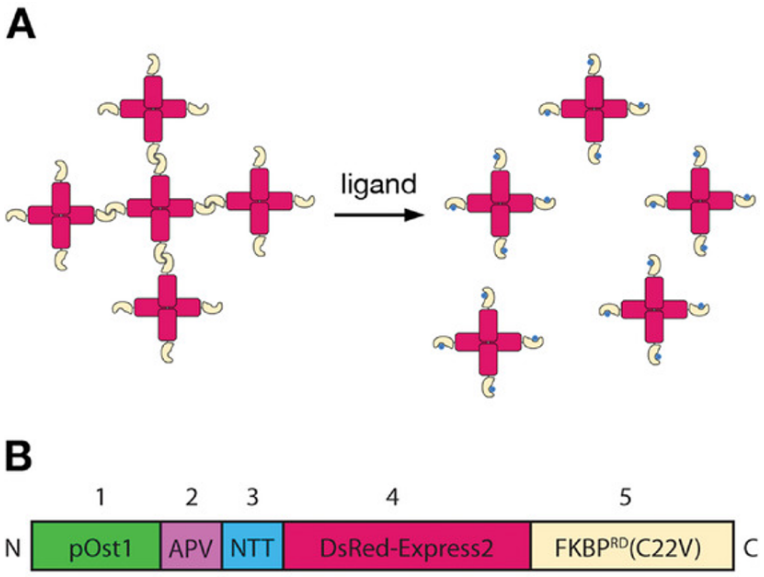

Figure 2.1: **A reversibly aggregating fluorescent secretory cargo. (A)** Strategy for generating and dissolving fluorescent aggregates. DsRed-Express2 tetramers (red) fused to a dimerizing variant of FKBP(gold) associate with one another to form aggregates. Addition of the FKBP ligand SLF (blue) blocks dimerization, thereby dissolving the aggregates into soluble tetramers. **(B)** Schematic of the functional segments of the regulatable secretory cargo polypeptide. (1) pOst1 (green): ER signal sequence that directs cotranslational translocation. (2) APV (pink): ER export signal tripeptide. (3) NTT (blue): N-linked glycosylation signal tripeptide. (4) DsRed-Express2 (red): tetrameric fluorescent protein. (5) FKBPRD(C22V) (gold): reversibly dimerizing variant of FKBP. The lengths of the different segments are not to scale.

aggregates that dissolved slowly and required high concentrations of SLF. Therefore, we rationally engineered a reversibly dimerizing FKBP mutant to form aggregates that dissolve faster and at lower SLF concentrations (Barrero et al., 2016). A further concern was that position 22 of FKBP was a cysteine, which could cause unwanted disulfide formation in the ER lumen. The corresponding residue in some FKBP homologs is valine (Galat, 2008), so we introduced a C22V mutation that does not alter the formation or dissolution of aggregates (Casler et al., 2019). We term the final reversibly dimerizing FKBP mutant FKBPRD(C22V) and the fusion construct DsRed-Express2-FKBPRD(C22V).

While optimizing the FKBP mutant, we discovered that yeast are adept at removing SLF via the action of pleiotropic drug transporters (Rogers et al., 2001). Removal of SLF causes reaggregation of the cargo. Deletion of the single drug transporter Pdr5 reduced but

did not abrogate the removal of SLF. A much more successful approach was to delete Pdr1 and Pdr3, which are transcription factors that control the expression of many pleiotropic drug transporters (Coorey et al., 2007; Schüller et al., 2007). In a *pdr1*Δ *pdr3*Δ background, addition of SLF allows for sustained dissolution of the aggregates (Barrero et al., 2016). The next challenge was to optimize entry into and exit from the ER. Many soluble yeast secretory cargo proteins undergo post-translational translocation (Ast et al., 2013; Ng, etl al., 1996), but it was essential to direct DsRed-Express2-FKBPRD(C22V) for cotranslational translocation to ensure its passage across the ER membrane. We appended the Ost1 signal sequence, which efficiently directs cotranslational translocation (Fitzgerald and Glick, 2014). Addition of this signal sequence generates ER-localized DsRed-Express2-FKBPRD(C22V) tetramers that form aggregates (see the red channel in Movie 2.1 and Figure 2.2). Upon addition of SLF, the aggregates quickly dissolve, and the solubilized tetramers fill the ER lumen (Casler et al., 2019).

Unfortunately, the solubilized tetramers exit the ER at the slow rate of bulk flow (Barlowe and Helenius, 2016). To circumvent this problem, we inserted the first six residues of the yeast α-factor pro region after the Ost1 signal sequence. That hexapeptide sequence is APVNTT, and it contains both the evolutionarily conserved ER export signal APV (Yun et al., 2018), which interacts with the cargo receptor Erv29 (Barlowe and Miller, 2013), and the N-linked glycosylation signal NTT (Kornfeld and Kornfeld, 1985). Addition of the hexapeptide to generate APVNTT-DsRed-Express2-FKBPRD(C22V) tetramers (Figure 2.1B) preserves the formation of aggregates in the ER lumen and allows rapid signal-mediated ER export upon addition of SLF. As shown in Figure 2.1B, the complete construct consists of the Ost1 signal sequence, the APVNTT hexapeptide, DsRed-Express2, and FKBPRD(C22V).

Another concern was that a significant fraction of the cargo molecules were diverted to the vacuole. This problem can be alleviated by introducing the *vps10-104* allele, which encodes a Vps10 protein that lacks one of the two sortilin homology domains (Jørgensen et al., 1999). The Vps10-104 mutant receptor continues to recognize endogenous vacuolar proteases but no

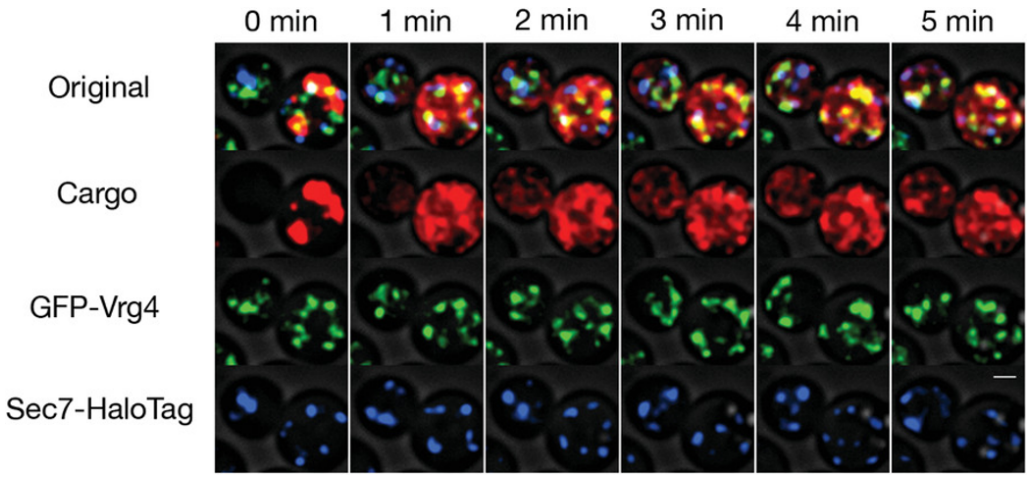

Figure 2.2: **Visualizing the secretory cargo together with Golgi markers.** A strain expressing pOst1-APVNTT-DsRed-Express2-FKBPRD(C22V), GFP-Vrg4 (early Golgi marker), and Sec7-HaloTag (late Golgi marker) was grown to mid-log phase in NSD, labeled with the HaloTag-JF$_{646}$ dye (Grimm et al., 2015), washed, mounted in a flow chamber, and imaged by 4D confocal microscopy while SLF was flowed over the cells. Images, taken from Movie 2.1, are average projected z-stacks at the indicated time points. Scale bar, 2 µm.

longer recognizes foreign secretory cargo proteins (Fitzgerald and Glick, 2014; Jørgensen et al., 1999). Our results also indicate that for unknown reasons, glycosylation of the secretory cargo further suppresses diversion to the vacuole (Casler et al., 2019). Thus, in a *vps10-104* strain, the glycosylated APVNTT-DsRed-Express2-FKBPRD(C22V) tetramers efficiently traverse the secretory pathway to the plasma membrane.

Basic Protocol 1: Generating a drug-sensitive yeast strain that expresses the regulatable secretory cargo

In this protocol we describe the construction of a *pdr1*Δ *pdr3*Δ *vps10-104* yeast strain suitable for tracking the regulatable fluorescent secretory cargo. The two gene deletions can be generated by standard PCR-based recombination techniques using G418-resistance and nourseothricin-resistance cassettes (Goldstein and McCusker, 1999; Wach et al., 1994); suitable primers are listed in Table 2.1. The *vps10-104* allele can be generated using pop-in/pop-out gene replacement with the plasmid vps10-104-YIplac211. Expression of the secretory

cargo is driven by the strong constitutive *TPI1* promoter and the *CYC1* terminator, and this is achieved by integrating an expression vector at either the *TRP1* or *LEU2* locus using the plasmid YIplac204-pOst1-APVNTT-DsRed-Express2-FKBP(LV,C22V) or YIplac128-pOst1-APVNTT-DsRed-Express2-FKBP(LV,C22V), respectively (Table 2.2). Single-copy integrants are verified by PCR.

Materials

- Plasmids of interest (see Table 2.2)
- PCR buffer
- 10 µM forward and reverse primers for PCR (see Table 2.1)
- dNTPs
- Herculase or Herculase II polymerase (e.g., Agilent, cat. nos. 600264, 600675)
- PEG/lithium acetate
- Yeast of interest (see Table 2.3)
- YPD selection plates (see recipe)
- Antibiotics for selection:
  - G418, disulfate salt (Teknova, cat. no. G5001)
  - Nourseothricin sulfate (Research Products International, cat. no. N51200-1.0)
  - 5-fluoroorotic acid (5-FOA; Oakwood Products, cat. no. 50204161)
- Restriction enzymes: HpaI, EcoRV, ClaI
- DNA cleaning kits (e.g., Qiagen, cat. nos. 28306, 28706)
- SD selection plates (see recipe)
- YPD medium (see recipe)
- Yeast DNA purification kit (e.g., Epicentre, cat. no. MPY80200)
- Thermal cycler
- 30°C incubator
- Fluorescence microscope
- Glass slides
- Glass coverslips (22 x 22 mm, no. 1.5)
- Additional reagents and equipment for agarose gel electrophoresis (Armstrong and Schulz, 2008), yeast transformation (Gietz and Woods, 2002), and colony PCR (Amberg et al., 2006)

Generate a pdr1Δ pdr3Δ strain

1. To delete *PDR1*, amplify a G418-resistance cassette from plasmid pFA6a-kanMX6 by PCR using the primers listed in Table 2.1 and the following reaction and thermal cycler conditions:

Herculase reaction conditions:

- 37.5 µl water
- 5 µl buffer
- 1.5 µl (150 ng) DNA
- 1 µl of 10 µM forward primer
- 1 µl of 10 µM reverse primer
- 2 µl of 10mM dNTPs
- 2 µl polymerase

Herculase II reaction conditions:

- 30.5 µl water
- 10 µl buffer
- 1.5 µl(~150 ng) DNA
- 2.5 µl of 10 µM forward primer
- 2.5 µl of 10 µM reverse primer
- 2 µl of 10 mM dNTPs
- 1 µl polymerase

Herculase thermal cycler conditions:

- Denature - 2 min - 92°C
- 30 cycles - 30 s - 92°C
- 30 s - 55°C
- 10 min - 68°C
- 1 cycle - 15 min - 68°C
- Hold - indefinite - 4°C

Herculase II thermal cycler conditions:

- Denature - 2 min - 92°C
- 10 cycles - 30 s - 92°C
- 30 s - 55°C
- 11 min - 68°C
- 20 cycles - 30 s - 92°C
- 30 s - 55°C
- 11 min + 30 s/cycle - 68°C
- 1 cycle - 12 min - 68°C
- Hold - indefinite - 4°C

The pFA6a-kanMX6 plasmid is available from Addgene (39296).

2. Run the PCR product on a 1 % agarose gel. Excise and purify the amplified 1583-bp fragment, and transform it into a yeast strain of choice (see Table 2.3) using PEG/lithium acetate.

When transforming yeast cells to obtain antibiotic resistance, spread the cells evenly on the plate because otherwise clumps of cells will generate pseudo-colonies.

3. Select for transformants on YPD plates containing G418 by incubating at 30°C for 2 to 3 days. Restreak colonies on fresh YPD plates containing G418 to ensure that the clones are truly drug resistant.

   To allow expression of the drug-resistance gene, we recommend incubating the transformed yeast cells in YPD for at least 4 hr prior to spreading on the selective plates.

4. Confirm deletion of *PDR1* by colony PCR (Amberg et al., 2006) using the primers listed in Table 2.1.

   The wild-type PDR1 allele will not yield an amplified fragment, whereas the pdr1Δ allele will yield an amplified fragment of 1155 bp.

5. Repeat steps 1 through 4 to delete *PDR3*, with the following modifications. In this case, amplification of the nourseothricin-resistance cassette from pAG25 will generate a 1349-bp fragment, and transformants will be selected on YPD plates containing nourseothricin. After colony PCR, the wild-type *PDR3* allele will not yield an amplified fragment, whereas the *pdr3*Δ allele will yield an amplified fragment of 1240 bp.

   The pAG25 plasmid is available from Addgene (35121). Both of the drug-resistance cassettes use the same promoter and terminator. Therefore, it is crucial when generating the second deletion to select on YPD plates that contain both nourseothricin and G418, to avoid selecting clones that have recombined at the previously deleted gene.

Introduce the vps10-104 allele by pop-in/pop-out gene replacement

6. Linearize plasmid vps10-104-YIplac211 with HpaI to direct integration at the *VPS10* locus. To linearize the plasmid, digest it thoroughly with HpaI, and then clean the DNA with a commercial kit.

    The vps10-104-YIplac211 plasmid, which contains the URA3 selectable marker, is available from Addgene (115426). This plasmid is suitable for pop-in/pop-out gene replacement (Rothstein, 1991). In this procedure, integration at the VPS10 locus generates adjacent wild-type and mutant alleles. Then counter-selection with 5-FOA selects for recombinants that have excised the URA3 gene. Recombination will either regenerate the wild-type VPS10 allele or cause a clean replacement of the wild-type allele with the mutant vps10-104 allele. Multiple pop-out clones need to be screened to ensure identification of a vps10-104 strain.

7. Using PEG/lithium acetate, transform the linearized DNA (~250 ng total) into a *ura3* auxotrophic yeast strain carrying the *pdr1*Δ and *pdr3*Δ alleles. Select for transformants on SD-Ura dropout plates by incubating at 30°C for 2 to 3 days. Restreak the colonies on fresh SD-Ura plates, and then work with single colonies from those plates.

    With dropout plates, only cells that have integrated the URA3-containing linearized plasmid will be able to grow and generate colonies.

8. Confirm successful pop-in integration by colony PCR (Amberg et al., 2006) with the primers listed in Table 2.1.

    The wild-type band is 3.2 kb, and the mutant band is 1.1 kb.

9. Grow a culture of a confirmed pop-in strain in YPD overnight.

We recommend working with two or three separate pop-in clones to increase the chance of obtaining successful pop-out clones. In theory, the pop-in clones should all be genetically identical. In practice, yeast transformation sometimes causes unexpected genomic rearrangements that elude detection by PCR, so it is good practice to work with several candidate clones.

10. Spread an aliquot from each pop-in clone culture on an SD plate containing 5-FOA. Incubate at 30°C for 2 to 3 days until colonies appear.

    Plating 50 µl of a saturated culture tends to give good colony density, but this amount may need to be determined empirically.

11. Restreak the pop-out clones on fresh YPD plates, and then work with single colonies from those plates.

12. Confirm the presence of the mutant *vps10-104* allele by the same colony PCR protocol described in step 9, using primers listed in Table 2.1.

    In our hands, out of 24 pop-out clones, 6 had the mutant allele.

Generate and confirm single-copy integrants of a cargo expression construct

14. Linearize plasmid YIplac204-pOst1-APVNTT-DsRed-Express2-FKBP(LV,C22V) with EcoRV, or plasmid YIplac128-pOst1-APVNTT-DsRed-Express2-FKBP(LV, C22V) with ClaI, to direct integration at the *TRP1* or *LEU2* locus, respectively. To linearize the plasmid, digest it extensively with the appropriate enzyme, and then clean the DNA with a commercial kit.

    These plasmids are available from Addgene (115420 and 115421). The choice of which plasmid to use will depend on whether a leu2 or trp1 auxotrophic marker is present in the yeast strain.

15. Transform the linearized DNA into a *pdr1*Δ *pdr3*Δ *vps10-104* yeast strain using PEG/lithium acetate.

    We recommend transforming with ~100 to 150 ng linearized DNA. Higher amounts of DNA increase the chance of multiple integrations.

16. Select for transformants on SD-Trp or SD-Leu dropout plates by incubating at 30°C for 2 to 3 days.

    With dropout plates, only cells that have integrated the TRP1- or LEU2-containing linearized plasmid will be able to grow and generate colonies.

17. Restreak 8 to 16 clones on fresh YPD plates.

18. Work with individual colonies to confirm expression of the construct by fluorescence microscopy. For this purpose, use a sterile toothpick to suspend a small amount of cells from a colony in 1 to 2 µl water on a glass slide. Then spread the cells by overlaying a glass coverslip, and examine the cells by widefield microscopy for the presence of red fluorescent aggregates.

19. For fluorescent clones, isolate high-purity genomic DNA.

    We typically use the MasterPure Yeast DNA Purification Kit (Epicentre, cat. no. MPY80200).

20. Verify single-copy integrants by PCR using the primers listed in Table 2.1 and the protocols listed in step 1.

    Some of the transformants will likely have experienced multiple tandem integrations of the linearized plasmid. Single-copy integrants are more genetically stable, and they will generate reliable results that allow for direct comparisons between different strains.

Basic Protocol 2: Visualizing secretory cargo in yeast cells by microscopy

This protocol describes a method to track the fluorescent secretory cargo by 4D confocal microscopy. Cells are immobilized on a coverslip dish that contains liquid medium, and the dish is viewed with an inverted microscope. An example of cargo solubilization and transport to Golgi compartments is shown in Figure 2.2 and Movie 2.1. In addition, we describe a fluorescence recovery after photobleaching (FRAP) procedure that detects secretory cargo transfer between cisternae during Golgi maturation (Casler et al., 2019).

When cells are grown in minimal medium to facilitate fluorescence microscopy, the secreted cargo becomes trapped between the plasma membrane and the cell wall (Casler et al., 2019). The resulting periplasmic fluorescence can complicate image analysis. To avoid this effect, imaging can be performed in minimal medium at a pH of 4 to quench the fluorescence of any extracellular DsRed-Express2 molecules, which have a chromophore pKa of 4.5 (Strack et al., 2009).

Materials

- 2 mg/ml concanavalin A (Sigma-Aldrich, cat. no. C2010) prepared in deionized water
- Yeast cells (see Table 2.3)
- NSD minimal medium, pH 4 (see recipe; Bevis et al., 2002)
- 100 mM SLF solution (Cayman Chemical, cat. no. 10007974) prepared in ethanol
- 1000× nocodazole (Thermo Fisher, cat. no. AC358240500) prepared in DMSO
- Coverslip dishes (e.g., MatTek P35G-1.5-14-C)
- 23°C shaking incubator
- 50-ml baffled flask, sterilized by autoclaving
- Spectrophotometer
- Confocal microscope with inverted optics (e.g., Leica SP8 or equivalent)

Prepare concanavalin A–coated coverslip dishes

1. Add 250 µl of 2 mg/ml concanavalin A in deionized water to a coverslip dish.

Aliquots of the concanavalin A solution can be frozen in liquid nitrogen, stored at –80°C, and thawed just before use.

2. Incubate at 23°C for 10 to 15 min to allow the concanavalin A to bind to the glass.

3. Wash gently with deionized water, and allow the glass surface to dry prior to adhering cells.

It is best to use coverslip dishes that have been coated with concanavalin A the same day.

Concanavalin A will bind carbohydrates in the yeast cell wall, thereby gently immobilizing the cells on the coverslip dish.

Prepare cells for 4D confocal microscopy

4. Inoculate a fresh culture of the yeast strain in 5 ml NSD in a 50-ml baffled flask. Allow the culture to grow overnight at 23°C with shaking at 225 rpm.

A saturated preculture of the yeast strain can be stored in a 15-ml culture tube at 4°C for up to a month. To initiate a fresh culture, dilute a small aliquot of the preculture in NSD. A typical dilution for overnight growth is 1:1000.

5. Verify that the OD_{600} is between 0.5 and 0.8. If it is too high, dilute the culture in fresh NSD to an OD_{600} of ~ 0.2, and let the culture grow for at least 2 more hr.

The OD_{600} is the optical density at 600 nm. It can be measured with a standard spectrophotometer using a disposable plastic cuvette.

6. Add 250 µl culture to a concanavalin A–coated coverslip dish. Allow the cells to settle and adhere for 10 min, and then gently wash with NSD. Add 1 ml NSD to cover the cells.

7. Prepare NSD supplemented with 200 µM SLF by adding 2 µl of 100 mM SLF stock solution to 1 ml NSD and mixing.

8. Place the dish on the microscope stage. Set microscope parameters as described in steps 10 through 18, and adjust the objective position so that cells immobilized on the coverslip are in focus.

9. Remove the dish from the microscope stage. Add 1 ml NSD/SLF medium (from step 7) to the dish to yield a final concentration of 100 µM SLF, and mix gently by swirling. Immediately replace the dish on the microscope stage, and identify the cells that will be imaged.

   Cargo aggregates will begin to dissolve immediately and will be fully dissolved within ~ 2 min.

   Appearance of the solubilized cargo in early and late Golgi compartments should be maximal at ~ 2 min and ~ 4 min after SLF addition, respectively.

Perform 4D confocal microscopy

The following parameters are suitable for a Leica SP8 with a 1.4-NA oil objective. Other confocal microscopes should have similar settings.

10. Choose a frame size of 256 × 128 pixels.

    The scan time is strongly influenced by the frame size. A 256 × 128 image should be sufficient to capture several cells.

11. Zoom to a pixel size of ~ 70 to 80 nm.

    This pixel size results in imaging at the Nyquist limit, thereby minimizing light exposure while theoretically avoiding information loss.

12. Choose the maximum scan speed. Enable bidirectional scanning for rapid imaging.

13. Adjust the pinhole to 1.2 Airy units.

    The standard recommendation for confocal microscopy is to use 1.0 Airy unit. But empirically, when imaging live cells, a setting of 1.2 Airy units yields significantly stronger signals with no discernible loss in image quality.

14. Use line accumulation of at least 2 (preferably 3 or 4 if the total scan time is under 3 sec).

15. Set the z-stack to ~ 20 to 30 steps at 0.25 to 0.35 µm/step to cover the entire cell with extra optical sections above and below.

    This step size results in imaging at the Nyquist limit, thereby minimizing light exposure while theoretically avoiding information loss. To avoid excessive scan times and photobleaching, keep the number of optical slices above and below the cells to the minimum needed to ensure full capture of the fluorescence signals.

16. Aim for the total time to capture a z-stack of between 1 and 3 sec.

17. With the laser set to 561 nm, set a range of 4 % to 7 % laser intensity, which typically provides an adequate, nonsaturated signal.

    Even though the regulatable fluorescent secretory cargo is expressed from an integrated construct that does not vary in copy number, heterogeneity between cells in the sizes of aggregates may require adjustment of the laser intensity on a cell-by-cell basis.

18. Perform deconvolution and bleach correction to compensate for the inherently noisy nature of 4D confocal microcopy data (Day et al., 2016).

During imaging, individual pixels may accumulate only one or a few photons, so structures will be difficult to see in the raw optical sections. Capturing data in this manner can be disconcerting. However, after deconvolution and projection of the z-stacks, structures should be readily visible and trackable through time.

Perform FRAP experiments with nocodazole-treated cells

1. Inoculate a fresh culture of the yeast strain in 5 ml NSD in a 50-ml baffled flask. Allow the culture to grow overnight at 23°C with shaking at 225 rpm.

2. Verify that the OD_{600} is between 0.5 and 0.8. If it is too high, dilute the culture in fresh NSD to an OD_{600} of 0.2, and let it grow for at least 2 more hr.

3. Add nocodazole to 8 µg/ml from a 1000× stock solution in DMSO, and incubate with shaking for 2 hr.

   Nocodazole depolymerizes microtubules, causing a yeast cell to arrest in mitosis with a large budded daughter that lacks a nucleus. After 2 hr, nearly every cell in the culture is arrested at this point in the cell cycle, but cellular function is not yet significantly compromised. The available evidence indicates that operation of the yeast secretory pathway is normal under these conditions (Casler et al., 2019).

4. Prepare cells for 4D confocal microscopy as described in steps 4 through 9, except wash and cover cells with NSD supplemented with 8 µg/ml nocodazole.

5. Add 1 ml NSD containing 200 µM SLF and 8 µg/ml nocodazole to the coverslip dish to yield a final concentration of 100 µM SLF, and mix gently.

6. Identify budded daughters by lack of perinuclear ER fluorescence in the cargo channel.

This identification can be performed within 2 min of adding SLF. The nuclear envelope comprises a large fraction of the ER in yeast cells. Because a budded daughter that lacks a nucleus has much less ER than an unperturbed yeast cell, imaging of Golgi dynamics in a budded daughter is relatively easy.

7. Draw a region of interest (ROI) around the entire budded daughter.

8. Increase the laser power to 100 % (with a background of 5 % outside the ROI), and bleach by taking about 20 z-stacks over a total period of 40 sec.

9. Drop the laser power to 4 % to 7 % and begin imaging normally. Look for recovery of cargo fluorescence in Golgi cisternae in the bleached daughter.

   Any recovered fluorescence is due to fluorescent cargo molecules that were originally present in the unbleached mother.

Basic Protocol 3: Detecting secreted cargo by immunoblotting

This protocol describes a method to track secretion of the cargo by immunoblotting. To enable release of the cargo from the periplasm, cells are grown in rich YPD medium to yield a more permeable cell wall (Casler et al., 2019; de Nobel et al., 1990). The secreted cargo is hyperglycosylated and is therefore treated with endoglycosidase H to remove the oligosaccharide and generate a sharp band when analyzed by SDS-PAGE (Casler et al., 2019).

Materials

- Yeast cells (see Table 2.3)
- YPD medium (see recipe)
- 100 mM SLF solution (Cayman Chemical, cat. no. 10007974) prepared in ethanol
- Phosphate-buffered saline (PBS)
- Protein precipitation kit (National Diagnostics, cat. no. EC-888)
- Acetone
- 70 % ethanol
- SDS-PAGE sample buffer containing β -mercaptoethanol

- Endoglycosidase H reaction kit (New England Biolabs, cat. no. P0702S) containing:
  - Glycoprotein denaturing buffer
  - Endoglycosidase H
  - Glycobuffer 3
- Anti-FKBP12 antibody, rabbit polyclonal (Abcam, cat. no. ab2918)
- Goat anti-rabbit secondary antibody conjugated to Alexa Fluor 647 (Thermo Fisher, cat. no. A21245)
- 50-ml baffled flask
- 23°C shaking incubator
- Spectrophotometer
- Centrifuge
- 1.7-ml snap-cap tubes
- Microcentrifuge
- 0.5-mm diameter glass beads (BioSpec Products)
- Vortex
- Heating block
- Additional reagents and equipment for SDS-PAGE (Gallagher, 2012) and immunoblotting (Gallagher et al., 2008)

Perform cargo secretion and cell lysis

1. Inoculate a fresh culture of the yeast strain in 5 ml YPD in a 50-ml baffled flask. Allow the culture to grow overnight at 23°C with shaking at 225 rpm.

   To detect secreted cargo, it is essential to grow the cells in rich medium. When cells are grown in minimal medium, most of the cargo becomes trapped in the periplasm.

2. Verify the OD_{600} is between 0.5 and 0.8. If it is too high, dilute the culture in fresh YPD to an OD_{600} of 0.2, and let it grow for at least 2 more hr.

3. Centrifuge sample 5 min at 1000 × g (3000 rpm), room temperature, and wash twice with fresh YPD.

4. Resuspend the cell pellet in the initial volume of YPD.

At this point the cargo is still in the form of ER-localized aggregates. Transfer of the cells to fresh medium has removed any cargo molecules that were secreted during growth of the culture.

5. Add 100 mM SLF to a final concentration of 100 µM. Continue to incubate the culture with shaking.

6. At each of the desired time points, transfer 1.6 ml culture to a 1.7-ml snap-cap tube.

   Secreted cargo molecules should begin to appear in the medium within about 10 min after SLF addition.

7. Using a microcentrifuge, centrifuge 2 min at 2400 × g (5000 rpm), room temperature, and separate the pellet (cells) and supernatant (secreted protein) fractions. Place the supernatant sample on ice in a 1.7-ml snap-cap tube.

   The supernatant sample is ready for protein precipitation, and the pellet sample is further processed as described in steps 8 through 11.

8. Wash the cell pellet once with deionized water by resuspending the cells and then centrifuging 2 min at 2400 × g (5000 rpm), room temperature.

9. Resuspend the cell pellet in 100 µl ice-cold PBS, and add 100 µl of 0.5-mm diameter glass beads.

10. Vortex sample for 1 minute followed by 1 minute on ice. Repeat twice.

    This procedure mechanically disrupts the cells, thereby ensuring that the intracellular cargo molecules will be efficiently solubilized when the sample is eventually boiled in SDS-PAGE sample buffer.

11. Add 800 µl ice-cold PBS to the lysed cell sample, mix briefly, and then transfer 800 µl liquid to a fresh snap-cap tube on ice.

Precipitate protein

12. Precipitate proteins using the National Diagnostics Protein Precipitation Kit, as follows:

    In our hands, this kit is more effective than standard protein precipitation methods that employ trichloroacetic acid.

    (a) Add 80 µl or 40 µl Reagent A to the secreted protein fraction or the lysed cell fraction, respectively. Warm the samples to room temperature.

    (b) Add 160 µl or 80 µl Reagent B to the secreted protein fraction or the lysed cell fraction, respectively.

    (c) Mix by inversion, and incubate at 23°C for 15 min.

    (d) Collect the precipitated proteins by centrifuging 10 min at 14,000 × g (12,000 rpm), room temperature.

    (e) Discard the supernatants, and resuspend each of the pellets in 1 ml acetone. For resuspension, vortexing typically works, but pipetting may be necessary.

    (f) Using a microcentrifuge, centrifuge 15 min at top speed, room temperature. Discard the supernatant.

    (g) Wash each pellet twice with 70 % ethanol.

13. Resuspend each final pellet in 50 µl SDS-PAGE sample buffer. Boil for 5 to 10 min.

Treat with endoglycosidase H and immunoblot

14. Add glycoprotein denaturing buffer to a 1× concentration to the protein samples in SDS-PAGE sample buffer.

    In our hands, 9 µl lysed cell fraction and 14 µl secreted protein fraction provide good signals.

15. Boil for 5 to 10 min to denature the proteins.

16. Add 2 µl endoglycosidase H, Glycobuffer 3 to a 1× concentration, and water to 20 µl.

17. Incubate at 37°C for at least 1 hr.

18. Perform SDS-PAGE using standard protocols.

19. Perform immunoblotting to detect the cargo using an anti-FKBP primary antibody together with a suitable secondary antibody.

    The protein band will have an apparent molecular weight of 38 to 39 kDa.

    For unknown reasons, we were unable to detect the cargo using anti-DsRed antibodies.

Reagents and solutions

Nonfluorescent vitamin mix, 500×

- 500 ml water
- 500 mg calcium pantothenate
- 2.5 g myo-inositol
- 100 mg niacin (nicotinic acid)
- 50 mg p-aminobenzoic acid
- 100 mg pyridoxine hydrochloride
- 100 mg thiamine hydrochloride
- Filter sterilize
- Store at 4°C for up to 6 months

Calcium pantothenate and p-aminobenzoic acid should be stored at 4˚C.

NSD

- 1 liter water
- 20 g glucose
- 5 g ammonium sulfate
- 0.79 g complete supplement mixture (CSM; Sunrise Science, cat. no. 1001-100) or CSM lacking a nutrient
- 1.7 g yeast nitrogen base
- 2 ml 500× nonfluorescent vitamin mix (see recipe)
- 2 ml 0.2 mg/ml biotin

- 2 ml 0.1 mg/ml CoCl2·6H2O
- 20 mg adenine sulfate
- Adjust pH with NaOH if desired
- Filter sterilize Store at room temperature for up to 6 months

  CSM lacking a nutrient can include CSM-Ura, CSM-Leu, CSM-Trp (Sunrise Science, cat. nos. 1004-10, 1005-100, 1007-100, respectively).

  Without pH adjustment, the pH is typically ~ 4.

SD plates for selection

- 1 liter water
- 20 g glucose
- 5 g ammonium sulfate
- 0.79 g CSM lacking a nutrient
- 1.7 g yeast nitrogen base
- 20 g agar
- Adjust pH to 5.5 with NaOH
- Sterilize by autoclaving, and let solution cool for ~ 30 min before pouring into plates
- Store plates at 4°C for up to 6 months

  CSM lacking a nutrient can include CSM-Ura, CSM-Leu, CSM-Trp (Sunrise Science, cat. nos. 1004-10, 1005-100, 1007-100, respectively).

SD plates containing 5-FOA for counterselection

- 700 ml water
- 20 g glucose
- 5 g ammonium sulfate
- 0.79 g CSM (Sunrise Science, cat. no. 1001-100)
- 1.7 g yeast nitrogen base
- 20 g agar
- Adjust pH to 5.5 with NaOH
- Sterilize by autoclaving, and let solution cool for ~ 30 min to ~ 60°C. Meanwhile, dissolve 1 g 5-FOA in 300 ml water with stirring and gentle heating. Filter sterilize 5-FOA solution, and slowly add with stirring to the autoclaved and cooled SD, avoiding bubbles. Pour into plates.

  Store plates at 4˚C for up to 6 months, shielded from light

YPD medium

- 1 liter water
- 10 g yeast extract
- 20 g peptone

- 20 g glucose
- Sterilize by autoclaving
- Store at 4°C for up to 6 months

YPD plates for growth and selection

- 1 liter water
- 20 g glucose
- 20 g peptone
- 10 g yeast extract
- 20 mg adenine sulfate
- 20 mg uracil
- Sterilize by autoclaving, and let cool for ~ 30 min
- If desired, add G418 to 200 µg/ml or nourseothricin to 100 µg/ml before pouring the plates
- Store plates at 4°C for up to 6 months

Purpose	**Primers**
PDR1 deletion	5'-CAGCCAAGAATATACAGAAAAGAATCCAA GAAACTGGAAGCGTACGCTGCAGGTCGAC-3' 5'-GGAAGTTTTTGAGAACTTTTATCTATACA AACGTATACGTATCGATGAATTCGAGCTCG-3'
PDR3 deletion	5'- ATCAGCAGTTTTATTAATTTTTTCTTAT TGCGTGACCGCACGTACGCTGCAGGTCGAC-3' 5'- TACTATGGTTATGCTCTGCTTCCCTATTT TCTTTGCGTTTATCGATGAATTCGAGCTCG-3'
*pdr1*Δ verification	5'-CCTAATGAGTGGCAATAAGAGGCGC-3' 5'-CACTCGCATCAACCAAACCGTTATTC -3'
*pdr3*Δ verification	5'-CCGTGCTCTGCTGCTTTCAG-3' 5'-GTGAACCCCATCCGCCGGTA-3'
vps10-104 verification	5'-CTCCCGTGGGCTTATGCGTTGCAG-3' 5'-GGAGGGATTCGTCGGTGACTGTGTC-3'
TRP1 integration	5'-GTGTACTTTGCAGTTATGACGCCAGATGG-3' 5'-AGTCAACCCCCTGCGATGTATATTTTCCTG-3'
LEU2 integration	5'-GGAGGTCGACTACGTCGTTAAGGC-3' 5'-GTCCTGTACTTCCTTGTTCATGTGTG-3'

Tables 2.1: PCR Primers for Generating and Verifying Yeast Strains

Plasmid	Marker	Addgene #	Notes
YIplac204-pOst1-APVNTT-DsRed-Express2-FKBP(LV,C22V)	*TRP1*	115420	Expresses cargo from a cassette integrated at *TRP1*
YIplac128-pOst1-APVNTT-DsRed-Express2-FKBP(LV,C22V)	*LEU2*	115421	Expresses cargo from a cassette integrated at *LEU2*
vps10-104-YIplac211	*URA3*	115426	Creates *vps10-104* allele by gene replacement

Tables 2.2: Integrating Plasmids for Engineering of Yeast Strains

Yeast strain	Genotype
yAG56	*pdr1*Δ *pdr*Δ *vps10-104*
yAK7	*pdr1*Δ*pdr*Δ *vps10-104 trp1*::PTPI1-pOst1-DsRed-Express2-FKBPRD(C22V)
yAL45	*pdr1*Δ*pdr*Δ *vps10-104 leu2*::PTPI1-pOst1-DsRed-Express2-FKBPRD(C22V)

Tables 2.3: Parental and Final Yeast Strains

Commentary

Background Information

Use of the regulatable secretory cargo requires a particular genetic background. The *pdr1 pdr3* mutations ensure that SLF will be effective, and the *vps10-104* mutation ensures that the

cargo will avoid being diverted to the vacuole. With such a strain, cargo transport through the secretory pathway is reproducibly efficient, and this process can be readily tracked by fluorescence microscopy and immunoblotting (Casler et al., 2019). After SLF addition, the ER-localized aggregates dissolve rapidly, and the fluorescent tetramers begin to exit the ER. Cargo molecules almost immediately become concentrated in ER exit sites and nascent early Golgi cisternae, so the punctate pattern of ER-localized aggregates is replaced by a different punctate pattern (Figure 2.2). The ER export signal present in the cargo protein leads to a "cargo wave" as defined by the sequential appearance of red fluorescence in early and late Golgi cisternae. Golgi labeling persists until the cargo drains from the ER and is fully secreted.

Our method for tracking yeast secretion has limitations but also opens additional possibilities. The main limitation is that the cargo is artificial and cannot easily be adapted to track natural or transmembrane cargoes. On the other hand, modification of the cargo with a vacuolar targeting signal should be feasible (Rothman et al., 1989), thereby enabling visualization of a fluorescent cargo as it transits through the Golgi and prevacuolar endosome to the vacuole. The use of fluorescent color variants of DsRed-Express2 (Strack et al., 2011) may allow plasma membrane and vacuole targeted cargoes to be tracked simultaneously in different color channels. We are actively exploring these options.

Critical Parameters and Troubleshooting

Because the secreted cargo becomes trapped in the periplasm when cells are grown in minimal medium, it is best to perform imaging in NSD medium at pH 4. This pH is below the chromophore pKa of DsRed-Express2 ($\sim$ 4.5), so the fluorescence signal in the periplasm is quenched while the intracellular signal is unaffected.

Although deletion of the Pdr1 and Pdr3 transcription factors dramatically inhibits the extrusion of SLF, a very small percentage of cells may show some reaggregation of the cargo.

This effect could be due to degradation or incomplete permeation of SLF. Any cells that show reaggregation should be excluded from analysis.

Even with an integrated single-copy expression construct, there is always considerable heterogeneity between cells with regard to the sizes of ER-localized aggregates. Thus, it may be necessary to adjust the 561-nm laser power for a given cell to obtain a stronger signal or to avoid saturating the detector.

Aggregation efficiency is temperature sensitive (Casler et al., 2019). Significant aggregation in the ER is seen at room temperature, but the extent of aggregation progressively declines at higher temperature and is negligible at 37°C. Therefore, it may be difficult to use this regulatable secretory cargo in certain experiments that employ thermosensitive mutants.

An SLF concentration of 100 µM should be well above the threshold needed for complete dissolution of the aggregates (Barrero et al., 2016). This concentration of drug does not seem to perturb yeast cells.

To avoid precipitation of SLF, we recommend allowing the SLF stock solution to warm to room temperature and diluting it into room temperature medium prior to adding the drug to cells. SLF can also be added directly to cell cultures.

To detect the secreted cargo by immunoblotting, the cells must be grown in rich medium. This requirement likely reflects higher permeability of the cell wall in rich medium than in minimal medium (de Nobel et al., 1990).

The secreted cargo is hyperglycosylated during transit through the Golgi. Therefore, to detect a clean band by immunoblotting, N-linked glycans must be removed enzymatically prior to SDS-PAGE. Endoglycosidase H works well for this purpose.

For unknown reasons,we have been unable to detect the cargo construct with commercially available anti-DsRed antibodies from TaKaRa or Clontech. However, an anti-FKBP antibody works well.

Anticipated Results

In an unperturbed wild-type yeast strain, addition of SLF will initiate rapid trafficking of the cargo. At room temperature, nearly all of the early Golgi compartments will contain visible cargo within 2 to 3 min, and nearly all of the late Golgi compartments will contain visible cargo within 4 to 5 min. Secreted cargo will begin to appear in the medium within 10 min. However, this cargo wave will not be completely synchronized, and cargo will continue to be visible inside the cell for up to 30 min. During this time, tracking of individual cisternae will reveal that the cargo remains in a given cisterna as resident Golgi proteins come and go.

In a yeast strain with a compromised membrane trafficking machinery, or in an unperturbed wild-type strain expressing a modified version of the cargo, the results may differ. Such experiments can be used to test mechanistic hypotheses about how a soluble cargo protein traverses the yeast secretory pathway.

Time Considerations

Basic Protocol 1: Generation of a cargo-expressing strain with the appropriate genetic background typically takes about 4 to 6 weeks.

Basic Protocol 2: After addition of SLF at room temperature, complete dissolution of the cargo aggregates in a cell takes about 1 to 2 min, depending on the size of the aggregates. The solubilized cargo fully populates early Golgi compartments within 2 to 3 min and late Golgi compartments within 4 to 5 min. Strong Golgi labeling persists for about 20 min, and secretion of the original pool of cargo is nearly complete in 30 min.

Basic Protocol 3: When cells are grown in rich medium at room temperature and then treated with SLF, secreted cargo in the medium can be detected by immunoblotting within 10 minutes.

Movie Associated with Chapter 2

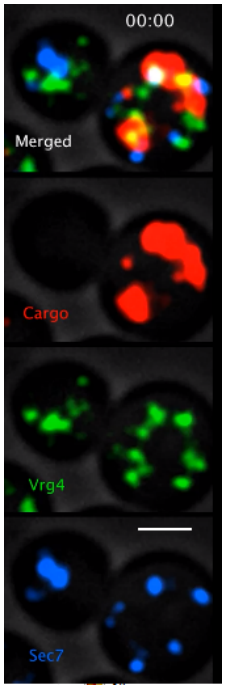

Movie 2.1: **Visualizing the solubilization and Golgi traffic of the secretory cargo.** A strain expressing pOst1-APVNTT-DsRed-Express2-FKBPRD(C22V), GFP-Vrg4 (early Golgi marker), and Sec7-HaloTag (late Golgi marker) was grown to mid-log phase in NSD, labeled with the HaloTag JF$_{646}$ dye, washed, mounted in a flow chamber, and imaged by 4D confocal microscopy while SLF was flowed over the cells. Full z-stacks were taken every 3 sec for 10 min, and the average was projected to create the movie frames. The top panel shows the complete movie, while the bottom three panels show the individual fluorescence channels. The cargo aggregates dissolve, and then the solubilized cargo appears in early and then in late Golgi compartments. Scale bar, 2 μm. See also Figure 2.2.

CHAPTER 3

MATURATION DRIVEN TRANSPORT AND AP-1 DEPENDENT RECYCLING OF A SECRETORY CARGO IN THE GOLGI

Abstract

Golgi cisternal maturation has been visualized by fluorescence imaging of individual cisternae in the yeast *Saccharomyces cerevisiae*, but those experiments did not track passage of a secretory cargo. The expectation is that a secretory cargo will be continuously present within maturing cisternae as resident Golgi proteins arrive and depart. We tested this idea using a regulatable fluorescent secretory cargo that forms ER-localized aggregates, which dissociate into tetramers upon addition of a ligand. The solubilized tetramers rapidly exit the ER and then transit through early and late Golgi compartments before being secreted. Early Golgi cisternae form near the ER and become loaded with the secretory cargo. As predicted, cisternae contain the secretory cargo throughout the maturation process. An unexpected finding is that a burst of intra-Golgi recycling delivers additional secretory cargo molecules to cisternae during the early-to-late Golgi transition. This recycling requires the AP-1 adaptor, suggesting that AP-1 can recycle secretory cargo proteins as well as resident Golgi proteins.

Introduction

Many features of the eukaryotic secretory pathway are well characterized. Soluble secretory cargo proteins are directed for translocation into the ER by an N-terminal signal sequence (Ng et al., 1996). After folding and assembly, newly synthesized secretory cargo proteins

This chapter is a version of a manuscript published in the Journal of Cell Biology 2019 May 6;218(5):1582-1601, with the same title and the following author list: J. C. Casler, E. Papanikou, J. J. Barrero, and B. S. Glick. I helped design the experiments, performed all of the experimental analyses, and produced initial drafts of the text and figures. E. Papanikou carried out extensive exploratory studies that laid the foundation for this project. J.J. Barrero refined the tools for generating the regulatable fluorescent secretory cargo. B.S. Glick supervised the project, helped design the experiments, performed the computer simulations, and prepared the final text and figures.

are packaged into COPII-coated vesicles at ER exit sites (ERES; Lord et al., 2013). Some secretory cargo proteins exit the ER by a nonselective bulk flow pathway, but many of them are concentrated in COPII vesicles with the aid of cargo receptors (Dancourt and Barlowe, 2010). After leaving the ER, secretory cargo proteins arrive in early (*cis*) cisternae of the Golgi apparatus, and then transit through the Golgi to late (*trans*) cisternae. In most cell types, the Golgi is organized as a stack of cisternae, and the secretory cargo proteins move in vectorial fashion across the stack (Dunphy and Rothman, 1985). Finally, secretory cargo proteins exit the Golgi in transport carriers for delivery to either the plasma membrane or the endosomal/lysosomal/vacuolar system (De Matteis and Luini, 2008).

The passage of secretory cargo proteins through the Golgi can be described by the cisternal maturation model (Glick and Nakano, 2009). According to this view, COPII vesicles fuse with one another to form early Golgi cisternae, which mature into late Golgi cisternae, which ultimately fragment into secretory vesicles and other types of transport carriers. During maturation of a cisterna, the secretory cargo proteins are continuously present but the population of resident Golgi proteins changes progressively. This change is thought to be driven by several mechanisms (Papanikou and Glick, 2014; Papanikou et al., 2015; Day et al., 2018). First, COPI-coated vesicles that bud from early cisternae transport resident Golgi proteins to other early cisternae or to the ER. Second, late Golgi proteins recycle to younger cisternae in clathrin-coated vesicles generated with the aid of the AP-1 adaptor. This AP-1–dependent recycling promotes the early-to-late Golgi transition. Third, peripheral membrane proteins dissociate from older cisternae and bind to younger cisternae. This model can explain how the Golgi transports diverse secretory cargoes, including large secretory cargoes that presumably must remain within the cisternae (Bonfanti et al., 1998).

Alternatively, other pathways have been postulated to operate in conjunction with or instead of cisternal maturation (Emr et al., 2009; Pfeffer, 2010; Glick and Luini, 2011). In mammalian cells, transient tubular connections between heterologous cisternae permit the rapid diffusion of some proteins across the Golgi stack (Beznoussenko et al., 2014).

Additional suggested vehicles for the transport of secretory cargo proteins through the Golgi include anterograde COPI vesicles or large cisterna-derived membrane carriers (Orci et al., 2000; Pfeffer, 2010; Lavieu et al., 2013; Dunlop et al., 2017). Because of these different possibilities, further work is needed to characterize how cisternae mature, and to determine whether cisternal maturation can plausibly be considered the major pathway for transporting secretory cargo proteins through the Golgi.

The budding yeast *Saccharomyces cerevisiae* is a uniquely powerful model system for studying cisternal maturation. Unlike most other eukaryotes, *S. cerevisiae* has a nonstacked Golgi, meaning that individual Golgi cisternae are optically resolvable by fluorescence microscopy (Preuss et al., 1992; Wooding and Pelham, 1998; Beznoussenko et al., 2016). We and the Nakano group employed two-color 4D fluorescence microscopy to visualize cisternal maturation directly in living yeast cells (Losev et al., 2006; Matsuura-Tokita et al., 2006). For those experiments, resident Golgi proteins were fluorescently tagged, and individual cisternae were tracked over time to confirm that each cisterna exchanges early Golgi markers for late Golgi markers. Subsequent studies showed that normal Golgi maturation requires the actions of Rab GTPases and COPI, and that COPI and clathrin are recruited sequentially to maturing cisternae (Rivera-Molina and Novick, 2009; Daboussi et al., 2012; Papanikou et al., 2015; Ishii et al., 2016; Kim et al., 2016).

In contrast, for yeast secretory cargo proteins, tools for visualizing transport through the Golgi have been limited. Such tools have been used with mammalian cells to document that secretory cargo proteins arrive at the cis face of the Golgi and move through the stack to the trans face (Mironov et al., 2001; Trucco et al., 2004; Tie et al., 2016). The prediction is that in yeast, secretory cargo proteins should be continuously present within the Golgi cisternae as they mature. Such a phenomenon should be observable by three-color fluorescence microscopy in which an early Golgi marker, a late Golgi marker, and a secretory cargo are labeled in different colors. The secretory cargo should stay visible while the early Golgi marker departs and the late Golgi marker arrives (Figure 3.1).

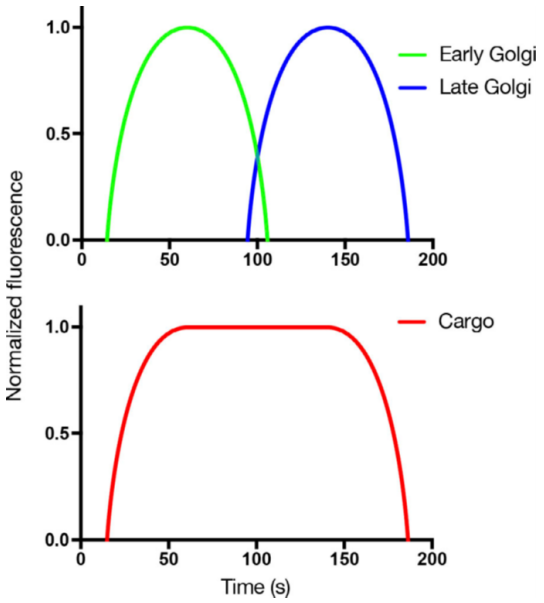

Figure 3.1: **Predicted cargo fluorescence signal in a maturing yeast Golgi cisterna.** Green and blue represent early and late resident Golgi proteins, respectively, and red represents the fluorescent secretory cargo. In the simplest envisioned scheme, the fluorescent cargo remains within a cisterna as it matures, so the cargo signal is constant before, during, and after the early-to-late transition.

To test this fundamental prediction of the cisternal maturation model, we engineered a regulatable fluorescent secretory cargo that can be accumulated in the ER and then released for transport through the secretory pathway. The approach builds on a previously described technique in which a GFP-tagged monomeric secretory cargo was fused to four copies of a dimerizing mutant of the FK506-binding protein FKBP, leading to the formation of fluorescent aggregates in the ER lumen (Rivera et al., 2000). Those aggregates could be dissolved by addition of an FKBP ligand, thereby allowing the monomeric protein to exit the ER. In our version of this technique, an improved dimerizing mutant of FKBP is fused to a tetrameric red fluorescent protein, thereby generating fluorescent aggregates that can be dissolved to yield soluble tetramers (Barrero et al., 2016). By targeting such a construct to the ER lumen and appending an ER export signal (Nam et al., 2014), we generated a secretory cargo that can be induced to exit the ER rapidly and move through the Golgi. Three-color 4D microscopy confirmed that this secretory cargo remains continuously visible

within maturing Golgi cisternae as predicted. Intriguingly, our data also indicate that the secretory cargo can recycle from older to younger cisternae during the early-to-late Golgi transition. The existence of such a recycling pathway could explain prior observations about the behavior of secretory cargo proteins in the Golgi.

Results

Designing a regulatable fluorescent secretory cargo for S. cerevisiae

The goal was to trap a fluorescent secretory cargo in the ER lumen and then release it for rapid transport through the secretory pathway. After exploring various approaches, including use of a thermosensitive COPII mutant to accumulate secretory cargo proteins in the ER (Castillon et al., 2009; Kurokawa et al., 2014), we chose to adapt a method that was previously developed for mammalian cells (Rivera et al., 2000). The highly soluble tetrameric red fluorescent protein DsRed-Express2 (Strack et al., 2008) was fused to a reversibly dimerizing variant of FKBP (Rollins et al., 2000; Barrero et al., 2016). An N-terminal signal sequence directs this fusion protein to the ER lumen, where it forms aggregates (Figure 3.2A). Addition of synthetic ligand of FKBP (SLF; Holt et al., 1993) disrupts FKBP dimerization and dissolves the aggregates, releasing soluble tetramers that can exit the ER (Figure 3.2A).

Although this approach is conceptually simple, implementation required careful engineering of the cargo and the yeast strain (Casler and Glick, 2018). A basic requirement was that the cargo aggregates must dissolve quickly and remain dissolved. We previously used rational mutagenesis to generate an improved reversibly dimerizing variant, here designated FKBPRD(C22V), which generates aggregates that dissolve within 1–2 min at low SLF concentrations (Barrero et al., 2016). FKBPRD(C22V) has a cysteine at residue 22, prompting the concern that disulfide bonds could form in the ER lumen. Based on an alignment of FKBP homologues (Galat, 2008), we introduced a C22V mutation and confirmed that this mutation does not significantly alter the formation or dissolution of aggregates (Figure 3.3A). The resulting variant was designated FKBPRD(C22V). Another challenge was that

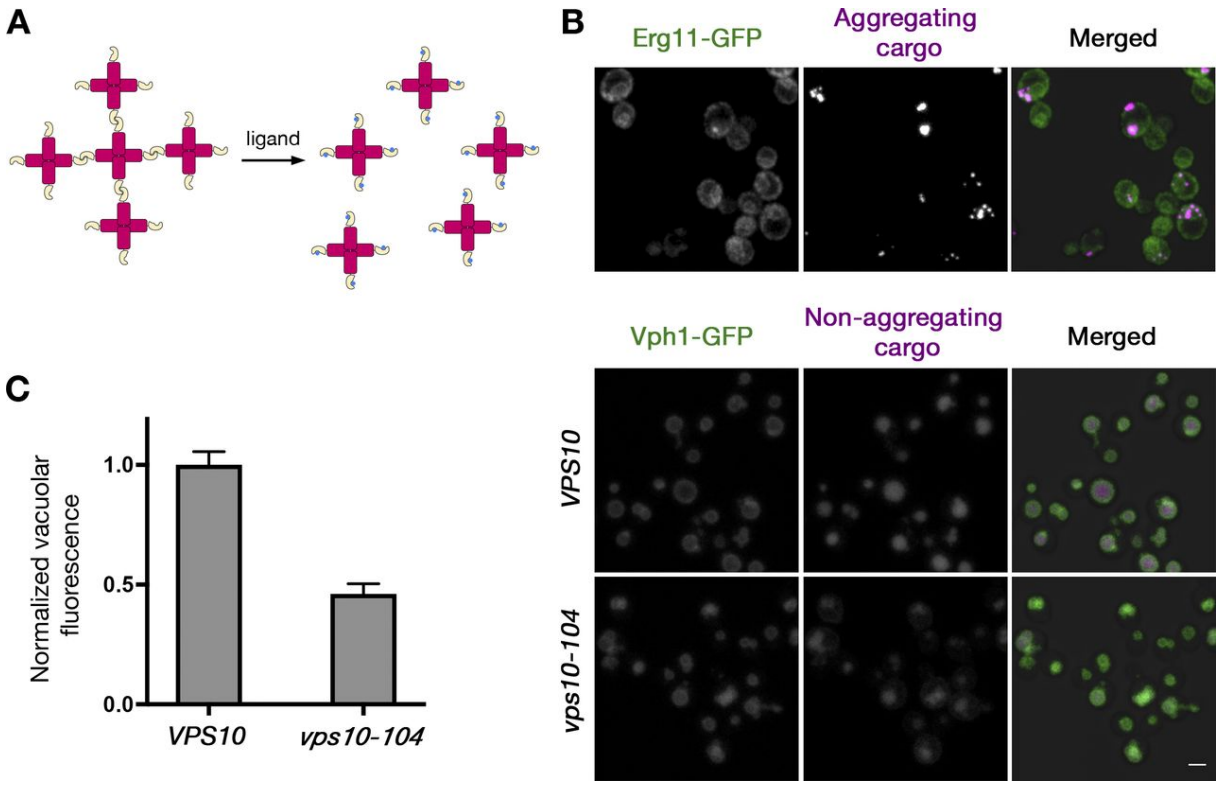

Figure 3.2: **A reversibly aggregating fluorescent secretory cargo. (A)** Strategy for generating and dissolving fluorescent aggregates. DsRed-Express2 tetramers (red) fused to a dimerizing variant of FKBP (gold) cross-link to form aggregates. Addition of the FKBP ligand SLF (blue) blocks dimerization, thereby dissolving the aggregates into soluble tetramers. **(B)** Dependence of aggregation on the dimerization of FKBP. A cargo construct containing the dimerizing FKBPRD(C22V) variant aggregated in the ER, which was marked by Erg11-GFP. By contrast, a cargo construct containing the monomeric FKBP(C22V) variant did not form ER aggregates, and the cargo was sorted to the vacuole, which was marked by Vph1-GFP. Introduction of the *vps10-104* mutation reduced the amount of the nonaggregating cargo in the vacuole. All images are projected confocal Z-stacks. Scale bar, 2 µm. **(C)** Quantification of the vacuolar fluorescence in B. For each cell, the green signal in the Vph1-GFP channel was used to create a mask for measuring the vacuolar fluorescence in the cargo channel. Data are average values from at least 110 cells for each strain. Error bars represent SEM.

yeast cells expel SLF by the action of pleiotropic drug transporters (Rogers et al., 2001). Removal of the transcription factors Pdr1 and Pdr3, which control the expression of many pleiotropic drug transporters (Schüller et al., 2007; Coorey et al., 2015), allows for sustained dissolution of aggregates in the presence of SLF (Barrero et al., 2016), so the strains used in this study contained the *pdr1*Δ *pdr3*Δ pair of gene deletions.

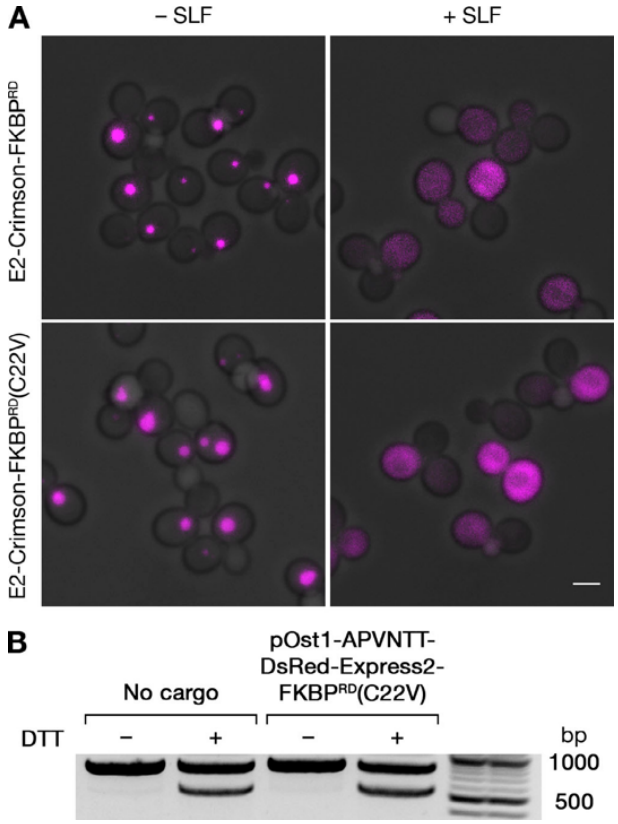

Figure 3.3: **Aggregated tetramers in the yeast cytosol and ER. (A)** Reversible aggregation of a cytosolic construct containing a dimerizing FKBP variant with the C22V mutation. Cells expressing cytosolic aggregates of either E2-Crimson-FKBPRD(C22V) (Barrero et al., 2016) or E2-Crimson-FKBPRD(C22V) were grown to midlog phase and imaged by confocal microscopy before and 3 min after addition of SLF. Shown are representative projected Z-stacks. Scale bar, 2 µm. **(B)** Lack of UPR activation by aggregated cargo in the ER. A parental *pdr1*Δ *pdr3*Δ *vps10-104* strain and a derivative strain that expressed pOst1-APVNTT-DsRed-Express2-FKBPRD(C22V) to generate ER-localized aggregates were grown overnight with shaking in minimal medium at 23°C to an OD_{600} of 0.6–0.8. Each culture was then split, and one half was mock treated while the other half was treated with 8 mM DTT for 30 min to activate the UPR. RNA was isolated from the cells, and RT-PCR was performed to measure the splicing of HAC1 mRNA. PCR products were separated by electrophoresis in a 1% agarose gel together with the 2-Log DNA Ladder (New England Biolabs; N0469S). The darker bands in the DNA ladder are at 500 and 1,000 bp. Unspliced HAC1 mRNA is 819 bp, and the spliced form is 567 bp

To ensure delivery of the DsRed-Express2-FKBPRD(C22V) construct to the ER lumen, we appended the Ost1 signal sequence, which efficiently directs cotranslational translocation (Willer et al., 2008; Fitzgerald and Glick, 2014; Barrero et al., 2018). The resulting construct was designated pOst1-DsRed-Express2-FKBPRD(C22V). After translocation, the

Ost1 signal sequence should be removed by signal peptidase (Paetzel et al., 2002) to generate aggregation-prone DsRed-Express2-FKBPRD(C22V) tetramers in the ER lumen.

Expression of the pOst1-DsRed-Express2-FKBPRD(C22V) construct yielded red fluorescent aggregates, which were in the ER as judged by labeling the ER membrane with Erg11-GFP (Shakoury-Elizeh et al., 2010; Figure 3.2B). As a control, we examined pOst1-E2-Crimson-FKBP(C22V), which contained a far-red derivative of DsRed-Express2 (Strack et al., 2009b) fused to the monomeric FKBP(C22V) variant. No aggregates were seen with this construct. However, strong fluorescence was visible in the vacuolar lumen as judged by labeling the vacuolar membrane with Vph1-GFP (Toshima et al., 2014; Figure 3.2B). We infer that after the E2-Crimson-FKBP(C22V) tetramers exited the ER, many of them were diverted to the vacuole. Sorting of fluorescent protein constructs to the *S. cerevisiae* vacuole can be inhibited by using the *vps10-104* allele (Jørgensen et al., 1999; Fitzgerald and Glick, 2014). Indeed, in a *vps10-104*, the vacuolar fluorescence seen with the pOst1-E2-Crimson-FKBP(C22V) construct was reduced (Figure 3.2BC). The combined results suggested that expression of the pOst1-DsRed-Express2-FKBPRD(C22V) construct in a *pdr1*Δ *pdr3*Δ *vps10-104* strain would enable us to achieve regulated secretion of a fluorescent secretory cargo.

Accelerating secretion with an ER export signal

Addition of SLF was expected to dissolve the ER-localized DsRed-Express2-FKBPRD(C22V) aggregates, allowing soluble tetramers to diffuse throughout the ER. We added SLF using a custom flow chamber while performing 4D confocal imaging of the yeast cells (Barrero et al., 2016). The fluorescent DsRed-Express2-FKBPRD(C22V) aggregates dissolved within 1–2 min, yielding soluble red fluorescent molecules that filled the ER as judged by colabeling with Erg11-GFP (Movie 3.1 and Figure 3.4). No ER-localized aggregates reappeared in the presence of SLF, indicating that we had efficiently reversed the dimerization of FKBPRD(C22V).

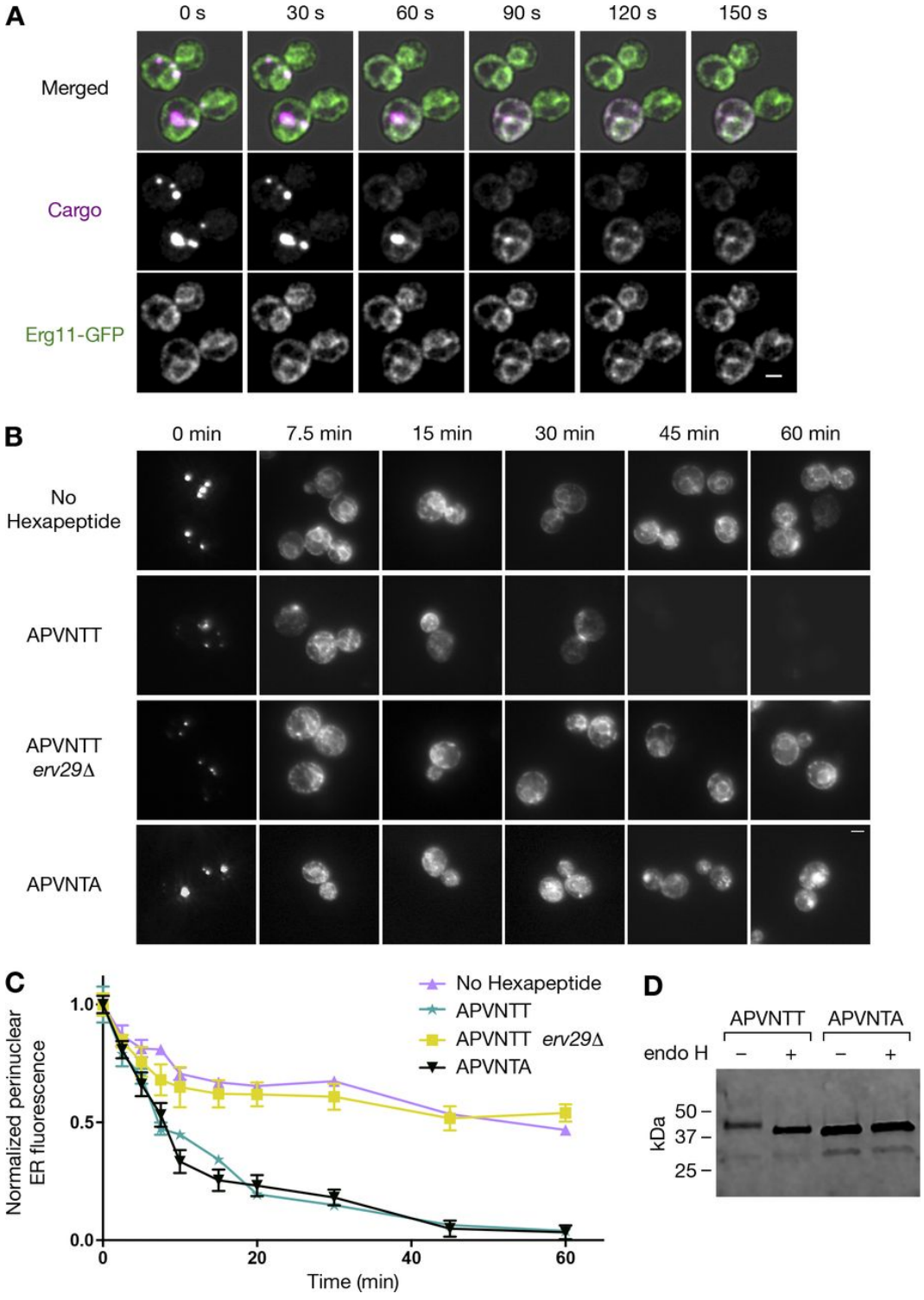

Figure 3.4: **Comparison of bulk flow-mediated versus signal-mediated ER export of fluorescent secretory cargo proteins.** *(continued on next page)*

Figure 3.4: **(A)** Projected Z-stacks from Movie 3.1 showing the dissolution of cargo aggregates. Cells containing ER-localized aggregates of the DsRed-Express2-FKBPRD(C22V) cargo were mounted in a flow chamber and imaged while SLF-containing medium entered the chamber. The solubilized cargo colocalized with the ER marker Erg11-GFP. Scale bar, 2 µm. **(B)** Loss of ER-associated fluorescence for various cargo constructs after SLF addition. Strains expressed cargo variants with no export signal, the APVNTT hexapeptide, the APVNTA hexapeptide, or the APVNTT hexapeptide in an *erv29*Δ background. Growing cells were fixed at the indicated time points after SLF addition, then imaged by wide-field fluorescence microscopy. Scale bar, 2 µm. **(C)** Quantification of the loss of ER-associated fluorescence in B. The perinuclear cargo signal was measured as described in Materials and methods. Plotted is the average fluorescence signal per unit area. Data were from 27–54 cells per time point, and error bars represent SEM. **(D)** Immunoblot to assess N-linked glycosylation of the cargo. Growing cells containing ER-localized aggregates of either the APVNTT-DsRed-Express2-FKBPRD(C22V) cargo or the APVNTA-DsRed-Express2-FKBPRD(C22V) cargo were lysed with glass beads and centrifuged, and the proteins released were precipitated. Resuspended samples were treated or mock treated with endo H, followed by SDS-PAGE and immunoblotting for FKBP. Numbers represent molecular weights of reference markers.

Exit of the solubilized DsRed-Express2-FKBPRD(C22V) tetramers from the ER was slow, presumably because this secretory cargo lacks an ER export signal and therefore leaves the ER by bulk flow (Barlowe and Helenius, 2016). In attempts to accelerate ER export, we inserted different versions of the pro region of the yeast α-factor mating pheromone after the Ost1 signal sequence (Barrero et al., 2018) to provide a signal for binding to the ER export receptor Erv29 (Otte and Barlowe, 2004; Fitzgerald and Glick, 2014). Unfortunately, those constructs either aggregated irreversibly or failed to become trapped in the ER (data not shown). As a simpler alternative, we inserted only the first six residues of the α-factor pro region after the Ost1 signal sequence, thereby adding an N-terminal hexapeptide to each subunit of the DsRed-Express2-FKBPRD(C22V) tetramer. This hexapeptide has the sequence APVNTT. The NTT tripeptide is a signal for asparagine-linked glycosylation (Kornfeld and Kornfeld, 1985), which could potentially enhance ER export through interaction with lectin-like receptors in the ER (Sato and Nakano, 2002; Appenzeller-Herzog et al., 2005). Moreover, the N-terminal APV tripeptide is an evolutionarily conserved ER export signal (Nam et al., 2014; Yin et al., 2018). We therefore predicted that the APVNTT hexapeptide would accelerate ER export.

This prediction was tested by comparing the rates at which various solubilized tetramers exited the ER after SLF addition. The original pOst1-DsRed-Express2-FKBPRD(C22V) construct was compared with the pOst1-APVNTT-DsRed-Express2-FKBPRD(C22V) construct, which was presumably cleaved by signal peptidase to generate tetramers with the N-terminal hexapeptide. Two controls were also performed. First, the APVNTT sequence was changed to APVNTA to eliminate the signal for asparagine-linked glycosylation (Kornfeld and Kornfeld, 1985). Second, the pOst1-APVNTT-DsRed-Express2-FKBPRD(C22V) construct was expressed in an *erv29*Δ strain to prevent recognition of the ER export signal. The results are shown in Figure 3.4 (B and C). In the absence of the hexapeptide, the DsRed-Express2-FKBPRD(C22V) tetramers exited the ER at the slow bulk flow rate, as indicated by a persistent fluorescence signal in the nuclear envelope portion of the ER. That persistent signal likely reflected a steady state in which slow ER exit was balanced by the accumulation of newly synthesized fluorescent molecules. In the presence of the hexapeptide, ER export was much faster, and the fluorescence signal in or near the nuclear envelope declined almost to zero with a half-time of 7.5 min. To confirm that the NTT signal resulted in asparagine-linked glycosylation, we showed that ER-localized molecules with the APVNTT hexapeptide had a slightly higher molecular weight than ER-localized molecules with the APVNTA hexapeptide, and that this difference was abolished by treatment with endoglycosidase H (endo H; Maley et al., 1989; Figure 3.4 D). Nonglycosylated tetramers with the APVNTA hexapeptide exited the ER at the same rapid rate as glycosylated tetramers with the APVNTT hexapeptide, indicating that glycosylation was not primarily responsible for the accelerated ER export. By contrast, when the effect of the APV signal was eliminated by the *erv29*Δ mutation, ER export occurred at the slow bulk flow rate. Thus, the APVNTT hexapeptide allows for rapid Erv29-dependent ER export.

A potential drawback of our approach is that aggregated APVNTT-DsRed-Express2-FKBPRD(C22V) tetramers in the ER lumen could trigger the unfolded protein response (UPR), thereby perturbing the secretory pathway (Wu et al., 2014). To exclude this possi-

bility, we examined HAC1 mRNA, which is spliced upon activation of the UPR (Cox and Walter, 1996; Di Santo et al., 2016). As a control, DTT activated the UPR and generated a spliced form of HAC1 mRNA (Figure 3.3 B). Expression of the pOst1-APVNTT-DsRed-Express2-FKBPRD(C22V) construct did not trigger HAC1 splicing (Figure 3.3 B). This result indicates that the presence of aggregated APVNTT-DsRed-Express2-FKBPRD(C22V) tetramers is compatible with normal ER function.

After an APVNTT-DsRed-Express2-FKBPRD(C22V) tetramer assembles in the ER, there will be a kinetic race between aggregation and Erv29-dependent ER export. This interpretation is supported by Figure 3.5. With the pOst1-APVNTT-DsRed-Express2-FKBPRD(C22V) construct, cells grown at 23°C or 30°C had abundant aggregates, but cells grown at 37°C had very few aggregates. If the APVNTT hexapeptide was absent, or if the strain carried an *erv29*Δ mutation, aggregates were seen even at 37°C (Figure 3.5, A and B). The implication is that at 37°C, the relative kinetics of aggregation and Erv29-dependent ER export favored escape of APVNTT-containing tetramers from the ER. Even at 23°C or 30°C, many of the APVNTT-containing tetramers probably escaped the ER in an Erv29-dependent manner, because the total fluorescence from aggregates could be increased by removing the APVNTT hexapeptide or by deleting Erv29 (Figure 3.5 C). Under the conditions of our experiments, which are performed at 23°C, there is evidently a balance such that aggregation of the APVNTT-DsRed-Express2-FKBPRD(C22V) tetramers is efficient enough to trap a fraction of the fluorescent secretory cargo molecules in the ER. Addition of SLF makes this population of molecules available for rapid ER export.

Compared with glycosylated tetramers with the APVNTT hexapeptide, nonglycosylated tetramers with the APVNTA hexapeptide yielded much stronger vacuolar labeling after prolonged incubation with SLF (Figure 3.4 B). The strain carried the *vps10-104* mutation, so this effect of glycosylation involves a separate, unknown mechanism that may or may not be relevant for natural secretory cargo proteins. For our purposes, the empirical finding is

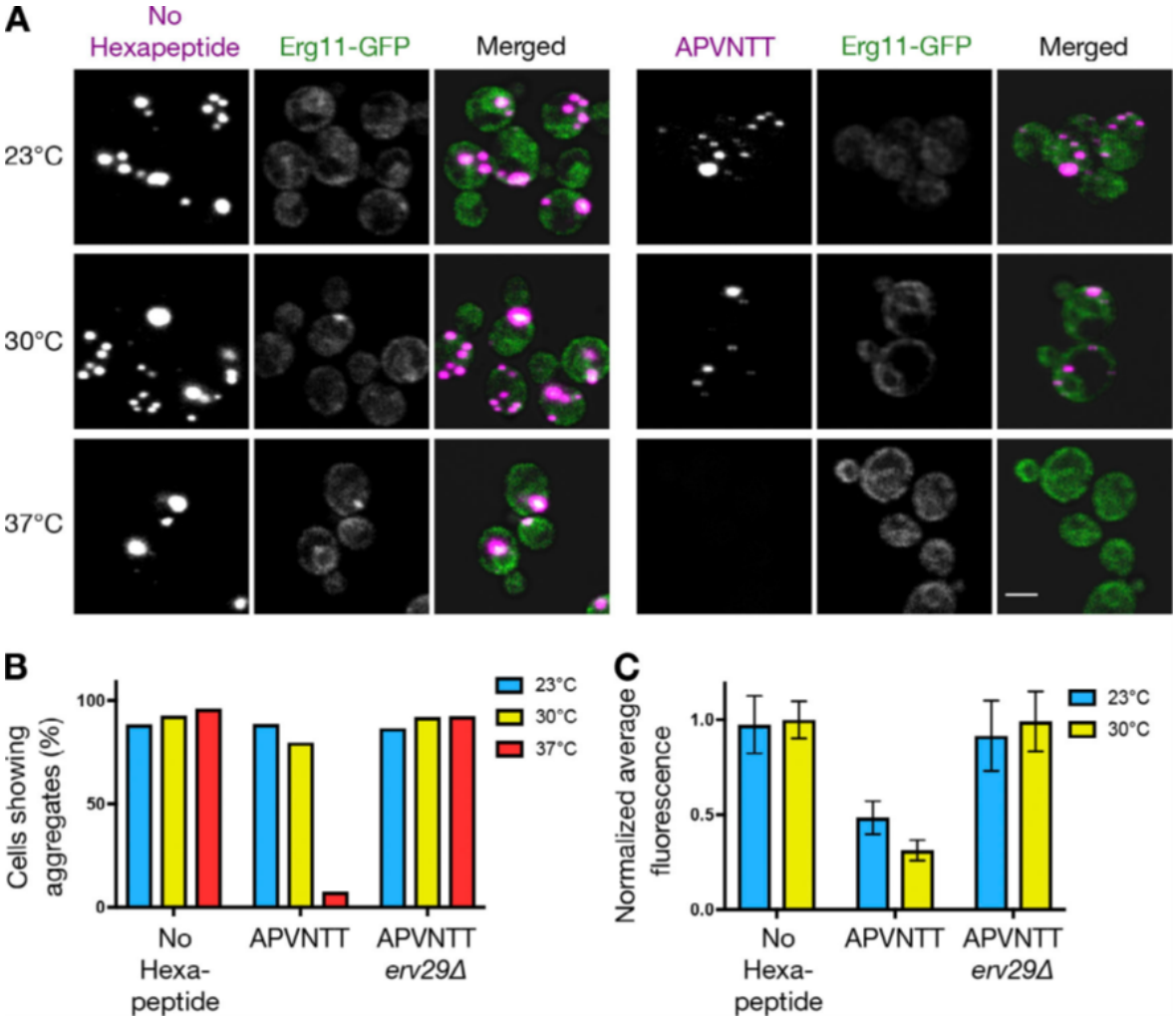

Figure 3.5: **Effect of temperature on the ER aggregation of cargo variants. (A)** Projected confocal Z-stacks of yeast cells expressing fluorescent cargo constructs after growth at the indicated temperatures. "APVNTT" indicates that an additional hexapeptide was present at the N terminus of the mature DsRedExpress2-FKBPRD(C22V) construct after cleavage of the signal sequence. The ER was labeled with Erg11-GFP. **(B)** Quantification of the percentages of cells with visible ER aggregates at different temperatures. For the samples in A, confocal projections of cells were manually scored for the presence or absence of visible aggregates. Measurements were taken from at least 40 cells per condition. **(C)** Average fluorescence of aggregates. For the samples in A, aggregates visible in confocal projections were selected using the Analyze Particles tool in ImageJ, and the fluorescence in a given cell was measured. Measurements were taken from at least 50 cells per condition. Error bars represent SEM.

that glycosylation helps to prevent the fluorescent secretory cargo from being diverted to the vacuole.

Tracking the fluorescent secretory cargo after ER export

At this point, we were ready to visualize the SLF-solubilized APVNTT-DsRed-Express2-FKBPRD(C22V) tetramers as they moved through the secretory pathway. The reference marker was the early Golgi protein GFP-Vrg4, the late Golgi protein Sec7-GFP, or the prevacuolar endosome (PVE) protein Vps8-GFP (Losev et al., 2006; Arlt et al., 2015; Day et al., 2018). This analysis was performed in strains that carried either the wild-type *VPS10* gene or the *vps10-104* allele. Cells were treated with SLF for 5 min, then fixed and imaged by two-color confocal microscopy. In the *VPS10* cells, the majority of the secretory cargo that was present in punctate structures colocalized with either the PVE marker or the early Golgi marker (Figure 3.6 A and B). Only occasional colocalization was seen with the late Golgi marker. By contrast, in the *vps10-104* cells, colocalization with the PVE marker was minimal, and strong colocalization was seen with both the early and late Golgi markers (Figure 3.6 A and B). These results support the view that the *vps10-104* mutation inhibits sorting of the secretory cargo to the PVE/vacuole system, thereby allowing the secretory cargo to traverse the entire Golgi for delivery to the cell surface.

If the secretory cargo were being secreted as expected in a *vps10-104* strain, the cargo molecules should have appeared in either the periplasm or the medium or both, depending on how efficiently the cargo molecules escaped through the cell wall. In our previous work, an artificial yeast secretory cargo was more efficiently recovered from rich medium than from minimal medium (Fitzgerald and Glick, 2014), consistent with evidence that the *S. cerevisiae* cell wall is more permeable after growth in rich medium (De Nobel et al., 1990). The results described below support the same interpretation for the APVNTT-DsRed-Express2-FKBPRD(C22V) tetramers.

Secretion into the medium was measured by immunoblotting. When SLF was added to cells growing in minimal medium, no secretory cargo was detected in the medium by immunoblotting (data not shown). We therefore performed this experiment using rich medium. When SLF was added to cells growing in rich medium, the ER-localized aggregates dissolved,

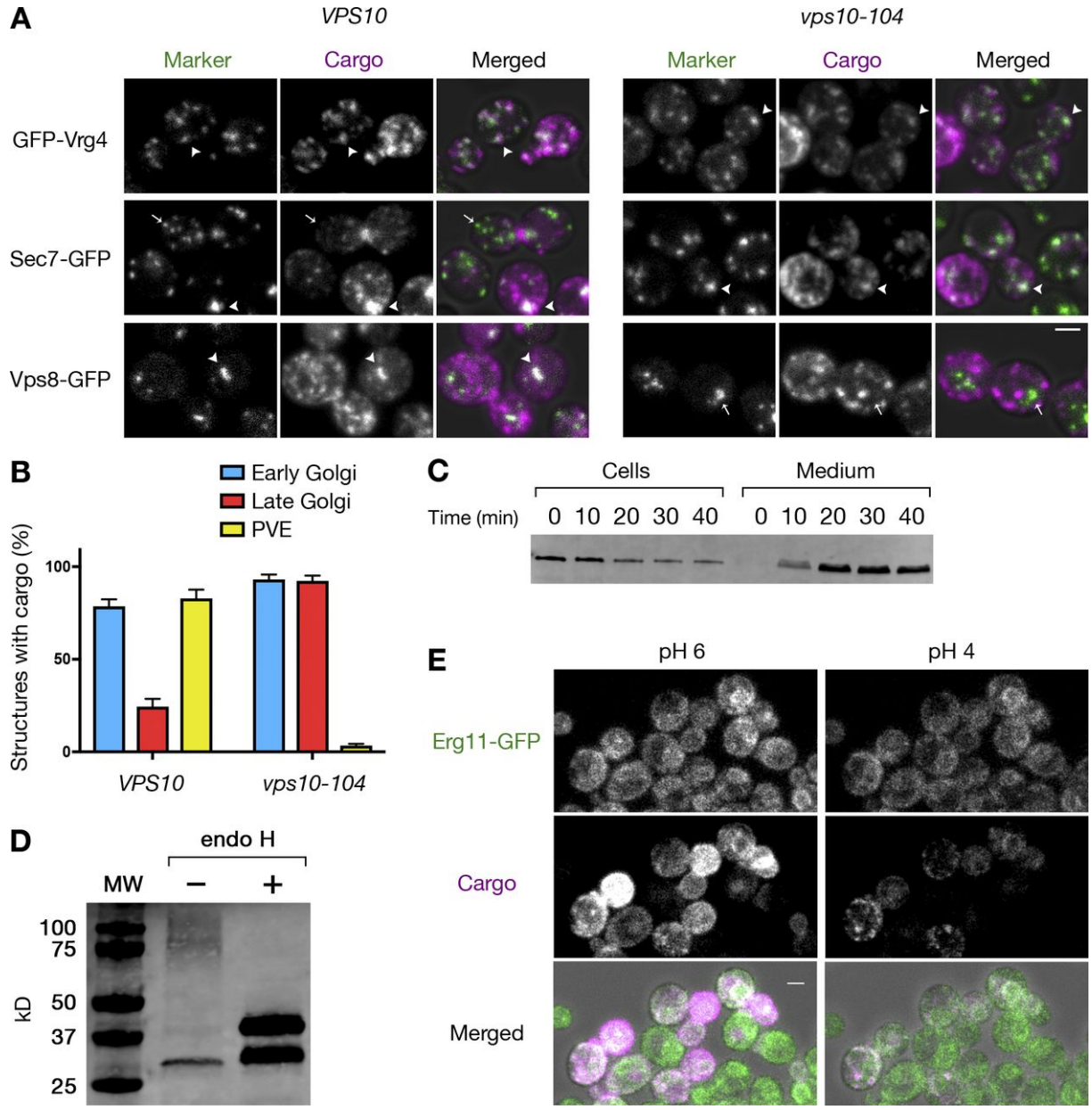

Figure 3.6: **Localization of the fluorescent secretory cargo after ER export. (A)** Colocalization of the cargo with Golgi and PVE markers soon after ER export. Cells expressing the APVNTT-DsRed-Express2-FKBPRD(C22V) cargo and either GFP-Vrg4 (early Golgi), Sec7-GFP (late Golgi), or Vps8-GFP (PVE) in a *pdr1*Δ *pdr3*Δ or *pdr1*Δ *pdr3*Δ *vps10-104* background were grown to mid-log phase, treated with SLF for 5 min, fixed, and imaged by confocal microscopy. Shown are representative projected Z-stacks. Arrowheads indicate examples of structures containing detectable cargo, and arrows indicate examples of structures lacking detectable cargo. Scale bar, 2 µm. **(B)** Quantification from A of the percentages of labeled structures containing detectable cargo. Data were obtained from at least 40 cells per condition. Error bars indicate SEM. *(continued on next page)*

Figure 3.6: **(C)** Immunoblot of cell-associated and secreted cargo after SLF addition in rich medium. Yeast were grown to mid-log phase in YPD, washed twice with fresh YPD, and treated with SLF. At the indicated time points, cell-associated and secreted fractions were separated by centrifugation, and then the sedimented cells were lysed and proteins from both fractions were precipitated. Samples were subjected to endo H treatment followed by SDS-PAGE and immunoblotting for FKBP. The visualized band corresponds to the upper band in the "+" lane of D. **(D)** Immunoblot demonstrating hyperglycosylation of the secreted cargo. Proteins were precipitated from rich medium 60 min after SLF addition. Samples were then treated or mock treated with endo H, followed by SDS-PAGE and immunoblotting for FKBP. A high-molecular-weight smear was seen only in the absence of endo H treatment. In the endo H–treated sample, the upper band is the full-length fusion protein, and the lower band is a minor species that was exaggerated by overloading the gel. The lower band might have been generated by Kex2 protease cleavage (Rockwell et al., 2002) of FKBP after the KR dipeptide at positions 17–18. MW, molecular weight marker, with the sizes of the reference proteins shown at the left. **(E)** Visualization of secreted cargo trapped in the periplasm in minimal medium. Cells expressing the aggregated cargo and the ER marker Erg11-GFP were grown to mid-log phase in NSD buffered at pH 6, then treated with SLF for 30 min and mounted in a flow chamber. Unbuffered NSD (pH 4) was flowed over the cells while imaging with a confocal microscope. Shown are projected Z-stacks from Movie 3.2. Scale bar, 2 µm.

and the fluorescent secretory cargo appeared in the Golgi with kinetics similar to those observed in minimal medium (data not shown). The secretory cargo signal was visible in the rich medium by 10 min after SLF addition, and was more prominent by 20 min (Figure 3.6 C). This time course was somewhat slower than expected, perhaps due to a delay in escape from the periplasm. The cargo molecules that remained in the cell pellet at later time points (Figure 3.6 C) probably included tetramers that were trapped in the periplasm plus newly synthesized tetramers that were still in the secretory pathway. These results verify that the secretory cargo is indeed secreted, although quantitative analysis of the efficiency and kinetics of secretion would require removal of the cell wall (Gaynor and Emr, 1997).

The immunoblotting protocol used endo H treatment to eliminate smearing of the protein band due to variable glycosylation. When endo H treatment was omitted, the secreted cargo molecules were not seen as a tight band, but could be seen as a high-molecular-weight smear if the gel lane was overloaded (Figure 3.6 D). The secretory cargo was evidently hyperglycosylated. Thus, the artificial secretory cargo behaves like glycoproteins that are naturally secreted by yeast cells (Trimble et al., 1983).

In minimal medium, most of the secreted cargo molecules presumably remained trapped in the periplasm. Because DsRed-Express2 fluorescence has a pKa of 4.5 (Strack et al., 2009a), the signal can be quenched by acidification. When cells were grown in minimal medium buffered at pH 6, SLF addition resulted in the frequent appearance of red fluorescence around the rim of a bud or at the bud neck (Figure 3.6 E). This signal was dramatically reduced by flowing in medium at pH 4.0 to quench DsRed-Express2 fluorescence (Movie 3.2 and Figure 3.6 E). We conclude that the fluorescent secretory cargo undergoes exocytosis at sites of polarized growth. Once again, this behavior is typical for secreted proteins in yeast (Field and Schekman, 1980; Finger and Novick, 1998).

The combined data indicate that APVNTT-DsRed-Express2-FKBPRD(C22V) acts as a regulatable secretory cargo in *vps10-104* cells. For the remainder of this study, the *vps10-104* allele was used, and the minimal medium was at pH 4.0 to suppress fluorescence from secreted cargo molecules in the periplasm.

Visualizing transport of the secretory cargo to the Golgi

According to the cisternal maturation model, Golgi cisternae are generated by the homotypic fusion of COPII vesicles that bud from ERES to carry secretory cargo proteins out of the ER (Glick and Nakano, 2009). This model makes two predictions that are pertinent for our analysis of *S. cerevisiae*. First, early Golgi cisternae should form near the ER. Second, the fluorescent secretory cargo should appear in newly formed early Golgi cisternae.

Do yeast Golgi cisternae form near the ER? Answering this question is tricky because chance alone gives a high probability that a cytoplasmic structure will be close to the nuclear envelope, the cortical ER, or the ER membranes that connect these two domains. To circumvent this problem, we added nocodazole for 2 h to generate cells that had large daughters lacking nuclei (Jacobs et al., 1988). The rationale was that the ER in those daughters was exclusively cortical, and the distance of a Golgi cisterna from the cortical ER was easy to measure. This approach was inspired by reports that nocodazole treatment does not perturb

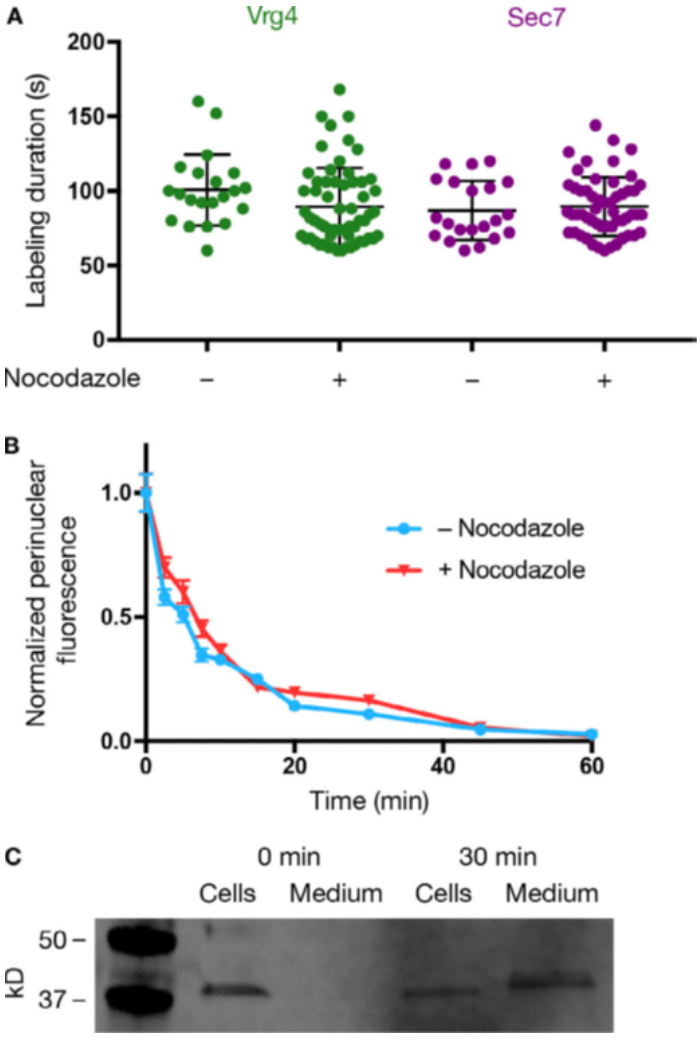

Figure 3.7: **Insensitivity of cisternal maturation rates and fluorescent secretory cargo traffic to nocodazole treatment. (A)** Scatter plot showing the durations of early and late Golgi maturation stages in untreated and nocodazole-treated cells. Cells expressing either GFP-Vrg4 (early Golgi) or Sec7-GFP (late Golgi) were grown to mid-log phase, either mock treated or treated with nocodazole for 2 h, and imaged by 4D confocal microscopy. For a given cisterna, the duration of an early or late Golgi stage was determined by measuring the time between the first and last movie frames in which the cisterna visibly displayed the relevant Golgi marker. Each scatter plot shows the mean duration of a Golgi stage and the standard deviation. **(B)** Comparison of ER export rates for the fluorescent secretory cargo in the presence or absence of nocodazole. The experiment was performed as in Figure 3.4 (B and C), except that cells expressing the APVNTT-DsRed-Express2-FKBPRD(C22V) cargo were either mock treated or treated with nocodazole for 2 h before SLF addition and imaging. **(C)** Immunoblot showing the appearance of the cargo in rich medium in the presence of nocodazole. The experiment was performed as in Figure 3.6 C, except that the cells were treated with nocodazole for 2 h before SLF addition. Numbers represent molecular weights of reference markers.

the yeast secretory pathway (Makarow, 1988; Vater et al., 1992). Indeed, our control experiments indicated that nocodazole had no effect on the average cisternal residence time of the early Golgi marker GFP-Vrg4 or the late Golgi marker Sec7-GFP (Figure 3.7 A), the rate at which the fluorescent secretory cargo exited the ER (Figure 3.7 B), or the appearance of the secretory cargo in rich medium after SLF addition (Figure 3.7 C). We examined nucleus-free daughters in nocodazole-treated cells and measured the distance from the cortical ER during transitions in which Golgi cisternae acquired or lost either GFP-Vrg4 or Sec7-GFP. The results were striking (Fig. 4 C). Newly formed early Golgi cisternae acquired GFP-Vrg4 in close proximity to the cortical ER (average ER–Golgi distance of 0.21 µm, near the resolution limit of our imaging system). By contrast, older Golgi cisternae lost GFP-Vrg4, and acquired and lost Sec7-GFP, throughout the daughter (average ER–Golgi distance of 0.44–0.61 µm). When early Golgi cisternae were tracked during the period in which they contained GFP-Vrg4, many of them could be seen to move away from the cortical ER (Movie 3.3 and Figure 3.8 A and B). We conclude that early Golgi cisternae form near the ER and then dissociate from sites of cisternal assembly.

The next step was to visualize the early trafficking of the fluorescent secretory cargo. Addition of SLF quickly dissolved the aggregates, but unlike the DsRed-Express2-FKBPRD(C22V) cargo visualized in Figure 3.4 A, the APVNTT-DsRed-Express2-FKBPRD(C22V) cargo immediately began to concentrate in punctate structures. To characterize those structures, we labeled the early Golgi with GFP-Vrg4 and simultaneously labeled ERES by tagging the COPII coat protein Sec31 with HaloTag conjugated to the far-red dye JF_{646} (Rossanese et al., 1999; Grimm et al., 2015; Day et al., 2018). The cargo-containing punctate structures were consistently next to ERES but were less numerous than ERES (Figure 3.9). A cargo-containing punctate structure was associated in some cases with a single ERES and in other cases with multiple ERES. This observation might mean that several ERES could export cargo to the same punctate structure, although due to the large number of ERES in *S. cerevisiae* cells (Rossanese et al., 1999), some of the associations were probably coincidental.

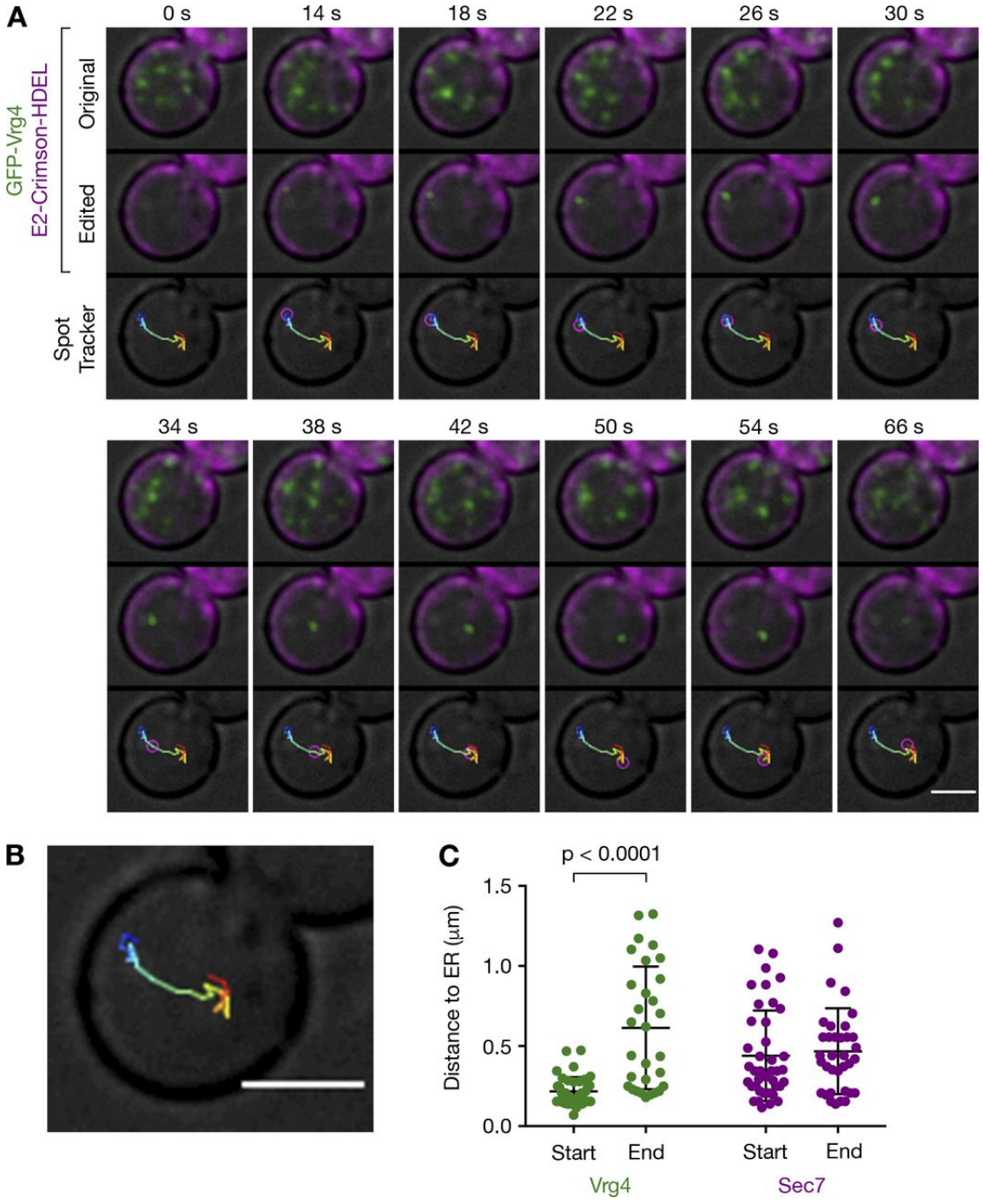

Figure 3.8: **Formation of new Golgi cisternae near the ER in nocodazole-treated cells. (A)** Tracking of a representative early Golgi cisterna. The early Golgi was labeled with GFP-Vrg4, and the ER lumen was labeled with E2-Crimson-HDEL (Strack et al., 2009b). From Movie 3.3, the top row is a projection of optical sections from the center of the cell, the middle row is the same projection after editing to highlight the tracked cisterna, and the bottom row illustrates the path followed by the tracked cisterna. Scale bar, 2 µm. *(continued on next page)*

Figure 3.8: **(B)** Enlargement of the track from part A. Time is indicated by a gradient from blue to red. Scale bar, 2 µm. **(C)** Quantification of the distances between cisternae and the ER during the arrival (Start) and departure (End) of early and late Golgi markers. Strains contained E2-Crimson-HDEL, together with either GFP-Vrg4 (early Golgi) or Sec7-GFP (late Golgi). Cells were grown to mid-log phase, treated with nocodazole for 2 h, and imaged by 4D confocal microscopy. Measurements were derived from the daughters, which lacked perinuclear ER fluorescence. Each of the chosen cisternae experienced a transition in GFP-Vrg4 or Sec7-GFP labeling while near the center of the cell along the vertical axis. At the time of a transition, 8–12 optical sections from the center of the cell were projected, and the distance to the cortical ER was measured using the Line tool in ImageJ. The scatter plot for a transition shows the mean distance from the ER and the standard deviation. For each condition, data were taken from events in at least 30 different cells visualized in seven or more movies. To determine statistical significance, the Vrg4 datasets were compared using the Mann–Whitney U test.

Many ERES were distant from the cargo-containing punctate structures (Figure 3.9), implying that only a subset of the ERES were active at a given time, or that different ERES were exporting distinct classes of proteins (Castillon et al., 2009). Each cargo-containing punctate structure either labeled with GFP-Vrg4 or soon acquired GFP-Vrg4 (Movie 3.4 and Figure 3.10 A). Taken together, these results indicate that after SLF addition, the fluorescent secretory appeared in early Golgi cisternae that had formed next to ERES.

Visualizing the behavior of the secretory cargo during Golgi maturation

An obvious prediction was that during the wave of fluorescent secretory cargo transport, the cargo should be visible first in the early Golgi and then in the late Golgi. To test this idea, we analyzed cells at various times after SLF addition and counted the percentages of early and late Golgi cisternae that contained detectable amounts of fluorescent secretory cargo. Labeling of the early Golgi cisternae was nearly maximal after 2 min, whereas labeling of the late Golgi cisternae was maximal after 4 min (Figure 3.10 B). Thus, the secretory cargo moved progressively through the Golgi.

We were now prepared to carry out the key experiment of visualizing the fluorescent secretory cargo in maturing Golgi cisternae. For this purpose, the secretory cargo was expressed in a strain that contained GFP-Vrg4 together with Sec7-HaloTag conjugated to JF_{646}. Consis-

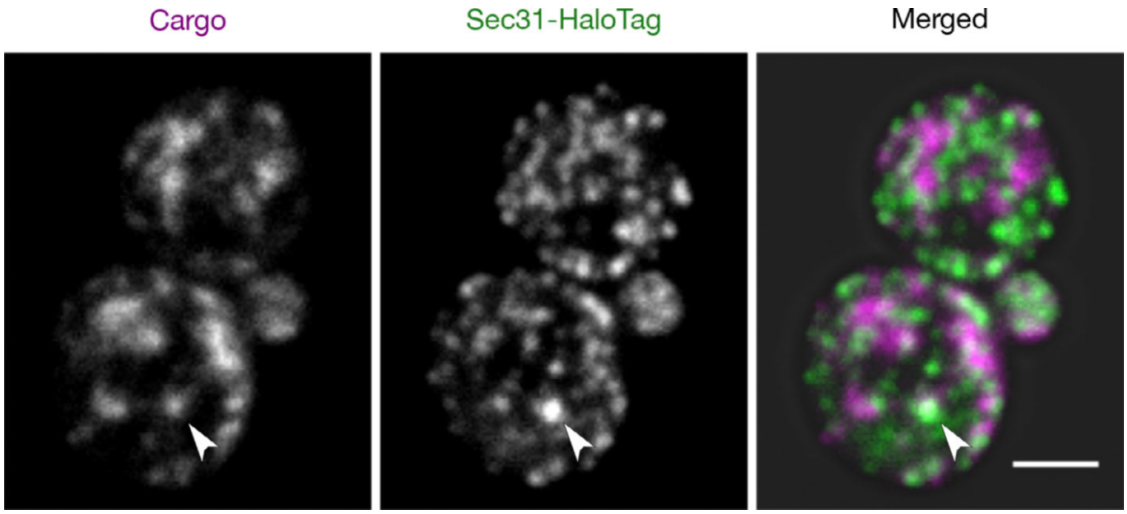

Figure 3.9: **Association of newly exported cargo with a subset of the ERES.** A strain expressing the APVNTT-DsRed-Express2-FKBPRD(C22V) cargo and the ERES marker Sec31-HaloTag was grown to mid-log phase, labeled with JF_{646}, treated with SLF for 2 min to trigger cargo solubilization and export, and fixed. The cells were compressed on a coverslip and imaged on a confocal microscope. This image is a representative projected Z-stack. The arrowhead marks an example of concentrated cargo in the vicinity of a single large ERES. Scale bar, 2 µm

tent with our earlier findings (Losev et al., 2006; Papanikou et al., 2015), individual cisternae acquired GFP-Vrg4, then lost GFP-Vrg4 as they acquired Sec7-HaloTag, and then lost Sec7-HaloTag, all over a time course of ~3 min. The presence of the fluorescent secretory cargo did not detectably alter Golgi morphology or maturation dynamics. Secretory cargo fluorescence was reproducibly visible throughout the period in which a cisterna contained early and late Golgi markers (Movie 3.5 and Figure 3.11 A). These data are quantified in Figure 3.11 B for the two cisternae analyzed in Movie 3.5. Our results verify the basic prediction that a secretory cargo should be present within maturing cisternae as the resident Golgi proteins come and go.

Interestingly, we often saw that the amount of fluorescent secretory cargo in a cisterna increased around the time of the early-to-late transition, and then decreased during the late stage of maturation (Figure 3.11 B). The transient increase raised the signal by an average of 70% (Figure 3.11 C). This phenomenon could reflect vesicular transport of secretory cargo molecules between cisternae. To test this possibility, we used FRAP to bleach the secretory

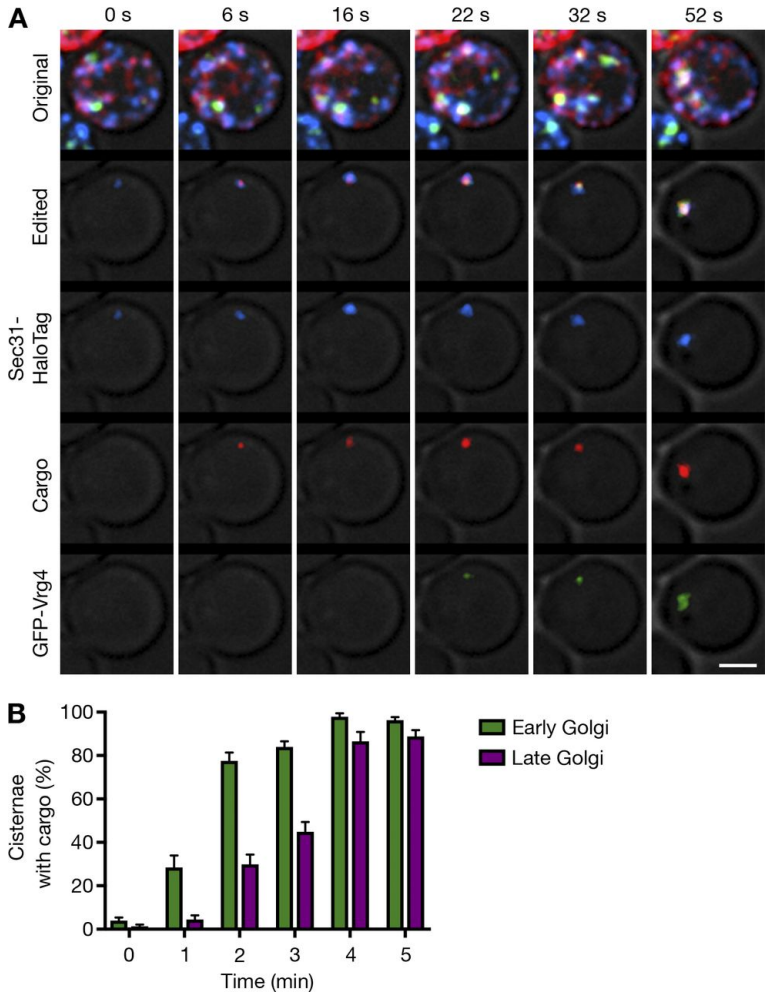

Figure 3.10: **Traffic of the fluorescent secretory cargo to Golgi compartments. (A)** Concentration of the cargo in a nascent Golgi cisterna that formed near an ERES. A strain expressing the APVNTT-DsRed-Express2-FKBPRD(C22V) cargo together with Sec31-HaloTag (ERES) and GFP-Vrg4 (early Golgi) was imaged by 4D microscopy during and after addition of SLF in a flow chamber. Depicted here is a representative example of the results, in frames from Movie 3.4. The top row is the complete projection, the second row is the same projection after editing to highlight the tracked compartments, and the remaining three rows are the individual channels for the edited projection. Time zero represents 45 s after the cells were exposed to SLF. The solubilized cargo became concentrated in a structure that was near an ERES, and then GFP-Vrg4 arrived at the same structure. Scale bar, 2 µm. **(B)** Sequential appearance of the cargo in early and then late Golgi cisternae. Cells expressing the aggregated cargo together with GFP-Vrg4 (early Golgi) and Sec7-HaloTag (late Golgi) were grown to mid-log phase, labeled with JF_{646}, and imaged by 4D confocal microscopy while flowing in medium containing SLF. Movies were analyzed by quantifying the percentages of the early and late Golgi cisternae that contained detectable cargo at the indicated time points. Data were taken from 27 cells in seven movies. Error bars represent SEM.

cargo molecules in early Golgi cisternae while leaving the resident Golgi markers unaffected, and then tracked the cisternae as they matured to detect any recovery of the secretory cargo signal. For convenience, this experiment was performed with nocodazole-treated cells, and all of the cargo fluorescence in a large daughter was bleached simultaneously. Identification of the daughter was unambiguous because the mother had brighter cargo fluorescence due to the presence of nuclear ER. Intense laser illumination of the daughter began 3 min after SLF addition and persisted for 40 s to ensure complete bleaching. The mother and daughter cytoplasms were interconnected, so vesicles carrying fluorescent secretory cargo molecules from the mother could potentially replenish the bleached cisternae in the daughter. For each early Golgi cisterna that we could track, there was an initial period during which cargo fluorescence showed no recovery, followed by a sudden return of cargo fluorescence around the time of the early-to-late transition (Movie 3.6 and Figure 3.12). We calculated the predicted level of fluorescence recovery as follows. In unbleached cells, cargo fluorescence increased by 70% during the early-to-late transition, suggesting that 70 of 170 or 40% of the secretory cargo molecules in late Golgi cisternae originated from other cisternae. In a FRAP experiment, approximately half of the secretory cargo molecules that arrive from other cisternae will have been rendered nonfluorescent by bleaching the daughter, so the recovered cargo fluorescence in the bleached cisternae should be on the order of 20% of the normal cargo fluorescence in unbleached cisternae. Indeed, by the time a cisterna showed maximal labeling with Sec7-HaloTag, the cargo fluorescence in the cisternae that had been bleached averaged 25% of the level seen for cisternae in unbleached nocodazole-treated daughters (Figure 3.13 B). These results are evidence for a burst of incoming secretory cargo traffic as an early cisterna matures into a late cisterna.

Probing the mechanism of secretory cargo transport between cisternae

For two reasons, we suspected that the carriers responsible for transporting the fluorescent secretory cargo between cisternae might be vesicles generated with the aid of the heterote-

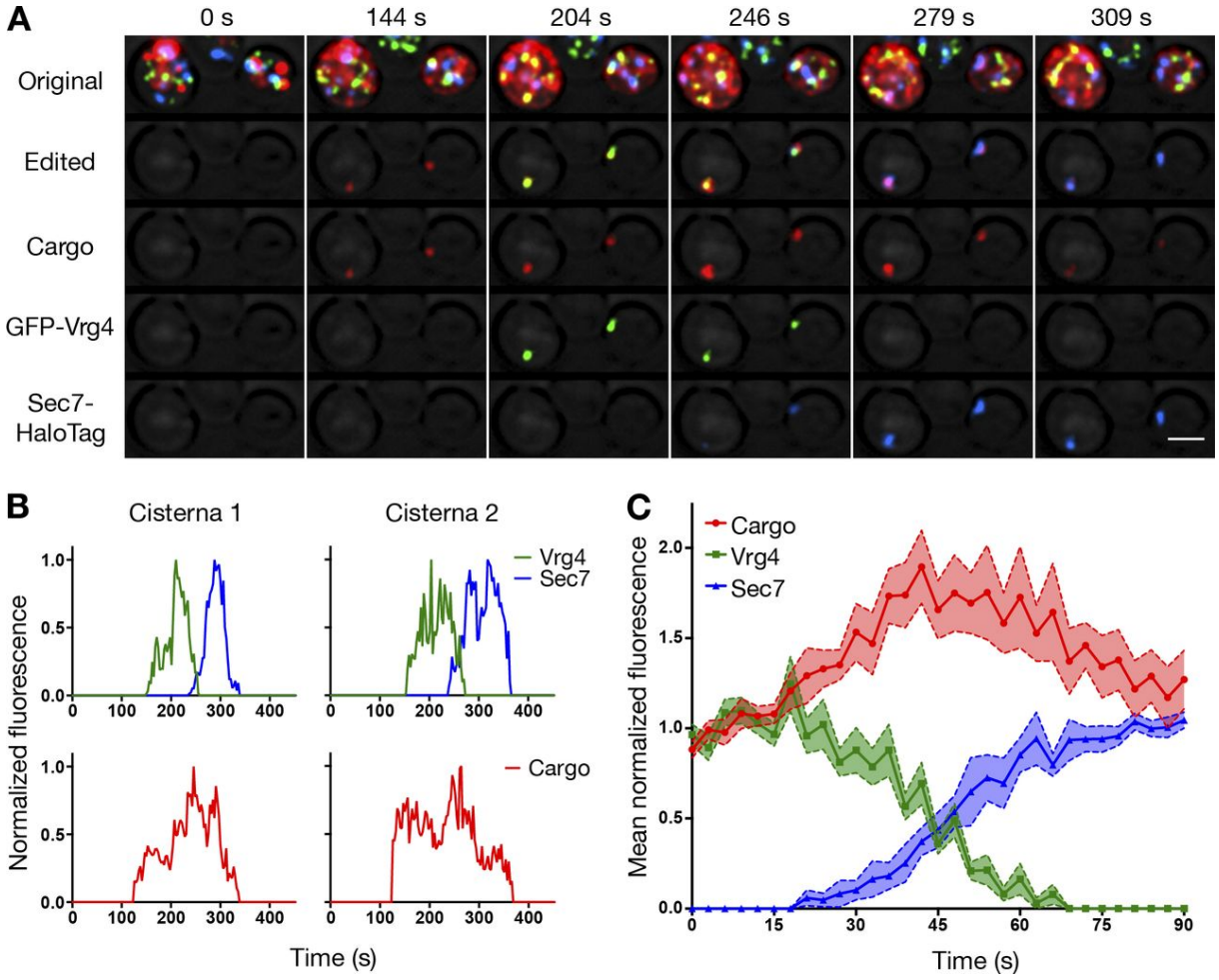

Figure 3.11: **Persistence of the fluorescent secretory cargo in maturing Golgi cisternae. (A)** Visualization of the cargo in maturing Golgi cisternae. Cells expressing the APVNTT-DsRed-Express2-FKBPRD(C22V) cargo together with GFP-Vrg4 (early Golgi) and Sec7-HaloTag (late Golgi) were grown to mid-log phase, labeled with JF_{646}, and imaged by 4D confocal microscopy while flowing in medium containing SLF. Shown are projected Z-stacks from the representative data in Movie 3.5. The top row is the complete projection, the second row is the same projection after editing to highlight the two cisternae that were tracked, and the remaining three rows are the individual channels for the edited projection. Scale bar, 2 µm. **(B)** Quantification of the fluorescence intensities of Golgi markers and cargo during typical maturation events. The graphs represent the cisternae tracked in A, with the signals normalized to a maximum value of 1.0. **(C)** Average cargo signal change during the early-to-late Golgi transition. For each of 19 separate maturation events, fluorescence was quantified over a period of 90 s with Z-stacks collected every 3 s. Normalization of a trace was performed by defining 1.0 as the average of the first six fluorescence values for Vrg4 or the cargo, or as the average of the last six fluorescence values for Sec7. Traces were aligned at the midpoints of the Vrg4-to-Sec7 transitions, and the normalized fluorescence signals were averaged. The shaded borders indicate SEM.

trameric AP-1 clathrin adaptor (Myers and Payne, 2013). First, arrival of secretory cargo molecules occurred during the early-to-late transition, and AP-1 apparently mediates intra-Golgi recycling from late to transitioning cisternae (Papanikou et al., 2015; Day et al., 2018). Second, the secretory cargo signal in a cisterna typically declined after the early-to-late transition, consistent with the idea that late Golgi cisternae were exporting fluorescent secretory cargo molecules to younger cisternae. To test this hypothesis, we deleted the Apl4 subunit of the AP-1 adaptor. Remarkably, in an *apl4*Δ strain, there was no increase in the amount of fluorescent secretory cargo during the early-to-late transition (Figure 3.13 A) and no recovery of cargo fluorescence in bleached cisternae (Figure 3.13 B). Our results are consistent with a role for AP-1 in recycling the fluorescent secretory cargo between cisternae.

This conclusion was somewhat surprising because AP-1 has been implicated in capturing transmembrane cargo proteins by binding their cytosolic tails (Hirst et al., 2012; Myers and Payne, 2013; Whitfield et al., 2016). By contrast, the artificial fluorescent secretory cargo is soluble in the cisternal lumen and is unlikely to contain signals for intra-Golgi recycling. A possible exception is the asparagine-linked oligosaccharide, which is present in four copies in the fluorescent tetramers. Those oligosaccharides could kinetically associate with transmembrane glycosylation enzymes that undergo AP-1–dependent recycling. In support of this possibility, when we tested the nonglycosylated fluorescent secretory cargo containing the APVNTA hexapeptide, there was only a minimal increase in the amount of fluorescent secretory cargo during the early-to-late transition (Figure 3.13 A), and no detectable recovery of cargo fluorescence in bleached cisternae (Figure 3.13 B). Thus, transport of the fluorescent secretory cargo between cisternae requires both AP-1 and asparagine-linked glycosylation.

Visualizing departure of the secretory cargo from the Golgi

Golgi maturation is believed to terminate with the dissolution of a late Golgi cisterna into transport carriers, including secretory carriers destined for the plasma membrane. We tried to observe this phenomenon by taking rapid 4D confocal movies of the fluorescent secretory

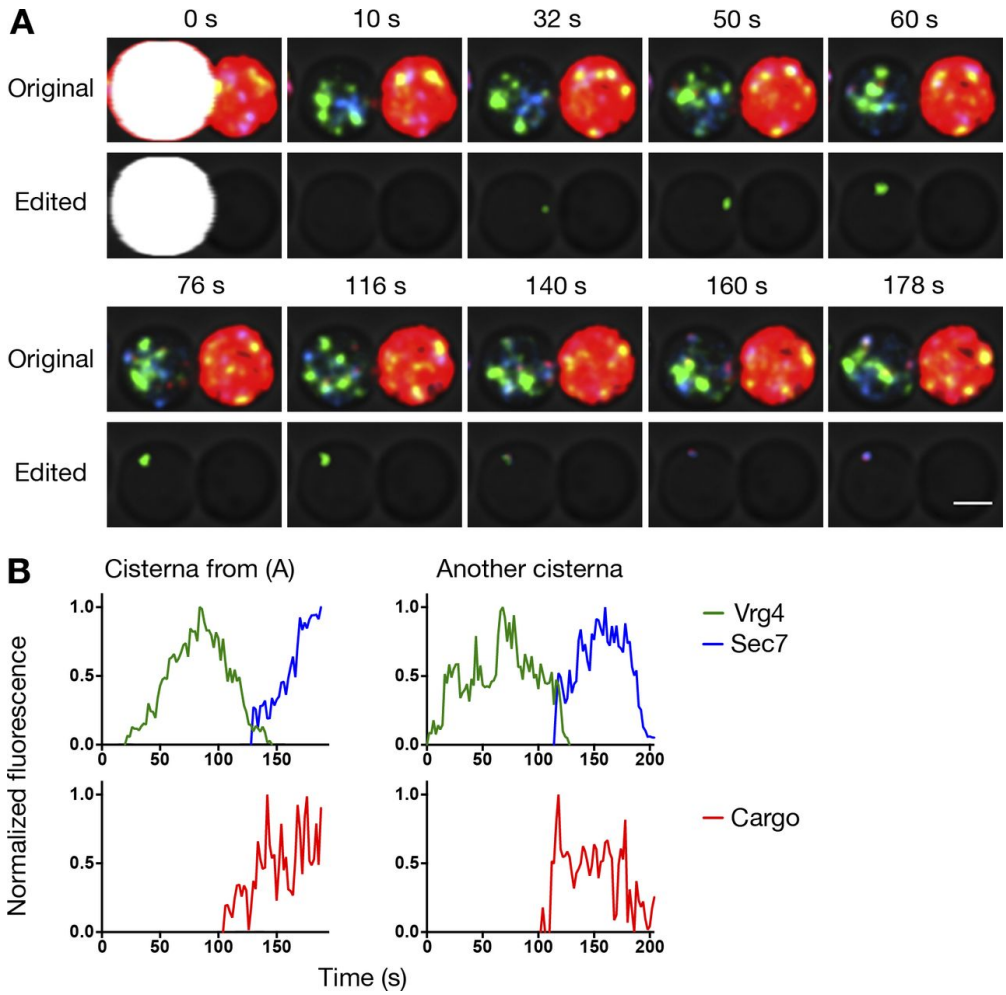

Figure 3.12: **Arrival of fluorescent secretory cargo molecules during the early-to-late Golgi transition. (A)** Visualizing traffic of the cargo to maturing cisternae. Cells expressing the APVNTT-DsRed-Express2-FKBPRD(C22V) cargo together with GFP-Vrg4 (early Golgi) and Sec7-HaloTag (late Golgi) were grown to mid-log phase, treated with nocodazole for 2 h, labeled with JF_{646}, and imaged by 4D confocal microscopy. SLF was added for 3 min to enable early Golgi cisternae to become loaded with cargo. At that point, the cargo fluorescence in an entire daughter was bleached by illuminating with the laser at maximum intensity for 40 s. Then individual cisternae in the daughter were tracked as in Figure 3.11 A by following the Golgi markers, which were not affected by the bleaching. Shown are projected Z-stacks from the representative data in Movie 3.6. The top row is the complete projection, and the bottom row is the same projection after editing to highlight the cisterna that was tracked. Scale bar, 2 µm. **(B)** Quantification of the Golgi markers and the fluorescence recovery of the cargo during typical maturation events in a daughter after cargo bleaching. The first graph represents the cisterna tracked in A, and the second graph represents another typical cisterna tracked in a similar movie. These data from two movies are representative of four total movies analyzed. As a control, when both the mother and daughter were bleached, no fluorescence recovery of the cargo was seen (not depicted).

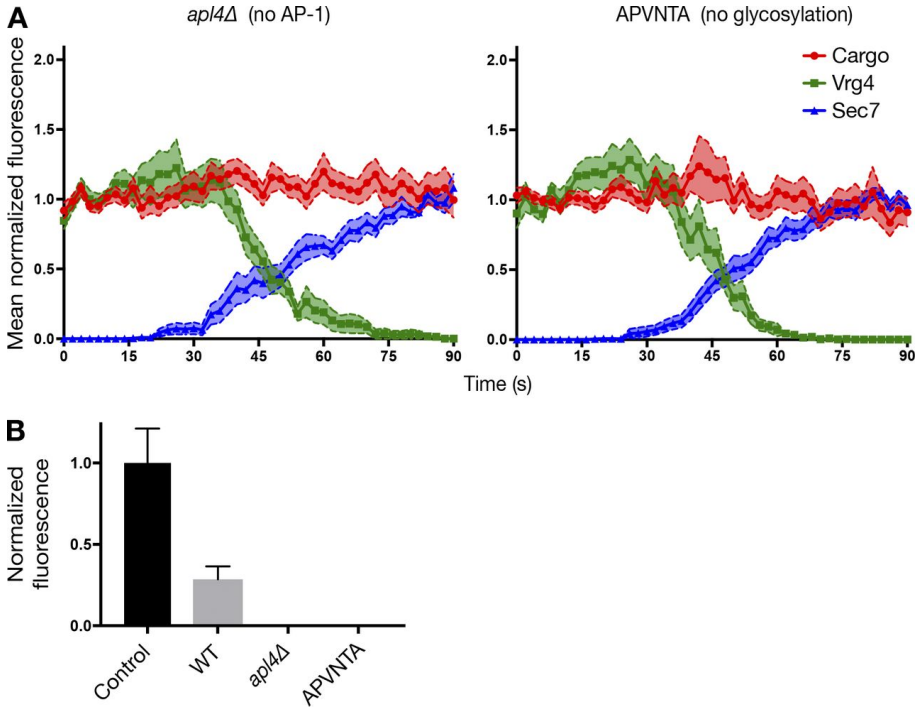

Figure 3.13: **Suppression of intercisternal transport of the fluorescent secretory cargo. (A)** Fluorescent secretory cargo levels during the early-to-late Golgi transition after eliminating AP-1 or asparagine-linked glycosylation. The analysis was performed as in Figure 3.11 C, except that Z-stacks were captured every 2 s. For each yeast strain, 17 early-to-late Golgi transitions visualized in at least nine movies were averaged. Where indicated, the cells lacked AP-1 due to an *apl4*Δ mutation, or the secretory cargo lacked asparagine-linked glycosylation due to the presence of the APVNTA hexapeptide. **(B)** Quantification of the average secretory cargo fluorescence in cisternae of nocodazole-treated daughters at the time of maximal Sec7 signal. The Control measurements were performed using the glycosylated secretory cargo in unbleached cells, and the other three measurements were performed after recovery from bleaching as in Figure 3.12. WT, cells with wild-type AP-1 and the glycosylated secretory cargo. The remaining two bars (for which virtually no signals were detected) are from the conditions described in A. Error bars represent SEM for measurements of at least four cisternae for each condition.

cargo in cells that expressed Sec7-HaloTag to mark the late Golgi as well as Apl2-GFP to mark AP-1 (Movie 3.7 and Figure 3.14). As we reported previously (Day et al., 2018), AP-1 arrived at late Golgi cisternae later than Sec7 and also departed somewhat later. Fluorescent secretory cargo was often detectable after Sec7 had departed, and disappeared in synchrony with AP-1. However, our microscopy system was unable to track the carriers that transported the fluorescent secretory cargo out of terminally maturing Golgi cisternae. A future challenge

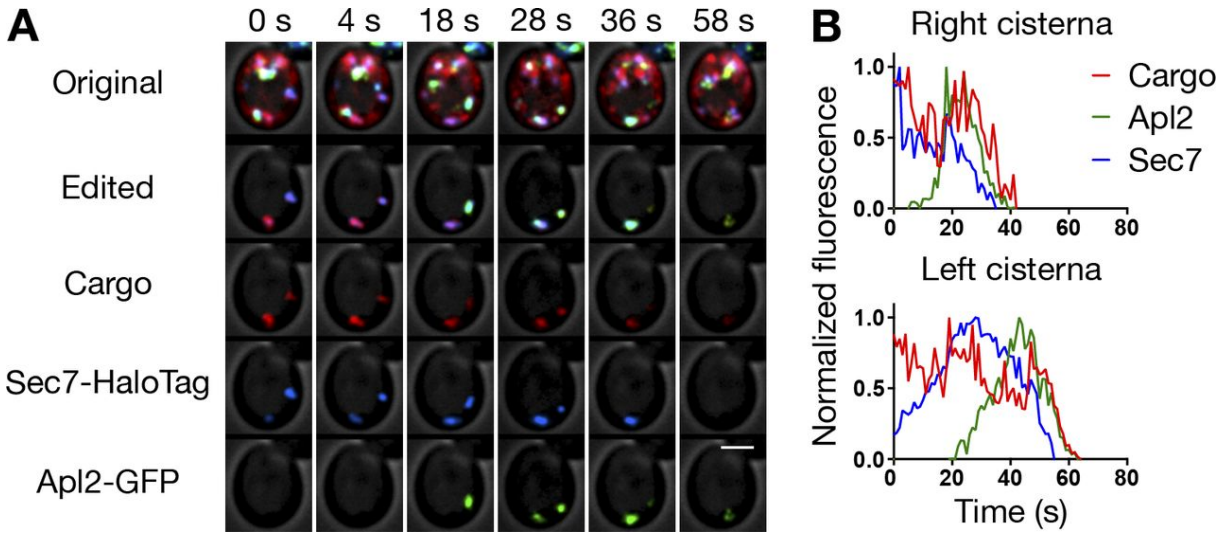

Figure 3.14: **Departure of the fluorescent secretory cargo from the late Golgi. (A)** Visualizing the cargo in terminally maturing cisternae. Cells expressing the APVNTT-DsRed-Express2-FKBPRD(C22V) cargo together with Sec7-HaloTag and Apl2-GFP were grown to mid-log phase, labeled with JF_{646}, treated with SLF for 5 min, and imaged by 4D confocal microscopy with an interval of 1 s between Z-stacks. Shown are projected Z-stacks from the representative data in movie 3.7. The top row is the complete projection, the second row is the same projection after editing to highlight the two cisternae that were tracked, and the remaining three rows are the individual channels for the edited projection. Scale bar, 2 µm. **(B)** Quantification of the Golgi markers and the fluorescent secretory cargo for the two cisternae tracked in A. These data are representative of five total movies in which one or more cisternae were analyzed per movie.

is to image the fluorescent secretory cargo as it travels from the late Golgi to the plasma membrane.

Discussion

Although budding yeast is extremely useful for studying membrane traffic, this system has lacked model cargo proteins that could be accumulated in the ER and then tracked by microscopy during their passage through the secretory pathway. For comparison, secretory cargo transport in animal cells has been visualized using model cargo proteins such as procollagen and the thermosensitive tsO45 mutant of vesicular stomatitis virus G protein (Presley et al., 1997; Mironov et al., 2001; Trucco et al., 2004). Those cargo proteins can be accumulated in the ER and then released for exit to the Golgi. A newer method is the retention using

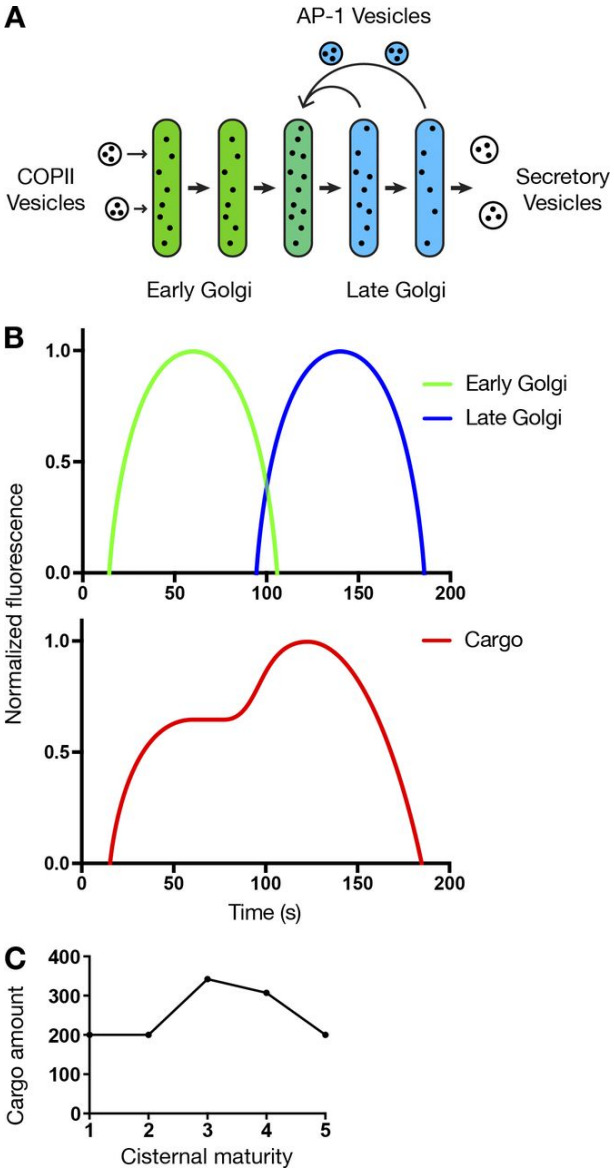

Figure 3.15: **Secretory cargo traffic during yeast cisternal maturation. (A)** Diagram illustrating the inferred behavior of the fluorescent secretory cargo in maturing yeast cisternae. Green and blue represent early and late resident Golgi proteins, respectively, and black dots represent fluorescent cargo molecules. Progressive maturation is depicted from left to right. The cargo molecules initially travel passively in the maturing cisternae. During the late stage of maturation, a fraction of the cargo molecules recycle in transport vesicles, which are generated with the aid of the AP-1 adaptor, to cisternae that are undergoing the early-to-late transition.**(B)** Qualitative prediction, according to the scheme in A, of the fluorescence signals from resident Golgi proteins and the secretory cargo in a maturing yeast Golgi cisterna. The cargo signal is constant during the early stage of maturation, then rises during the early-to-late transition, then declines during the late stage of maturation. Compare to the simpler scheme in Figure 3.1.

Figure 3.15: **(C)** Computer simulation of steady state cargo levels in maturing Golgi cisternae according to the scheme in A. Details of the simulation procedure are given in Materials and methods. The horizontal axis indicates cisternae of varying maturity, from the newly formed cisterna 1 to the terminally mature cisterna 5. The vertical axis indicates the number of simulated cargo molecules in each cisterna. A cargo molecule in cisterna 4 or 5 could recycle to cisterna 3 with a specified probability. For the simulation shown, the probability of recycling from cisterna 4 was 0.10, and the probability of recycling from cisterna 5 was 0.35, where the increasing probability reflects the late recruitment of AP-1 to the Golgi. Those probability values were chosen for illustrative purposes because they produce a reasonable match to the experimental data, with 70% more cargo molecules in the transitioning cisterna 3 than in earlier cisternae.

selective hooks (RUSH) system, which allows a variety of cargo proteins to be trapped in the ER and then released (Boncompain et al., 2012; Chen et al., 2017). Yet another approach generates reversible aggregates in the ER by fusing four copies of a dimerizing FKBP variant to a GFP-tagged cargo protein (Rivera et al., 2000). Addition of an FKBP ligand dissolves the aggregates and allows the solubilized fluorescent protein to exit the ER. For yeast, we adapted this last strategy with modifications. A dimerizing FKBP variant was fused to the tetrameric fluorescent protein DsRed-Express2 (Strack et al., 2008), and this construct was targeted to the ER lumen with a signal sequence. The result is that the cells accumulate red fluorescent aggregates that can be dissolved to trigger ER exit.

This approach required overcoming a series of technical hurdles to ensure that the fluorescent secretory cargo reaches the ER lumen, that the cargo aggregates dissolve efficiently, and that the cargo traverses the secretory pathway without being diverted to the vacuole (Casler and Glick, 2018). A key step was to add a tripeptide ER export signal to the cargo (Nam et al., 2014; Yin et al., 2018). As a result, the solubilized cargo exits the ER and passes through the Golgi in a nearly synchronous wave.

The anticipated behavior of this secretory cargo was guided by earlier work with endogenous yeast secretory cargo proteins such as invertase and α-factor (Gaynor and Emr, 1997; Brigance et al., 2000), and with mammalian secretory cargo proteins such as procollagen and vesicular stomatitis virus G protein. We expected that the secretory cargo would appear first in early and then in late Golgi cisternae. As a result of passage through the Golgi, the

asparagine-linked oligosaccharide should be modified. Finally, the secretory cargo should be delivered to secretion sites, which for much of the yeast cell cycle are sites of polarized growth (Finger and Novick, 1998). Each of these predictions was confirmed for the fluorescent secretory cargo. The time scale for transit from the ER to the late Golgi is minutes, consistent with the kinetics for transport of α-factor through the yeast secretory pathway (Losev et al., 2006). Thus, by all of the available criteria, our artificial fluorescent fusion protein construct behaves like a bona fide secretory cargo.

Using the fluorescent secretory cargo, we visualized traffic through the yeast secretory pathway, beginning with transfer from the ER to the early Golgi. The prevailing model is that new Golgi cisternae form by the coalescence of COPII vesicles that have encapsulated secretory cargo proteins while budding from ERES. In support of this idea, previous work revealed associations of early Golgi cisternae with ERES in *S. cerevisiae* (Levi et al., 2010; Okamoto et al., 2012; Kurokawa et al., 2014). However, those associations were seen for only a subset of the labeled compartments, and the data were not integrated with studies of maturation kinetics. We now show that early Golgi cisternae form next to the ER, presumably at ERES, and then dissociate from the ER as they mature. Furthermore, within 1 min after SLF addition, the fluorescent secretory cargo begins to accumulate in punctate structures that are associated with ERES. Those punctate structures subsequently acquire the early Golgi marker Vrg4. Our interpretation is that the fluorescent secretory cargo exits the ER in COPII vesicles and becomes concentrated in newly forming early Golgi cisternae.

The next step was to track the secretory cargo as a cisterna matured from early to late. This transition can be visualized by using different fluorescent colors to tag the early Golgi marker Vrg4 and the late Golgi marker Sec7 (Losev et al., 2006). To image those two Golgi markers together with the red fluorescent secretory cargo, Vrg4 was tagged with GFP while Sec7 was tagged with HaloTag conjugated to the far-red dye JF_{646} (Grimm et al., 2015). We reproducibly found that a Golgi cisterna labels continuously with the secretory cargo as the cisterna loses Vrg4 and acquires Sec7. This result verifies a core prediction of the cisternal

maturation model. Substantially similar results for a yeast membrane protein are reported in the accompanying manuscript in this issue from the Nakano laboratory (Kurokawa et al., 2019).

Continuous labeling of cisternae with a secretory cargo does not necessarily mean that each cargo molecule remains within a particular cisterna. Alternatively, some cargo molecules could exchange between cisternae in vesicles. Possible pathways for intercisternal vesicular traffic of a secretory cargo include COPI-dependent exchange between early Golgi cisternae and clathrin-dependent recycling from late to transitioning cisternae (Orci et al., 2000; Pellett et al., 2013; Papanikou et al., 2015). Initial evidence for intercisternal traffic of our fluorescent secretory cargo came from the finding that around the time of the early-to-late Golgi transition, the amount of secretory cargo within a cisterna typically increases. To test more directly whether the secretory cargo moves between cisternae, we photobleached the cargo molecules in a subset of the early cisternae and then imaged. There was no recovery of fluorescence until the early-to-late transition, at which point there was sudden recovery. The cargo molecules that arrive during the early-to-late transition likely originate not from the ER but rather from late Golgi cisternae, for the following reasons. First, if the ER were continuing to supply cargo to Golgi cisternae, the fluorescence signal after photobleaching should have recovered gradually throughout maturation instead of recovering suddenly during the early-to-late transition. Second, by the time of the early-to-late transition, a cisterna has dissociated from the ER and is probably no longer competent to receive COPII vesicles. Third, after the increase in cargo signal during the early-to-late transition, the signal often declines during the late stage of maturation, suggesting that late Golgi cisternae are exporting rather than receiving cargo. The combined results fit best with the idea that maturing late Golgi cisternae produce retrograde carriers that recycle certain components, including the fluorescent secretory cargo, to younger cisternae that are undergoing the early-to-late transition (Figure 3.15 A and B). A simple computer simulation confirmed that such a re-

cycling pathway could generate a transient increase in the secretory cargo concentration in a maturing cisterna (Figure 3.15 C).

What type of carrier recycles the fluorescent secretory cargo? The most likely candidate is vesicles formed with the aid of the AP-1 clathrin adaptor, which functions in an intra-Golgi recycling pathway (Valdivia et al., 2002; Papanikou et al., 2015; Spang, 2015; Day et al., 2018). In support of this hypothesis, disruption of AP-1 abolishes intra-Golgi recycling of the fluorescent secretory cargo even though cisternal maturation is preserved. We were somewhat surprised to see normal Golgi dynamics in the absence of AP-1. A possible explanation is that late Golgi proteins that ordinarily recycle with the aid of AP-1 now reach the plasma membrane and then recycle in endocytic vesicles, which in yeast fuse directly with Golgi cisternae during the early-to-late transition (Day et al., 2018). In any case, the straightforward interpretation of our data are that AP-1 vesicles recycle the fluorescent secretory cargo.

The question then becomes, how is the fluorescent secretory cargo packaged into AP-1 vesicles, which typically incorporate transmembrane cargo proteins that contain cytosolic trafficking signals (Hirst et al., 2012; Myers and Payne, 2013; Whitfield et al., 2016)? One possibility is that the asparagine-linked oligosaccharides on the soluble cargo are kinetically bound to transmembrane glycosylation enzymes, which in turn are packaged into AP-1 vesicles. Indeed, removal of the glycosylation signal from the fluorescent secretory cargo prevents intra-Golgi recycling. This observation leads us to speculate that intra-Golgi recycling of glycosylated secretory cargo proteins is a quality control mechanism to ensure that oligosaccharides are efficiently processed. Further work will be needed to explore the detailed mechanism that drives recycling of the glycosylated fluorescent secretory cargo and to determine whether a similar pathway exists for other secretory cargo proteins.

These findings focus interest on the early-to-late Golgi transition, which is special in that the recycling secretory cargo arrives specifically during this time. We can therefore define a transitional stage of yeast Golgi maturation by the presence of machinery that captures AP-1 vesicles as well as other incoming carriers such as endocytic vesicles (Day et al., 2018).

Building on earlier ideas (Day et al., 2013; Papanikou and Glick, 2014; Papanikou et al., 2015; Kim et al., 2016), we envision that Golgi maturation can be divided into early and late stages that produce COPI and clathrin-coated vesicles, respectively, plus an overlapping transitional stage that captures incoming vesicles. This mechanistic view of Golgi organization may be more tractable than the loosely defined concepts of *cis*, *medial*, *trans*, and *trans*-Golgi network (TGN) compartments.

If intra-Golgi recycling of secretory cargo proteins turns out to be a general phenomenon, it could explain three observations from the literature. First, a study of mammalian cells reported that several secretory cargo proteins exited the Golgi with exponential kinetics rather than with the linear kinetics predicted from a simple maturation scheme (Patterson et al., 2008). The exponential kinetics could be explained by repeated recycling of a fraction of the secretory cargo molecules from late to transitioning cisternae. Second, secretory cargo proteins were found to exchange between Golgi stacks after fusion of mammalian cells (Pellett et al., 2013). That exchange could have been due to intra-Golgi recycling by means of vesicles that traveled long distances in the cytoplasm. Third, an intra-Golgi recycling pathway could explain how certain components accumulate in the TGN even though that compartment turns over rapidly. Accumulation in the TGN can occur when secretory cargo proteins are mutated or incompletely assembled, or when specific components of the trafficking machinery are inactivated (Koval et al., 1997; Gut et al., 1998; von Blume et al., 2012; Guo et al., 2013). Such perturbations may cause the secretory cargo proteins to recycle repeatedly rather than to partition into secretory vesicles. Similarly, when a pulse of a membrane-associated fluorescent dye was internalized to the yeast late Golgi, which is equivalent to the TGN, the dye labeled the late Golgi for much longer than the turnover time of that compartment, implying that membrane was recycling from older to younger cisternae (Day et al., 2018). In yeast, the plasma membrane protein Fus1 can be accumulated in the Golgi by mutations in the exomer complex or in Fus1 itself, and disruption of AP-1 restores transport to the plasma membrane (Barfield et al., 2009), consistent with a role for AP-1 in intra-Golgi

recycling of Fus1. A potentially conserved role for mammalian AP-1 in intra-Golgi recycling merits further investigation.

Our results demonstrate the value of using a regulatable fluorescent secretory cargo in a model eukaryote. The same secretory cargo is expected to behave similarly in other cell types, especially because the ER export signal and its cognate receptor are well conserved (Mitrovic et al., 2008; Nam et al., 2014; Saegusa et al., 2018; Yin et al., 2018). For a cell type of interest, if a suitable signal sequence is available to drive cotranslational translocation, and if the SLF ligand can readily penetrate the cells, then it should be possible to achieve aggregation of the fluorescent secretory cargo in the ER followed by rapid transit through the secretory pathway.

Materials and methods

Yeast growth and transformation

The parental haploid *S. cerevisiae* strain was JK9-3da (*leu2-3,112 ura3-52 rme1 trp1 his4*; Heitman et al., 1991). Yeast cells were grown in baffled flasks with shaking at 23°C in nonfluorescent minimal glucose dropout medium (NSD; Bevis et al., 2002) or in rich glucose medium (YPD) supplemented with adenine and uracil. Unless otherwise indicated, cells were grown and imaged in unbuffered NSD. To generate budded cells in which the daughters had yet to inherit nuclei, cells from a logarithmically growing culture were treated for 2 h with 8 µg/ml nocodazole (Thermo Fisher Scientific; AC358240500; stored as a 1,000× stock in DMSO).

The *vps10-104* mutation was generated via pop-in/pop-out mutagenesis as previously described (Fitzgerald and Glick, 2014). Deletion of the *PDR1*, *PDR3*, and *ERV29* genes was accomplished by replacement with a G418, nourseothricin, or hygromycin resistance cassette from pFA6a-kanMX6, pAG25, or pAG32, respectively (Wach et al., 1994; Goldstein and McCusker, 1999). The primers used for amplifying these cassettes were:

5'-CAGCCAAGAATATACAGAAAAGAATCCAAGAAACTGGAAGCGTA

CGCTGCAGGTCGAC-3' and
5'-GGAAGTTTTTGAGAACTTTTATCTATACAAACGTATACGTATCG
ATGAATTCGAGCTCG-3' for deleting *PDR1*,
5'-ATCAGCAGTTTTATTAATTTTTTCTTATTGCGTGACCGCACGT
ACGCTGCAGGTCGAC-3' and
5'-TACTATGGTTATGCTCTGCTTCCCTATTTTCTTTGCGTTTATC
GATGAATTCGAGCTCG-3' for deleting *PDR3*, and
5'-GACTCAAAAAAAGTGAAAACAAAACTGAAAGGATAGATCACGT
ACGCTGCAGGTCGAC-3' and
5'-GAGTGAACAGAAGGGACATAAAGAAAAGATTTCCTTTACAATATC
GATGAATTCGAGCTCG-3' for deleting *ERV29*.

Yeast cells were transformed with an amplified fragment and selected for resistance to the appropriate antibiotic.

Native yeast proteins were tagged by gene replacement using the pop-in/pop-out method to maintain endogenous expression levels. Secretory cargo proteins were expressed using a *TRP1* integrating vector with the strong constitutive *TPI1* promoter and the *CYC1* terminator (Fitzgerald and Glick, 2014). To ensure similar expression of secretory cargo proteins between strains, single-copy integrants were confirmed by PCR using primers 5'-GTGTACTTTGCAGTTATGACGCCAGATGG-3' and 5'-AGTCAACCCCCTGCGATGTATATTTTCCTG-3'. All plasmids used in this study are documented in the online supplemental material ZIP file with annotated map/sequence files that can be opened with SnapGene Viewer. Newly generated plasmids have been submitted to Addgene.

Fluorescence microscopy and FRAP experiments

For live-cell fluorescence imaging, yeast strains were grown in NSD (pH 4) or in phosphate-buffered NSD at pH 6 and were imaged at room temperature (23°C). Where indicated,

SLF was diluted from a 100-mM stock in ethanol (Cayman Chemical; 10007974) to a final concentration of 100 µM. For static live-cell imaging, cells were attached to a concanavalin A–coated coverglass-bottom dish containing NSD (Losev et al., 2006) on a Leica SP8 confocal microscope equipped with a 1.4 NA/63× oil objective, using a 60–80-nm pixel size, a 0.25–0.30-µm Z-step interval, and 20–30 optical sections. Z-stacks were captured at intervals of 1–3 s. For 4D live-cell imaging in a flow chamber (Barrero et al., 2016), a 24 × 50-mm coverslip was coated with freshly dissolved 2 mg/ml concanavalin A (Sigma-Aldrich; C2010) for 10 min, then washed with water and allowed to dry. A 250-µl aliquot of the culture was overlaid on the coverslip, and cells were allowed to adhere for 10 min, followed by several rounds of gentle washing with NSD. The coverslip was placed in the flow chamber and sealed while ensuring that the cells remained immersed in NSD the entire time. NSD was pushed through the flow chamber with a syringe to remove any bubbles, and then the Tygon tubing was clamped. The flow chamber was placed on the stage of an SP8 inverted confocal microscope. One end of the Tygon tubing was connected to a negative pressure pump (Moscovici et al., 2010), while the other end was placed in a culture tube with appropriate medium. To initiate flow of medium, the clamp was removed. Z-stacks were then captured as described above.

For imaging of fixed cells, an aliquot of yeast culture was mixed with an equal volume of 2× ice-cold fixative (100 mM potassium phosphate at pH 6.5, 2 mM MgCl2, 8% formaldehyde, and 0.5% glutaraldehyde) while vortexing. After 1 h on ice, the fixed cells were washed twice with PBS and then resuspended in PBS for viewing.

Static images were converted to 16-bit and average projected (Hammond and Glick, 2000), then range-adjusted to the minimum and maximum pixel values in ImageJ (National Institutes of Health). Movies were deconvolved with Huygens Essential (Scientific Volume Imaging) using the classic maximum likelihood estimation algorithm (Day et al., 2017). Movies were converted to hyperstacks and average projected, then range-adjusted to maximize contrast in ImageJ. Custom ImageJ plugins were used to generate montages of time

series, select individual structures and remove background structures, convert edited montages to hyperstacks, and measure fluorescence intensities (Day et al., 2016). Spot tracking was performed using the TrackMate plugin for Fiji.

Perinuclear ER fluorescence was measured as follows (Papanikou et al., 2015). Cells were fixed as described above and then stained with DAPI to mark the nucleus. Cells were compressed under a coverslip, and images of the central regions of the cells, defined along the vertical axis, were collected by wide-field microscopy on a Zeiss Axioplan 2 epifluorescence microscope equipped with a 1.4-NA/100× oil objective and a Hamamatsu digital camera. The DAPI signal was selected using the Magic Wand tool in ImageJ and expanded by 12 pixels to include the nuclear envelope. The cargo signal within this area was then quantified.

FRAP experiments were performed on an SP8 confocal microscope with a 1.4-NA/63× oil objective. Nocodazole-treated cells were adhered to a concanavalin A–coated coverglass-bottom dish and incubated with 100 µM SLF for 3 min before imaging. Daughters (defined by the lack of visible perinuclear ER fluorescence) were selected manually and subjected to photobleaching by 100% intensity laser power at 561 nm. Fluorescence recovery was then monitored by imaging at a standard laser power (5–7%).

HaloTag labeling

To visualize proteins fused to HaloTag, the JF_{646} ligand, kindly provided by Luke Lavis (Janelia Research Campus, Ashburn, VA), was added to 0.5 ml of culture medium to a final concentration of 1 µm from a 1-mM stock in DMSO. The medium was cleared of any precipitate by spinning at 17,000 g (13,000 rpm) in a microcentrifuge for 1 min. Then the cleared medium containing the JF_{646} ligand was added to 0.5 ml of yeast culture, and the cells were incubated with shaking at 23°C for 30 min. Excess dye was removed by filtration through and washing on a 0.22-µm syringe filter (Millipore; SLGV004SL). The washed cells were resuspended in NSD and adhered to a concanavalin A–coated coverglass-bottom dish. movies were captured immediately with an SP8 confocal microscope.

Immunoblotting of yeast cell lysate and secreted protein

A 5- to 25-ml yeast culture was grown in YPD overnight with shaking in a baffled flask to an OD_{600} of 0.7–1.0. The cells were collected by a brief spin in a microcentrifuge, washed twice with fresh YPD, and resuspended in the original volume of fresh YPD. Cultures were treated with 100 µM SLF, and 1.6 ml was removed at each time point. The cells were collected by spinning at 2,500 x g (5,000 rpm) for 2 min in a microcentrifuge. The culture medium supernatant was transferred to a fresh microcentrifuge tube on ice, and the cells were washed once with deionized water. Then the cells were resuspended in 100 µl PBS. Glass beads (0.5 mm; BioSpec Products) were added to bring the total volume to 200 µl, and the sample was vortexed three times for 1 min each separated by 1-min intervals on ice. Finally, 800 µl of PBS was added, the solution was mixed, and 800 µl of the cell lysate was transferred to a fresh microcentrifuge tube.

Protein samples were precipitated using the ND Protein Precipitation Kit (National Diagnostics; EC-888). Briefly, a sample was supplemented with 1/20 volume reagent A followed by 1/10 volume reagent B. Samples were mixed by inversion and incubated at 23°C for 15 min followed by spinning at 17,000 x g (13,000 rpm) for 10 min in a microcentrifuge. Each pellet was resuspended in 1 ml acetone and spun as before for 15 min, and then the supernatant was removed. The resulting pellet was washed twice with 70% ethanol and resuspended in 50 µl SDS-PAGE sample buffer.

Treatment with endo H was performed as described by the manufacturer (New England Biolabs; P0702S). Briefly, Glycoprotein Denaturing Buffer was added to the protein sample, which was boiled for 5–10 min, followed by addition of GlycoBuffer 3 and endo H. The reaction was performed at 37°C for at least 1 h.

For immunoblotting, 9 µl of each cell lysate and 14 µl of each secreted protein sample were run on a 4–20% Tris-glycine gel (Bio-Rad; 4561094) together with a molecular weight marker (Bio-Rad; Precision Plus Protein Dual Color Standards; 1610374). The separated proteins were transferred to a PVDF membrane (Bio-Rad; 1704156) using the Trans-Blot Turbo

system (Bio-Rad). The membrane was blocked with 5% nonfat dry milk in TBST (50 mM Tris-HCl at pH 7.6, 150 mM NaCl, and 0.05% Tween 20) with shaking at room temperature for 1 h, and then incubated with 1:1,000 polyclonal rabbit anti-FKBP12 antibody (Abcam; ab2918, raised against an N-terminal peptide from FKBP) in 5% milk/TBST with shaking overnight at 4°C. After four 5-min washes in TBST, the membrane was incubated with a 1:1,000 dilution of goat anti-rabbit secondary antibody conjugated to Alexa Fluor 647 (Thermo Fisher Scientific; A21245) for 1 h at room temperature. The membrane was then washed twice with TBST and twice with 50 mM Tris-HCl at pH 7.6 and 150 mM NaCl. Analysis was performed with a LI-COR Odyssey CLx imaging system.

Analysis of HAC1 mRNA splicing

RNA isolation was performed using the Qiagen RNeasy Mini Kit (74104). 1 ml of yeast culture at an OD600 of 0.6–0.8 was centrifuged for 1 min at 2,400 g (5,000 rpm) in a microcentrifuge. The liquid was removed, and the cell pellet was resuspended in 600 µl of RLT buffer that had been supplemented with 10 µl -mercaptoethanol per ml of buffer. Cells were lysed by addition of 600 µl of glass beads followed by vortexing three times for 1 min each, with intervals of 1 min on ice between rounds of vortexing. After lysis, RNA purification was performed as detailed in the kit handbook.

cDNA synthesis was performed using the ProtoScript II First Strand cDNA Synthesis Kit from New England Biolabs (E6560S). Briefly, 6 µl of the isolated RNA was combined with 10 µl of 2× ProtoScript II Reaction Mix, 2 µl of primer d(T)23 VN, and 2 µl of 10× ProtoScript II Enzyme Mix. Samples were incubated at 42°C for 1 h followed by heat inactivation of the enzymes at 80°C for 5 min.

PCR was performed using primers 5'-ACGACGCTTTTGTTGCTTCT-3' and 5'-TCTTCGGTTGAAGTAGCACAC-3', which flank the intron of the HAC1 mRNA. A 10-µl aliquot of each PCR product was subjected to agarose gel electrophoresis.

Computer simulations

A Java program was used to simulate transport of a solubilized cargo through the yeast secretory pathway. Ten thousand simulated cargo molecules were initially located in the ER. During each of step of the simulation, 200 cargo molecules exited the ER. The Golgi was modeled as five cisternae of increasing maturity, where cisternae 1–3 represented the early Golgi, cisternae 3–5 represented the late Golgi, and cisterna 3 represented a transitioning cisterna with properties of both the early and late Golgi. Maturation was modeled as forward movement of the cargo molecules in each cisterna to the next cisterna, or for cisterna 5, as forward movement to a post-Golgi status. To simulate recycling, cargo molecules in cisternae 4 and 5 had specified probabilities of traveling back to cisterna 3 instead of moving forward. After 25 steps of the simulation, half of the cargo molecules had exited the ER, and the system was assumed to be at steady-state. Five thousand simulations of 25 steps each were performed, and the average number of cargo molecules in each location was calculated.

Movies Associated with Chapter 3

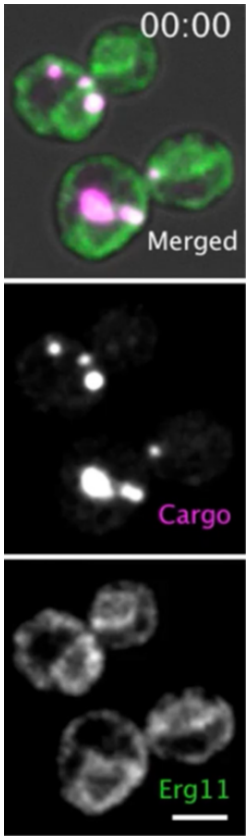

Movie 3.1. **Dissolution of cargo aggregates in the ER lumen.** Cells expressed the DsRed-Express2-FKBPRD(C22V) cargo, together with Erg11-GFP to mark the ER. Medium that contained SLF was added while imaging on a confocal microscope, with a Z-stack collected every 2 s. The top panel merges the cargo, Erg11-GFP, and bright-field channels, while the middle panel is the cargo alone and the bottom panel is the Erg11-GFP channel alone. The movie shows projections of 10 optical sections from the centers of the cells. Scale bar, 2 µm. Frames from this movie are shown in Figure 3.4.

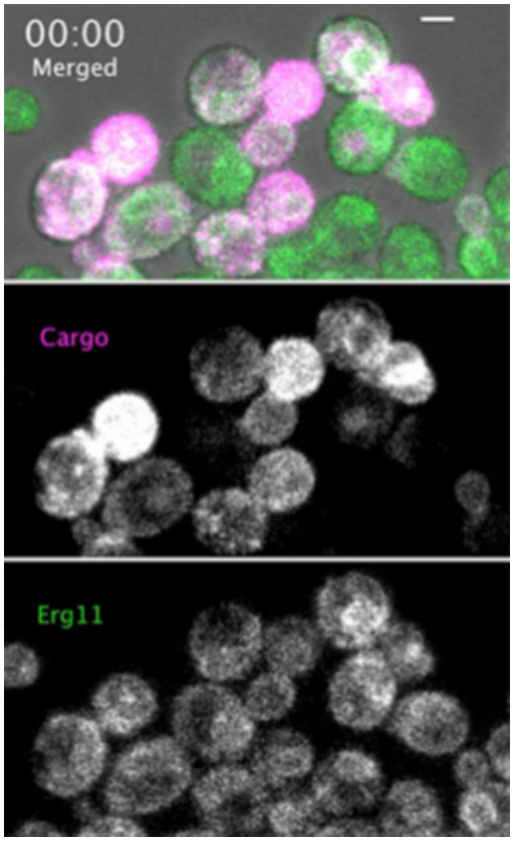

Movie 3.2. **Quenching of periplasmic cargo fluorescence by low pH.** Cells expressed the APVNTT-DsRed-Express2-FKBPRD(C22V) cargo, together with Erg11-GFP to mark the ER. A culture was grown to mid-log phase in NSD buffered at pH 6, treated with SLF for 30 min to allow secretion of the cargo, and mounted in a flow chamber. Unbuffered NSD (pH ~4) was added while imaging on a confocal microscope, with a Z-stack collected every 3 s. The top panel merges the cargo, Erg11-GFP, and bright-field channels, while the middle panel is the cargo alone and the bottom panel is the Erg11-GFP channel alone. The movie shows projections of the full Z-stacks. Scale bar, 2 µm. Frames from this movie are shown in Figure 3.6.

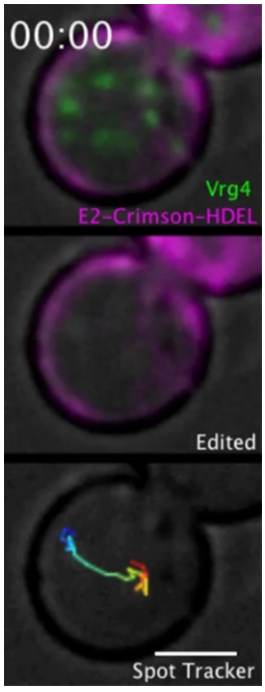

Movie 3.3. **Localization of a typical early Golgi cisterna relative to the cortical ER in a nocodazole-treated cell.** Cells expressed GFP-Vrg4 to mark early Golgi cisternae, together with E2-Crimson-HDEL to mark the ER. After treatment for 2 h with nocodazole, the daughter was imaged on a confocal microscope, with a Z-stack collected every 2 s. The top panel shows projections of eight optical sections from the center of the cell. The middle panel was edited to show only the cisterna being tracked. The bottom panel shows the results of analyzing the movements of that cisterna with the TrackMate plugin, with the start position marked in blue and the end position marked in red. Bright-field images of the cell are present in all panels. Because only the center of the cell is shown, the cortical ER appears primarily as a ring around the periphery of the cell, but some of the projections also include cortical ER signal from the top or bottom of the cell. Scale bar, 2 µm. Frames from this movie are shown in Figure 3.8 (A and B).

Movie 3.4. **Concentration of exported secretory cargo in a newly forming Golgi cisterna near an ERES.** Cells expressed the APVNTT-DsRed-Express2-FKBPRD(C22V) cargo, together with Sec31-HaloTag to mark ERES and GFP-Vrg4 to mark the early Golgi. A culture was grown to mid-log phase, labeled with JF_{646}, washed, and mounted in a flow chamber. Medium that contained SLF was added while imaging on a confocal microscope, with a Z-stack collected every 2 s. Cells were exposed to SLF 45 s before the beginning of the movie. The top panel shows the complete movie, with projections of the full Z-stacks. The second panel shows an edited movie of a representative cargo-containing structure and the associated ERES and early Golgi structures. The bottom three panels show the individual fluorescence channels. Bright-field images of the cell are present in all panels. Scale bar, 2 µm. Frames from this movie are shown in Figure 3.10.

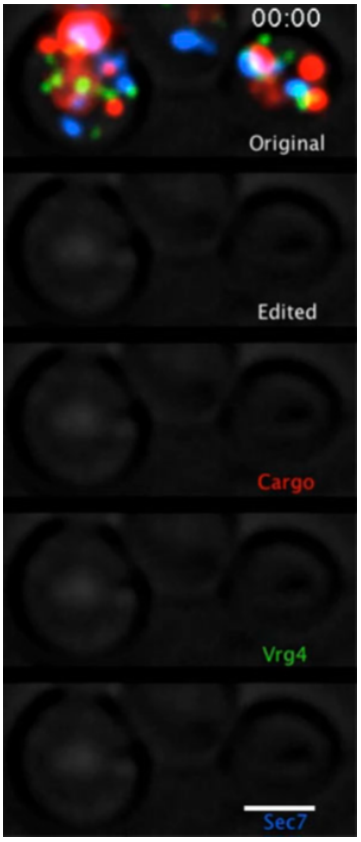

Movie 3.5. **Continuous presence of the fluorescent secretory cargo within maturing Golgi cisternae.** Cells expressed the APVNTT-DsRed-Express2-FKBPRD(C22V) cargo, together with GFP-Vrg4 to mark the early Golgi and Sec7-HaloTag to mark the late Golgi. A culture was grown to mid-log phase, labeled with JF_{646}, washed, and mounted in a flow chamber. Medium that contained SLF was added while imaging on a confocal microscope, with a Z-stack collected every 3 s. The top panel shows the complete movie, with projections of the full Z-stacks. The second panel shows an edited movie of two representative cisternae. The bottom three panels show the individual fluorescence channels. Bright-field images of the cells are present in all panels. Scale bar, 2 µm. Frames from this movie are shown in Figure 3.11.

Movie 3.6. **Traffic of cargo to a bleached cisterna during the early-to-late Golgi transition.** Cells expressed the APVNTT-DsRedExpress2-FKBPRD(C22V) cargo, together with GFP-Vrg4 to mark the early Golgi and Sec7-HaloTag to mark the late Golgi. A culture was grown to mid-log phase, treated for 2 h with nocodazole, labeled with JF_{646}, washed, and mounted in a flow chamber. Medium that contained SLF was added for 3 min before imaging on a confocal microscope. The cargo fluorescence in the entire daughter (identified by lack of a nuclear envelope signal) was bleached by illumination with 561-nm laser light at maximum intensity for ~40 s. Then Z-stacks were captured every 2 s. The movie begins shortly before the end of the bleaching period. The top panel shows the complete movie, with projections of the full Z-stacks. The second panel shows an edited movie of a representative cisterna. The bottom three panels show the individual fluorescence channels. Bright-field images of the cells are present in all panels. Scale bar, 2 µm. Frames from this movie are shown in Figure 3.12.

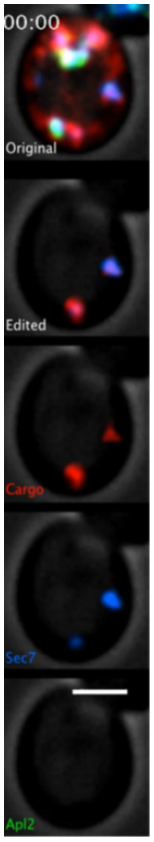

Movie 3.7. **Departure of cargo during terminal maturation of the late Golgi.** Cells expressed the aggregated APVNTT-DsRedExpress2-FKBPRD(C22V) cargo, together with Sec7-HaloTag to mark the late Golgi and Apl2-GFP to mark AP-1. A mid-log-phase culture was labeled with JF_{646}, then treated with SLF for 5 min before imaging with a confocal microscope. Z-stacks were captured every 1 s. The top panel shows the complete movie, with projections of the full Z-stacks. The second panel shows an edited movie of two representative cisternae. The bottom three panels show the individual fluorescence channels. Bright-field images of the cell are present in all panels. Scale bar, 2 µm. Frames from this movie are shown in Figure 3.14.

CHAPTER 4

A MICROSCOPY-BASED KINETIC ANALYSIS OF YEAST VACUOLAR PROTEIN SORTING

Abstract

The yeast *Saccharomyces cerevisiae* is amenable to studying membrane traffic by live-cell fluorescence microscopy. We used this system to explore two aspects of cargo protein traffic through prevacuolar endosome (PVE) compartments to the vacuole. First, at what point during Golgi maturation does a biosynthetic vacuolar cargo depart from the maturing cisternae? To address this question, we modified a regulatable fluorescent secretory cargo by adding a vacuolar targeting signal. Traffic of the vacuolar cargo requires the GGA clathrin adaptors, which arrive during the early-to-late Golgi transition. Accordingly, the vacuolar cargo begins to exit the Golgi near the midpoint of maturation, significantly before exit of a secretory cargo. Second, how are cargoes delivered from PVE compartments to the vacuole? To address this question, we tracked biosynthetic and endocytic cargoes after they had accumulated in PVE compartments. The results suggest that stable PVE compartments repeatedly deliver material to the vacuole by a kiss-and-run mechanism.

Introduction

Budding yeast has been instrumental for defining mechanisms of membrane traffic. Genetic screens of *Saccharomyces cerevisiae* have identified many conserved components of the biosynthetic and endocytic machineries (Kaiser et al., 1997; Novick et al., 1980). In addition, 4D (time-lapse 3D) fluorescence microscopy of *S. cerevisiae* has been powerful for characterizing membrane traffic pathways (Day et al., 2016; Kurokawa et al., 2013). Unlike most eukaryotes, *S. cerevisiae* has a non-stacked Golgi in which individual cisternae are optically

This chapter is a version of a manuscript published in eLife June 2020;9:e56844, with the same name and the following author list: J. C. Casler and B. S. Glick. I designed and carried out all experiments and wrote the manuscript. B. S. Glick helped design experiments, edited the manuscript, and supervised the project.

resolvable by fluorescence microscopy (Preuss et al., 1992; Wooding and Pelham, 1998). This property enabled the first direct visualization of Golgi cisternal maturation (Losev et al., 2006; Matsuura-Tokita et al., 2006) as well as later studies of how maturation is regulated by GTPases and vesicle coat proteins (Ishii et al., 2016; Kim et al., 2016; Papanikou et al., 2015; Rivera-Molina and Novick, 2009; Suda et al., 2013; Thomas and Fromme, 2020).

Observations of the yeast Golgi can be synthesized in the following scheme (Pantazopoulou and Glick, 2019). New Golgi cisternae arise at ER exit sites and capture biosynthetic cargoes from the ER. These cisternae then mature by recycling resident Golgi proteins to the ER and to younger cisternae. During the early stage of maturation, one set of resident Golgi membrane proteins recycles with the aid of the COPI vesicle coat, whereas during the late stage of maturation, another set of resident Golgi membrane proteins recycles with the aid of the AP-1 clathrin adaptor. Biosynthetic cargoes are present in the cisternae throughout the maturation process (Casler et al., 2019; Kurokawa et al., 2019). Finally, the terminally mature Golgi cisternae fragment into secretory vesicles.

Recently, we expanded this analysis by examining the *S. cerevisiae* endocytic pathway. Our work was based on earlier studies of prevacuolar endosome (PVE) compartments, which are multivesicular bodies reminiscent of mammalian late endosomes (Ma and Burd, 2020; Pelham, 2002). The evidence indicates that *S. cerevisiae* has a minimal endomembrane system in which the late Golgi, also known as the *trans*-Golgi network (TGN), plays an additional role as an early and recycling endosome (Day et al., 2018). According to this view, yeast cells have two types of endosomes: (a) the late Golgi/TGN, and (b) PVE compartments that are typically attached to the vacuole.

4D microscopy can integrate these pictures of the biosynthetic and endocytic pathways by enhancing our understanding of cargo delivery to the vacuole. Such experiments require a way to visualize the transport of a biosynthetic vacuolar cargo in live yeast cells. To this end, we built on our recent engineering of a regulatable fluorescent secretory cargo (Casler and Glick, 2019; Casler et al., 2019). A tetrameric red fluorescent protein is fused to

an improved dimerizing variant of the FK506-binding protein FKBP, and this construct is targeted to the ER lumen to generate aggregates, which are then solubilized with a ligand to create a fluorescent cargo wave that passes through the Golgi. We have now modified this construct by appending a tetrapeptide vacuolar targeting signal from the precursor to carboxypeptidase Y (CPY) (Valls et al., 1990). This targeting signal is recognized in the Golgi by the Vps10 cargo receptor (Marcusson et al., 1994), which in turn is packaged, with the aid of the GGA adaptors Gga1 and Gga2, into clathrin-coated vesicles destined for PVE compartments (reviewed in Myers and Payne, 2013). The result is that we have a regulatable fluorescent biosynthetic vacuolar cargo, which can be tracked as it moves from the ER through the Golgi to PVE compartments and then to the vacuole.

Our data extend prior results from other methods, which revealed the existence of traffic pathways for both biosynthetic and endocytic vacuolar cargoes. Biosynthetic vacuolar cargoes initially move from the ER to the Golgi. Some vacuolar membrane proteins traffic directly from the Golgi to the vacuole with the aid of the Golgi-associated AP-3 adaptor complex (Cowles et al., 1997; Llinares et al., 2015; Odorizzi et al., 1998). By contrast, CPY and certain other vacuolar hydrolases first traffic from the Golgi to PVE compartments (Conibear and Stevens, 1998; Vida et al., 1993). The same PVE compartments also contain endocytosed cargoes, such as the methionine permease Mup1, that are in transit to the vacuole (Menant et al., 2006). Within PVE compartments, transmembrane cargo proteins such as Mup1 are packaged into intraluminal vesicles that are transferred from the PVE compartments to the vacuole, where the intraluminal vesicles are degraded (MacDonald et al., 2012). Despite these insights, the understanding of vacuolar protein sorting remains incomplete. We have focused on two questions.

First, how is traffic from the Golgi to PVE compartments coordinated with cisternal maturation? The conventional view is that biosynthetic cargoes all travel together through the Golgi until reaching a terminal sorting stage (De Matteis and Luini, 2008; Griffiths and Simons, 1986), implying that vacuolar cargoes would remain in a cisterna throughout the

maturation process. However, this idea is called into question by studies of GGA dynamics at the Golgi. We have now replicated work from the Payne lab showing that GGAs arrive earlier than AP-1 and at about the same time as Sec7 (Daboussi et al., 2012), an Arf guanine nucleotide exchange factor that is recruited and activated during the early-to-late Golgi transition (Losev et al., 2006; McDonold and Fromme, 2014). In addition, as described below, we have now tracked the passage of a fluorescent biosynthetic vacuolar cargo through the Golgi. The results indicate that the vacuolar cargo begins to depart when GGAs arrive, well before the final maturation of late Golgi cisternae into secretory vesicles. Thus, the late/TGN stage of Golgi maturation can be divided into a first sub-stage marked by the exit of vacuolar cargoes to PVE compartments, followed by a second sub-stage marked by AP-1-dependent intra-Golgi recycling and by the exit of secretory cargoes to the plasma membrane.

Second, how is material transferred from PVE compartments to the vacuole? Again, the answer was thought to be known, but 4D microscopy offers a new perspective. By analogy to mammalian cells, it was assumed that in yeast, early endosomes would mature into PVE compartments that would be consumed by fusing with the vacuole (Balderhaar and Ungermann, 2013; Feyder et al., 2015). Yet maturation of PVE compartments has not been observed—and indeed, if we are correct that yeast cells lack distinct early endosomes, then maturation of yeast endosomes is logically precluded (Day et al., 2018). The implication is that PVE compartments are not continually regenerated and must therefore be stable organelles. In support of this concept, our previous live-cell imaging revealed that PVE compartments undergo fusion and fission but otherwise persist indefinitely (Day et al., 2018). Evidence presented here suggests that stable PVE compartments deliver their contents to the vacuole by transient kiss-and-run fusion events.

Results

Addition of a tetrapeptide generates a fluorescent biosynthetic vacuolar cargo

To create a wave of fluorescent vacuolar cargo, we modified a recently developed regulatable fluorescent secretory cargo (Casler and Glick, 2019; Casler et al., 2019). Our secretory cargo consists of the tetrameric red fluorescent protein DsRed-Express2 fused to a dimerizing variant of FKBP, with a cleavable N-terminal signal sequence to direct cotranslational translocation into the ER. The signal sequence is followed by a tripeptide ER export signal (Yin et al., 2018) and a signal for N linked glycosylation (Figure 4.1B). This fusion protein forms fluorescent aggregates within the ER lumen, and the aggregates can be dissolved by adding a synthetic ligand of FKBP (SLF) that blocks dimerization of FKBP (Figure 4.1A). Soluble tetramers then exit the ER in a nearly synchronized wave. Efficient dissolution of the aggregates requires a drug-sensitive yeast strain. Thus, all of our experiments with the regulatable cargoes employed yeast strains containing deletions of the transcription factors Pdr1 and Pdr3, which mediate pleiotropic drug resistance (Barrero et al., 2016; Casler et al., 2019; Coorey et al., 2015; Schüller et al., 2007). We found previously that the regulatable secretory cargo persists in cisternae through the early-to-late transition of Golgi maturation, and that a fraction of the cargo molecules are recycled within the Golgi in an AP-1-dependent manner (Casler et al., 2019). The goal was to perform similar experiments with a modified cargo that was targeted to the vacuole.

Our strategy was to augment the fusion protein with a vacuolar targeting signal. An obvious candidate for this signal was the propeptide of the vacuolar hydrolase CPY. Prior studies showed that within the propeptide, the tetrapeptide QRPL is necessary and sufficient to direct CPY from the Golgi to PVE compartments by means of the sorting receptor Vps10 (Johnson et al., 1987; Marcusson et al., 1994; Valls et al., 1987; Valls et al., 1990). We flanked QRPL with glycine/serine spacers by appending at the C ¬terminus of the fusion protein the peptide GSQRPLGGS (Figure 4.1B). The C terminus was chosen because insertion of

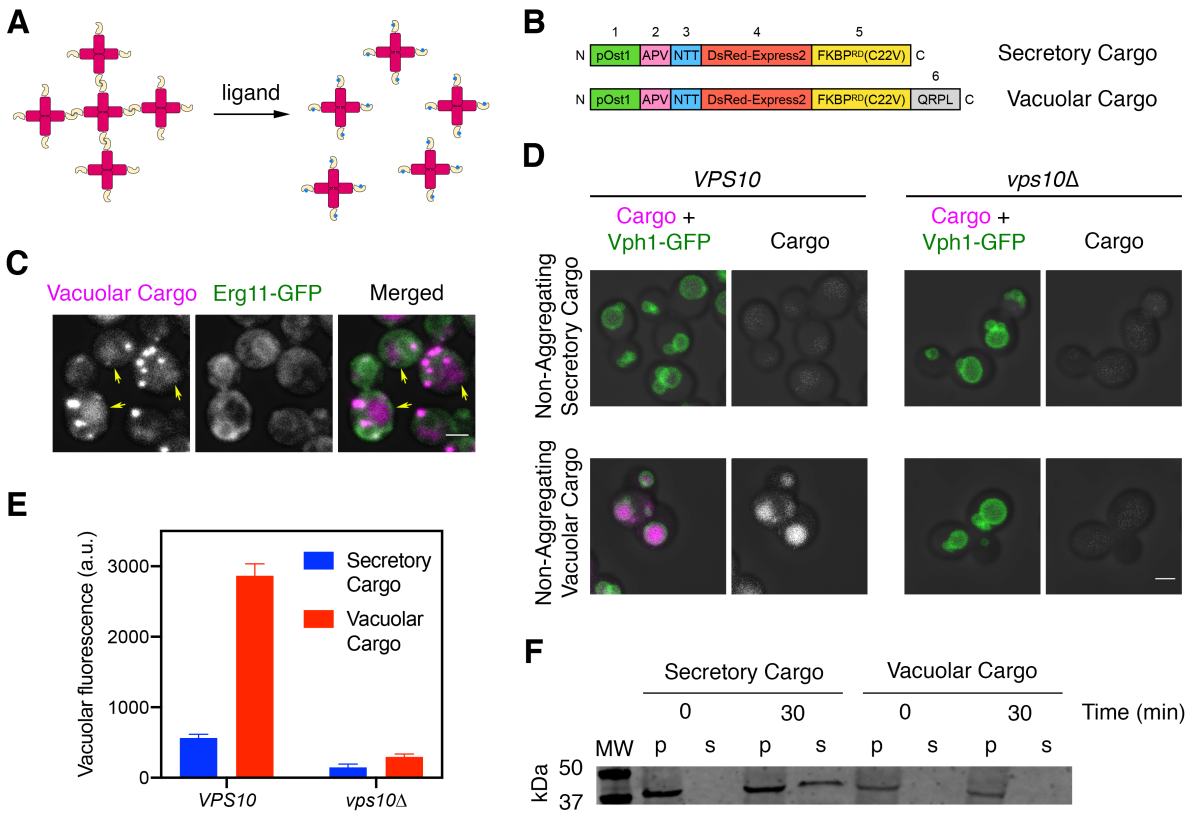

Figure 4.1: **A regulatable vacuolar cargo. (A)** General strategy for the use of reversibly aggregating fluorescent cargoes. DsRed-Express2 tetramers (red) are linked to a dimerizing FKBP variant (gold), so the tetramers associate to form aggregates. Addition of the FKBP ligand SLF (blue) blocks dimerization, thereby dissolving the aggregates into soluble tetramers that can exit the ER. **(B)** Functional regions of the reversibly aggregating secretory and vacuolar cargoes. The lengths of the regions are not to scale. 1: pOst1 (green) is an ER signal sequence that directs cotranslational translocation. 2: APV (pink) is a tripeptide signal for ER export. 3: NTT (blue) is a tripeptide signal for N-linked glycosylation. 4: DsRed-Express2 (red) is a tetrameric red fluorescent protein. 5: $FKBP^{RD}$(C22V) (gold) is a reversibly dimerizing variant of FKBP. 6: QRPL (gray) is a tetrapeptide signal for vacuolar targeting. **(C)** Aggregation in the ER of the vacuolar cargo. The ER membrane marker Erg11-GFP (green) confirms that the aggregates (magenta) are in the ER. Yellow arrows point to leaked cargo molecules that have accumulated in the vacuole. Shown are projected confocal Z-stacks. Scale bar, 2 µm. **(D)** Vacuolar targeting by the QRPL tetrapeptide. Non-aggregating variants of the secretory and vacuolar cargoes were expressed in *VPS10* wild-type or *vps10*Δ cells to visualize receptor-dependent targeting to the vacuole, which was marked by the vacuolar membrane marker Vph1-GFP. Significant vacuolar accumulation was seen only in the *VPS10* background when the QRPL signal was present. Shown are projected confocal Z stacks. Scale bar, 2 µm.

Figure 4.1: **(E)** Quantification of the cargo fluorescence signals in (D). The Vph1-GFP signal was used to create a mask for measuring cargo fluorescence in the vacuole. Data are average values from at least 69 cells for each strain. Fluorescence is plotted in arbitrary units (a.u.). Bars represent SEM. **(F)** Immunoblot to measure cell-associated and secreted levels of the secretory and vacuolar cargoes after SLF addition in rich medium. Cells expressing either the secretory or vacuolar cargo were grown to mid-log phase in YPD, washed with fresh YPD, and treated with SLF. At the 0- and 30-min time points, cell-associated pellet ("p") and secreted soluble ("s") fractions were separated by centrifugation. Samples were treated with endglycosidase H to trim N linked glycans, and were analyzed by SDS-PAGE and immunoblotting. Shown is a representative example from four separate experiments. MW, molecular weight markers. The predicted molecular weights for the mature cargoes are ~38-39 kDa. In some samples, the cell-associated vacuolar cargo at the 30-min time point showed evidence of degradation, presumably due to exposure to vacuolar proteases (data not shown).

QRPL near the N terminus of the mature protein prevented robust ER aggregation (data not shown). Addition of the QRPL-containing peptide at the C terminus preserved the formation of aggregates within the lumen of the ER, which was marked by GFP-tagged Erg11 (Figure 4.1C). Some cargo molecules were already present in the vacuole prior to dissolution of the aggregates (arrows in Figure 4.1C), presumably because signal-dependent ER exit allowed a fraction of the cargo molecules to escape from the ER and reach the vacuole while others became trapped in ER-localized aggregates (Casler et al., 2019). Based on these observations, the QRPL-containing construct was a candidate for a regulatable fluorescent vacuolar cargo. To test if the QRPL signal worked as intended, we tested non-aggregating (and therefore non-regulatable) versions of the secretory and vacuolar cargoes. The vacuolar membrane was visualized with Vph1-GFP. Compared to the non-aggregating secretory cargo, which accumulated at low levels in the vacuole (Casler et al., 2019), the non-aggregating vacuolar cargo accumulated at high levels in the vacuole in a Vps10-dependent manner (Figure 4.1D,E). A final control experiment employed the regulatable versions of the cargoes once again. At 30 min after addition of SLF, the regulatable secretory cargo was detected in the culture medium whereas the regulatable vacuolar cargo was not (Figure 4.1F). These results confirm that the vacuolar cargo traffics efficiently to the vacuole. For

convenience, from now on we will refer to the regulatable fluorescent secretory cargo and the regulatable fluorescent vacuolar cargo as the secretory and vacuolar cargoes, respectively.

Traffic of the vacuolar cargo can be visualized

We first measured the overall rate of cargo traffic from the ER to the vacuole. A *VPS10* wild-type strain and a *vps10*Δ mutant strain expressed the vacuolar cargo together with the vacuole marker Vph1-GFP. After SLF was added to initiate cargo transport, the cells were imaged by 4D confocal microscopy for 60 min (Movie 4.1 and Figure 4.2A-C). With *VPS10* cells, we saw a gradual accumulation of fluorescence in the vacuole. With *vps10*Δ cells, virtually no fluorescence appeared in the vacuole, presumably because the cargo exited the cell in secretory vesicles (see below, Figure 4.11). In typical *VPS10* cells, small amounts of the cargo were detected in the vacuole within 8-15 min after SLF addition, and full delivery to the vacuole required at least 40 min (Figure 4.2B,C). Individual cells showed significant variations in the timing of cargo traffic. About 35% of the cells required more than 15 min and in some cases, more than 25 min—before any cargo appeared in the vacuole (Figure 4.2B,D). On average, the cell population showed a gradual increase in vacuolar fluorescence over a time course of an hour (Figure 4.2C).

A potential concern with this analysis is that during the time interval examined, new cargo molecules were being synthesized, and some of those molecules could have become fluorescent and reached the vacuole. We addressed this issue by repeating the experiment after pre-treating the cells with cycloheximide to block protein synthesis. Following SLF addition, untreated and cycloheximide-treated cells showed similar traffic kinetics, with cycloheximide causing only a modest reduction in the amount of cargo accumulating in the vacuole even though cell growth was arrested (Figure 4.3). We conclude that to a close approximation, the kinetics observed in the absence of cycloheximide reflect traffic of the vacuolar cargo molecules that were originally in ER-localized aggregates.

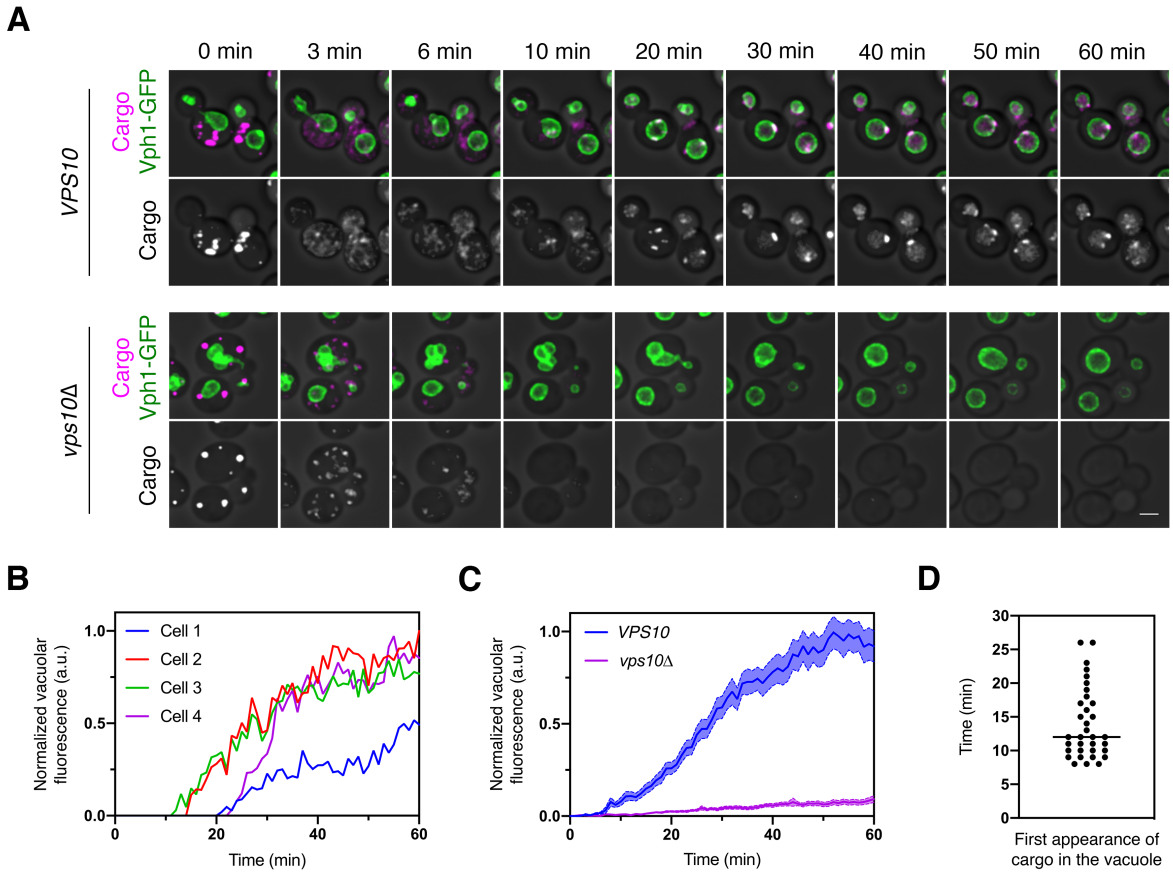

Figure 4.2: **Traffic kinetics of the vacuolar cargo. (A)** Visualizing cargo traffic. The vacuolar cargo expressed in *VPS10* wild-type or *vps10*Δ strains was imaged by 4D confocal microscopy. Prior to the movie, fluorescence from leaked cargo molecules was bleached by illuminating the vacuole with a 561-nm laser at maximum intensity for 20-30 s. Then SLF was added, and Z-stacks were captured every minute for 60 min. The top panel shows the cargo (magenta) together with the vacuolar membrane marker Vph1-GFP (green), while the bottom panel shows only the cargo. Fluorescence data are superimposed on brightfield images of the cells. Shown are representative frames from Movie 1. Scale bar, 2 µm. **(B)** Quantification of the vacuolar fluorescence from each of the four *VPS10* cells in (A). The Vph1-GFP signal was used to create a mask for measuring cargo fluorescence in the vacuole. Fluorescence is plotted in arbitrary units (a.u.). **(C)** Quantification of the average vacuolar fluorescence in *VPS10* and *vps10*Δ cells after addition of SLF. For each strain, at least 39 cells were analyzed from four movies. Quantification was performed as in (B). The shaded borders represent SEM. **(D)** Quantification of the first appearance of cargo fluorescence in the vacuole. Data are from the same set of *VPS10* cells analyzed for (C). Appearance in the vacuole was scored as the first time point at which the vacuolar cargo fluorescence reached at least 5% of its final value.

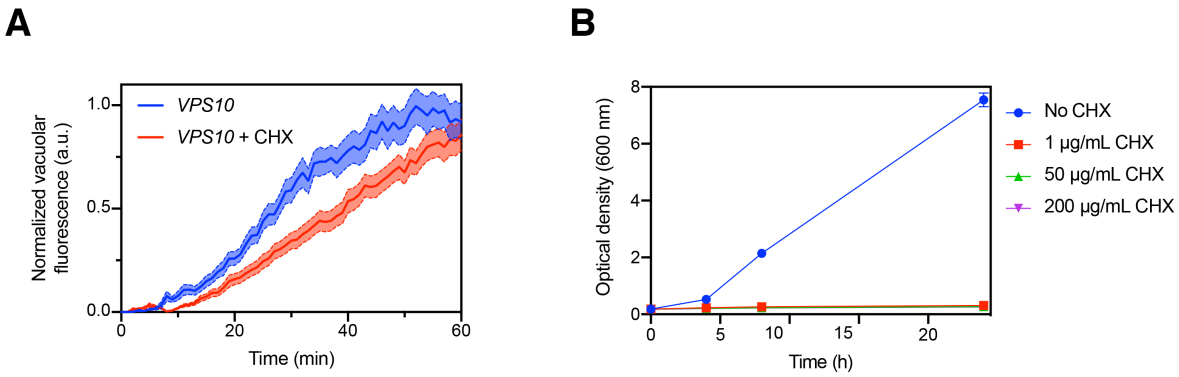

Figure 4.3: **Minor effect of cycloheximide treatment on the kinetics of cargo traffic to the vacuole. (A)** Comparison of traffic kinetics in the absence or presence of cycloheximide (CHX). Data from Figure 4.2C were re-plotted with the additional analysis of *VPS10* cells that had been pretreated with 200 µg/mL cycloheximide starting 15 min prior to addition of SLF. **(B)** Control experiment to confirm that cycloheximide potently inhibited protein synthesis. A log-phase culture of *VPS10* cells in YPD medium was diluted to an OD_{600} of 0.2, and growth of the culture was measured over 24 h with or without addition of cycloheximide at the indicated concentrations.

Why is traffic to the vacuole so slow? For comparison, secretory cargo molecules can travel from the ER to the plasma membrane within 5-10 min, and nearly all of them are secreted within 20 min (Casler et al., 2019; Losev et al., 2006). This effect is seen in the *vps10*Δ cells because in the absence of a sorting receptor, the vacuolar cargo behaves like a secretory cargo (Figure 4.2A). To understand the slow kinetics of cargo delivery to the vacuole, we set out to track the different steps of this pathway by fluorescence microscopy.

The vacuolar cargo transits rapidly through the Golgi and accumulates in PVE compartments

Early work suggested that the rate-limiting step in biosynthetic cargo transport to the vacuole is exit from PVE compartments (Vida et al., 1993). To test this idea, we used 4D confocal movies to visualize the vacuolar cargo together with organellar markers. PVE compartments were labeled by tagging Vps8, a subunit of the CORVET tethering complex (Arlt et al., 2015; Markgraf et al., 2009). We showed previously that tagged Vps8 colocalized strongly with a

variety of other PVE compartment markers, and that the observed dynamics of PVE compartments were similar when using either tagged Vps8 or other markers (Day et al., 2018). For three-color 4D movies, the red fluorescent vacuolar cargo was visualized together with the early Golgi marker GFP-Vrg4 and the late Golgi marker Sec7-HaloTag, or together with the PVE marker Vps8-GFP and the vacuole marker Vph1-HaloTag (Arlt et al., 2015; Day et al., 2018; Losev et al., 2006). In this and subsequent experiments, HaloTag was conjugated to the far-red dye JF_{646} (Grimm et al., 2015). After the cargo aggregates were solubilized with SLF, a strain expressing the vacuolar cargo plus the Golgi markers was imaged every 30 s for 29.5 min, and a strain expressing the vacuolar cargo plus the PVE and vacuole markers was imaged every 60 s for 60 min. The results showed cargo accumulation within Golgi compartments 1-5 min after SLF addition, followed by nearly complete transfer of the cargo to PVE compartments by 10 min (Movie 4.2, Movie 4.3, and Figure 4.4A-D). After 10 min, puncta that contained the cargo invariably labeled with Vps8-GFP, confirming that Vps8 is a reliable marker for PVE compartments. The cargo gradually exited the PVE compartments and then accumulated in the vacuole as described above. Interestingly, even though the PVE compartments contained cargo by 10 min, some of them did not immediately begin to transfer cargo to the vacuole (see Figure 4.2B,D), suggesting that PVE compartments can be temporarily quiescent with regard to cargo delivery. These results verify that the rate-limiting step in traffic to the vacuole is not movement through the Golgi, but rather transfer of the cargo from PVE compartments to the vacuole.

Interestingly, although most of the early Golgi cisternae contained detectable vacuolar cargo at early time points, only about half of the late Golgi cisternae ever contained detectable vacuolar cargo (Figure 4.4C). By contrast, we previously saw that the fluorescent secretory cargo was present in nearly all of the late Golgi cisternae, where it persisted until the final phase of maturation (Casler et al., 2019). A possible explanation is that the vacuolar cargo departed during the late stage of Golgi maturation, so that as late Golgi cisternae

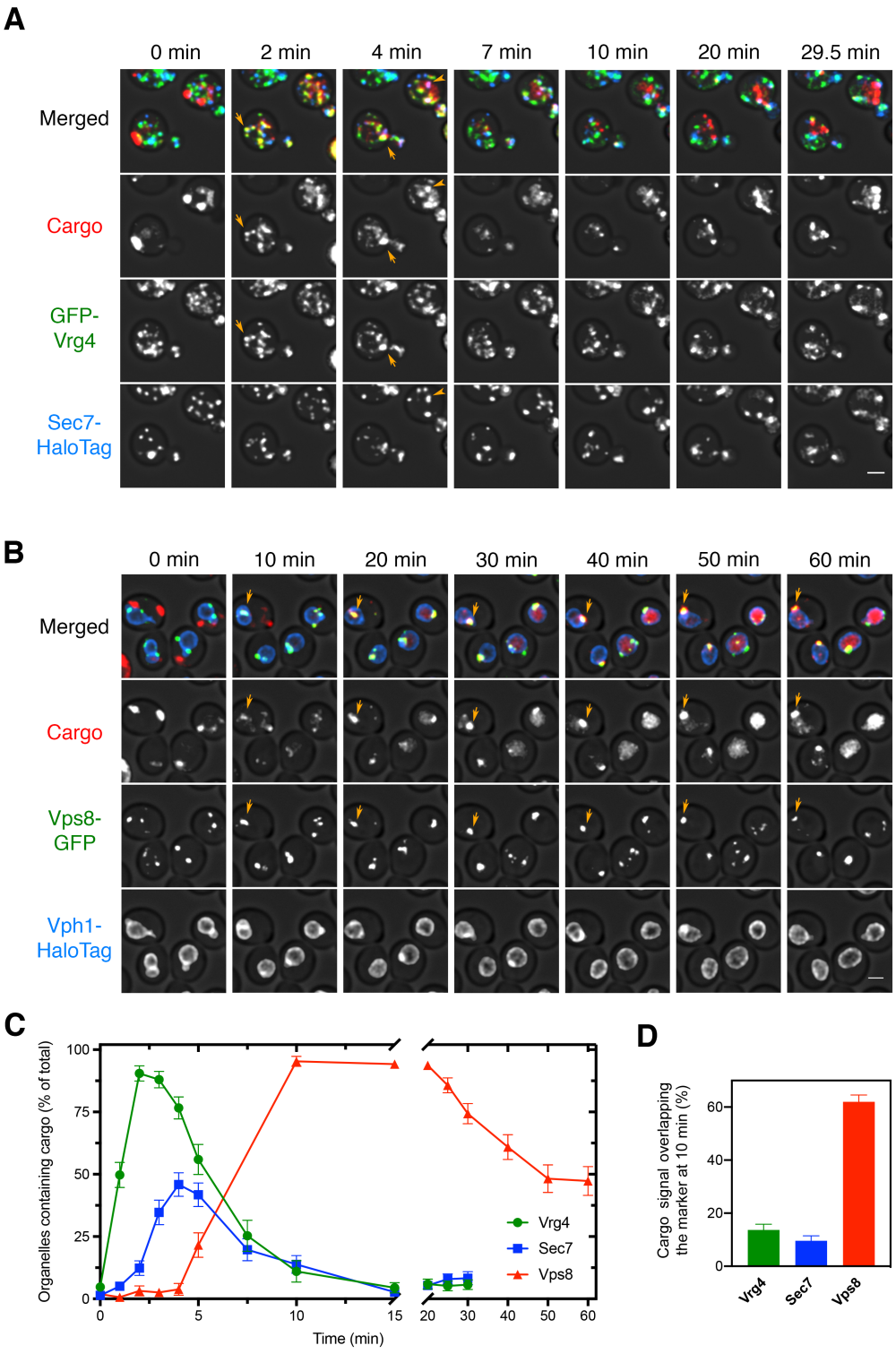

Figure 4.4: **Sequential appearance of the vacuolar cargo in Golgi and PVE compartments.** *continued on next page.*

Figure 4.4: **(A)** Appearance of the vacuolar cargo in early Golgi compartments marked with GFP-Vrg4 and in late Golgi compartments marked with Sec7-HaloTag. Cells were grown to mid-log phase, labeled with JF_{646}, and imaged by 4D confocal microscopy. Prior to beginning the movie, fluorescence from leaked cargo molecules in the vacuole was bleached by illuminating with maximum intensity 561 nm laser power for 20-30 s. SLF was added directly to the dish between the first and second Z-stacks, and then additional Z-stacks were captured every 30 s for 29.5 min. Images are representative time points from Movie 4.2. The top panel shows the merged images, and the other panels show the individual fluorescence channels for cargo, Vrg4, and Sec7. Scale bar, 2 µm. **(B)** Appearance of the vacuolar cargo in PVE compartments marked with Vps8-GFP and in the vacuole marked with Vph1-HaloTag. The procedure was as in (A), except that Z stacks were captured every 60 s for 60 min. Images are representative time points from Movie 4.3. The top panel shows the merged images, and the other panels show the individual fluorescence channels for cargo, Vps8, and Vph1. Scale bar 2 µm. **(C)** Quantification of the percentage of compartments containing detectable cargo from (A) and (B). Confocal movies were average projected and manually scored for the presence of cargo in labeled compartments. For each strain, at least 26 cells were analyzed from four movies. The bars represent SEM. **(D)** Quantification of the percentage of the total cargo fluorescence present in early Golgi, late Golgi, and PVE compartments 10 min after SLF addition. The fluorescence for a compartment marker was used to generate a mask to quantify the corresponding cargo fluorescence. Data were taken from at least 26 cells from four movies. The bars represent SEM.

became more mature, they no longer contained fluorescent cargo. To test this hypothesis, we next visualized the dynamics of the vacuolar cargo in maturing Golgi cisternae.

The vacuolar cargo begins to exit the Golgi near the midpoint of cisternal maturation

To determine when the vacuolar cargo departs from maturing cisternae, we performed 4D confocal microscopy of yeast cells expressing the vacuolar cargo, the early Golgi marker GFP-Vrg4, and the late Golgi marker Sec7-HaloTag. As previously described, we readily detected Golgi maturation events in which GFP-Vrg4-labeled cisternae lost the GFP-Vrg4 signal as they acquired Sec7-HaloTag, which they subsequently lost in the final phase of maturation (Casler et al., 2019; Losev et al., 2006). Intriguingly, the vacuolar cargo signal always began to decline near the midpoint of maturation (Movie 4.4, Figure 4.5A,B, and Figure 4.6A-C). The rate of decline varied between cells, and qualitative observations indicated that the

decline was slower in cells expressing very high levels of the vacuolar cargo (data not shown), probably because the sorting machinery was saturated. Therefore, we focused the analysis on cells expressing moderate levels of the vacuolar cargo. The average behavior from 21 maturation events is depicted in Figure 4.5C.

We predicted that removal of the Vps10 sorting receptor would prevent normal exit of the vacuolar cargo, which would then behave like a secretory cargo. This prediction was tested by tracking the vacuolar cargo during Golgi maturation in a *vps10*Δ mutant. In the absence of Vps10, the vacuolar cargo signal no longer declined during the early-to-late transition (Movie 4.5, Figure 4.5D-F, and Figure 4.6D-F). Instead, *vps10*Δ cells actually displayed a transient increase in the cargo signal during the early-to-late transition, likely due to AP-1-dependent recycling from older cisternae as previously shown for the fluorescent secretory cargo (Casler et al., 2019). These data indicate that in wild-type cells, the vacuolar cargo begins to exit the Golgi in a Vps10-dependent manner around the time of the early-to-late transition.

GGAs but not AP-1 are required to sort the vacuolar cargo

To characterize how the vacuolar cargo exits the Golgi, we tested the roles of the AP-1 clathrin adaptor and of the GGA clathrin adaptors Gga1 and Gga2. AP-1 was originally proposed to mediate transport of proteins from the TGN to endosomes (reviewed in Hinners and Tooze, 2003), but subsequent work implicated GGAs in TGN-to-endosome traffic in both yeast and mammalian cells (Black and Pelham, 2000; Dell'Angelica et al., 2000; Hirst et al., 2000; Zhdankina et al., 2001). In *S. cerevisiae*, AP-1 localizes exclusively to the late Golgi, and it mediates intra-Golgi recycling of some resident late Golgi proteins and secretory cargoes (Casler and Glick, 2019; Day et al., 2018; Liu et al., 2008; Papanikou et al., 2015; Spang, 2015; Valdivia et al., 2002). It was previously reported that yeast GGAs function upstream of AP 1 and that GGAs display similar kinetics of arrival and departure as the late Golgi reference marker Sec7 (Daboussi et al., 2012). However, a somewhat different

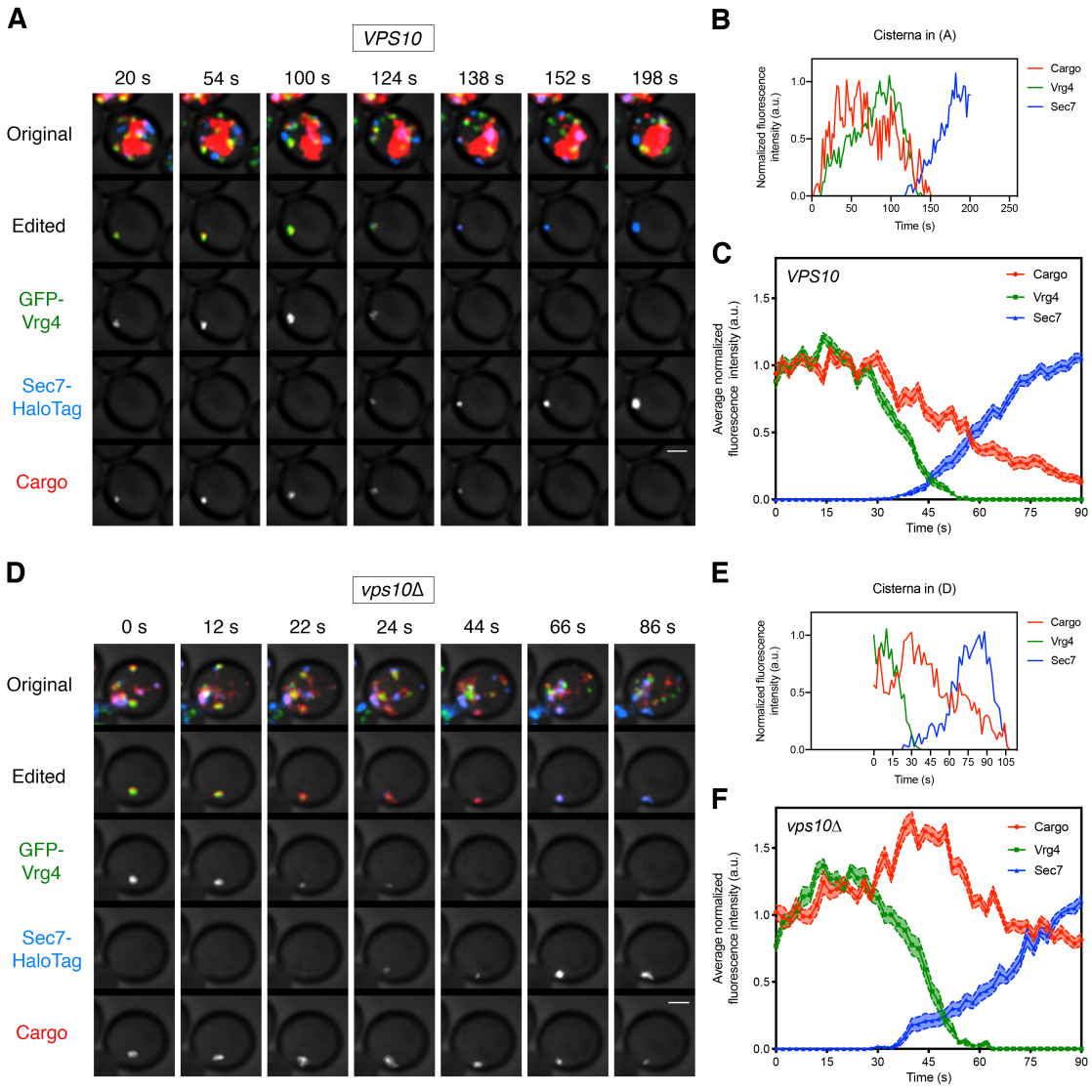

Figure 4.5: **Visualizing the vacuolar cargo during Golgi maturation. (A)** Visualizing the vacuolar cargo in a *VPS10* wild-type strain. Cells expressing the vacuolar cargo together with the early Golgi marker GFP-Vrg4 and the late Golgi marker Sec7-HaloTag were grown to mid-log phase, labeled with JF_{646}, and imaged by 4D confocal microscopy. SLF was added 1-3 min before imaging. Shown are average projected Z-stacks at representative time points from Movie 4.4. The top row shows the complete projection, the second row shows an edited projection that includes only the cisterna being tracked, and the other rows show the individual fluorescence channels from the edited projection. The large red structure is the vacuole, which contained cargo molecules that had escaped from the ER prior to SLF addition as described in Figure 4.1. Scale bar, 2 µm. **(B)** Quantification of the fluorescence intensities of the Golgi markers and the vacuolar cargo during a typical maturation event. Depicted are the normalized fluorescence intensities in arbitrary units (a.u.) of the cisterna tracked in (A).

Figure 4.5: **(C)** Average cargo signal during the early-to-late Golgi transition. For 21 maturation events from 18 movies of cells expressing moderate levels of the vacuolar cargo, fluorescence was quantified over a 90 s window with Z-stacks collected every 2 s. Normalization was performed by defining the maximum value as the average of the first six fluorescence values for the cargo and Vrg4, or of the last six fluorescence values for Sec7. Traces were aligned at the midpoint of the Vrg4-to-Sec7 transition, and the normalized fluorescence signals were averaged. The shaded borders represent SEM. **(D)** Visualizing the vacuolar cargo in a *vps10*Δ strain. The experiment was performed as in (A). Shown are average projected Z stacks at representative time points from Movie 4.5. **(E)** Quantification of the fluorescence intensities of the Golgi markers and the vacuolar cargo during a typical maturation event in the *vps10*Δ strain. Depicted are the normalized fluorescence intensities in arbitrary units (a.u.) of the cisterna tracked in (D). **(F)** Average cargo signal during the early-to-late Golgi transition in a *vps10*Δ strain. The experiment was performed as in (C). Data were collected for 12 maturation events from 12 movies of cells expressing moderate levels of the vacuolar cargo.

conclusion was presented in a more recent study, which reported that GGAs arrived at Golgi cisternae significantly later than Sec7 (Tojima et al., 2019). To clarify the functions of these adaptors in sorting the vacuolar cargo, we combined a kinetic analysis of AP-1 and GGA dynamics with tests of deletion mutants.

If a given adaptor is involved in transporting the vacuolar cargo out of the Golgi, then arrival of that adaptor is expected to coincide with initiation of cargo departure. In a kinetic analysis, we first compared Sec7 with the AP-1 subunit Apl2 and with the major GGA isoform Gga2 (Myers and Payne, 2013). Three-color imaging was performed with Apl2-GFP, Gga2-HaloTag, and Sec7-mScarlet. Gga2 consistently showed arrival and departure kinetics nearly identical to those of Sec7, whereas Apl2 consistently arrived ∼20-40 s later and departed ∼10-15 s later than Gga2 and Sec7 (Movie 4.6, Figure 4.7A,B and 4.8A-C). Thus, GGAs arrive at the Golgi at about the same time that the vacuolar cargo begins to depart. Indeed, when the vacuolar cargo was visualized in maturing cisternae together with the early Golgi marker GFP-Vrg4 and with Gga2-HaloTag, the first appearance of Gga2 occurred at about the same time that the vacuolar cargo signal started to decline (Movie 4.7, Figure 4.7C,D, and Figure 4.8D). Interestingly, the cargo signal sometimes began to drop a short time before Gga2 was visible at the Golgi. A potential explanation is that

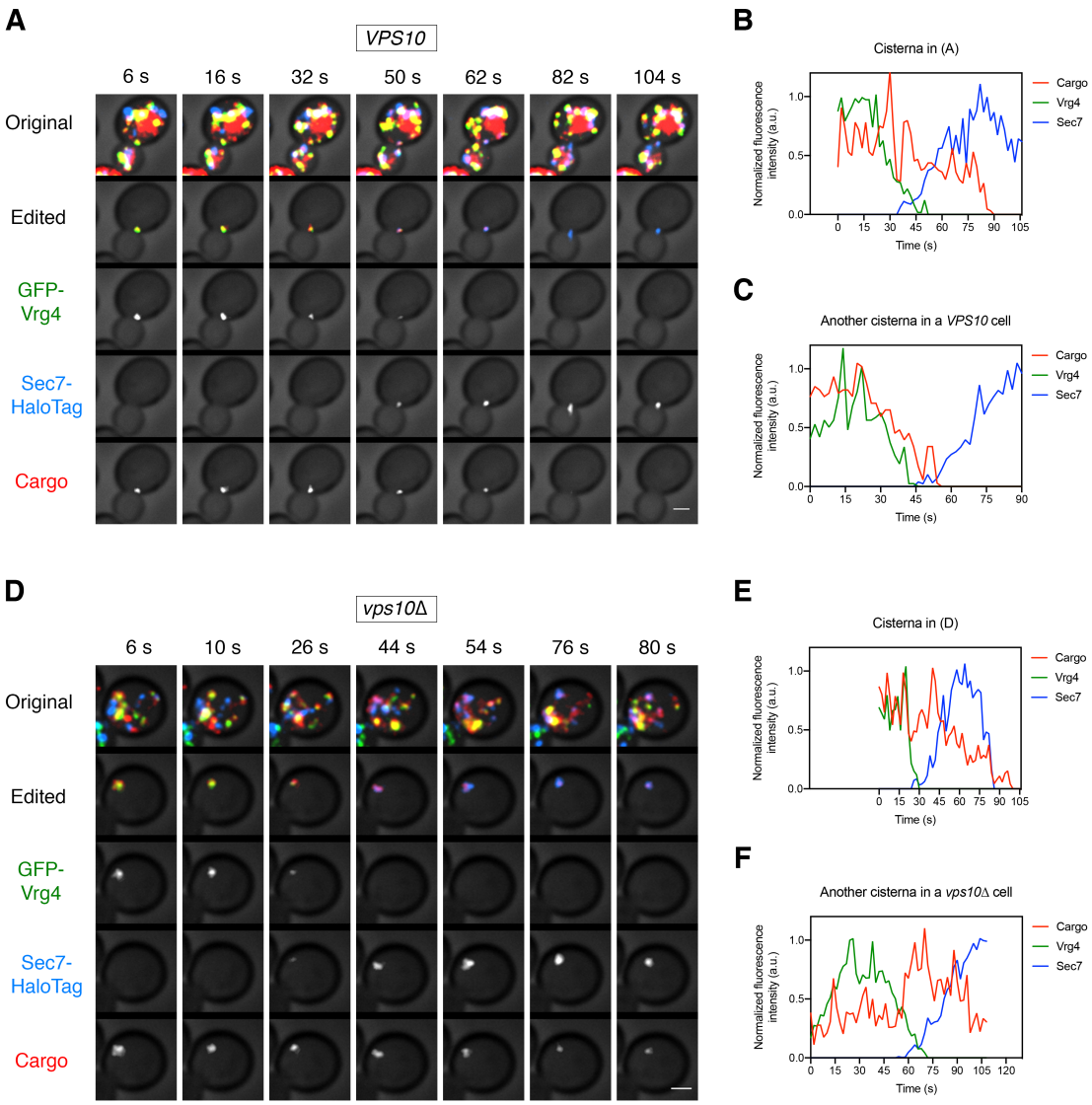

Figure 4.6: **Additional examples of vacuolar cargo traffic during Golgi maturation.** **(A)** Vacuolar cargo traffic in a VPS10 wild-type strain. The experiment was performed as in Figure 4.5A. Shown are average projected Z-stacks at representative time points from an additional movie. The top row shows the complete projection, the second row shows an edited projection that includes only the cisterna being tracked, and the other rows show the individual fluorescence channels from the edited projection. Scale bar, 2 µm. **(B)** Quantification of the fluorescence intensities of the Golgi markers and the vacuolar cargo during maturation of the cisterna tracked in (A). The procedure was as in Figure 4.5B. **(C)** Quantification of a maturation event from an additional movie of a *VPS10* cell. **(D)** – **(F)** Same as (A) – (C), except that the analysis was performed with a *vps10*Δ strain.

when GGAs are first recruited, they are immediately packaged into vesicles that transport vacuolar cargoes from the Golgi, so the pool of Golgi-associated Gga2 initially remains low.

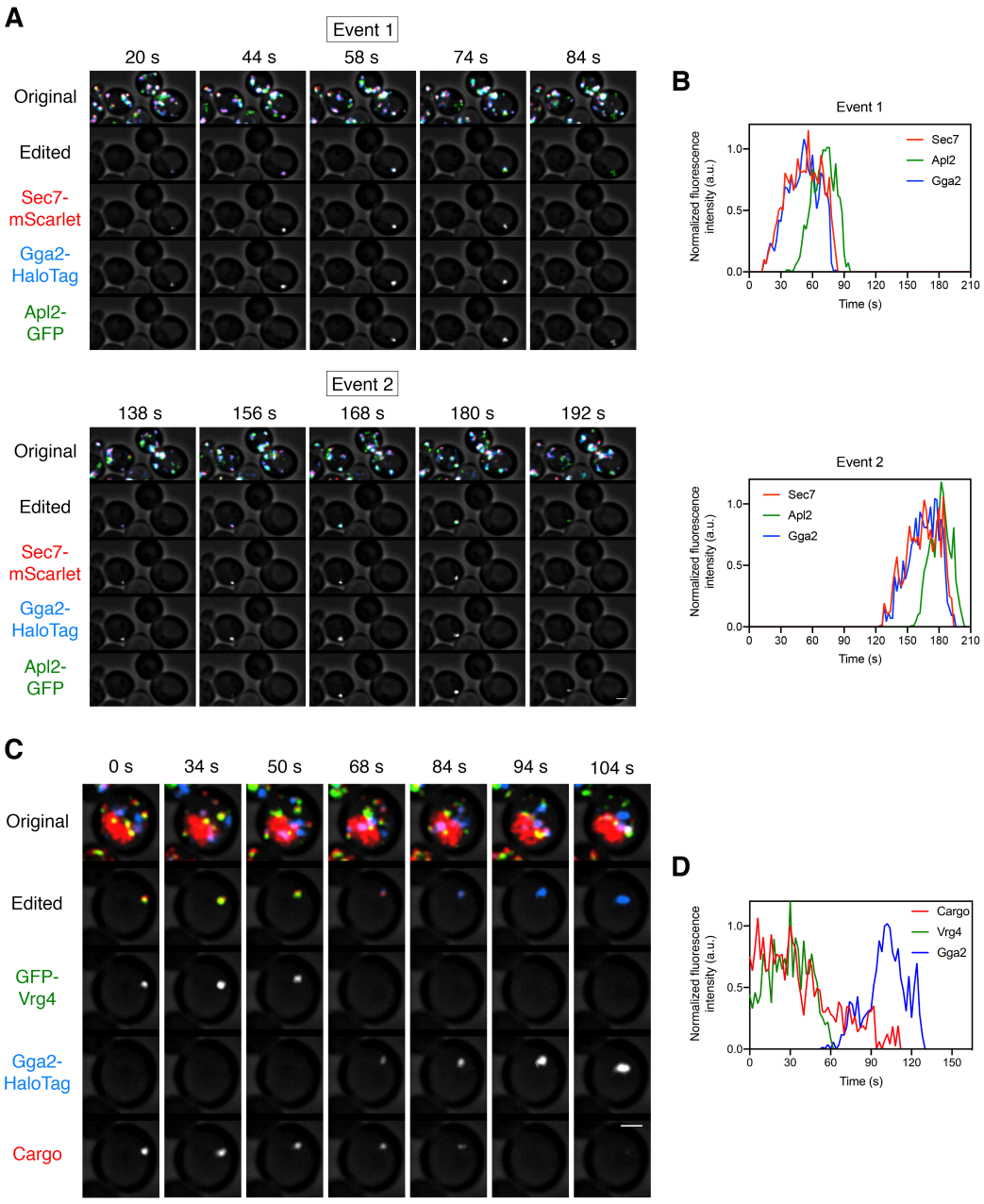

Figure 4.7: **Kinetics of GGA arrival at the Golgi. (A)** Visualizing the dynamics of the GGA and AP-1 adaptors during cisternal maturation. A strain expressing the GGA protein Gga2-HaloTag, the AP-1 subunit Apl2-GFP, and the late Golgi marker Sec7-mScarlet was grown to mid-log phase, labeled with JF_{646}, and imaged by 4D confocal microscopy. Shown are average projected Z-stacks at representative time points from Movie 4.6. The top row shows the complete projection, the second row shows an edited projection that includes only the cisterna being tracked, and the other rows show the individual fluorescence channels from the edited projection. Two maturation events are highlighted. Scale bar, 2 µm.

Figure 4.7: **(B)** Quantification of the fluorescence intensities of the late Golgi marker and the adaptors during typical maturation events. Depicted are the normalized fluorescence intensities in arbitrary units (a.u.) of the two cisternae tracked in (A). **(C)** Visualizing Vrg4 and Gga2 together with the vacuolar cargo. The experiment was performed as in Figure 4.5A, except that the Golgi markers were GFP-Vrg4 and Gga2-HaloTag. Shown are average projected Z-stacks at representative time points from Movie 4.7. The top row shows the complete projection, the second row shows an edited projection that includes only the cisterna being tracked, and the other rows show the individual fluorescence channels from the edited projection. Scale bar, 2 µm. **(D)** Quantification of the fluorescence intensities of the Golgi markers together with the vacuolar cargo during a typical maturation event. Depicted are the normalized fluorescence intensities in arbitrary units (a.u.) of the cisterna tracked in (C).

Regardless of whether this interpretation is correct, GGA arrival kinetics closely match the departure kinetics of the vacuolar cargo, whereas AP-1 arrival kinetics do not.

If a given adaptor is involved in transporting the vacuolar cargo out of the Golgi, then loss of that adaptor should disrupt normal sorting. We generated an *apl4*Δ deletion strain to inactivate AP-1 and a *gga1*Δ *gga2*Δ double deletion strain to inactivate GGAs, and then tracked the vacuolar cargo together with the early Golgi marker GFP-Vrg4 and the late Golgi marker Sec7-HaloTag. In the *apl4*Δ strain, the vacuolar cargo signal began to decline during the early-to-late transition of Golgi maturation in a manner indistinguishable from that seen in wild-type cells (Movie 4.8, Figure 4.9A-C, and Figure 4.10A-C). Strikingly, in the *gga1*Δ *gga2*Δ strain, the vacuolar cargo persisted during the early-to-late transition (Movie 4.9, Figure 4.9D-F, and Figure 4.10D-F). In most of the events analyzed for the *gga1*Δ *gga2*Δ strain, the vacuolar cargo could be detected within the cisterna until the Sec7 signal disappeared or even afterwards (Figure 4.9D, E and Figure 4.10D,E). A caveat is that the *gga1*Δ *gga2*Δ strain displayed somewhat altered Vrg4 and Sec7 maturation kinetics, as indicated by abnormally shallow slopes for the arrival and departure curves of the Golgi markers (Figure 4.10F). Nevertheless, maturation events could be readily identified in the *gga1*Δ *gga2*Δ strain, and the results strongly suggest that GGAs are needed for the vacuolar cargo to exit the Golgi.

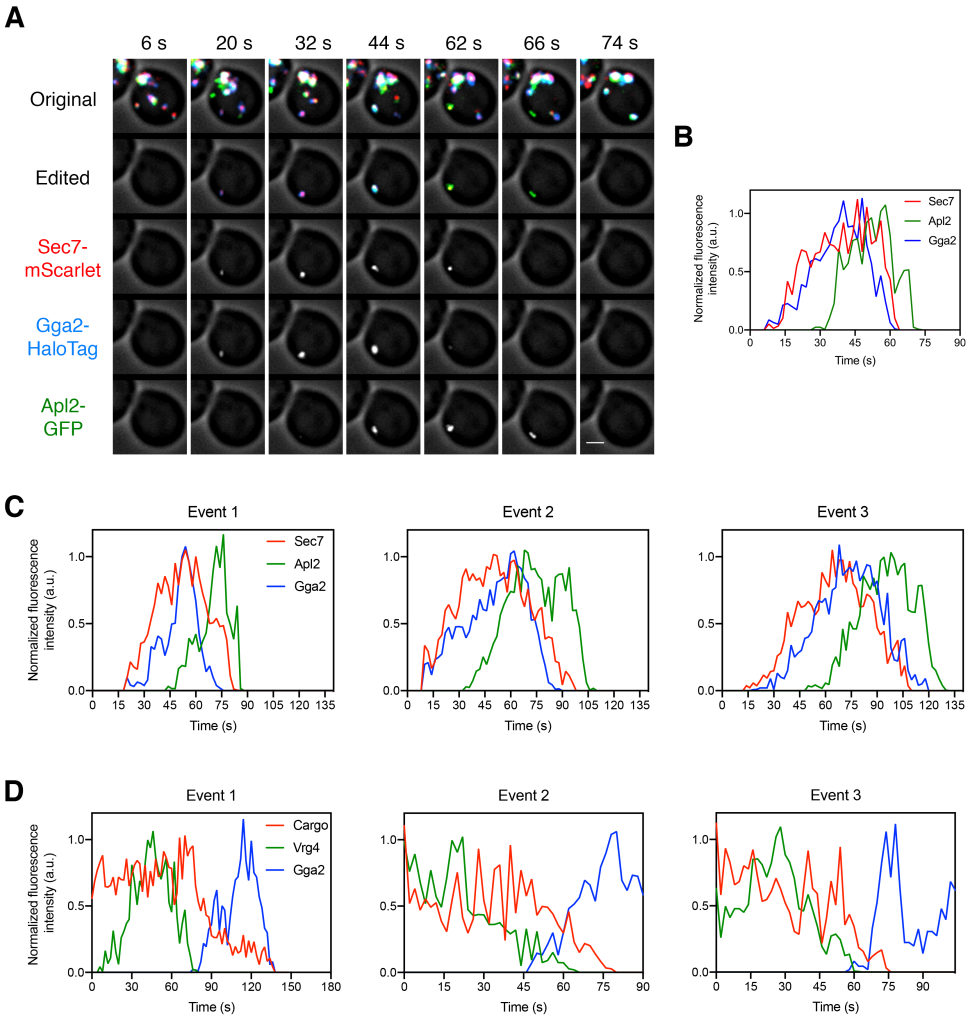

Figure 4.8: **Additional examples of adaptor dynamics and of the relationship between GGA arrival and vacuolar cargo departure. (A)** Visualizing the dynamics of the GGA and AP-1 adaptors during cisternal maturation. The experiment was performed as in Figure 4.7A. Shown are average projected Z-stacks at representative time points from an additional movie. The top row shows the complete projection, the second row shows an edited projection that includes only the cisterna being tracked, and the other rows show the individual fluorescence channels from the edited projection. Scale bar, 2 µm. **(B)** Quantification of the fluorescence intensities of the late Golgi marker and the adaptors during a typical maturation event. Depicted are the normalized fluorescence intensities in arbitrary units (a.u.) of the cisterna tracked in (A). **(C)** Quantification of the fluorescence intensities of the late Golgi marker and the adaptors during three additional maturation events from three additional movies. The analysis was performed as in (B). **(D)** Quantification of the fluorescence intensities of the Golgi markers GFP-Vrg4 and Gga2-HaloTag together with the vacuolar cargo during three additional maturation events from three additional movies. The analysis was performed as in Figure 4.7D.

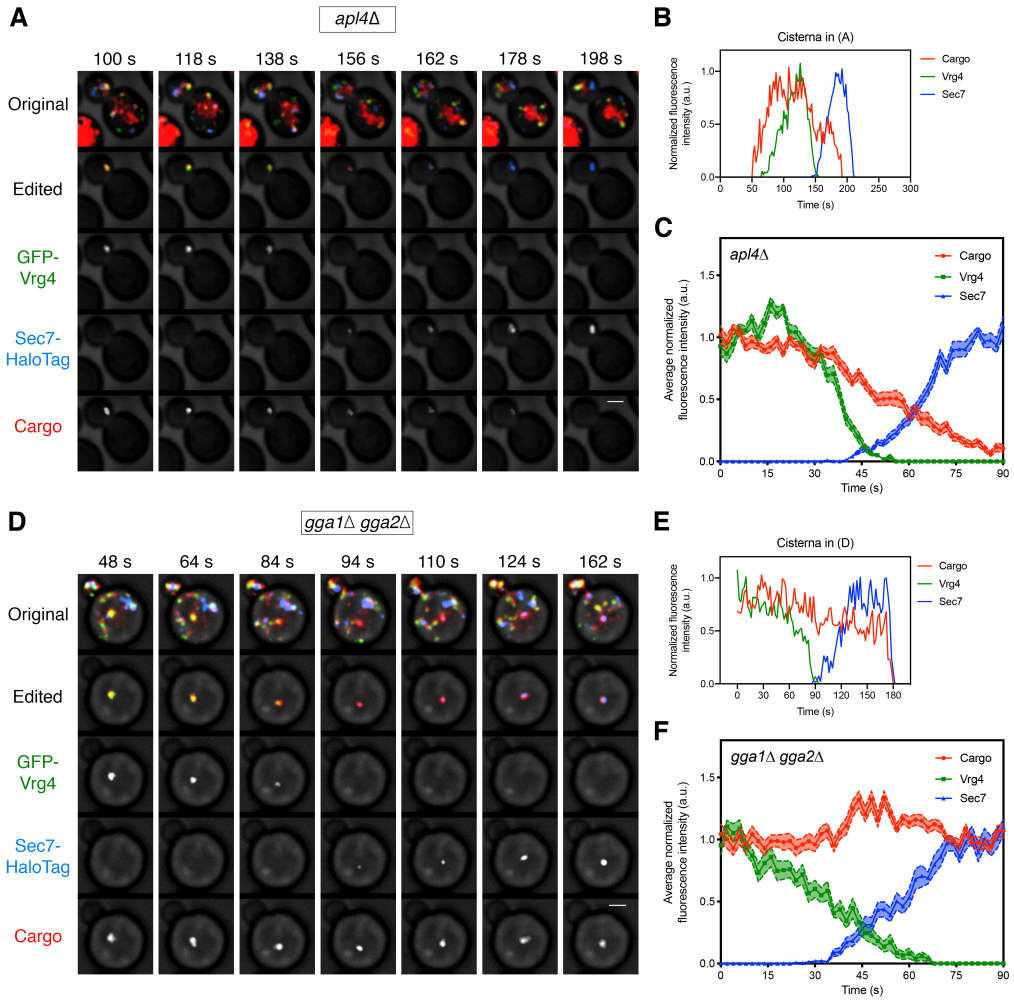

Figure 4.9: **Requirement for the GGAs but not AP-1 during Golgi-to-PVE traffic.** **(A)** Visualizing vacuolar cargo traffic during Golgi maturation in a strain lacking AP-1. The experiment was performed as in Figure 4.5A, except that an *apl4*Δ strain was used. Shown are average projected Z-stacks at representative time points from Movie 4.8. The top row shows the complete projection, the second row shows an edited projection that includes only the cisterna being tracked, and the other rows show the individual fluorescence channels from the edited projection. Scale bar, 2 µm. **(B)** Quantification of the fluorescence intensities of the Golgi markers and the vacuolar cargo during a typical maturation event in the *apl4*Δ strain. Depicted are the normalized fluorescence intensities in arbitrary units (a.u.) of the cisterna tracked in (A). **(C)** Average cargo signal during the early-to-late Golgi transition in the *apl4*Δ strain. The analysis was performed as in Figure 4.5C, based on 17 maturation events from 13 movies of cells expressing moderate levels of the vacuolar cargo. **((D) – (F))** Same as (A) – (C) except with a *gga1*Δ *gga2*Δ strain lacking GGAs. The analysis in (C) was based on 15 maturation events from 12 movies of cells expressing moderate levels of the vacuolar cargo. Shown in (D) are average projected Z-stacks at representative time points from Movie 4.9.

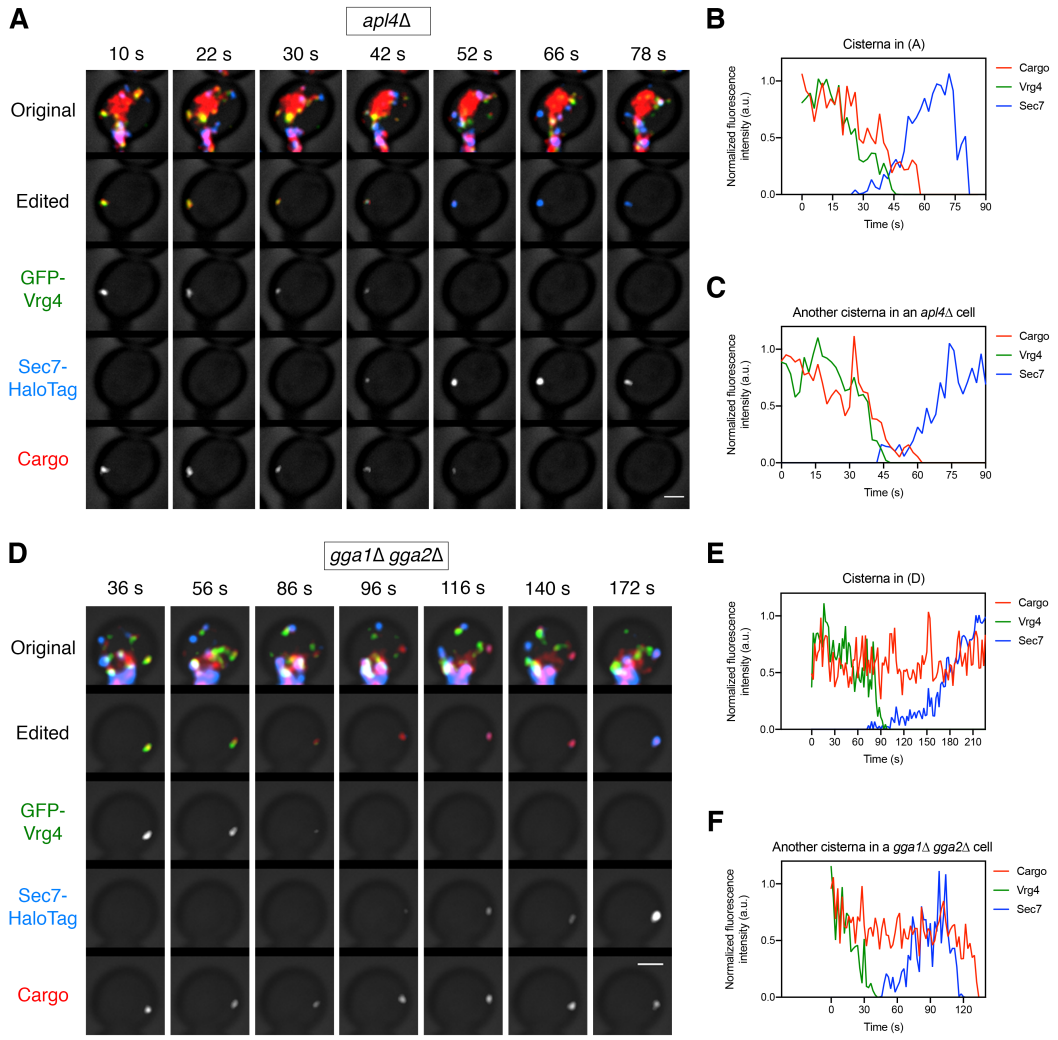

Figure 4.10: **Additional examples of cargo dynamics during cisternal maturation in strains lacking AP-1 or GGAs. (A)** Visualizing vacuolar cargo traffic during Golgi maturation in a strain lacking AP-1. The experiment was performed with an *apl4*Δ strain as in Figure 4.9A. Shown are average projected Z-stacks at representative time points from an additional movie. The top row shows the complete projection, the second row shows an edited projection that includes only the cisterna being tracked, and the other rows show the individual fluorescence channels from the edited projection. Scale bar, 2 µm. **(B)** Quantification of the fluorescence intensities of the Golgi markers and the vacuolar cargo during maturation of the cisterna tracked in (A). The procedure was as in Figure 4.9B. **(C)** Quantification of a maturation event from an additional movie of an *apl4*Δ cell. **(D) - (F)** Same as (A) – (C) except with a *gga1*Δ *gga2*Δ strain lacking GGAs.

As a further test of this interpretation, we hypothesized that loss of GGAs would cause the vacuolar cargo to be secreted, as is true for native CPY (Dell'Angelica et al., 2000; Hirst et al., 2000; Zhdankina et al., 2001). This prediction was tested by an immunoblot of

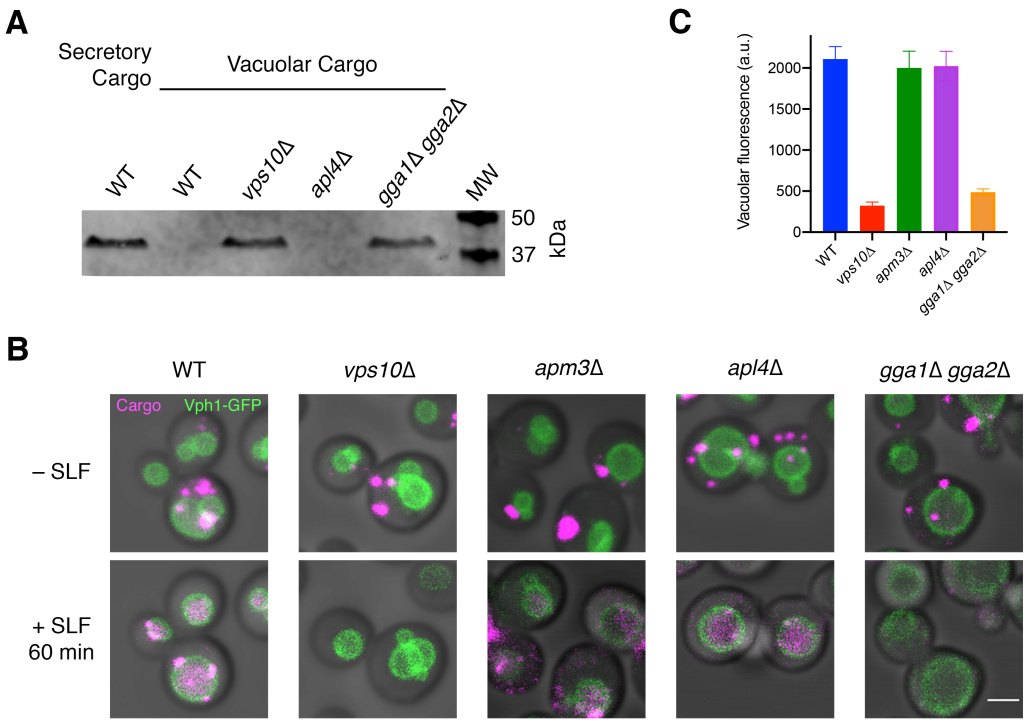

Figure 4.11: **Secretion of the vacuolar cargo in cells lacking either Vps10 or GGAs.** **(A)** Immunoblot of secreted cargoes after SLF addition in rich medium. Wild-type (WT) cells expressing the secretory cargo and wild-type, *vps10*Δ, *apl4*Δ, and *gga1*Δ *gga2*Δ cells expressing the vacuolar cargo were grown to mid-log phase in YPD, washed with fresh YPD, and treated with SLF. After 30 min, the secreted fractions were isolated by centrifugation, treated with endoglycosidase H to trim N-glycans, and analyzed by SDS-PAGE and immunoblotting. Shown is a representative example from four separate experiments. MW, molecular weight markers. The predicted molecular weights for the mature cargoes are ~38-39 kDa. **(B)** Accumulation of the vacuolar cargo in the vacuole after SLF addition in various genetic backgrounds. The vacuolar cargo was expressed in wild-type, *vps10*Δ, *apm3*Δ, *apl4*Δ, and *gga1*Δ *gga2*Δ cells that also contained the vacuolar membrane marker Vph1-GFP. The experiment was performed as in Figure 4.2A. **(C)** Quantification of the amount of cargo reaching the vacuole in (B). The Vph1-GFP signal was used to create a mask for measuring cargo fluorescence in the vacuole. Data are average values from at least 37 cells for each strain. Fluorescence is plotted in arbitrary units (a.u.). Bars represent SEM.

media samples collected 30 min after solubilizing the vacuolar cargo with SLF in wild-type, *vps10*Δ, *apl4*Δ, and *gga1*Δ *gga2*Δ strains. Secreted cargo was consistently observed with the *vps10*Δ and *gga1*Δ *gga2*Δ strains but not with the wild-type or *apl4*Δ strains (Figure 4.11A). As another readout for mistargeting of the vacuolar cargo, we compared the total amount of cargo present in the vacuole 60 min after solubilizing the cargo with SLF in wild-type,

*vps10*Δ, *apm3*Δ, *apl4*Δ, and *gga1*Δ *gga2*Δ strains. Apm3 serves as an additional control because it is a subunit of the AP-3 adaptor complex, which functions in a parallel pathway that targets certain membrane proteins directly from the Golgi to the vacuole (Myers and Payne, 2013; Odorizzi et al., 1998). The wild-type, *apl4*Δ, and *apm3*Δ strains all showed similar amounts of vacuolar cargo, while the *vps10*Δ and *gga1*Δ *gga2*Δ strains showed very little vacuolar cargo (Figure 4.11B,C). The combined results indicate that the vacuolar cargo is sorted to PVE compartments after the early-to-late Golgi transition, with the aid of Vps10 and GGAs but with no significant contribution from AP-1.

Soluble and transmembrane cargoes apparently transit from PVE compartments to the vacuole by kiss-and-run events

Based on the observation that PVE compartments are indefinitely long-lived, we have speculated that PVE compartments deliver cargoes to the vacuole via kiss-and-run fusion events that generate transient pores (Day et al., 2018). Such pores would allow the passage of soluble cargoes as well as intraluminal vesicles that carry membrane-bound cargoes (Henne et al., 2011). This type of partial fusion mechanism could explain why the movement of cargoes from PVE compartments to the vacuole is relatively slow. To test this concept, we developed an assay in which a pool of labeled cargo molecules in a PVE compartment can be tracked during passage to the vacuole. This approach had two technical hurdles: (1) prior to imaging, a fraction of the fluorescent cargo molecules are in the vacuole or other non-PVE compartments, and (2) a typical cell contains several PVE compartments that can undergo fusion and fission (Day et al., 2018), making it difficult to follow individual organelles. The problem with background fluorescence was addressed by photobleaching cargo molecules outside the PVE compartments. Bleaching occurred in the interior of the vacuole and in the portion of the cell outside the vacuole, leaving a ring of non-bleached fluorescence that included vacuole-associated PVE compartments. The problem of tracking multiple PVE compart-

ments was addressed by focusing on cells that happened to contain just one or two punctate PVE structures.

Traffic of the biosynthetic vacuolar cargo from PVE compartments to the vacuole was visualized by generating a yeast strain expressing the vacuolar cargo together with the PVE marker Vps8-GFP and the vacuole marker Vph1-HaloTag. At 10-15 min after SLF addition, the majority of the cargo molecules had passed through the Golgi and accumulated in PVE compartments (see Figure 4.4C above). 4D confocal imaging was then performed after photobleaching the signal outside the PVE compartments. As previously documented (Day et al., 2018), the Vps8-GFP-labeled PVE compartments were persistent structures. Meanwhile, cargo fluorescence moved from PVE compartments to the vacuole. This process was examined by capturing 10-min movies. Some PVE compartments were quiescent for cargo delivery as described above, so the analysis focused on PVE compartments that were active throughout the imaging period. During the majority of a typical time course, the fluorescence in a PVE compartment gradually declined, and this decrease was matched by a gradual increase of fluorescence in the vacuole (Movie 4.10 and Figure 4.12A,B). Occasionally, a discrete event rapidly transferred a substantial fraction of the cargo fluorescence to the vacuole (Movie 4.11 and Figure 4.12C,D). Although the Vps8-GFP signal varied, and sometimes dropped after a discrete event, the punctate PVE compartments marked with Vps8-GFP were never seen to disappear. Our interpretation is that the vacuolar cargo moves from long-lived PVE compartments to the vacuole by a series of kiss-and-run events that are frequently small and sometimes large.

We wondered whether the putative kiss-and-run events could also deliver transmembrane cargoes that are encapsulated in intraluminal vesicles within PVE compartments (Henne et al., 2011). This experiment employed the methionine permease Mup1 as a model transmembrane cargo (Menant et al., 2006). In the absence of methionine in the culture medium, Mup1 resides in the plasma membrane, and upon addition of methionine, Mup1 is ubiquitinated, internalized, and sent to the vacuole for degradation (Lin et al., 2008). We generated

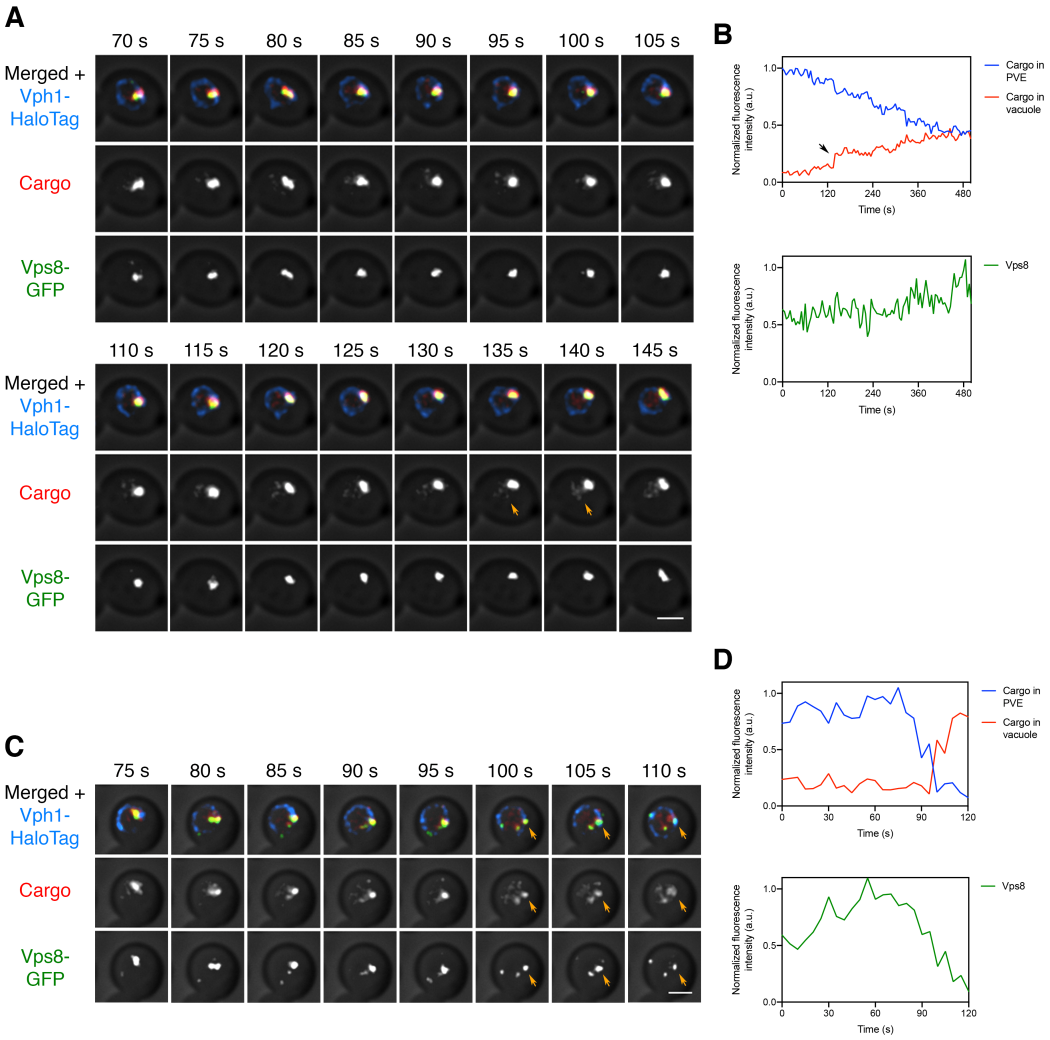

Figure 4.12: **Visualizing transfer of the vacuolar cargo from PVE compartments to the vacuole. (A)** Gradual movement of the vacuolar cargo from a PVE compartment to the vacuole. A strain expressing the vacuolar membrane marker Vph1-HaloTag, the PVE marker Vps8-GFP, and the vacuolar cargo was grown to mid-log phase, attached to a confocal dish, and treated with SLF for 10-15 min to enable the cargo to reach PVE compartments. Prior to imaging, a region that excluded PVE compartments was photobleached by illumination with maximum intensity 561-nm laser light for 40 s. Shown are frames from Movie 4.10. The top row shows the complete projection, the middle row shows the cargo fluorescence, and the bottom row shows the Vps8-GFP fluorescence. Orange arrows indicate sudden transfer of a small amount of cargo from the PVE compartment to the vacuole. Scale bar, 2 µm. **(B)** Quantification from (A) of the time course of cargo fluorescence in the PVE compartment and the vacuole, and of the Vps8 signal. To quantify the cargo signal at each time point, the Vph1 or Vps8 signal was selected in a 3D volume and then the cargo fluorescence within that volume was measured. Normalized data are plotted in arbitrary units (a.u.). The black arrow points to the same cargo transfer event that is marked by the orange arrows in (A).

Figure 4.12: **(C)** Example of sudden transfer of a large amount of cargo from a PVE compartment to the vacuole. The experiment was performed as in (A). Shown are frames from Movie 4.11. Orange arrows indicate an event in which nearly all of the cargo moved from the PVE compartment to the vacuole. **(D)** Quantification of (C), performed as in (B).

a strain expressing Mup1-mScarlet, together with Vps8-GFP to label PVE compartments and Vph1-HaloTag to label the vacuole. Methionine was added for 10-15 min to redistribute Mup1 to PVE compartments, and then cells were subjected to 4D confocal imaging after photobleaching the signal outside the PVE compartments, as described above for the soluble vacuolar cargo. Once again, apparent kiss-and-run transfer was readily observed. The Mup1 cargo moved from PVE compartments to the vacuole, sometimes gradually and sometimes in discrete bursts (Movie 4.12 and Figure 4.13A,B). Rarely, a dramatic event results in transfer of virtually all of the Mup1 in a single burst (Movie 4.13 and Figure 4.13C,D). We never observed complete loss of Vps8 as would be expected for a full fusion event, although a subset of the larger discrete events led to substantial reduction of the Vps8 signal (Movie 4.14 and Figure 4.14). For both the vacuolar cargo and Mup1, quantification revealed that gradual transfer to the vacuole was punctuated, about once every 5 min on average, by bursts in which more than 15% of the remaining cargo moved to the vacuole. The average amount of remaining cargo transferred during a burst was ~35-40%. Individual PVE compartments differed greatly in the total fraction of the cargo that was transferred in bursts, but on average this number was ~75%. These results favor a PVE-to-vacuole traffic mechanism involving repeated kiss-and-run events of varying size.

Discussion

Live-cell fluorescence microscopy complements other methods by providing unique insights into membrane traffic (Lippincott-Schwartz et al., 2000). Recently, we engineered a regulatable fluorescent secretory cargo that can be visualized during yeast Golgi maturation (Casler and Glick, 2019; Casler et al., 2019). This secretory cargo is present in Golgi cisternae throughout the maturation process, and a fraction of the cargo molecules recycle from

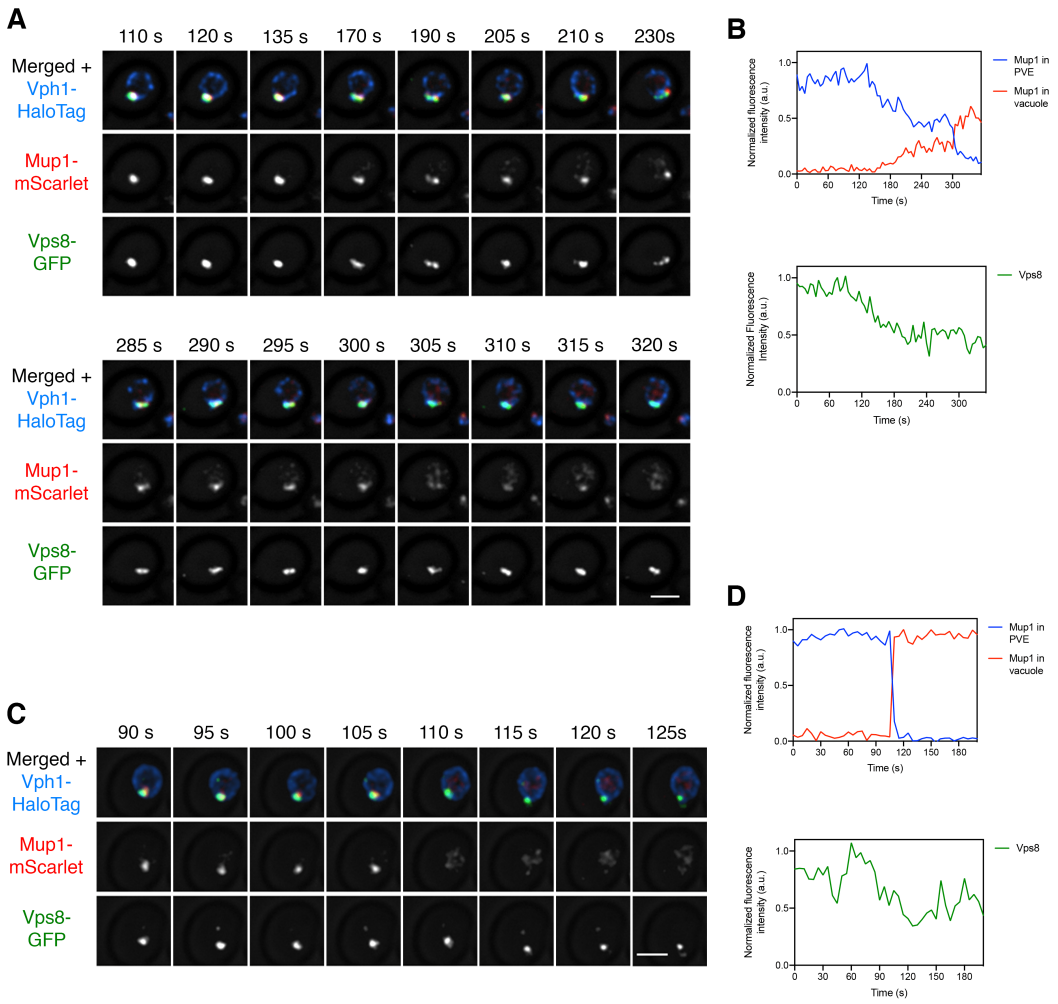

Figure 4.13: **Visualizing transfer of Mup1 from PVE compartments to the vacuole.** **(A)** Movement of Mup1 from a PVE compartment to the vacuole. A strain expressing the vacuolar membrane marker Vph1-HaloTag, the PVE marker Vps8-GFP, and Mup1-mScarlet was grown to mid-log phase in NSD lacking methionine, attached to a confocal dish, and exposed to NSD containing methionine for 10-15 min to promote internalization of Mup1 to PVE compartments. Prior to imaging, a region that excluded PVE compartments was photobleached by illumination with maximum intensity 561-nm laser light for 5 s. Shown are frames from Movie 4.12, which illustrates a typical example of putative kiss-and-run fusion at about 300 s. The top row shows the complete projection, the middle row shows the Mup1-mScarlet fluorescence, and the bottom row shows the Vps8-GFP fluorescence. Scale bar, 2 µm. **(B)** Quantification of (A), performed as in Figure 4.12B. At about 300 s, a significant amount of Mup1 moved from the PVE compartment to the vacuole. **(C)** Example of an unusually large cargo transfer event. The experiment was performed as in (A), and frames are shown from Movie 4.13. Between the 105-s and 110-s time points, virtually all of the Mup1 moved from the PVE compartment to the vacuole.**(D)** Quantification of (C), performed as in Figure 4.12B.

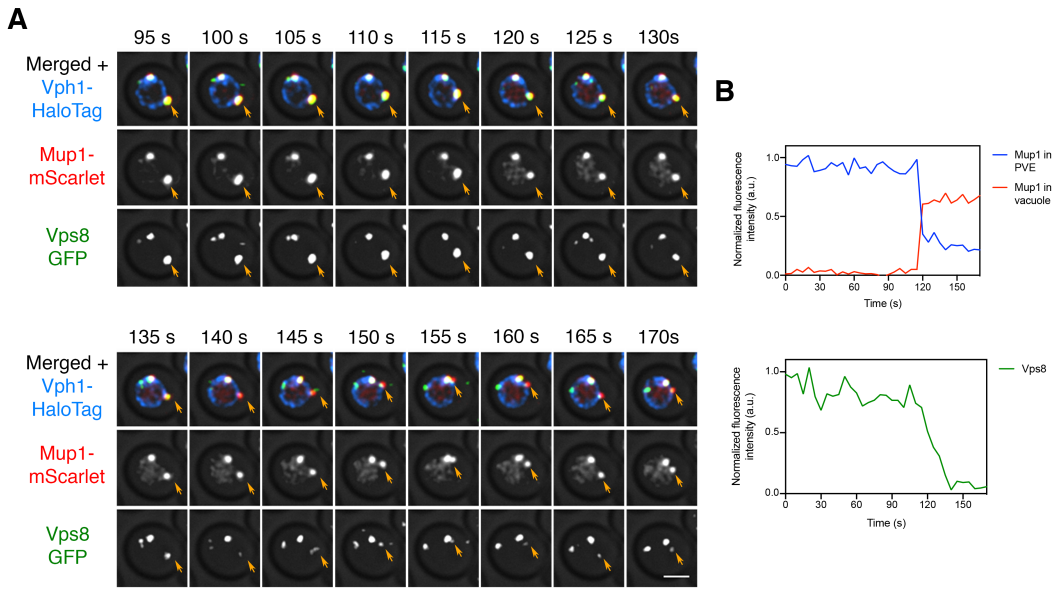

Figure 4.14: **Reduction in Vps8 labeling of a PVE compartment after a large cargo transfer event. (A)** Sudden movement of Mup1 from a PVE compartment to the vacuole. The experiment was performed as in Figure 4.13A, and frames are shown from Movie 4.14. Orange arrows indicate the PVE compartment that was tracked. **(B)** Quantification of (A), performed as in Figure 4.12B. Between the 115-s and 120-s time points, a large fraction of the Mup1 moved from the PVE compartment to the vacuole, and the Vps8-GFP fluorescence began a steep decline.

older to younger cisternae by an AP-1-dependent pathway (Casler et al., 2019). As an extension of that work, we have now generated a regulatable fluorescent vacuolar cargo that can be tracked in yeast cells. This vacuolar cargo follows the well characterized pathway by which CPY travels from the Golgi to PVE compartments, with the aid of Vps10 and GGAs, before reaching the vacuole (Bowers and Stevens, 2005; Hecht et al., 2014).

The convenience of working with an artificial vacuolar cargo is accompanied by some caveats. Compared to CPY, which is monomeric (Endrizzi et al., 1994), our vacuolar cargo is a tetramer and thus contains four copies of the Vps10 recognition signal. Moreover, Vps10 has a quality control domain that recognizes the fluorescent protein component of the cargo (Casler et al., 2019; Fitzgerald and Glick, 2014), so there are multiple points of interaction between Vps10 and the artificial vacuolar cargo. A consequence is that our vacuolar cargo might dissociate from Vps10 more slowly than CPY dissociates, leading to slower PVE-

to-vacuole delivery. However, this possible effect on traffic kinetics should not compromise interpretations about the pathway of cargo transport from the Golgi to the vacuole.

Using the vacuolar cargo, we asked a basic question: at what point during cisternal maturation does the vacuolar cargo depart from the Golgi? Unlike the regulatable fluorescent secretory cargo, which persists in Golgi cisternae until they are terminally mature (Casler et al., 2019), the vacuolar cargo begins to depart during the early-to-late Golgi transition. Departure of the vacuolar cargo begins at about the same time that GGAs arrive at the Golgi, and well before AP-1 arrives. Moreover, departure of the vacuolar cargo is abolished by deleting the GGAs but is unaffected by deleting AP-1. These results fit with previously published data indicating that the CPY pathway from the Golgi to the PVE involves GGAs but not AP-1 (Dell'Angelica et al., 2000; Hirst et al., 2001; Hirst et al., 2000; Zhdankina et al., 2001). The new insight is that departure of the vacuolar cargo from the Golgi begins relatively early, about halfway through the time course of cisternal maturation (Figure 9A).

Superficially, these results are at odds with the established view that various types of biosynthetic cargoes travel through the entire Golgi until being packaged into distinct carriers at the TGN (De Matteis and Luini, 2008; Griffiths and Simons, 1986). While there is evidence that biosynthetic cargoes begin to segregate early in the mammalian Golgi, all of those cargoes are thought to reach the terminal TGN compartment (Chen et al., 2017). But we suggest that there is actually no discrepancy between the yeast and mammalian data. In a typical cultured mammalian cell, the early Golgi consists of about six cisternae whereas the clathrin-labeled TGN is a single cisterna (Ladinsky et al., 1999; Mogelsvang et al., 2004). In yeast, the ratio is different because the clathrin-labeled late Golgi/TGN stage occupies about half of the maturation time course (Figure 4.15B). In both cell types, GGA-dependent transport occurs during the TGN stage, but the yeast system has allowed us to define a first TGN sub-stage marked by GGA activity followed by a second TGN sub-stage marked by AP 1 activity (Figure 4.15A). Mammalian TGN structures probably undergo a similar kinetic evolution because the interactions of clathrin adaptors at the mammalian TGN resemble

those at the yeast TGN (Daboussi et al., 2017). A proposed unified view is that during traffic to either yeast PVE compartments or mammalian late endosomes, GGA-dependent export from the TGN begins prior to secretory vesicle formation and AP-1-dependent intra-Golgi recycling (Pantazopoulou and Glick, 2019).

After the vacuolar cargo reaches PVE compartments, how does it move to the vacuole? Previously, based on evidence that PVE compartments are long-lived organelles that rarely if ever fuse completely with the vacuole, we proposed that transfer of material from PVE compartments to the vacuole might involve kiss-and-run fusion events (Day et al., 2018). This model seemed plausible because mammalian cells can employ kiss-and-run fusion to exchange material between lysosomes and late endosomes (Bright et al., 2016; Bright et al., 2005; Saffi and Botelho, 2019). Here, we have tested the kiss-and-run hypothesis by fluorescence microscopy. A photobleaching protocol generated a cell in which we could image a single PVE compartment containing fluorescent vacuolar cargo molecules, and the fate of that cohort of molecules was tracked over time. We observed gradual transfer of the cargo molecules to the vacuole over tens of minutes, punctuated by occasional larger events involving sudden transfer of a significant fraction of the cargo molecules. The PVE compartments persisted after cargo transfer. Qualitatively similar results were seen when PVE compartments were loaded with fluorescently tagged molecules of the methionine permease Mup1, which is internalized for degradation after methionine is added to the medium (Menant et al., 2006). Mup1 is packaged into intraluminal vesicles within PVE compartments (Lin et al., 2008), so kiss-and-run fusion pores would need to be large enough to transfer intraluminal vesicles. The observed fluctuations in the rate of cargo delivery from PVE compartments to the vacuole suggest that kiss-and-run fusion events vary in size and duration.

Our inference about the kiss-and-run mechanism is based on fluorescence microscopy and will benefit from validation by other techniques. Notably, an electron tomographic reconstruction carried out by the Odorizzi group (McNatt et al., 2007), shows tubular membrane connections between PVE compartments and the vacuole. Our results suggest that

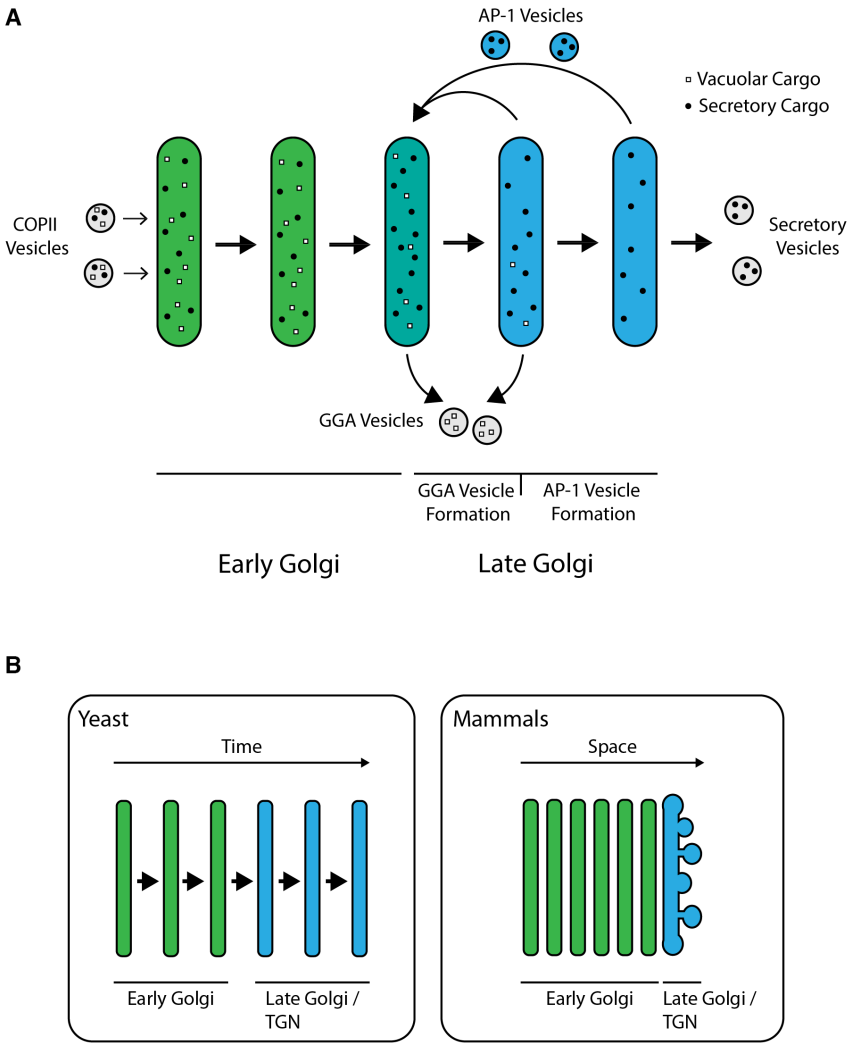

Figure 4.15: **Model for sorting of biosynthetic cargoes in the late Golgi. (A)** Sequential formation of GGA vesicles and AP-1 vesicles in yeast cells. The thick arrows represent progressive maturation of a Golgi cisterna over time. During the early-to-late Golgi transition of cisternal maturation, GGA adaptors arrive, and GGA vesicles that carry vacuolar cargoes (white squares) begin to form. Subsequently, the AP-1 adaptor arrives, and AP-1 vesicles that recycle resident Golgi proteins (not shown) as well as some secretory cargoes (black dots) begin to form. GGAs depart before AP-1 departs, but the formation phases for GGA vesicles and AP-1 vesicles overlap. **(B)** Comparison of Golgi structures in yeast and mammalian cells. In *S. cerevisiae*, the late Golgi or TGN stage accounts for about half of the maturation process, so the sequential arrival times and activities of GGAs and AP-1 are easy to detect. In mammalian cells, Golgi cisternae are stacked, with the youngest early Golgi cisterna at the opposite side of a stack from the oldest late Golgi/TGN cisterna. Only the trans-most cisterna of a mammalian Golgi stack functions as late Golgi/TGN, but during the lifetime of this cisterna, GGAs and AP-1 may arrive and act sequentially as in yeast.

such tubular connections should be common, so their prevalence could be quantified in future morphological studies. A separate electron tomographic analysis highlighted a possible complication—PVE compartments were sometimes observed to form clusters (Adell et al., 2017). If a single PVE compartment in a cluster fused completely with the vacuole, the fluorescence from the remaining PVE compartments in the cluster would persist, yielding a false impression of kiss-and-run fusion. Although we cannot rule out this scenario, it seems unlikely, because some PVE compartments are presumably solitary and yet we have never seen one disappear by fusing completely with the vacuole. The kiss-and-run hypothesis could be revisited if new methods make it possible either to prevent clustering of PVE compartments or to identify solitary PVE compartments by fluorescence microscopy.

If kiss-and-run transfer occurs between PVE compartments and the vacuole, the transient continuities between these organelles might permit exchange of transmembrane proteins. For example, the transmembrane precursor to the vacuolar hydrolase carboxypeptidase S is normally internalized into intraluminal vesicles of PVE compartments, but a mutant carboxypeptidase S precursor that cannot be internalized moves from the limiting membranes of PVE compartments to the vacuole membrane (Katzmann et al., 2001). Although other transmembrane proteins such as Vps10 and the SNARE protein Pep12 normally reside in PVE compartments and not the vacuole membrane, overexpressed Vps10 and Pep12 do reach the vacuole membrane (Black and Pelham, 2000; Cereghino et al., 1995; Chi et al., 2014). It seems plausible that during transient fusions of PVE compartments with the vacuole, saturable interactions with the trafficking machinery retain proteins such as Vps10 and Pep12 in the PVE compartments. Hence, the kiss-and-run model can explain how some transmembrane PVE proteins avoid reaching the vacuole, whereas this phenomenon would be hard to understand if PVE compartments fused completely with the vacuole.

Cargo transfer from PVE compartments to the vacuole is slow relative to other membrane traffic steps in budding yeast. Historically, kinetics of traffic to the vacuole have been measured by pulse-chase experiments that rely on the maturation of CPY by vacuolar pro-

teases (Stevens et al., 1982; Vida et al., 1993), but those results may be misleading because kiss-and-run fusion could result in some vacuolar proteases being present and active in PVE compartments (Bright et al., 2016). As judged by fluorescence microscopy, PVE-to-vacuole transfer often requires 30 min or more to reach completion. By comparison, transit from the ER to the PVE along the biosynthetic pathway or from the plasma membrane to the PVE along the endocytic pathway is largely complete within 10 min (Casler et al., 2019; Day et al., 2018; Losev et al., 2006). A possible reason for PVE-to-vacuole traffic being rate-limiting is that the cell has the option to "change its mind" by recycling membrane proteins from the PVE instead of degrading them (Ma and Burd, 2020). Meanwhile, the AP-3-driven pathway of direct Golgi-to-vacuole traffic offers an alternative for rapid delivery of membrane proteins to the vacuole (Odorizzi et al., 1998).

Materials and methods

Yeast growth and strain construction

The parental haploid strain was JK9-3da (*leu2-3,112 ura3-52 rme1 trp1 his4*) (Kunz et al., 1993). Yeast were grown with shaking in baffled flasks at 23°C in nonfluorescent minimal glucose dropout medium (NSD) (Bevis et al., 2002) or in rich glucose medium (YPD) supplemented with adenine and uracil. Deletion of the *PDR1*, *PDR3*, and *GGA1* genes was accomplished by replacement with a G418, nourseothricin, or hygromycin resistance cassette from pFA6a-kanMX6, pAG25, or pAG32, respectively (Goldstein and McCusker, 1999; Wach et al., 1994). Deletion of *VPS10*, *APM3*, and *APL4* was accomplished by using overlap extension PCR to generate a hygromycin resistance cassette, amplified from pAG32, flanked by 500 bp upstream and downstream of the gene. Deletion of *GGA2* was accomplished in the same manner, except that the *LEU2* gene from *K. lactis* was amplified from pUG73 (Gueldener et al., 2002). Yeast proteins were tagged by gene replacement using the pop-in/pop-out method to maintain endogenous expression levels (Rossanese et al., 1999; Rothstein, 1991). Secretory and vacuolar cargo proteins were expressed using a *TRP1* integrating vector with

the strong constitutive *TPI1* promoter and the *CYC1* terminator (Fitzgerald and Glick, 2014). To ensure consistent expression levels, each strain was verified to have a single copy of the integrated plasmid by PCR with the primers listed in Table 1. All plasmids used in this study are documented in the online supplemental material ZIP file, which contains annotated map/sequence files that can be opened with SnapGene Viewer (Insightful Science; https://www.snapgene.com/snapgene-viewer/). Newly generated plasmids will be submitted to Addgene.

Fluorescence microscopy and photobleaching

For live-cell fluorescence imaging, yeast strains were grown in NSD (pH ~5.5) at 23°C. Where indicated, SLF was diluted from a 100 mM stock solution in ethanol (Cayman Chemical; 10007974) to a final concentration of 100 µM, and cycloheximide was added from a 100 mg/mL stock solution in DMSO. Cells were attached to a concanavalin A-coated coverglass-bottom dish containing NSD (Losev et al., 2006) for imaging on a Leica SP8 or Leica SP5 confocal microscope equipped with a 1.4 NA/63x oil objective, using a pixel size of 60-80 nm, a Z step interval of 0.25-0.30 µm, and 20-30 optical sections. The intervals between Z stacks were based on the requirements for the individual experiments. Static images and 4D movies were processed as follows. Static images were converted to 16-bit and average projected (Hammond and Glick, 2000), then range-adjusted to the minimum and maximum pixel values with ImageJ (Schneider et al., 2012). Movies were deconvolved with Huygens Essential (Scientific Volume Imaging) using the classic maximum likelihood estimation algorithm (Day et al., 2017). Movies were converted to hyperstacks and average projected, then range-adjusted to maximize contrast in ImageJ. Custom ImageJ plugins were used to generate montages of time series, select individual structures and remove extraneous structures, convert edited montages to hyperstacks, and measure fluorescence intensities (Johnson and Glick, 2019). Each kinetic trace of a fluorescent Golgi marker was normalized to the average of the three highest values measured, a method that provided better results than relying on

the single highest signal from a noisy data set. For photobleaching prior to 4D imaging, a region of interest was drawn to include all fluorescent structures within the cell except for the PVE compartments. The regulatable vacuolar cargo and Mup1-mScarlet were bleached by maximum-intensity illumination with a 561 nm laser for 40 s or 5 s, respectively. These bleaching durations were chosen by determining the minimal times needed to bleach the fluorescence signals completely. To quantify the frequency at which bursts of cargo moved from PVE compartments to the vacuole, each 10-min movie was examined at 10-s intervals. Bursts were scored as intervals in which more than 15% of the remaining cargo transferred to the vacuole. Six movies for the vacuolar cargo and seven movies for Mup1 were analyzed. The two cargoes displayed similar frequencies of large bursts as well as similar amounts of cargo transferred per burst, so the data were combined to obtain the averaged numbers stated in the text.

HaloTag labeling

Proteins modified with HaloTag were labeled as previously described (Casler et al., 2019). Briefly, 1 µL of a 1-mM stock solution of JF_{646} ligand (Grimm et al., 2015) in DMSO was diluted in 500 µL NSD and then spun at maximum speed in a microcentrifuge to remove precipitated material, and the supernatant was mixed with a 500 µL aliquot of cells. Labeling was performed for 30 min with shaking at 23°C. To remove excess dye, cells were filter-washed by pushing 3 mL of fresh media through the filter. Washed cells were resuspended by pipetting on the filter. The resulting cell mixture was diluted to its original density, and the cells were attached to confocal dishes.

Immunoblotting of yeast cell lysates and secreted proteins

Immunoblotting was performed as follows (Casler et al., 2019). A 5 mL yeast culture was grown in YPD overnight with shaking in a baffled flask to an OD_{600} of 0.7-1.0. The cells were collected by a brief spin in a microcentrifuge, washed twice with fresh YPD, and re-

suspended in the original volume of fresh YPD. Cultures were treated with 100 µM SLF, and 1.6 mL was removed at each time point. The cells were collected by spinning at 2500xg (5000 rpm) for 2 min in a microcentrifuge. The culture medium supernatant was transferred to a fresh microcentrifuge tube on ice, and the cells were washed once with deionized water. Then the cells were resuspended in 100 µL 4% trichloroacetic acid. Glass beads (0.5-mm; BioSpec Products) were added to bring the total volume to 200 µL, and the sample was vortexed three times for 1 min each separated by 1-min intervals on ice. Finally, 800 µL of PBS was added, the solution was mixed, and 800 µL of the cell lysate was transferred to a fresh microcentrifuge tube. Supernatant protein samples were precipitated with 4% trichloroacetic acid on ice for 20 min. Precipitated proteins were centrifuged at maximum speed in a microcentrifuge for 15 min at 4°C. Finally, each protein pellet was resuspended in 50 µL SDS-PAGE sample buffer. Treatment with endoglycosidase H was performed as described by the manufacturer (New England Biolabs; P0702S). Briefly, Glycoprotein Denaturing Buffer was added to the protein sample, which was boiled for 5–10 min, followed by addition of GlycoBuffer 3 and endoglycosidase H. The reaction was performed at 37°C for at least 1 h. For immunoblotting, 9 µL of each cell lysate and 14 µL of each secreted protein sample were run on a 4–20% Tris-glycine gel (Bio-Rad; 4561094) together with the Precision Plus Protein Dual Color Standards molecular weight marker (Bio-Rad; 1610374). The separated proteins were transferred to a PVDF membrane (Bio-Rad; 1704156) using the Trans-Blot Turbo system (Bio-Rad). The membrane was blocked with 5% nonfat dry milk in TBST (50 mM Tris-HCl at pH 7.6, 150 mM NaCl, and 0.05% Tween 20) with shaking at room temperature for 1 h, and then incubated with 1:1000 polyclonal rabbit anti-FKBP12 antibody (Abcam; ab2918) in 5% milk/TBST with shaking overnight at 4°C. After four 5 min washes in TBST, the membrane was incubated with a 1:1000 dilution of goat anti-rabbit secondary antibody conjugated to Alexa Fluor 647 (Thermo Fisher Scientific; A21245) for 1 h at room temperature. The membrane was then washed twice with TBST and twice with

50 mM Tris-HCl at pH 7.6, 150 mM NaCl. Analysis was performed with a LI-COR Odyssey CLx imaging system.

Movies Associated with Chapter 4

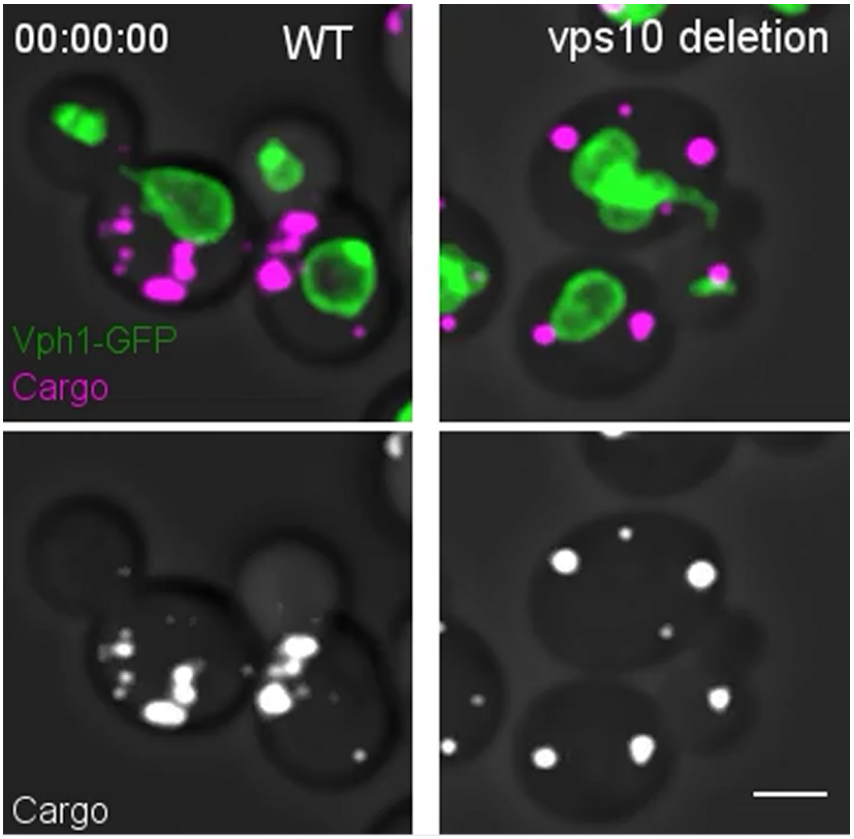

Movie 4.1. **Visualizing traffic of the vacuolar cargo from the ER to the vacuole.** The cargo expressed in *VPS10* wild-type (WT) and *vps10*Δ strains was imaged by 4D confocal microscopy together with the vacuolar membrane marker Vph1-GFP. Prior to the movie, fluorescence from leaked cargo molecules was bleached by illuminating the vacuole with a 561 nm laser at maximum intensity for 20-30 s. Then SLF was added, and Z-stacks were captured every minute for 60 min. In these average projected Z stacks, fluorescence data are superimposed on brightfield images of the cells. The top panels show the cargo (magenta) together with Vph1-GFP (green), while the bottom panels show only the cargo. Frames from this movie are shown in Figure 4.2A. Scale bar, 2 µm.

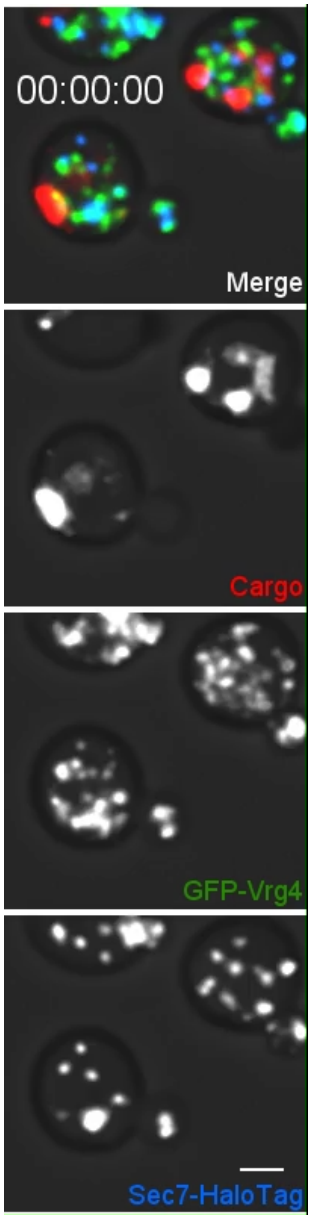

Movie 4.2. **Visualizing traffic of the vacuolar cargo together with Golgi markers.** Cells expressing the cargo together with the early Golgi marker GFP-Vrg4 and the late Golgi marker Sec7-HaloTag were grown to mid-log phase, labeled with JF_{646}, and imaged by 4D confocal microscopy. Prior to imaging, fluorescence from leaked cargo molecules in the vacuole was bleached by illuminating with maximum intensity 561 nm laser power for 20-30 s. SLF was added directly to the dish between the first and second Z-stacks, and then additional Z stacks were captured every 30 s for 29.5 min. In these average projected Z stacks, fluorescence data are superimposed on brightfield images of the cells. The top panel shows the merged images, and the other panels show the individual fluorescence channels for cargo, Vrg4, and Sec7. Frames from this movie are shown in Figure 4.4A. Scale bar, 2 µm.

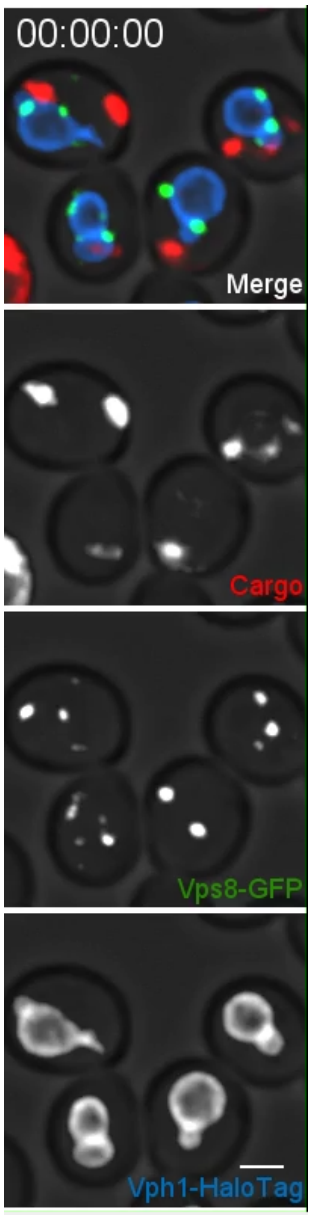

Movie 4.3. **Visualizing traffic of the vacuolar cargo together with PVE and vacuole markers.** Cells expressing the cargo together with the PVE marker Vps8-GFP and the vacuolar membrane marker Vph1-HaloTag were grown to mid-log phase, labeled with JF_{646}, and imaged by 4D confocal microscopy. Prior to imaging, fluorescence from leaked cargo molecules in the vacuole was bleached by illuminating with maximum intensity 561 nm laser power for 20-30 s. SLF was added directly to the dish between the first and second Z-stacks, and then additional Z-stacks were captured every 1 min for 60 min. In these average projected Z stacks, fluorescence data are superimposed on brightfield images of the cells. The top panel shows the merged images, and the other panels show the individual fluorescence channels for cargo, Vps8, and Vph1. Frames from this movie are shown in Figure 4.4B. Scale bar, 2 µm.

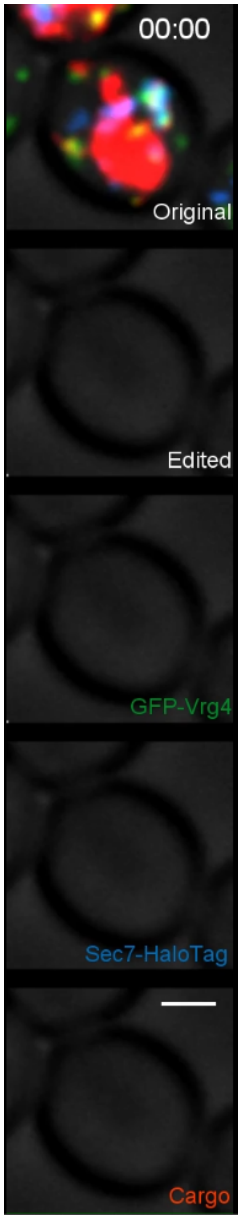

Movie 4.4. **Visualizing traffic of the vacuolar cargo during Golgi maturation.** Cells expressing the cargo together with the early Golgi marker GFP-Vrg4 and the late Golgi marker Sec7-HaloTag were grown to mid-log phase, labeled with JF_{646}, and imaged by 4D confocal microscopy. SLF was added 1-3 min before imaging. In these average projected Z stacks, fluorescence data are superimposed on brightfield images of the cells. The top panel shows the complete projection, the second panel shows an edited projection that includes only the cisterna being tracked, and the other panels show the individual fluorescence channels from the edited projection. Frames from this movie are shown in Figure 4.5A. Scale bar, 2 µm.

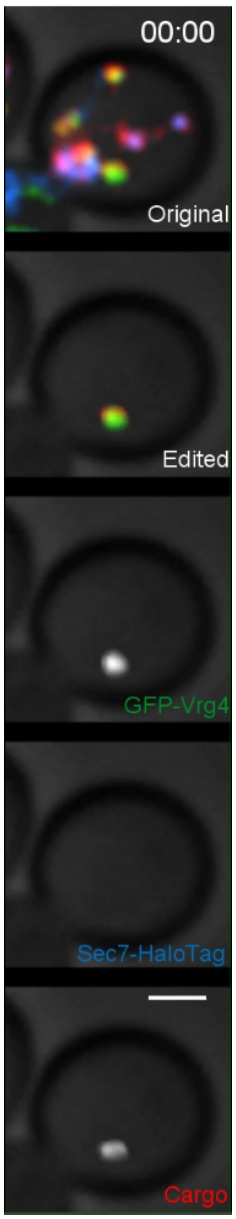

Movie 4.5. **Visualizing traffic of the vacuolar cargo during Golgi maturation in a strain lacking Vps10.** The procedure was as in Movie 4.4 except that a *vps10*Δ strain was used. Frames from this movie are shown in Figure 4.5D. Scale bar, 2 µm.

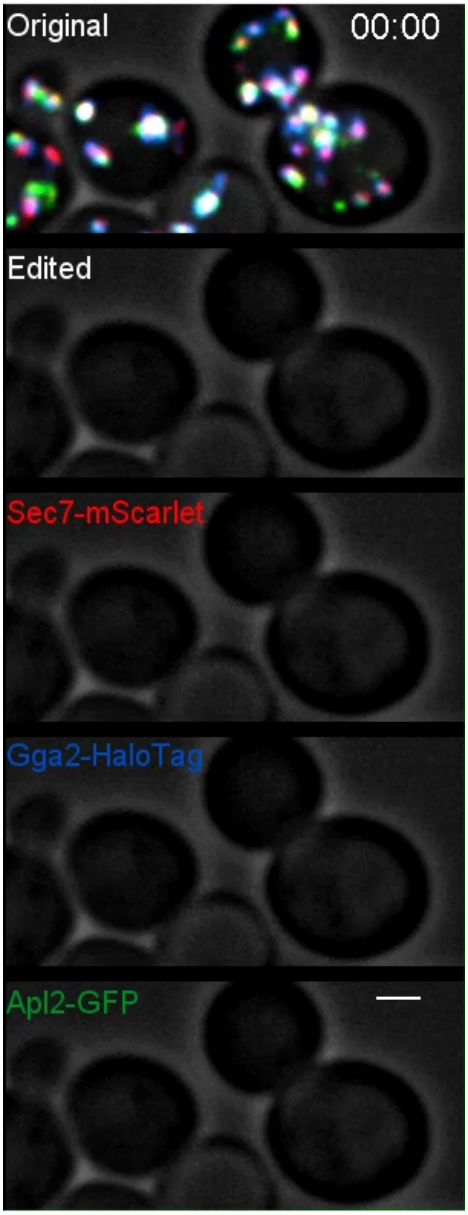

Movie 4.6. **Visualizing the dynamics of the GGA and AP-1 clathrin adaptors during Golgi maturation.** Cells expressing the GGA protein Gga2-HaloTag, the AP-1 subunit Apl2-GFP, and the late Golgi marker Sec7-mScarlet were grown to mid-log phase, labeled with JF_{646}, and imaged by 4D confocal microscopy. In these average projected Z stacks, fluorescence data are superimposed on brightfield images of the cells. The top panel shows the complete projection, the second panel shows an edited projection that includes only the cisterna being tracked, and the other panels show the individual fluorescence channels from the edited projection. Two maturation events are highlighted. Frames from this movie are shown in Figure 4.7A. Scale bar, 2 µm.

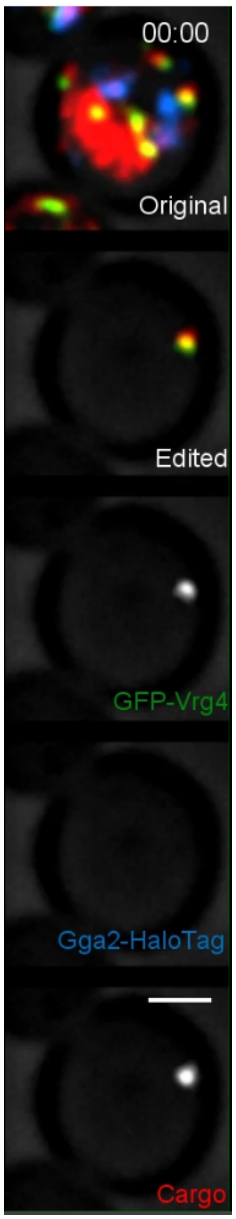

Movie 4.7. **Visualizing the vacuolar cargo together with a GGA adaptor.** Cells expressing the cargo together with the early Golgi marker GFP-Vrg4 and the GGA protein Gga2-HaloTag were grown to mid-log phase, labeled with JF_{646}, and imaged by 4D confocal microscopy. SLF was added 1-3 min before imaging. In these average projected Z stacks, fluorescence data are superimposed on brightfield images of the cells. The top panel shows the complete projection, the second panel shows an edited projection that includes only the cisterna being tracked, and the other panels show the individual fluorescence channels from the edited projection. Frames from this movie are shown in Figure 4.7C. Scale bar, 2 µm.

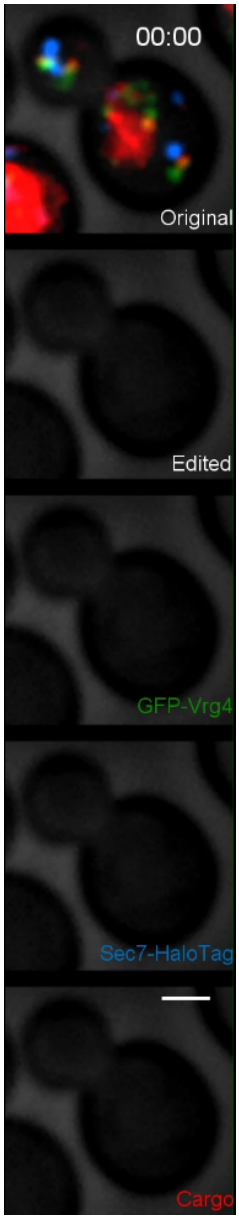

Movie 4.8. **Visualizing traffic of the vacuolar cargo during Golgi maturation in a strain lacking AP-1.** The procedure was as in Movie 4.4 except that an *apl4*Δ strain was used. Frames from this movie are shown in Figure 4.9A. Scale bar, 2 µm.

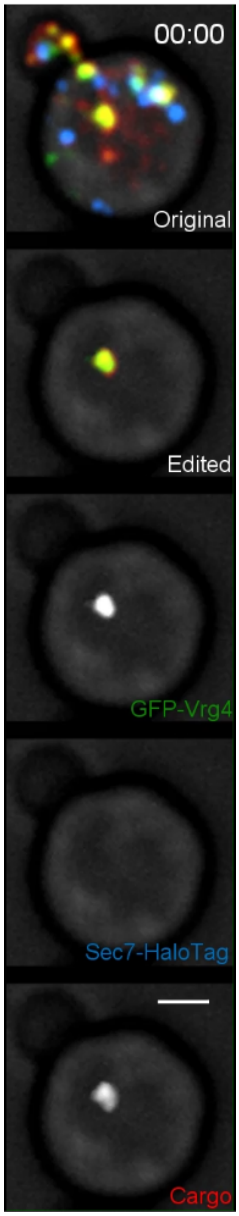

Movie 4.9. **Visualizing traffic of the vacuolar cargo during Golgi maturation in a strain lacking GGAs.** The procedure was as in Movie 4.4 except that a *gga1*Δ *gga2*Δ strain was used. Frames from this movie are shown in Figure 4.9D. Scale bar, 2 µm.

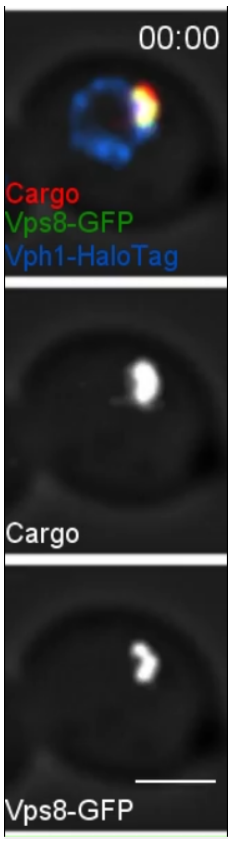

Movie 4.10. **Visualizing movement of the vacuolar cargo from a PVE compartment to the vacuole.** Cells expressing the cargo together with the vacuolar membrane marker Vph1-HaloTag and the PVE marker Vps8-GFP were grown to mid-log phase, attached to a confocal dish, and treated with SLF for 10-15 min to enable the cargo to reach PVE compartments. Prior to imaging, a region that excluded PVE compartments was photobleached by illumination with maximum intensity 561 nm laser light for 40 s. The top panel shows the complete projection, the middle panel shows the cargo fluorescence, and the bottom panel shows the Vps8-GFP fluorescence. Frames from this movie are shown in Figure 4.12A. Scale bar, 2 µm.

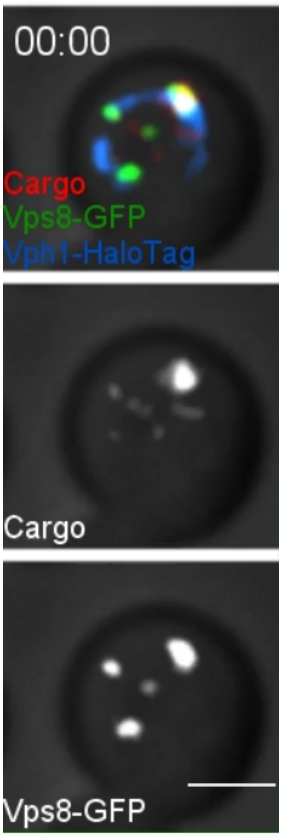

Movie 4.11. **Visualizing sudden movement of the vacuolar cargo from a PVE compartment to the vacuole.** The procedure was as in Movie 4.10. Frames from this movie are shown in Figure 4.12C. Scale bar, 2 µm.

Movie 4.12. **Visualizing movement of Mup1 from a PVE compartment to the vacuole.** Cells expressing the vacuolar membrane marker Vph1-HaloTag, the PVE marker Vps8-GFP, and Mup1-mScarlet were grown to mid-log phase in NSD lacking methionine, attached to a confocal dish, and exposed to NSD containing methionine for 10-15 min to promote internalization of Mup1 to PVE compartments. Prior to imaging, a region that excluded PVE compartments was photobleached by illumination with maximum intensity 561-nm laser light for 5 s. The top panel shows the complete projection, the middle panel shows the Mup1-mScarlet fluorescence, and the bottom panel shows the Vps8-GFP fluorescence. Frames from this movie are shown in Figure 4.13A. Scale bar, 2 µm.

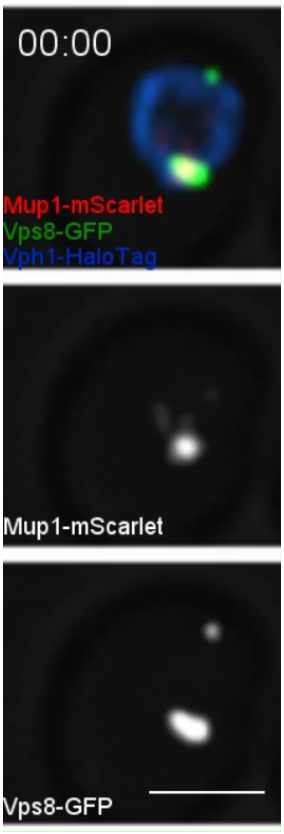

Movie 4.13. **Visualizing sudden movement of Mup1 from a PVE compartment to the vacuole.** The procedure was as in Movie 4.12. Frames from this movie are shown in Figure 4.13C. Scale bar, 2 µm.

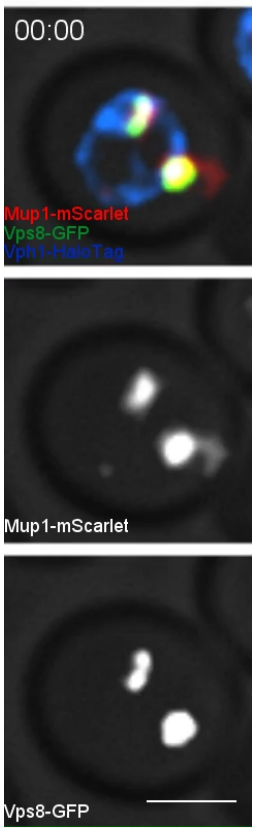

Movie 4.14. **Reduction in the apparent size of a PVE compartment after a large cargo transfer event.** The procedure was as in Movie 4.12. Frames from this movie are shown in Figure 4.14A. Scale bar, 2 µm.

CHAPTER 5

ESCARGO: A REGULATABLE FLUORESCENT SECRETORY CARGO FOR DIVERSE MODEL ORGANISMS

Abstract

Membrane traffic can be studied by imaging a protein cargo during its transport through the secretory pathway. The best tools for this purpose initially block exit of the secretory cargo from the endoplasmic reticulum (ER), and then release the block to generate a cargo wave. However, previously developed regulatable secretory cargoes are often tricky to use or specific for a single model organism. To overcome these hurdles for budding yeast, we recently optimized an artificial fluorescent secretory protein that exits the ER with the aid of the Erv29 cargo receptor, which is homologous to mammalian Surf4. The fluorescent secretory protein forms aggregates in the ER lumen and can be rapidly disaggregated by addition of a ligand to generate a nearly synchronized cargo wave. Here we term this regulatable secretory protein ESCargo (Erv29/Surf4-dependent Secretory Cargo) and demonstrate its utility not only in yeast cells, but also in cultured mammalian cells, cultured *Drosophila* cells, and the ciliate *Tetrahymena thermophila*. Kinetic studies of ESCargo variants lacking the ER export signal indicate that rapid transport out of the ER requires recognition by Erv29/Surf4. By choosing an appropriate ER signal sequence and expression vector, this simple technology can likely be used with many model organisms.

This chapter is a version of a manuscript in preparation for publication. It contains the following author list: Jason C. Casler, Allison L. Zajac, Daniela Sparvoli, Aaron P. Turkewitz, Sally Horne-Badovinac and Benjamin S. Glick. JCC helped design all experiments, created all new plasmids, performed the *Saccharomyces* and mammalian tissue culture experiments, and wrote the manuscript. AZ helped design and performed all *Drosophila* experiments. DS helped design and performed all of the *Tetrahymena* experiments. APT supervised the *Tetrahymena* experiments. SHB supervised the *Drosophila* experiments. BSG helped design all experiments, supervised the project, and wrote the manuscript.

Introduction

Our knowledge of the secretory pathway has gradually moved beyond morphological observations to studies of the underlying molecular machinery. Most of the key players have been identified, and they are being increasingly characterized at the biochemical and structural levels. Yet fundamental questions remain about how these components work together to drive membrane traffic. In this regard, a powerful technique is the tracking of secretory cargoes in live cells using fluorescence microscopy (Lippincott-Schwartz et al., 2000). A natural or artificial secretory cargo is typically labeled with a fluorescent protein. It is beneficial to trap the secretory cargo initially in the ER, for two reasons. First, a residence period in the ER gives the fluorescent protein portion of the cargo enough time to acquire a mature chromophore. Second, when the accumulated cargo is released to allow ER exit, the resulting wave of transport can be tracked to visualize the stages of cargo movement through the secretory pathway (Trucco et al., 2004; Boncompain and Perez, 2013).

Several strategies have been used to generate regulatable secretory cargoes for mammalian cells. Tagged versions of thermosensitive tsO45 mutant of the viral glycoprotein VSV-G can be made to accumulate in the ER at 40°C, and can be released for ER exit by dropping the temperature to 32°C (Presley et al., 1997; Scales et al., 1997). Similarly, procollagen can be made to accumulate in the ER at 40°C, and can be released for ER exit by reducing the temperature and adding ascorbic acid (Mironov et al., 2001). These regulatable secretory cargoes are unlikely to be suitable for other model organisms. A newer approach is retention using streptavidin "hooks" (RUSH) (Boncompain et al., 2012; Boncompain and Perez, 2013; Chen et al., 2017). Streptavidin is fused to a resident ER protein, and it traps a secretory cargo that is tagged with the streptavidin-binding peptide (SBP). Addition of biotin to the medium inhibits the streptavidin/SBP interaction and releases the secretory cargo for ER exit. RUSH has the major advantage of being compatible with a variety of natural secretory cargoes, but the initial trapping event requires a low biotin concentration. In our hands, this limitation has prevented the RUSH method from being adapted to yeast cells (data

not shown), and similar issues might arise with other model organisms. A more versatile regulatable secretory cargo was described by Rivera et al. (2000). They fused GFP to four copies of the reversibly dimerizing F36M mutant of FK506-binding protein (FKBP). When this construct was targeted to the ER, dimerization of the FKBP domains created aggregates, which could be dissolved by adding a ligand that interfered with FKBP dimerization. We adapted this approach for yeast, with modifications. Improved FKBP variants with F36L and I90V mutations exhibit an increased affinity for the ligand and faster disaggregation (Barrero et al., 2016). When a single copy of such an FKBP variant, termed FKBPRD(C22V), was fused to the highly soluble tetrameric fluorescent protein DsRed-Express2 (Strack et al., 2008), the result was red fluorescent aggregates that could be dissolved readily upon addition of the drug SLF, a synthetic ligand of FKBP (Figure 5.1A) (Holt et al., 1993; Barrero et al., 2016; Casler et al., 2019). This construct was targeted to the ER lumen in yeast strains defective for drug transporters (Barrero et al., 2016). Fluorescent aggregates formed in the ER lumen without causing detectable cellular stress, and addition of SLF dissolved the aggregates to produce soluble tetramers that exited the ER (Casler et al., 2019).

For the basic DsRed-Express2- FKBPRD(C22V) secretory cargo, ER export was expected to occur at the relatively slow rate of bulk flow (Barlowe and Helenius, 2016). A crucial enhancement was to fuse the tripeptide APV to the N terminus of the mature secretory cargo. This tripeptide is recognized by the Erv29 cargo receptor, and it confers rapid transport from the ER to the Golgi (Barlowe and Helenius, 2016; Yin et al., 2018). The final fusion protein consisted of a cleavable ER signal sequence that drove cotranslational translocation into the ER lumen, followed by a tripeptide ER export signal, followed by a tripeptide N glycosylation signal, followed by DsRed-Express2, followed by FKBPRD(C22V) (Figure 5.1B) (Casler and Glick, 2019). Here we designate the mature fusion protein "ESCargo" for Erv29-dependent Secretory Cargo. Addition of SLF generated a wave of fluorescent ESCargo that could be tracked in maturing Golgi cisternae (Casler et al., 2019). This approach was subsequently extended by adding a C-terminal vacuolar targeting peptide to ESCargo,

thereby enabling a kinetic analysis of biosynthetic traffic to the yeast vacuole (Casler and Glick, 2020). We anticipated that the original secreted version of ESCargo could be used in other cell types, including cultured mammalian cells. Efficient ER export should be conserved because mammalian Surf4 is an Erv29-related ER export receptor that recognizes the same type of tripeptide signals (Mitrovic et al., 2008; Yin et al., 2018). To adapt ESCargo for use in a given organism, the requirement is to append an appropriate ER signal sequence and then express this construct using a suitable vector. By comparing ESCargo with a version that lacks the tripeptide recognized by Erv29/Surf4, the kinetics can be measured for bulk flow ER export versus signal-dependent ER export (Casler et al., 2019). We now document the utility of ESCargo as a regulatable fluorescent secretory cargo in diverse eukaryotes.

Results and Discussion

ESCargo undergoes signal-dependent ER export in yeast

ESCargo was originally developed to track secretion in yeast (Casler and Glick, 2019; Casler et al., 2019). This protein is targeted to the ER by the Ost1 signal sequence, which drives cotranslational translocation (Willer et al., 2008; Fitzgerald and Glick, 2014), thereby ensuring that fluorescent aggregates form in the ER lumen. The precursor protein containing the yeast signal sequence is here designated ESCargo-Y.

For the present analysis, we used a modified assay to verify the earlier finding that ER export of solubilized ESCargo is accelerated by Erv29 (Casler et al., 2019). Instead of measuring loss from the ER by quantifying static images taken after SLF addition (Casler et al., 2019), we tracked the total fluorescence signals in individual cells using 4D confocal microscopy, and then averaged the resulting traces. The analyzed cells were chosen to have similar levels of fluorescent aggregates. Although the expression vector for ESCargo Y was integrated into the genome as a single copy, there was cell-to-cell variation in the amount of aggregated ESCargo in the ER, and we reasoned that high levels of ESCargo would saturate the ER export system. Thus, the experiment focused on cells containing moderate amounts

of aggregated ESCargo. The quantification was performed in parallel using *ERV29* wild-type and *erv29*Δ strains.

Figure 5.1C and Movie 5.1 show images of two cells: an *ERV29* wild-type cell and an *erv29*Δ cell that expressed ESCargo-Y. One limitation of ESCargo is that after SLF is added, this drug must be present continuously inside the cells to prevent reaggregation. Yeast cells have pleiotropic drug transporters, so our strains carried deletions of *PDR1* and *PDR3*, which encode transcription factors that drive expression of multiple drug transporters (Schüller et al., 2007; Coorey et al., 2015; Barrero et al., 2016). The strains also carried the *vps10-104* allele, which prevents fluorescent proteins from being diverted to the vacuole by the sortilin homolog Vps10 (Fitzgerald and Glick, 2014; Casler et al., 2019). Addition of SLF dissolved the ESCargo aggregates rapidly in both the *ERV29* and *erv29*Δ cells (Figure 5.1C and Movie 5.1). In the *ERV29* cell, the solubilized ESCargo initially appeared in dynamic puncta, some of which contained the early Golgi marker, and then largely disappeared from the cell within 10 min (Casler et al., 2019). By contrast, in the *erv29*Δ cell, the solubilized ESCargo persisted in the ER. Quantification of those cellular fluorescence signals is shown in Figure 5.1D, and quantification of averaged fluorescence signals from multiple cells is shown in Figure 5.1E. For the *ERV29* strain, ESCargo levels began to drop rapidly about 5 min after addition of SLF. This effect reflects a rapid wave of ER export followed by transport through the Golgi to the plasma membrane (Casler et al., 2019). For the *erv29*Δ strain, the signal declined much more gradually. Presumably, ER export in this strain occurred at the slow rate of bulk flow. In support of this interpretation, an immunoblot of ESCargo in the culture medium confirmed that secretion was rapid for the *ERV29* strain but much slower for the *erv29*Δ strain (Figure 5.1F). Thus, ESCargo undergoes signal-dependent ER export mediated by the Erv29 receptor in an *ERV29* wild-type strain, or bulk flow ER export in an *erv29*Δ strain.

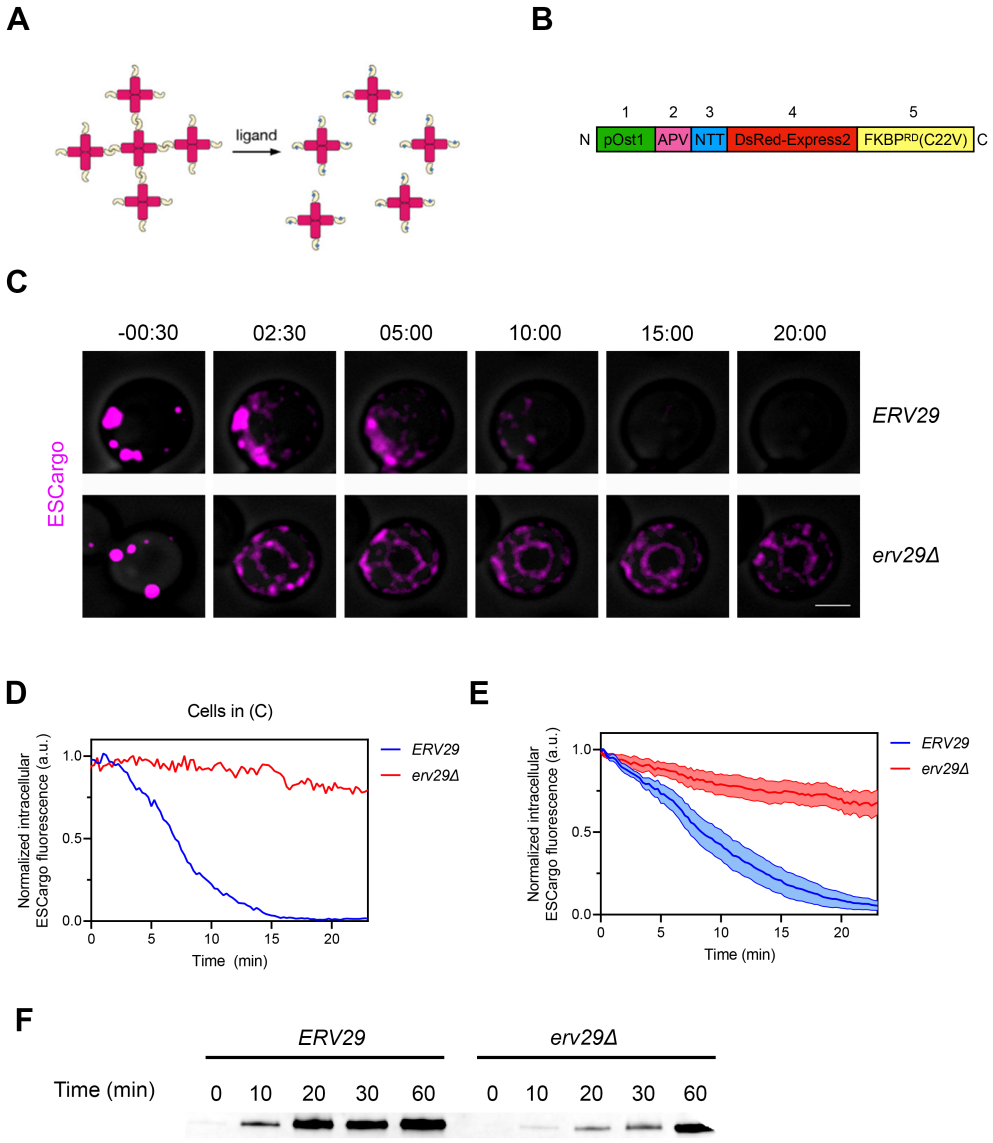

Figure 5.1: ESCargo traffic in *Saccharomyces cerevisiae.* **(A)** Strategy for generating and dissolving fluorescent aggregates. DsRed-Express2 tetramers (red) fused to an dimerizing variant of FKBP (gold) cross-link to form aggregates. Addition of the FKBP ligand SLF (blue) blocks dimerization, thereby dissolving the aggregates into soluble tetramers. **(B)** Cartoon depiction of the functional domains of the reversibly aggregating cargo. (1) pOst1 (green): ER signal sequence that directs cotranslational translocation. (2) APV (pink): ER export signal tripeptide. (3) NTT (blue): N-linked glycosylation signal tripeptide. (4) DsRed-Express2 (red): tetrameric red fluorescent protein. (5) FKBPRD(C22V) (gold): reversibly dimerizing variant of FKBP. The lengths of the different segments are not to scale. *Continued on next page.*

Figure 5.1: **(C)** Comparing secretion of ESCargo in yeast containing or lacking Erv29. *ERV29* and *erv29*Δ *Saccharomyces* strains expressing ESCargo were grown overnight to mid log phase in NSD, adhered to a ConA treated confocal dish, and imaged on a Leica SP5 confocal microscope. Images were captured every fifteen seconds for twenty five minutes. After the first two frames, SLF was added directly to the dish to a concentration of 100μM. Shown are representative images from Movie 5.1. Scale bar 2μm. **(D)** Quantification of the total intracellular ESCargo fluorescence from the cells in (C). The brightfield image was used to select the cell profile and quantify the total ESCargo fluorescence at each timepoint. **(E)** Average total intracellular ESCargo fluorescence. Data taken from at least 8 cells from 3 movies. Error bars represent SEM. **(F)** Detecting ESCargo secretion into the medium via immunoblot. The strains imaged in (C) were grown overnight in rich YPD medium to an OD of 0.7-1.0. Cultures were washed twice with deionized water and resuspended in YPD to the same optical density. The cultures were then treated with 100μM SLF to dissolve the ESCargo aggregates. Secreted ESCargo was precipitated with TCA at the indicated timepoints, subjected to EndoH treatment to trim N-glycans, and analyzed via immunoblotting with an anti-FKBP antibody.

ESCargo undergoes signal-dependent ER export in cultured mammalian cells

To express ESCargo in mammalian cells and target it to the ER, we subcloned the ESCargo gene cassette into a vector that contained the EF-1α promoter followed by an IgH signal sequence (Strack et al., 2009b). A control ESCargo variant lacked both the tripeptide ER export signal and the tripeptide N-glycosylation signal. That control variant, here termed ESCargo*, has no known signals for ER export and was therefore expected to be a bulk flow secretory cargo. Both constructs were transfected into a Flp-In 293 T-REx cell line, which stably expressed the Golgi marker GalNAc-T2-GFP to label the juxtanuclear Golgi ribbon (Storrie et al., 1998). When the cells expressed ESCargo*, nearly all of them accumulated brightly red fluorescent round aggregates that dissolved upon SLF addition to fill the ER. A representative cell is shown in Figure 5.2A and Movie 5.2, with the data quantified in Figure 5.2B. In this cell, ESCargo* fluorescence began to appear in the Golgi by 10 min after SLF addition, and reached a plateau level in the Golgi of about 20-25% of the total initial fluorescence by 20 min. The cargo signal in the Golgi remained at nearly the same level for at least 60 min. Meanwhile, substantial cargo signal remained in the ER for the entire time course. The cells had been treated with cycloheximide to suppress new protein synthesis, so

the persistent ER signal was apparently due to slow ER export. These results were typical of the cells in the population, as indicated by the averaged data in Figure 5.2C. Thus, ESCargo* acts as expected for a bulk flow secretory cargo. When the cells instead expressed the original ESCargo containing the APV tripeptide, red fluorescence was once again observed, but for most of the cells, the fluorescence pattern showed little change upon SLF addition. This effect highlights a limitation of ESCargo: as previously documented for yeast cells, there is a kinetic competition between aggregation in the ER and signal-dependent ER export (Casler et al., 2019; Casler and Glick, 2020). In mammalian cells, ER export tends to win the race, and so much of the ESCargo accumulates in post-ER compartments. This problem was overcome by using a less potent ER export signal (Yin et al., 2018). The FTV tripeptide gave satisfactory results, with nearly all of the cells exhibiting fluorescent aggregates that dissolved upon SLF addition to fill the ER (Figure 5.2A and Movie 5.2). We therefore used the FTV variant of ESCargo for further experiments with mammalian cells. The precursor protein containing the mammalian signal sequence and the FTV tripeptide is here designated ESCargo M, and the bulk flow version of this precursor protein is designated ESCargo* M. After SLF addition, ESCargo (with the FTV tripeptide) rapidly exited the ER and accumulated in the Golgi, with about 80% of the total initial fluorescence in the Golgi by 20 min after SLF addition (Figure 5.2 and Movie 5.2). Then ESCargo fluorescence in the Golgi progressively declined. Starting at ~25 min after SLF addition, small, mobile ESCargo-containing structures were visible near the Golgi. These structures were presumably secretory carriers (Hirschberg et al., 1998; Toomre et al., 1999; Polishchuk et al., 2000). At the 60 min time point, most of the ESCargo fluorescence had left the cells, although some signal remained in the Golgi (Figure 5.2 and Movie 5.2). The combined results indicate that ESCargo transits the mammalian secretory pathway in a manner that involves receptor-dependent ER export.

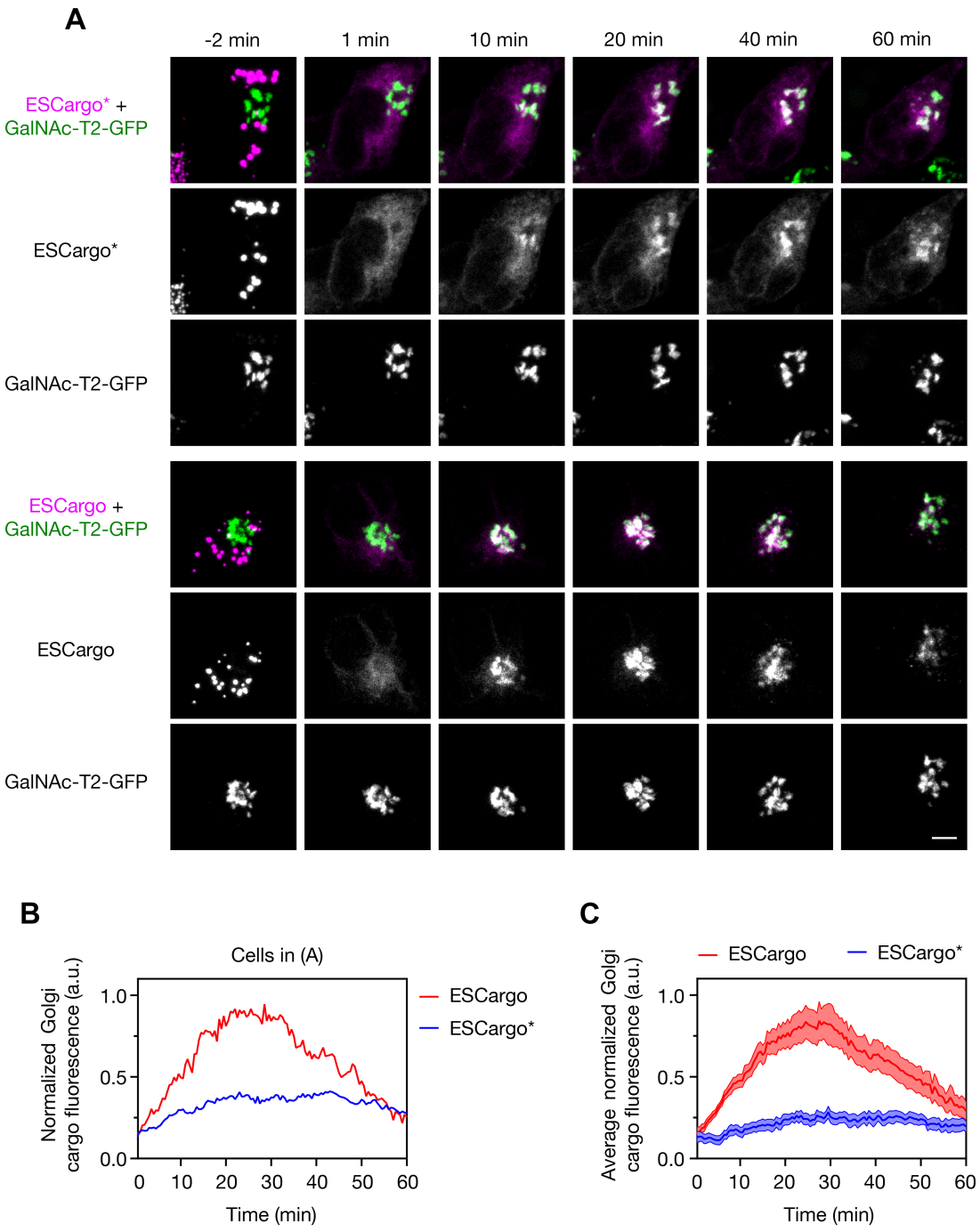

Figure 5.2: **ESCargo traffic in cultured mammalian cells.** *Continued on next page.*

ESCargo undergoes signal-dependent ER export in Drosophila cells

In a procedure similar to the one described above for mammalian cells, the *Drosophila* BiP signal sequence (Ohmuro-Matsuyama and Yamaji, 2018) was fused to ESCargo and

Figure 5.2: **(A)** Comparison of the bulk flow ESCargo* variant with signal-containing ESCargo. Flp-In 293 T-REx cells stably expressing the Golgi marker GalNAc-T2-GFP were grown on PEI-coated confocal dishes, and transfected with pIgH-ESCargo* (top) or pIgH-ESCargo (bottom) 24 – 48 h before imaging by 4D confocal microscopy. Following cycloheximide treatment, SLF was added directly to the dish to a final concentration of 50 μM at time 0. For each cargo variant, the top row shows the merged images while the other two rows show the red and green channels. Images are average projected Z-stacks. Scale bar, 5 μm. (B) Quantification of Golgi-associated cargo fluorescence for the cells in (A). The GalNAcT2-GFP signal was used to create masks to quantify the Golgi-associated fluorescence in the cargo channel. (C) Quantification was performed as in (B) to generate averaged time courses, using at least 7 cells from 6 movies for each variant. Error bars represent SEM.

ESCargo* to yield the precursor proteins ESCargo D and ESCargo* D, respectively. ESCargo D contained the original APV tripeptide. The two constructs were expressed in *Drosophila* S2 cells together with the Golgi marker ManII-GFP, which labeled the multiple individual Golgi stacks present in those cells (Zhou et al., 2014). Both ESCargo and ESCargo* formed red fluorescent round aggregates that dissolved rapidly upon addition of SLF (Figure 5.3A,B and Movie 5.3). ESCargo* was visible in the ER throughout the time course, and was also persistently visible in the Golgi starting at 5-10 min. By contrast, ESCargo showed only a very transient distribution throughout the ER, and then transferred completely to the Golgi within 2 min (Figure 5.3A,B and Movie 5.3). Most of the ManII-GFP-labeled structures acquired ESCargo fluorescence. The remaining ManII-GFP-labeled structures were probably not Golgi stacks, because separate triple-label experiments (Figure 5.5) indicated that the cells contained some ManII-GFP-labeled structures that were distant from the ER exit site marker Tango1 and the Golgi marker GM130. Starting at about 10 min after SLF addition, ESCargo began to depart from the Golgi stacks in small mobile carriers, and by 20 min, the cellular ESCargo fluorescence was almost completely gone (Figure 5.3A,B and Movie 5.3). These results indicate that ESCargo exits the *Drosophila* ER in a signal-dependent manner and then travels rapidly through the secretory pathway. *Drosophila* also presented an opportunity to test whether ESCargo could be used in a multicellular organism. We generated a *Drosophila* line containing the ESCargo-D construct inserted on chromosome 3R. Expression in follicular epithelial cells in the egg chamber resulted in large red fluorescent

aggregates (Figure 5.3C). After incubation with SLF for 5 min, much of the red fluorescence had redistributed to Golgi stacks marked by YFP-Rab10 (Figure 5.3C) (Lerner et al., 2013). This result suggests that ESCargo behaves similarly in cultured cells and in an intact tissue.

ESCargo undergoes regulated secretion in Tetrahymena thermophila*

So far our analysis had been limited to opisthokonts, which are closely related to one another from an evolutionary standpoint. We therefore turned to the evolutionarily distant ciliate *Tetrahymena thermophila*. In addition to its specialized organelles, *Tetrahymena* contains standard secretory pathway organelles including the ER and Golgi, and this model organism has been used extensively to study membrane traffic (Nusblat et al., 2012). For translocation into the *Tetrahymena* ER, we used the signal sequence of the mucocyst protein Grl1 (Chilcoat et al., 1996). The cleavage site of this signal sequence has not been experimentally determined, so it was not possible to create a construct in which the APV tripeptide was located at the N terminus of the mature protein. Instead, the Grl1 signal sequence was simply fused to ESCargo*. This construct was expressed under control of a cadmium-inducible *Tetrahymena* promoter (Shang et al., 2002). No fluorescence was seen before induction (Figure 5.5), but after induction, the cells contained scattered punctate fluorescent structures that were presumably ER-localized aggregates (Figure 5.4A). The puncta remained stable for at least an hour (Figure 5.5). Upon addition of SLF, the puncta disappeared, and the cells exhibited dispersed fluorescence in an ER-like pattern throughout a 30-min time course (Figure 5.4A). By 30 min, some punctate fluorescence had returned (Figure 5.4A), perhaps due to reaggregation caused by extrusion or degradation of SLF. Within 5 min of adding SLF, secreted protein could be detected in the medium by immunoblotting (Figure 5.4B). A full analysis would involve experiments that are beyond the scope of this study, including identification of the signal sequence cleavage site, testing of putative tripeptide ER export signals, colocalization tests with organelle markers, and a time course of secretion. However,

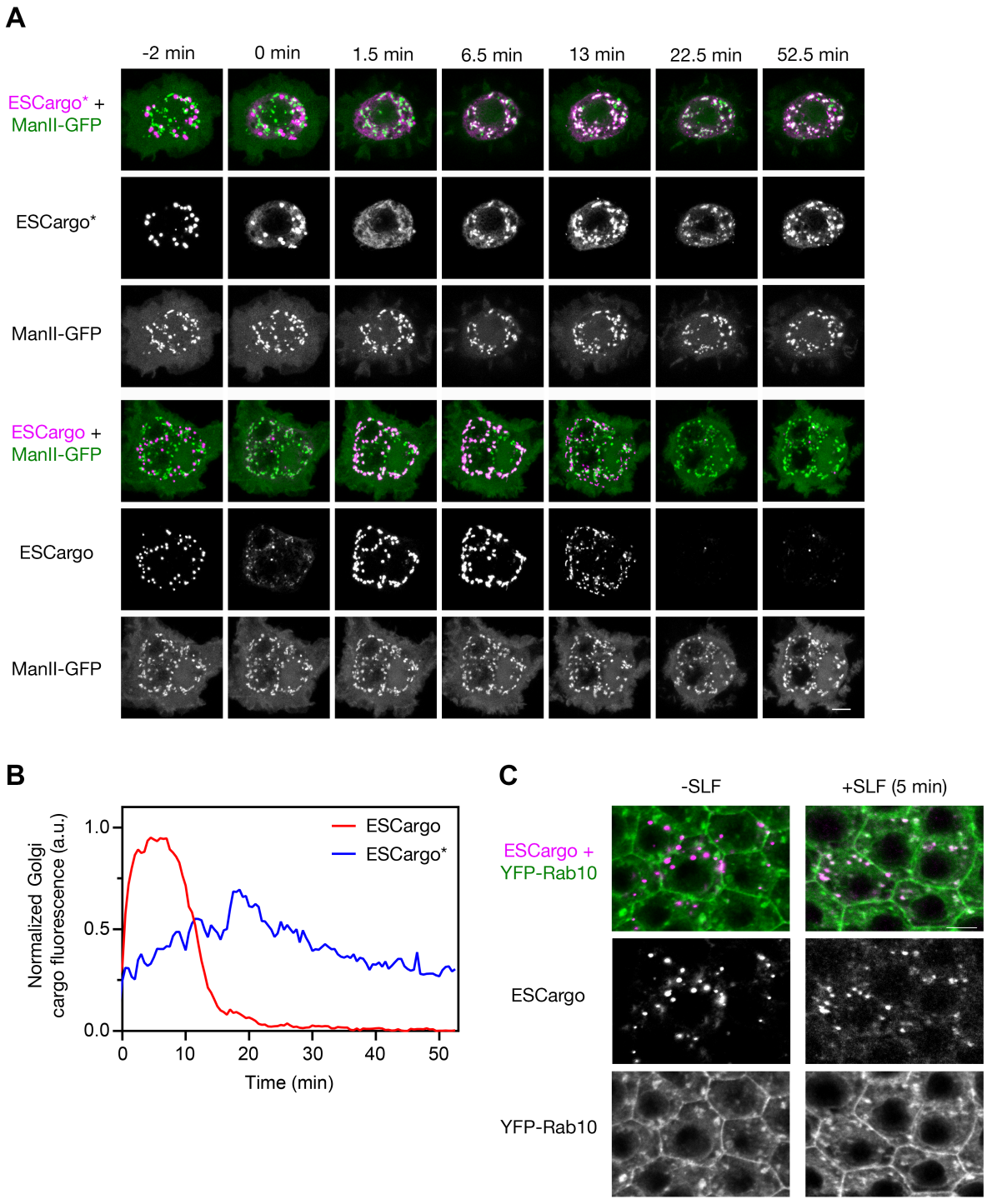

Figure 5.3: **ESCargo traffic in *Drosophila melanogaster*.** *Continued on next page.*

the available results suggest that ESCargo* can serve as a regulatable secretory cargo in *Tetrahymena*.

Figure 5.3:. **(A)** Comparison of the bulk flow ESCargo* variant with signal-containing ES-Cargo in *Drosophila* S2 cells. The cells were transfected 3 – 4 days before imaging with Ubi-GAL4, pUASt-ManII-eGFP, and either pUASt-ssBiP-ESCargo* (top) or pUASt-ssBiP-ESCargo (bottom). Cells were adhered to ConA-coated confocal dishes for 30 min before imaging on a Zeiss LSM 880 laser scanning confocal microscope. After 2 min of imaging, SLF was added directly to the dish to a final concentration of 50 μM. For each cargo variant, the top row shows the merged images while the other two rows show the red and green channels. Images are average projected Z-stacks. Scale bar, 5 μm. (B) Quantification of Golgi-associated cargo fluorescence for the cells in (A). The ManII-GFP signal was used to create masks to quantify the Golgi-associated fluorescence in the cargo channel. (C) Colocalization of ESCargo with the Golgi in Drosophila egg chamber follicular epithelial cells. Egg chambers from a Drosophila line (w; traffic jam-Gal4/+; UASt-ssBiP-ESCargo/UASp-YFP-Rab10) expressing ESCargo and YFP-Rab10 were fixed before and 5 min after introducing 50 μM SLF. Imaging was performed on a Zeiss LSM 880 laser scanning confocal microscope. Shown are average projected Z-stacks of the central four slices. the top row shows the merged images while the other two rows show the red and green channels. Scale bar, 5 μM.

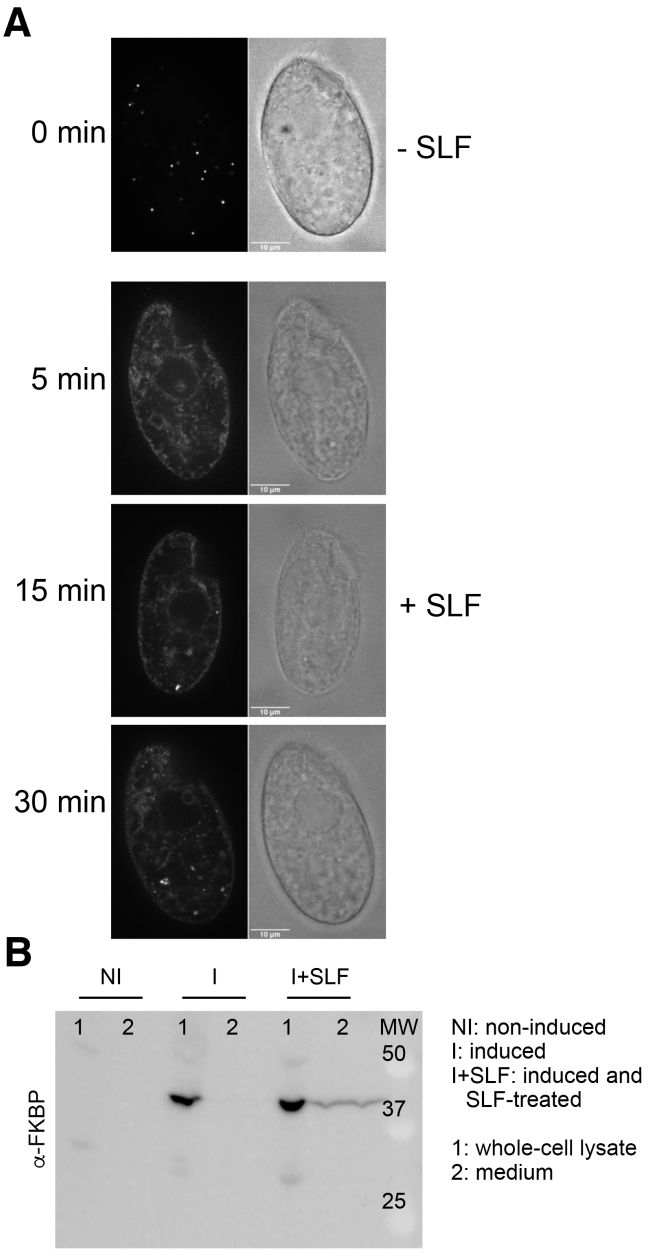

Figure 5.4: **ESCargo traffic in *Tetrahymena thermophila*.** *Continued on next page.*

Figure 5.4: **(A)** Confocal cross sections of fixed *Tetrahymena* expressing ESCargo* with paired DIC images. Protein expression was induced with 0.5 μg/ml CdCl2 prior to SLF treatment. From the top to the bottom: the first panel shows images of cells fixed immediately after induction (0 min), while the second, third, and fourth panels show images of CdCl2-induced cells treated with 12.5 μM SLF for 5, 15 and 30 minutes, respectively. 100-ms exposure time was used to image cells at time 0, while 400-ms were used for other time points. The bright fluorescent puncta visible at time 0 disappeared after 5 min incubation with SLF, replaced by dispersed fluorescence in ER-like membranes including the nuclear envelope. At 30 min, some punctate fluorescence reappeared. Scale bars, 10m. **(B)** Secretion ESCargo* into the growth media was monitored by western blot. *Tetrahymena* expressing EScargo* were treated with 12.5 μM SLF for 5 minutes. TCA-precipitated cell pellets and cell-free medium were analyzed by SDS-PAGE and Western blotting with anti-FBKP antibodies. The expected full-length proteins were detected in whole cell lysates (1) of untreated (I) and SLF-treated (I+SLF) CdCl2-induced cells, but only in the supernatant of (2) of SLF-treated (I+SLF) cells. Bulk flow and signal mediated cargo were not detected in non-induced cells (NI).

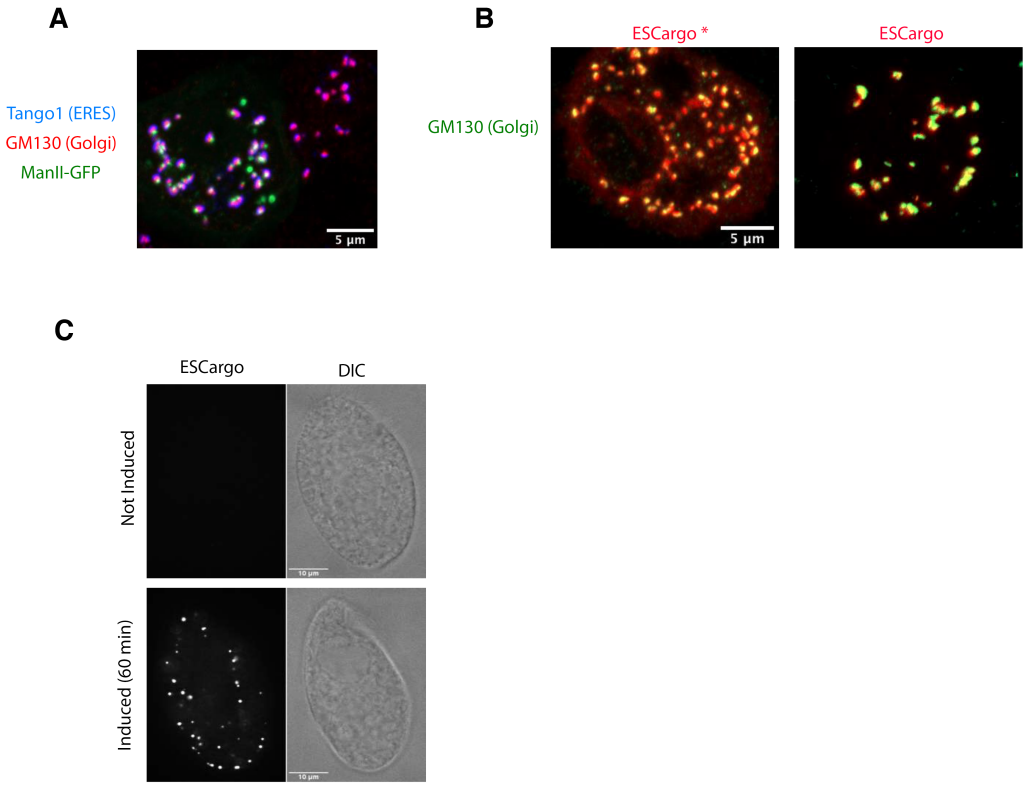

Figure 5.5: **Organelle marker and induction controls. (A)** Some ManII-GFP puncta do not colocalize with Golgi or ERES markers. *Drosophila* S2 cells expressing ManII-GFP were fixed and stained for GM130 (Golgi marker) and Tango1 (ERES marker). Note the few ManII-GFP puncta that do not contain GM130 or Tango1 signal. Scale bar 5μm. **(B)** ESCargo accumulates in all Golgi stacks. *Drosophila* S2 cells expressing EScargo* or ES-Cargo were treated with 50μM SLF for 5 minutes, fixed, and stained for GM130 (Golgi marker). Note that all GM130 puncta have corresponding ESCargo signal. Scale bar 5μMm. **(C)** Confocal cross sections of fixed *Tetrahymena*. The top panel shows non-induced cells, while the bottom shows CdCl2-induced cells expressing ESCargo*, with paired DIC images. ESCargo expression was induced as in figure 5.4A, after which cells were suspended in drug-free medium for 60 minutes before fixation. 100-ms and 400-ms exposure times were used to image induced and non-induced cells, respectively. ESCargo puncta were not detected in non-induced cells, but persisted for at least 60 minutes in CdCl2-induced (SLF-untreated) cells. Scale bars, 10μm.

Conclusions

Our analysis shows that ESCargo can be used as a regulatable red fluorescent secretory cargo in model organisms. If a different fluorescent color is desired, the DsRed-Express2 portion of the cargo can be replaced with a DsRed-Express2 variant, either the orange E2 Orange (Strack et al., 2009a) or the far-red E2 Crimson (Strack et al., 2009b). We have seen good results with those variants (data not shown). In *S. cerevisiae*, *Drosophila*, and mammalian cells, SLF can be used to trigger rapid dissolution and Erv29/Surf4-dependent ER export of ESCargo. It is unknown whether more evolutionarily distant organisms such as plants have Erv29/Surf4 homologs that recognize tripeptide ER export signals. However, initial results with the ciliate Tetrahymena thermophila suggest that in a wide range of eukaryotes, ESCargo aggregates can be generated in the ER and then dissolved with SLF to trigger secretion.

The ESCargo method has two limitations. First, when ESCargo molecules containing the APV tripeptide enter the ER, they experience a kinetic competition between aggregation and signal-dependent ER export (Casler et al., 2019; Casler and Glick, 2020). As a result, a substantial fraction of the newly synthesized ESCargo molecules are either secreted or delivered to post-ER compartments. Although this phenomenon did not interfere with our studies of biosynthetic traffic in yeast, it did prevent efficient trapping of ESCargo aggregates in mammalian cells. We solved this problem by using the FTV tripeptide, which is a less potent ER export signal (Yin et al., 2018) that allows for aggregate formation while still conferring rapid ER export of the solubilized ESCargo tetramers. Other tripeptide ER export signals might be optimal for different model organisms. Second, some cells efficiently extrude SLF, thereby preventing complete and sustained dissolution of ESCargo aggregates. We overcame that hurdle for *S. cerevisiae* by blocking the expression of pleiotropic drug transporters (Barrero et al., 2016; Casler and Glick, 2019), but in the budding yeast *Pichia pastoris*, we have been unable to solubilize ER-localized ESCargo aggregates with SLF (data

not shown). Perhaps better results could be obtained with other FKBP ligands. However, in general, ESCargo is best suited to cells with limited capacity to export drugs.

We envision that ESCargo will be useful for addressing open questions about how the secretory pathway operates in diverse organisms. In particular, the available data support a cisternal maturation model for the traffic of secretory cargoes through the yeast Golgi (Casler et al., 2019, Kurokawa et al., 2019), but the mechanism of Golgi traffic in mammalian cells is ambiguous (Glick and Luini, 2011). According to a simple version of the maturation model, after secretory cargo molecules arrive at the mammalian Golgi, they should exhibit a lag period due to transit through the Golgi stack, and should then depart with linear kinetics. According to the rapid partitioning model, after secretory cargo molecules arrive at the Golgi, they should begin to exit immediately, and should depart with exponential kinetics (Patterson et al., 2008). We found that in mammalian cells, ESCargo showed a pronounced lag period in the Golgi before appearing in secretory carriers, as predicted by the maturation model, but some ESCargo molecules persisted in the Golgi for an extended time, as predicted by the rapid partitioning model. In *Drosophila* cells, ESCargo showed a lag period before appearing in secretory carriers, and then departed from the Golgi with close to linear kinetics, fulfilling both predictions of the maturation model. Although these observations are very preliminary and will require rigorous follow-up studies, they provide encouragement that new tools will help to paint a unified picture of the secretory pathway.

Materials and methods

Yeast growth, transformation, and microscopy

The parental haploid strain was JK9-3da (*leu2-3,112 ura3-52 rme1 trp1 his4*) (Kunz et al., 1993). Yeast were grown with shaking in baffled flasks at 23°C in the nonfluorescent minimal glucose dropout medium NSD (Bevis et al., 2002) or in the rich glucose medium YPD supplemented with adenine and uracil. Introduction of the *vps10-104* mutation and deletion of the *PDR1* and *PDR3* genes were performed as previously described (Casler

and Glick, 2019). Secretory cargo proteins were expressed using a *TRP1* integrating vector with the strong constitutive *TPI1* promoter and the *CYC1* terminator. To ensure similar expression between strains, each clone was verified to have a single copy of the integrated plasmid by PCR using primers 5' GTGTACTTTGCAGTTATGACG-3' and 5' AGTCAACCCCCTGCGATGTATATTTTCCTG-3'.

For live-cell fluorescence microscopy, yeast strains were grown in NSD (pH 4) at 23°C. Where indicated, SLF was diluted from a 100 mM stock solution in ethanol (Cayman Chemical; 10007974) to a final concentration of 100 µM. Cells were attached to a concanavalin A (ConA)-coated coverglass-bottom dish containing NSD (Losev et al., 2006), and were imaged on a Leica SP8 confocal microscope equipped with a 1.4 NA/63x oil objective using a 60 to 80 nm pixel size, a 0.25 to 0.30 µm Z-step interval, and 20-30 optical sections. Movies were deconvolved with Huygens Essential (Scientific Volume Imaging) using the classic maximum likelihood estimation algorithm, then converted to hyperstacks and average projected, then range-adjusted to maximize contrast in ImageJ (Johnson and Glick, 2019).

Mammalian cell culture, engineering, and microscopy

Flp-In 293 T-REx cells (Thermo Fisher; R78007) were maintained in 5% CO2 at 37°C in DMEM supplemented with 10% fetal bovine serum (GenClone; 25-550). Cells were transfected with 3 µg of DNA using FuGENE HD (Promega; E2311). Cells were regularly checked for mycoplasma contamination using a Mycoplasma Detection Kit (SouthernBiotech; 131001). To generate the Flp-In 293 T-REx cell line stably expressing GalNAc-T2-GFP, cells were transfected with pcDNA5-GalNAc-T2-GFP together with the Flp-recombinase expression vector pOG44 (Thermo Fisher; V600520). After two days, the medium was supplemented with 200 µg/mL hygromycin. Over the next two weeks, the media was replaced every few days until colonies were visible on the dish. Individual clones were scraped onto a new dish and expanded. Successful integration was confirmed by visualizing GalNAc-T2-GFP fluo-

rescence in all cells, newly acquired sensitivity to Zeocin (400 µg/mL), and resistance to hygromycin (200 µg/mL).

For live-cell fluorescence microscopy, cells were grown on coverglass-bottom dishes coated with polyethyleneimine (PEI) (Vancha et al., 2004). A dish was incubated with 250 µL of 25 µg/mL PEI (Sigma; 181978) in 150 mM NaCl for 10 min, and then the dish was washed and allowed to dry completely before adding cells. Prior to imaging, cells were treated with 100 µg/mL cycloheximide from a 100 mg/mL stock in DMSO for 15-30 min, and the medium was buffered with 15 mM Na+ HEPES, pH 7.4. Imaging was performed at 37°C on a Leica SP5 confocal microscope equipped with an incubator stage and a 1.4 NA/63x oil objective, using a 100 nm pixel size, a 0.5 µm Z-step interval, and ~30-40 optical sections. Z-stacks were average projected to make movies.

ImageJ was used to quantify the Golgi-associated secretory cargo signals in the movies. The first step was to measure background cellular fluorescence from a control movie of non-transfected cells. Then for each time point, the GalNAc-T2-GFP signal was used to create a mask, and the background-subtracted cargo signal within the mask was measured. These values were normalized to the initial cargo fluorescence, which was measured by quantifying the total background-subtracted cellular fluorescence at 1 min after SLF addition.

Drosophila cell culture, engineering, and microscopy

S2-DGRC cells were obtained from the *Drosophila* Genomic Resource Center (cell line 6). Cells were grown in Insect-XPRESSTM Protein-fee Insect Cell Medium supplemented with 1X antibiotic-antimycotic in a 25°C incubator. The DNA constructs used were Ubi-GAL4 (a gift of Richard Fehon), pUASt-ManII-eGFP (a gift of Bing Ye), and either pUASt-ssBiP-DsRed-Express2-FKBP(LV,C22V) or pUASt-ssBiP-APVNTT-DsRed-Express2-FKBP(LV,C22V). Transfection was performed using the dimethyldioactadecylammonium (DDAB) method (Han, 1996). DDAB and cell culture medium were mixed in a 1:2 ratio and incubated at room temperature for 10 min. To transfect a well in a 6 well plate, 1 μg of DNA was mixed

with 144 μL of the DDAB/medium solution and incubated for 15 min at room temperature, and this mixture was added to 2.6x10^6 cells in 2 mL of medium. The transfected cells were allowed to grow for 3-4 days before imaging.

For immunofluorescence microscopy, coverslips were incubated in 100 μg/mL ConA for 1 h, washed 3x in deionized water, and dried before use. Transfected cells were detached by pipetting, and 250 L of a cell suspension was added to a fresh 6-well plate containing a ConA-coated coverslip and 1.75 mL of media. Cells were allowed to spread for 1 h, and were then fixed in 4% formaldehyde diluted in phosphate buffered saline (PBS) for 10 min at room temperature. The fixed cells were washed, and permeabilized with PBS containing 0.1% Triton X-100 (PBST) 3x for 5 min each. Anti-GM130 antibody (Abcam; ab30637) and anti-Tango1 antibody (Lerner et al., 2013) were diluted 1:500 in PBST. A 100 μML drop of the antibody mixture was placed on a piece of parafilm in a humidified chamber, and the cell-coated coverslip was inverted onto this drop and incubated for 1 h at room temperature. The coverslip was washed 3x for 5 min each in PBST. Secondary antibodies (Thermo Fisher; A-27039 and A-2145) diluted 1:500 in PBST were added for 1 h at room temperature, and the samples were washed 3x for 5 min each in PBST. Finally, the coverslip was mounted in ProLongTM Gold (Thermo Fisher; P36930) and sealed with nail polish. Imaging was performed on a Zeiss LSM 800 laser scanning confocal microscope with Zen blue software and a 63x Plan Apo 1.4 NA oil objective.

For live imaging of S2 cells, transfected cells were detached by pipetting, and 250 μML of cells and 750 μML of fresh media were added to a 35 mm glass bottom dish coated with ConA using the procedure described above for coverslips. Cells were allowed to attach for 30 min, and were then imaged at room temperature on a Zeiss LSM 880 laser scanning microscope with Zen black software and a 63x Plan Apochromat 1.4 NA oil objective. Every 30 s for 1 h, a Z stack of 2-5 μm, depending on cell height, was captured using steps of 0.37 μm. After the first 2 min of imaging, 1 mL of medium containing 100 μM SLF was

added, yielding a final SLF concentration of 50 μM. The Z-stacks were average projected and quantified as described above for cultured mammalian cells.

Transgenic flies containing the pUASt-ssBiP-APVNTT-DsRed-Express2-FKBP(LV,C22V) plasmid were generated using PhiC31-mediated recombination. Insertions were generated on chromosomes 2L(attP40) and 3R(VK20) by GenetiVision. Both lines express well, and the VK20 insertion was used for all experiments in this paper. The egg chamber follicle cell driver traffic jam-Gal4 from the Drosophila Genetic Resource Center in Kyoto (DGRC 104055) was used to express both UASt-ssBiP-APVNTT-DsRed-Express2-FKBP(LV,C22V) and UASp-YFP-Rab10 from the Bloomington *Drosophila* Stock Center (BDSC 9789).

To examine ESCargo traffic in egg chambers, transgenic flies were reared on cornmeal molasses agar at 25°C using standard techniques. 1- to 2-day old females were aged on yeast with males for 2 days at 25°C. Ovary dissection was performed as described (Cetera et al., 2016). Ovaries were removed from yeasted females in dissection/live cell imaging medium (Schneider's *Drosophila* medium containing 15% FBS and 200 g/mL insulin). Ovariole strands were mechanically removed from muscle with forceps. Egg chambers older than stage 9 were cut away from the ovariole strand using a 27-gauge needle. To trigger a wave of ESCargo traffic, egg chambers were transferred to a 1.5 mL tube, and were incubated in fresh imaging medium for 5 min at room temperature with 50 M SLF, or without SLF as a negative control. Egg chambers were fixed in 4% formaldehyde in PBST for 15 min at room temperature, washed 3x for 10 min each in PBST, and mounted in 35 L ProLongTM Gold on a slide with a 22x50mm coverslip. The coverslip was then sealed with nail polish. Imaging was performed on a Zeiss LSM 800 laser scanning confocal microscope with Zen blue software and a 63x Plan Apo 1.4 NA oil objective.

Tetrahymena cell culture, engineering, and microscopy

Tetrahymena thermophila were grown overnight in SPP (2% proteose peptone, 0.1% yeast extract, 0.2% dextrose, 0.003% ferric-EDTA) supplemented with 250 μg/mL penicillin G,

250 μg/mL streptomycin sulfate, and 0.25 μg/mL amphotericin B fungizone, to medium density (0.6-2.0 x 10^5 cells/mL). For biolistic transformation, growing cells were subsequently starved in 10 mM Tris buffer, pH 7.4, for 18-20 h. Fed and starved cells were kept at 30°C with agitation at 99 rpm, unless otherwise indicated. Culture densities were measured using a Z1 Coulter Counter (Beckman Coulter Inc.).

Transformants were generated and selected after biolistic transformation as previously described (Kaur et al., 2017; Sparvoli et al., 2018). Transformants were serially transferred 6x per week in increasing concentrations of blasticidin and decreasing concentrations of CdCl2 (up to 90 μg/mL of blasticidin and 0.1 μg/mL CdCl2) for at least 3 weeks before further testing.

For fluorescence microscopy, cells were grown overnight in 20 mL SPP at 30°C with agitation at 99 rpm to 2.0x105 cells/mL. Transgene expression was induced with 0.5 g/mL CdCl2 for 90 min. Cells were then washed once with 20 mL SPP and resuspended in 20 mL of medium without CdCl2, prior to treatment with SLF. Incubation with 12.5 M SLF was for 5, 10, or 30 min in a 24-well plate (2 mL/well) at 30°C without agitation. Cells were then fixed by addition of ice-cold 4% paraformaldehyde, and incubated for 30 min at room temperature . Controls included CdCl2-induced cells fixed before the treatment with SLF (time 0) or kept for 60 min in SPP without SLF. Non-induced cells were grown, fixed, and imaged in parallel. Fixed cells were washed three times with PBS, mounted with Trolox (1:1000) to inhibit bleaching, and imaged at room temperature on a Marianas Yokogawa-type spinning disk inverted confocal microscope using a 100x 1.45 NA oil objective with SlideBook 6 software (Intelligent Imaging Innovations, Denver, CO). Z-stack images were denoised and adjusted for brightness and contrast using Fiji software (Schindelin et al., 2012).

To detect secreted proteins by immunoblotting, cells were grown overnight in 20 mL SPP to 0.6-0.8x10^5 cells/ml. 1.0x10^5 cells were transferred into 2 mL SPP for each experimental condition: non-induced, CdCl2-induced, and CdCl2-induced and SLF-treated. Protein expression was induced with 0.5 μg/mL CdCl2 for 90 min at 30°C. CdCl2-induced cells were

washed once with SPP and resuspended in 1 mL SPP without or with 12.5 μM SLF for 5 min at room temperature. Non-induced cells were washed and resuspended in SPP for 5 min without SLF. Cells were pelleted by centrifugation, and 500 μL of cell-free supernatant were precipitated by adding one-tenth volumes of 2% deoxycholate and 100% trichloroacetic acid (TCA). In parallel, the corresponding pellet fractions were precipitated with 10% TCA. TCA-insoluble pellets were suspended in 100°C LDS (lithium dodecyl sulfate) sample buffer containing 40 mM DTT, and analyzed by SDS-PAGE and immunoblotting as previously described (Sparvoli et al., 2018). A rabbit monoclonal anti-FBKP antibody (Abcam; ab2918) was diluted 1:1000 in blocking solution. Proteins were visualized with 1:20,000 anti-rabbit IgG (whole molecule)-peroxidase secondary antibody and SuperSignal West Femto Maximum Sensitivity Substrate (Thermo Fisher; 34095).

Movies Associated with Chapter 5

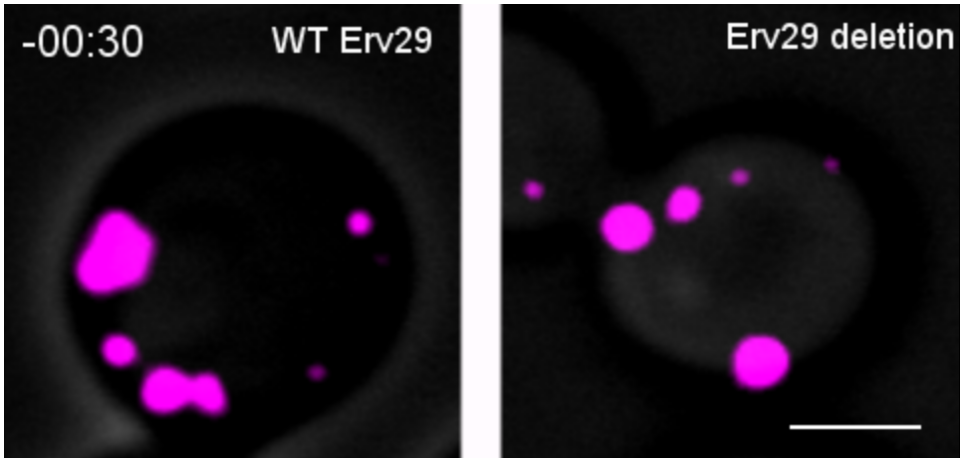

Movie 5.1. **ESCargo in *Saccharomyces cerevisiae*.** Visualizing ESCargo trafficking after release from the ER in *Saccharomyces cerevisiae*. WT *ERV29* and *erv29*Δ cells expressing ESCargo were grown to mid-log phase in NSD, adhered to a ConA treated confocal dish, and imaged via 4D confocal microscopy. SLF was added directly to the dish to 100μM at time 0. Z-stacks were taken every 15s. Shown are average projected Z-stacks. Images from this movie are shown in Figure 5.1C. Scale bar 2μm.

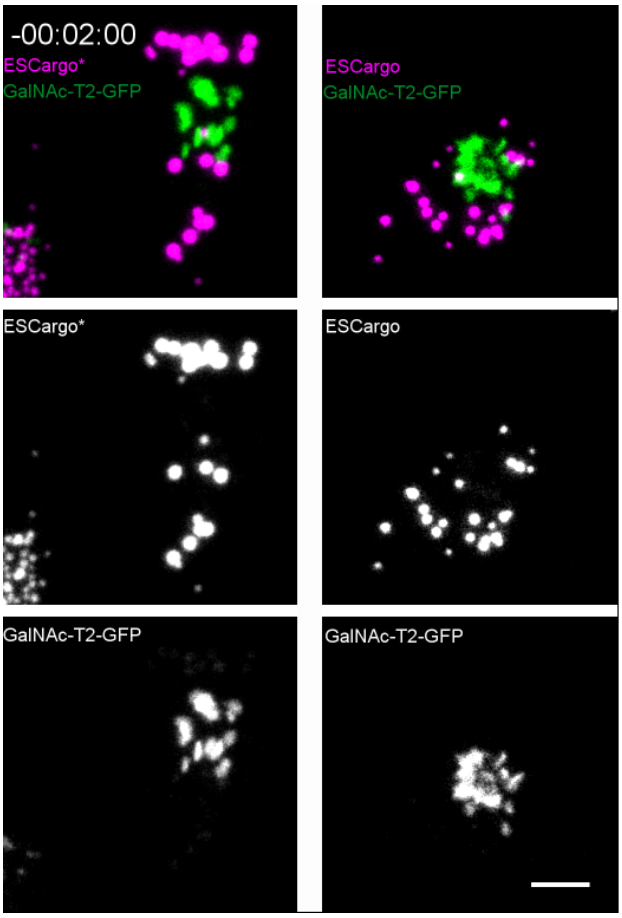

Movie 5.2. **ESCargo in mammalian tissue culture.** Visualizing ESCargo trafficking after release from the ER in Flp-In 293 T-REx cells stably expressing the Golgi marker GalNAc-T2-GFP. Cells were grown on PEI coated confocal dishes in DMEM + 10% FBS and transfected with either pIgH-ESCargo* or pIgH-ESCargo 24-48 hours before imaging. Media was buffered with 15mM HEPES and 100μg/mL cycloheximide was added 15-30 minutes prior to imaging. 4D confocal microscopy was performed on an incubated Leica SP5 incubated at 37C. SLF was added directly to the dish to 50μM at time 0. Z-stacks were taken every 30 s for one hour. Shown are average projected Z-stacks. Images from this movie are shown in Figure 5.2A. The top row shows a merged image and the subsequent channels show the ESCargo and GFP fluorescence channels respectively. Scale bar 5μm.

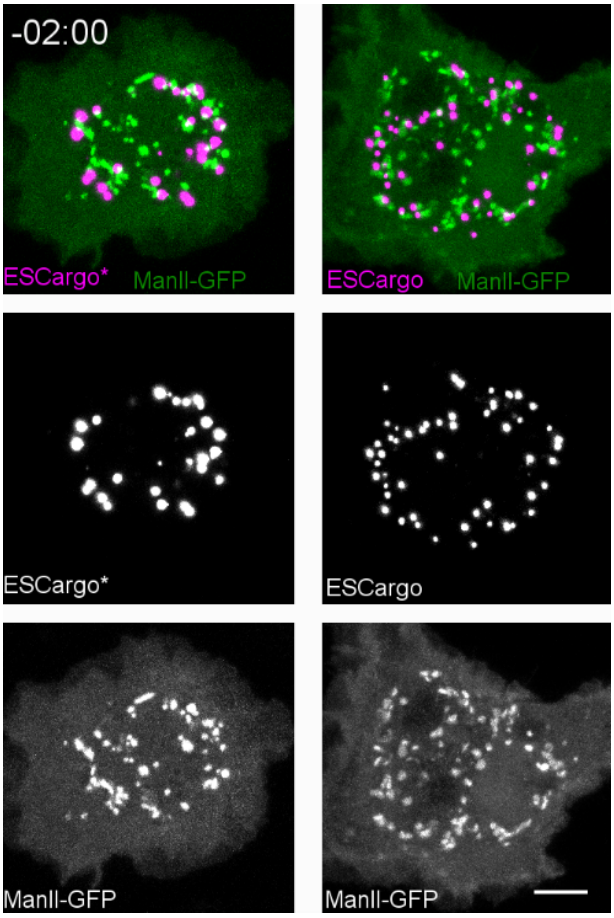

Movie 5.3. **ESCargo in *Drosophila* S2 cells.** Visualizing ESCargo trafficking after release from the ER in *Drosophila* S2 cells. Cells were transfected 3-4 days before imaging with Ubi-GAL4, pUASt-ManII-GFP, and either pUASt-ssBip-ESCargo* or pUASt-ssBip-ESCargo. Cells were adhered to ConA coated confocal dishes for thirty minutes before imaging. Imaging was performed on a Zeiss LSM 880 laser scanning confocal microscope. SLF was added directly to the dish to a final concentration of 50μM after 2 minutes of imaging. Shown are max projected Z-stacks. The top row shows a merged image and the subsequent channels show the ESCargo and GFP fluorescence channels respectively. Scale bar 5μm.

CHAPTER 6

THE AP-1 ADAPTOR COMPLEX DRIVES CISTERNAL MATURATION BY RECYCLING RESIDENT LATE GOLGI PROTEINS AND SECRETORY CARGO

Abstract

The AP-1 adaptor complex has been implicated in the formation of clathrin coated vesicles at the TGN. While some evidence supports AP-1 acting in an intra-Golgi recycling pathway the precise function of AP-1 has been ambiguous. To clarify the function of AP-1 at the TGN we sought to characterize how AP-1 interacts with secretory cargo and resident Golgi proteins. First, we demonstrated that secretory cargo can be recycled within the Golgi in a manner that specifically requires AP-1 and the mannosyltransferase Mnn1. Further, in AP-1 mutants inhibiting endocytosis causes the mislocalization of a subset of resident Golgi enzymes to the plasma membrane and severely disrupts cisternal maturation. Finally, a kinetic analysis of putative AP-1 cargoes revealed that some, but not all, resident Golgi proteins show altered kinetics in AP-1 mutants. Thus, AP-1 is involved in an intra-Golgi recycling pathway that drives cisternal maturation.

Introduction

Golgi maturation is driven by the continued recycling of resident Golgi proteins in vesicular carriers (Glick and Nakano 2009). COPI has been shown to be essential for the recycling of early but not late Golgi proteins (Papanikou et al., 2015; Ishii et al., 2016). Therefore, it is likely that a second intra-Golgi recycling pathway exists that operates at the late Golgi. The best candidate is the AP-1 clathrin adaptor complex. AP-1 was originally postulated to mediate the recycling of proteins from the early endosome to the TGN (Hinners and Tooze,

This chapter describes a series of experiments that will be included in a manuscript for publication in the near future. In this chapter, all experiments, figure design, and writing were performed by me, Jason C. Casler. Benjamin S. Glick supervised the project.

2003). A recent analysis of yeast endosomes, however, demonstrated that the TGN acts as both a recycling and early endosome in budding yeast (Day et al., 2018). Endocytic vesicles fuse directly with the TGN and all canonical early endosome markers localize to the TGN or PVE, demonstrating that no distinct early endosome exists. A kinetic analysis of AP-1 during Golgi maturation revealed that it resides exclusively on late Golgi cisternae (Day et al., 2018). Some late Golgi proteins, such as the chitin synthase Chs3, the Golgi SNARE Tlg1, and the aminophospholipid translocase Drs2, have been shown to mislocalize in AP-1 mutants (Valdivia et al., 2002; Liu et al., 2008). Recently, we have identified AP-1 as being involved in the intra-Golgi recycling of some secretory cargo (Casler et al., 2019). Thus, AP-1 is an excellent candidate for mediating an intra-Golgi recycling pathway at the late Golgi.

Interestingly, AP-1 mutants show only mild phenotypes. Without AP-1 Golgi maturation occurs at rates indistinguishable from wild type and many late Golgi proteins continue to localize normally (Casler et al., 2019). In contrast, COPI is essential and disrupting functionality has severe consequences on Golgi function and cell growth (Papanikou et al., 2015). If AP-1 mediates a critical intra-Golgi recycling pathway, why is Golgi maturation seemingly unaffected in AP-1 mutants? One possibility is that a parallel pathway operates to retrieve resident Golgi proteins in the absence of AP-1. Due to the yeast TGN functioning as an early endosome, one possible candidate is endocytosis. Terminal Golgi maturation results in the formation of secretory vesicles destined for the plasma membrane (Glick and Nakano 2009). Thus, in cells where intra-Golgi recycling is compromised one would expect to find resident Golgi proteins at the plasma membrane. Endocytosis could act as a retrieval mechanism to bring leaked proteins back to the Golgi (Figure 6.9). If this were the case, inhibition of endocytosis should disrupt Golgi maturation and enhance the mislocalization of late Golgi proteins in AP-1 mutants.

Here we provide evidence that AP-1 mediates an intra-Golgi recycling pathway that operates at the late Golgi to drive cisternal maturation by recycling resident Golgi proteins and secretory cargo. Removing AP-1 or the mannosyltransferase Mnn1 prevents the intra-Golgi

recycling of secretory cargo. Further, some late Golgi enzymes mislocalize in AP-1 mutants and mislocalization can be exaggerated by blocking endocytosis. Inhibiting endocytosis in AP-1 mutants leads to a severe disruption in cisternal maturation. Finally, putative AP-1 cargoes show kinetic signatures consistent with AP-1 mediated intra-Golgi recycling and at least one cargo, Drs2, shows altered kinetics in an AP-1 mutant.

Results and Discussion

AP-1 and Mnn1 are required for the intra-Golgi recycling of a secretory cargo

Our hypothesis was that AP-1 exclusively mediates an intra-Golgi recycling pathway that recycles resident Golgi proteins and secretory cargo from the late Golgi to younger cisternae. To test this, we first built on our previous work by probing the recycling of an artificial secretory cargo. During the early-to-late Golgi transition we saw a significant increase in the amount of cargo present in the maturing cisterna. This increase was lost when AP-1 was absent or when the cargo lacked N-glycans (See Chapter 3 Figure 3.11 and 3.13, Casler et al., 2019). If AP-1 is responsible for the increase in cargo signal during the early-to-late transition, then removing unrelated trafficking pathways should have no effect. To test this, we repeated the tracking of secretory cargo during the early-to-late transition in AP-3 and Gga mutants. AP-3 functions at the late Golgi to bring cargo directly to the vacuole while the Ggas function at the late Golgi to bring cargo to the PVE (Odorizzi et al., 1998; Myers and Payne, 2013). Deleting either of these trafficking routes did not prevent the transient increase in cargo signal seen during the early-to-late transition (Figure 6.1). Of note, the *gga1*Δ *gga2*Δ strain showed a shallower but broader increase in the cargo signal. The *gga1*Δ *gga2*Δ strain also showed slightly altered kinetics of cisternal maturation, as seen by the shallower Vrg4 and Sec7 slopes. One possibility is that cisternal maturation is slower in this background and the period of time when AP-1 vesicles can fuse is broader. Alternatively, it is possible that removal of the Ggas partially disrupts AP-1 function. In support of this,

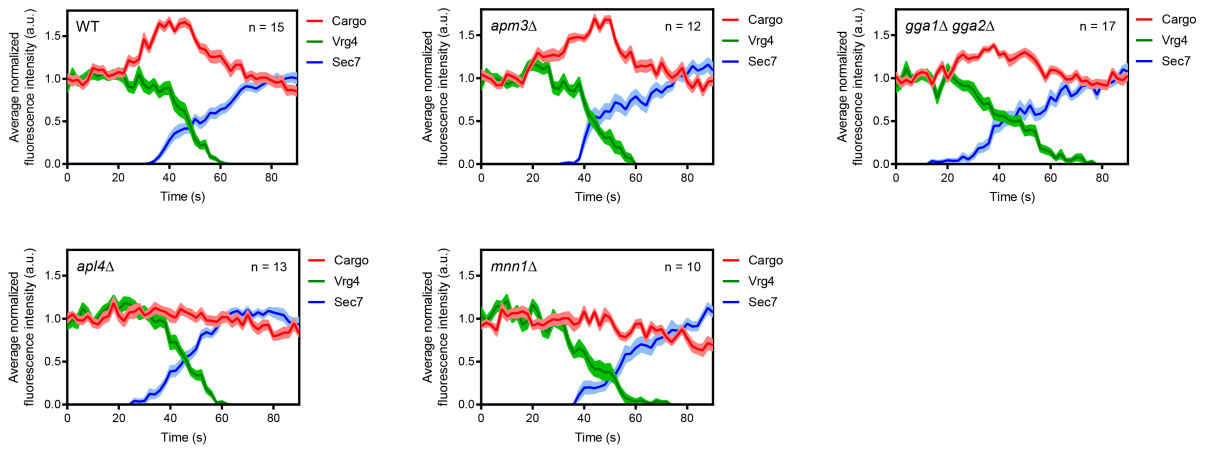

Figure 6.1: **AP-1 and Mnn1 are required for intra-Golgi secretory cargo recycling.** Plotting the average cargo signal during the early-to-late Golgi transition in the indicated genetic backgrounds. Cells expressing the early Golgi marker GFP-Vrg4, the late Golgi marker Sec7-HaloTag, and the artificial secretory cargo, pOst1-APVNTT-DsRedExpress2-FKBP(LV)(C22V), were grown to mid-log phase overnight, labeled with JF_{646}, treated with 100μM SLF for 3 minutes to release the cargo, and imaged via 4D confocal microscopy. In each genetic background fluorescence was quantified over a 90s window during the early-to-late Golgi transition with Z-stacks collected every 2s. Maturation events were aligned based on the midpoint of the GFP-Vrg4 to Sec7-HaloTag transition. Normalization was performed by defining 1.0 as the average of the first six fluorescence values for Vrg4 and the cargo or the average of the last six fluorescence values for Sec7. Shaded borders indicate SEM. The number of events analyzed are indicated in the top right corner of each graph.

the Ggas are partially responsible for recruiting Pik1 which is important for AP-1 function (Wang et al., 2003; Daboussi et al., 2012).

To probe the mechanism by which N-glycosylation causes incorporation of secretory cargo into AP-1 recycling vesicles we examined secretory cargo trafficking in a glycosylation mutant. Mnn1 localizes to the late Golgi and displays α1,3-mannosyltransferase activity, which is the last step in the sequential maturation of N-linked oligosaccharides in *S. cerevisiae* (Munro 2001). Interestingly, Mnn1 is also a strong candidate to be an AP-1 dependent recycling cargo as its TGN localization is dependent on clathrin (Graham et al., 1994). Deleting Mnn1 also completely blocked the increase of secretory cargo signal during the early-to-late transition (Figure 6.1). Thus, hypermannosylation is required for secretory cargo recycling.

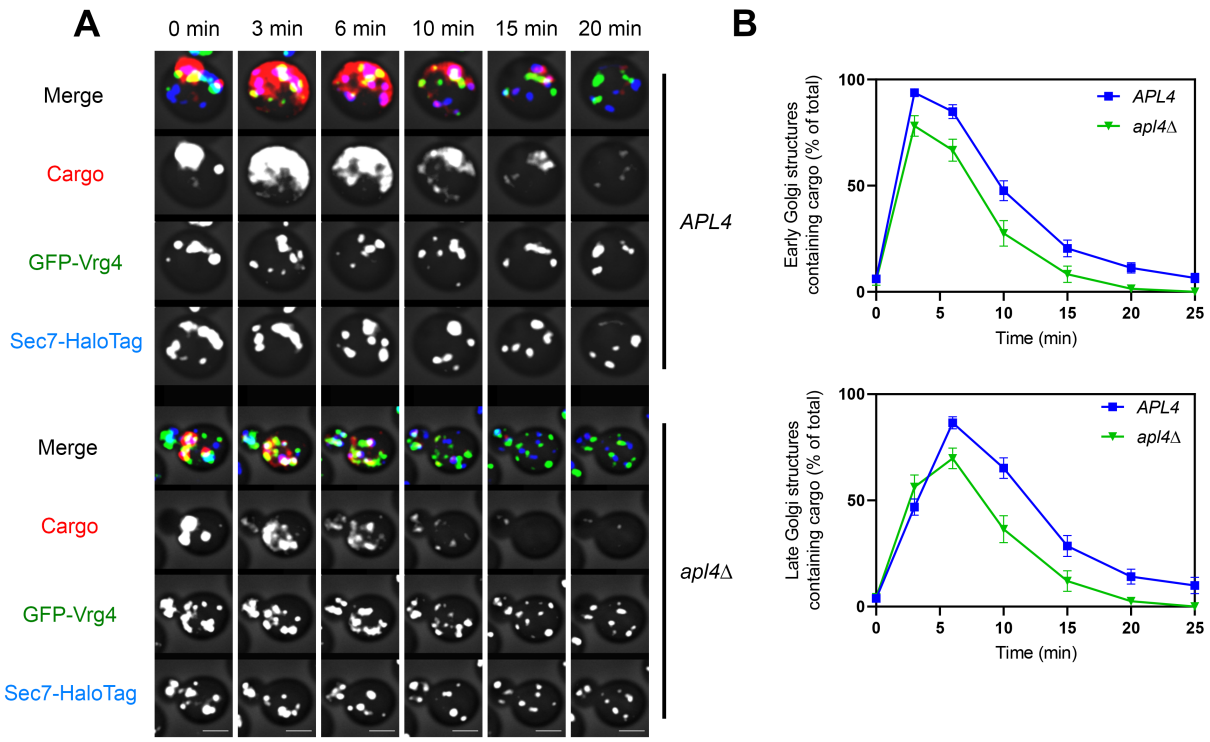

Figure 6.2: **A cargo wave traverses the secretory pathway faster in the absence of AP-1. (A)**. *APL4* (top) or *apl4*Δ (bottom) cells expressing an artificial secretory cargo, pOst1-APVNTT-DsRedExpress2-FKBP(LV)(C22V), GFP-Vrg4 (early Golgi marker), and Sec7-HaloTag (late Golgi marker), were grown to mid-log phase overnight in NSD, labeled with JF_{646}, and imaged via 4D confocal microscopy. SLF was added to 100μM directly after time point zero. The top panel shows the unedited image, and the following rows depict the individual fluorescent channels. Images are average projected Z-stacks. Scale bar 2μm.**(B)** Quantification of the percentage of Golgi cisternae containing cargo after release from the ER. Movies were average projected and manually scored for the presence or absence of cargo at the indicated time points. Only cells displaying a similar, moderate cargo expression level were analyzed. Error bars indicate SEM.

It is not obvious how an artificial soluble secretory cargo could partition into AP-1 recycling vesicles. AP-1 is thought to specifically recognize motifs in the cytosolic tails of transmembrane cargo proteins (Traub and Bonifacino, 2013). The observation that glycosylation is required for incorporation into AP-1 vesicles provides a potential link. Cargo molecules could remain kinetically associated with Mnn1 during glycan extension while Mnn1 is incorporated into AP-1 recycling vesicles. Thus secretory cargo would not be specifically recognized by AP-1 but would be incorporated into AP-1 vesicles indirectly via the interaction with an

AP-1 cargo. This would result in secretory cargo having an increased residence time in the Golgi and could serve as a quality control mechanism to ensure proper post-translational modification prior to secretion. Of course, this is speculative and will require a more rigorous characterization of the biochemical interaction between the secretory cargo and Mnn1 and assays to probe the glycosylation state of cargo in AP-1 vesicles.

In the absence of intra-Golgi secretory cargo recycling, cargo should transit the secretory pathway faster. To test this hypothesis, we tracked the Golgi localization of secretory cargo after release from the ER over a 25 minute time course in the presence or absence of AP-1. With AP-1 present, cargo localization at the early Golgi peaks within 3 minutes, followed by a later peak with the late Golgi (Figure 6.2 A and B). At 10 minutes half of the Golgi structures still contain cargo and by 25 minutes most cargo has left the cell. In the absence of AP-1, cargo localization at the early Golgi peaks at 3 minutes (or slightly before) followed by a peak with the late Golgi soon after (Figure 6.2 A and B). By 10 minutes only a quarter of the Golgi structures have detectable cargo and by 20 minutes essentially no cargo remains. Thus a cargo wave transits the secretory pathway faster in the absence of AP-1.

Endocytosis becomes essential for the localization of some late Golgi proteins and cisternal maturation in the absence of AP-1

If AP-1 is responsible for recycling resident late Golgi enzymes, then removal of the adaptor should cause those proteins to mislocalize. This has been reported for the chitin synthase Chs3 but does not seem to be a generalized phenomenon (Valdivia et al., 2002). Because the yeast TGN acts as an early endosome, it is possible that some late Golgi enzymes are being recycled via endocytosis in AP-1 mutants. In this case, inhibition of endocytosis in AP-1 mutants should cause accumulation of leaked late Golgi proteins on the plasma membrane (Figure 6.9). Indeed this has already been reported for the aminophospholipid translocase Drs2 (Liu et al., 2008). Unfortunately there has not been a rigorous characterization of yeast AP-1 cargoes. To identify a set of AP-1 cargoes, we compared the localization of GFP-tagged

late Golgi proteins with Sec7-mScarlet, as a reference late Golgi protein, in the presence or absence of AP-1 after inhibiting endocytosis. Sec7 is a peripheral membrane protein that would not be expected to display altered localization in AP-1 mutants. To inhibit endocytosis we used the drug CK-666 which disrupts Arp2/3 mediated actin patch formation (Hetrick et al., 2013). To ensure sensitivity to the drug, we worked with strains lacking the Pdr1 and Pdr3 transcription factors that control expression of drug transporters (Barrero et al., 2016, Coorey et al., 2015). As a control for the functionality of the drug, we examined an endocytic patch protein, Abp1, and the endocytic tracer dye FM 4-64. After preincubation with CK-666 for 15 minutes no internalized FM4-64 puncta can be seen and the Abp1 signal redistributes from punctate structures to a cytosolic haze (Figure 6.3). Thus, CK-666 is a potent inhibitor of endocytosis. From our panel of potential AP-1 candidates we saw a mixed set of results. In an AP-1 deletion background alone the chitin synthase Chs3 already largely redistributed to the plasma membrane and vacuole with only weak intracellular punctate fluorescence seen (Figure 6.4). CK-666 treatment caused a complete redistribution of Chs3 to the plasma membrane and vacuole within 15 minutes. As a control, the early Golgi protein Vrg4, which likely recycles via COPI, showed no change in localization (Figure 6.4). Drs2 showed normal Golgi localization in the AP-1 mutant but strongly redistributed to the plasma membrane after treatment with CK-666 (Figure 6.4). Tvp23, a protein of unknown function whose mammalian homolog is enriched in AP-1 vesicles (Hirst et al., 2012), and Stv1, a subunit of the Golgi localized V-ATPase that controls acidification of the late Golgi (Banerjee and Kane, 2017), largely remained in punctate structures, but by 15 minutes some signal could be detected at the plasma membrane. The other candidate proteins showed no obvious change in localization.

This assay is likely an imperfect way to identify AP-1 cargoes. First, the rate of endocytosis of a particular cargo will vary. Second, the Golgi does not seem to completely break down as evidenced by the continual presence of Sec7 punctate signal even after 30 minutes of drug treatment (See Figure 6.5). If the Golgi was terminally maturing and not being regen-

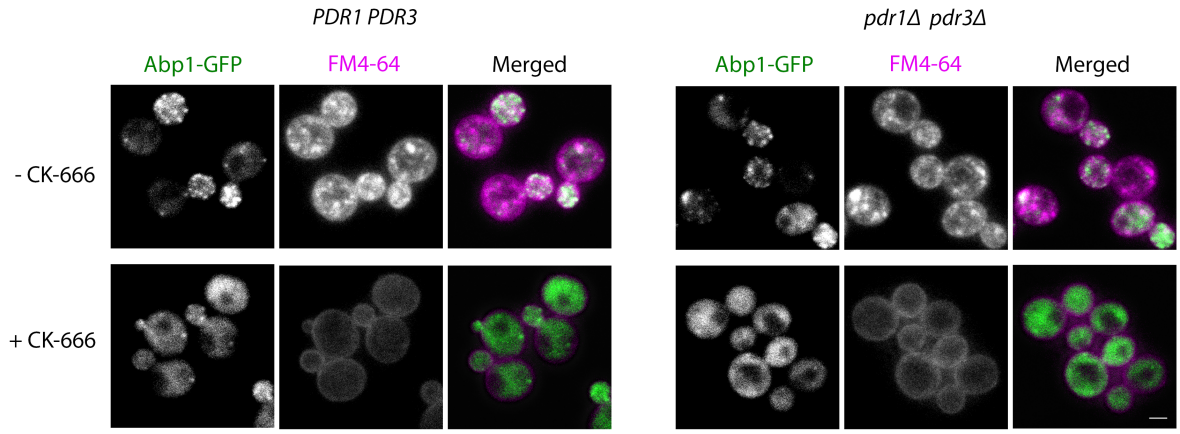

Figure 6.3: **Potent inhibition of endocytosis by the drug CK-666.** *PDR1 PDR3* or *pdr1*Δ *pdr3*Δ cells expressing Abp1-GFP to label endocytic patches were mock treated or treated with 100μM CK-666 for 15 minutes and were imaged via confocal microscopy 5 minutes after adding 0.8μM FM 4-64X. Scale bar 2μm.

erated, then there should not be any Golgi membranes remaining after 15 minutes, as the Golgi turns over within ~3-5 minutes (Losev et al., 2006). Thus, it seems likely that some Golgi-like membranes remain though their functionality is probably severely compromised. For these reasons negative results do not rule out AP-1 dependent recycling but positive results imply that a protein is likely an AP-1 cargo. These results also suggest that a functional intra-Golgi recycling pathway for late Golgi proteins may still be operating in the absence of AP-1.

What happens to Golgi maturation when endocytosis is inhibited in AP-1 mutants? If endocytosis acts as a retrieval pathway for leaked late Golgi proteins essential for maturation, then endocytosis should become essential for cisternal maturation in AP-1 mutants. To test this, we examined the kinetics of cisternal maturation before and after CK-666 treatment in the presence or absence of AP-1. As seen previously, we readily identified transitions where new Vrg4 positive cisternae formed, lost the Vrg4 signal as they acquired Sec7 signal, which was then subsequently lost (Figure 6.5 A) (Losev et al., 2006; Casler et al., 2019). After CK-666 treatment, wild type cells showed no obvious change in the rate of cisternal maturation (Figure 6.5 B), but the AP-1 mutant displayed remarkably altered kinetics (Figure 6.5 C-

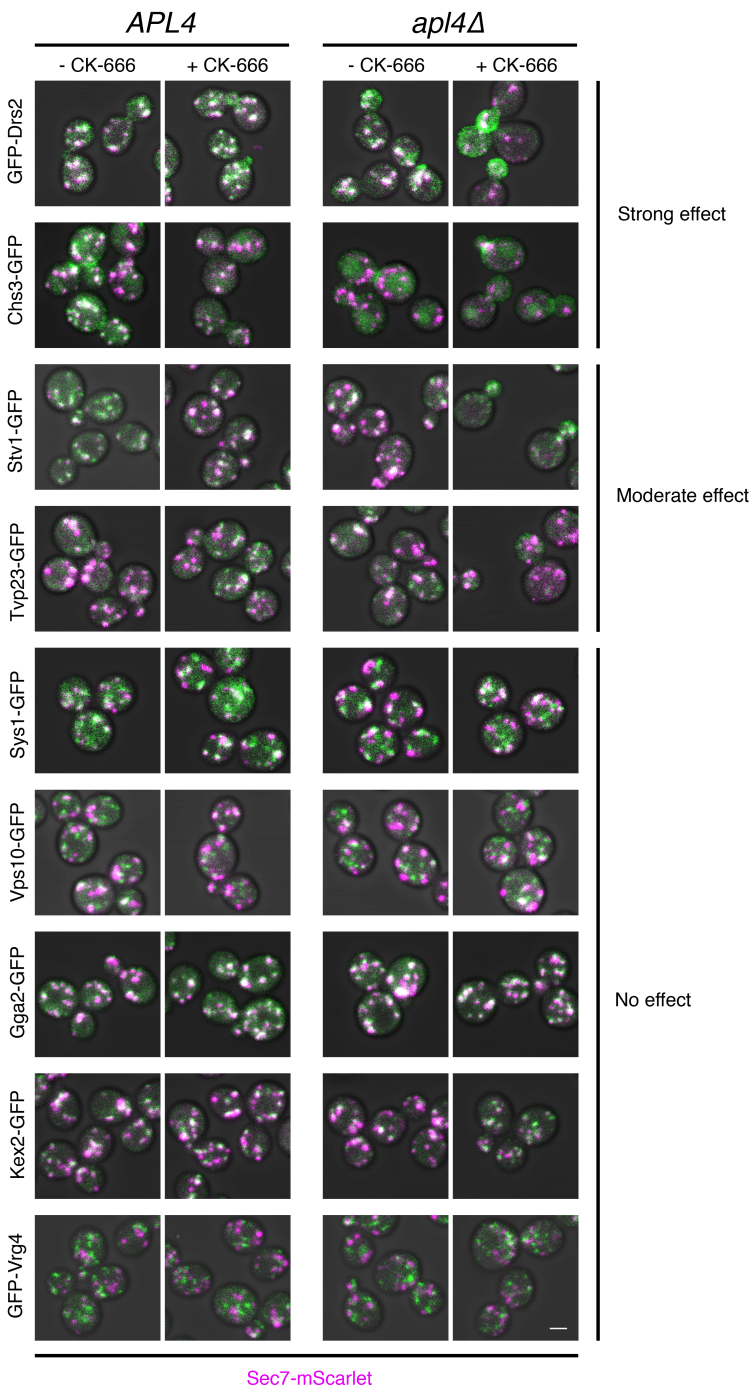

Figure 6.4: **A subset of TGN proteins mislocalize in AP-1 mutants when endocytosis is inhibited.** *APL4* (left) or *apl4*Δ (right) cells expressing the indicated GFP tagged Golgi proteins and Sec7-mScarlet (reference late Golgi marker) were grown to mid-log phase in NSD, and imaged on a Leica SP5 confocal microscope before and fifteen minutes after introduction of 100μM CK-666. Scale bar 2μm.

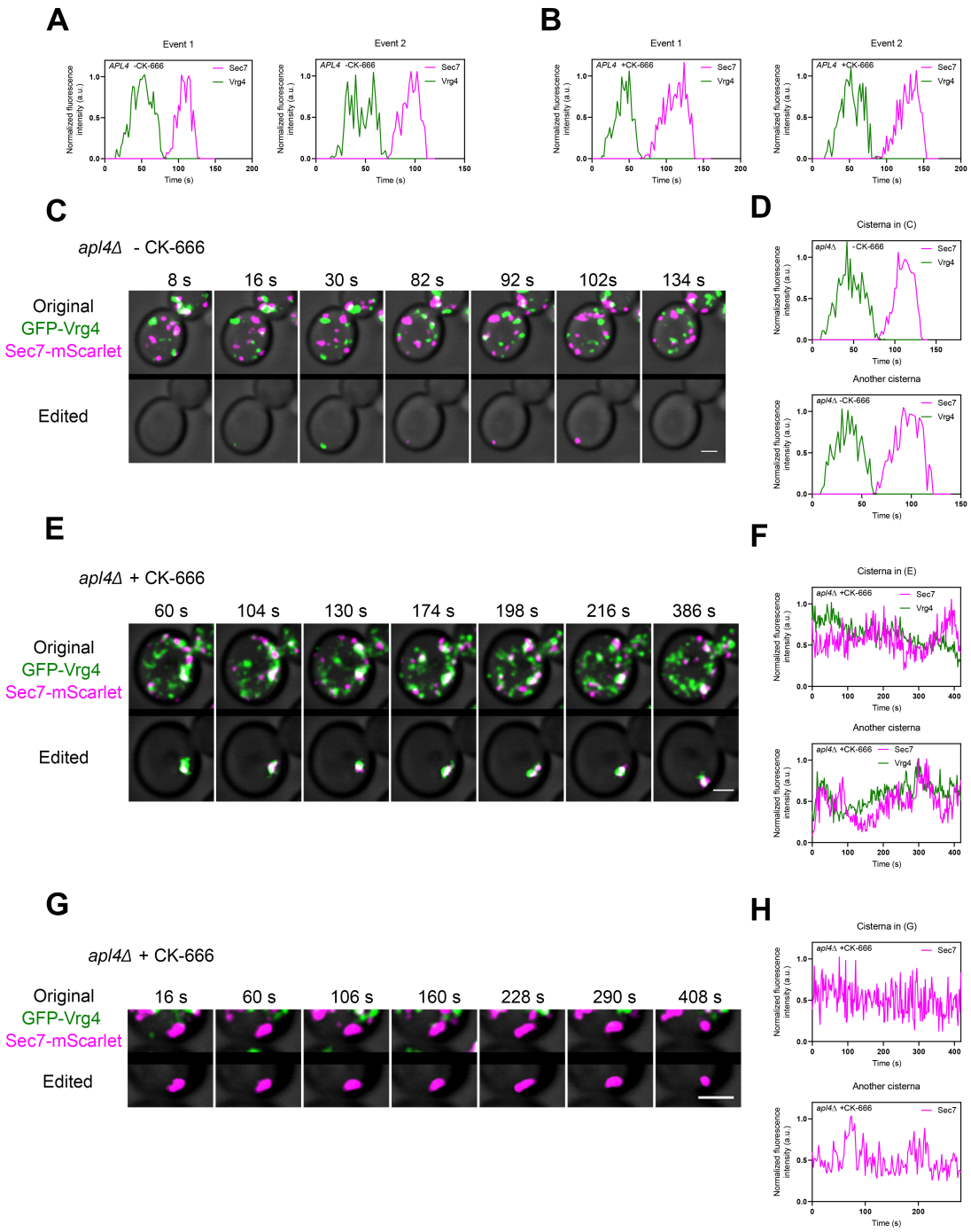

Figure 6.5: **Disruption of cisternal maturation in AP-1 mutants when endocytosis is inhibited. (A)** *APL4* cells expressing GFP-Vrg4 (early Golgi marker) and Sec7-mScarlet (late Golgi marker) were grown overnight in NSD to mid-log phase, and imaged via 4D confocal microscopy. Shown are the quantifications of two representative maturation events. *(continued on next page)*

Figure 6.5: **(B)** Cells were grown and imaged as in (A) except they were treated with 100μM CK-666 for 30 minutes prior to imaging. Shown are the quantifications of two representative maturation events. **(C)** *apl4*Δ cells were grown, treated, and imaged as in (A). Images depict a representative cisternal maturation event. The top panel shows the unedited images while the bottom panel shows only the cisterna being tracked. Scale bar 2μm. (D) Quantification of the maturation event in (C) and another representative event. **(E)** *apl4*Δ cells were grown, treated, and imaged as in (B). Shown is a representative example of the coalescence of the early and late Golgi markers. The top panel shows the unedited images while the bottom panel shows only the cisterna being tracked. Scale bar 2μMm. **(F)** Quantification of the event in (E) and another representative event. **(G)** *apl4*Δ cells were grown, treated, and imaged as in (B). Shown is a representative example of an individual late Golgi cisterna persisting for at least seven minutes. The top panel shows the unedited images while the bottom panel shows only the cisterna being tracked. Scale bar 2μMm. **(H)** Quantification of the event in (G) and another representative event.

H). Within fifteen minutes of drug treatment the overall rate of cisternal maturation began to decrease and the effect was strongest by thirty minutes. After thirty minutes of CK-666 treatment cells began to show significantly increased colocalization of Vrg4 and Sec7 in large punctate structures that can be tracked for at least seven minutes (Figure 6 E and F). It was also possible to identify individual late Golgi structures, with no detectable early Golgi signal, that also persisted for upwards of seven minutes (Figure 6 G and H). The early Golgi marker GFP-Vrg4 displayed a more dispersed pattern and it was difficult to track individual structures. Based on this result, we conclude that endocytosis is essential for cisternal maturation in the absence of AP-1.

The maturation kinetics of some Golgi proteins are altered in AP-1 mutants

Another way to characterize AP-1 cargoes is by examining the kinetics of the protein during cisternal maturation. If a protein is an AP-1 cargo, then it should arrive at the late Golgi when AP-1 vesicles begin to fuse, and leave the Golgi when AP-1 vesicles are formed. Based on our previous results, AP-1 vesicles likely fuse with the Golgi at or slightly before the Vrg4-to-Sec7 transition and AP-1 vesicles start forming about halfway through the late Golgi lifetime (Day et al., 2018, Casler et al., 2019, Casler and Glick 2020). In the absence of AP-1, AP-1 dependent recycling late Golgi proteins should persist to the latest stages

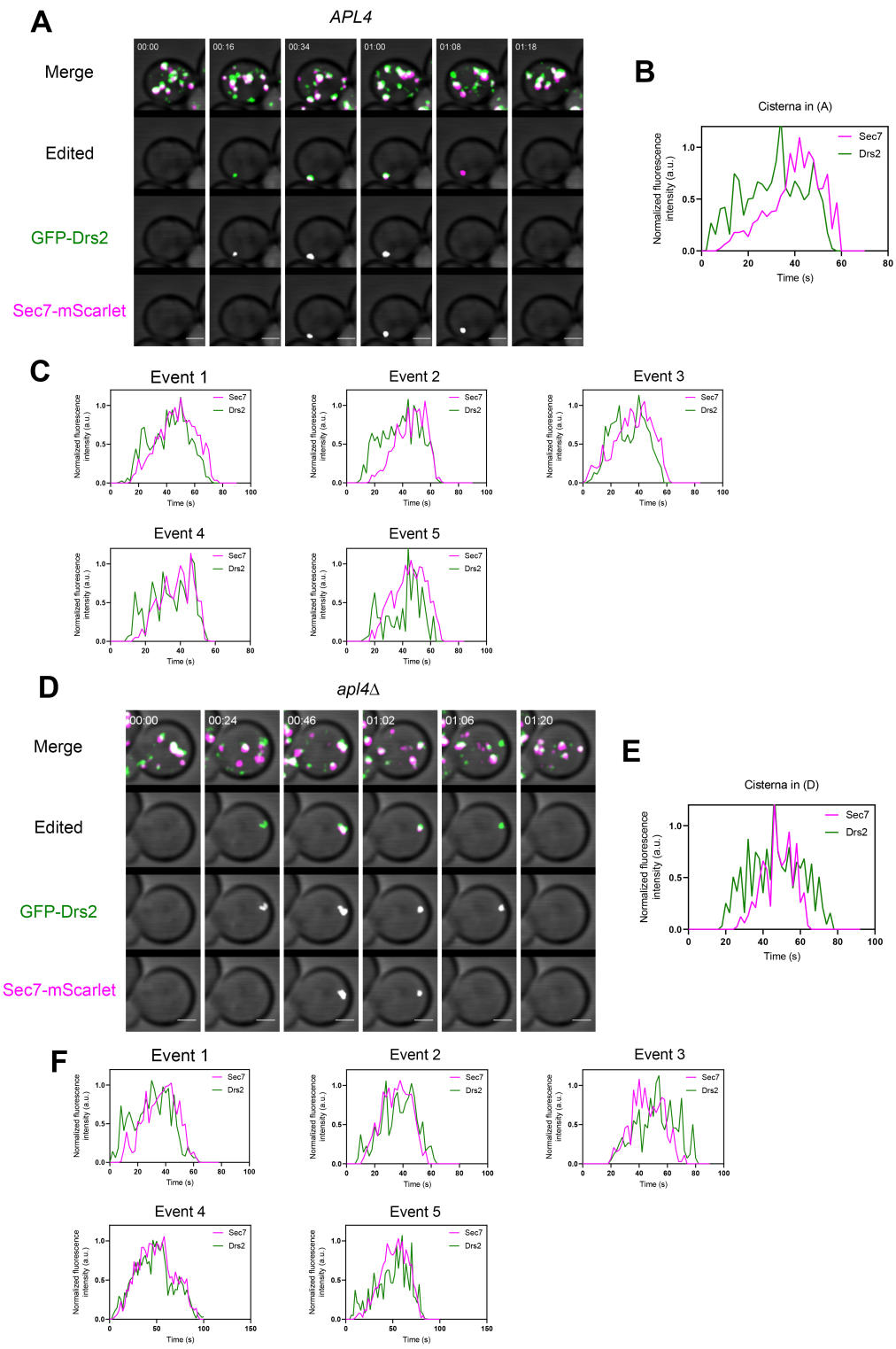

Figure 6.6: **Kinetics of putative AP-1 cargo Drs2 in wild type and AP-1 mutant cells.** *(continued on next page)*

Figure 6.6: **(A)** Cells expressing GFP-Drs2 and Sec7-mScarlet were grown to mid-log phase in NSD and imaged via 4D confocal microscopy. Images depict a representative maturation event. The top panel shows the unedited image, the next shows only the cisterna being tracked, and the following rows depict the individual fluorescence channels in grayscale. Scale bar 2μM. **(B)** Quantification of the fluorescence intensity of the markers from (A). **(C)** Examples of five additional maturation traces of experiments performed as in (A). **(D)** *apl4*Δ cells containing the same markers as (A) were grown and imaged as in (A). Scale bar 2μM. **(E)** Quantification of the fluorescence intensity of the Golgi markers from (D). **(F)** Examples of five additional maturation traces of experiments performed as in (D).

of maturation where they are packaged into secretory vesicles. To test this, we examined the kinetics of three likely AP-1 cargoes, Drs2, Tvp23, and Stv1 together with Sec7 in the presence or absence of AP-1. Drs2 arrived slightly before Sec7 and also departed slightly before Sec7 (Figure 6.6 A-C). In an AP-1 deletion some maturation events showed Drs2 signal persisting beyond the Sec7 signal while others showed them depart at nearly the same time (Figure 6.6 D-F). Tvp23 and Stv1 showed similar kinetics with functional AP-1. Both Tvp23 and Stv1 arrived ~10-20 seconds before Sec7 and left near the midpoint of the Sec7 trace (Figure 6.7 A-C, Figure 6.8 A-C). These kinetics were not obviously altered in an AP-1 deletion (Figure 6.7 D-F, Figure 6.8 D-F). Thus, some, but not all, late Golgi proteins show altered kinetics in AP-1 mutants.

There could be several explanations as to why Tvp23 and Stv1 did not show altered kinetics in AP-1 mutants. First, they may not be bona fide AP-1 dependent recycling cargoes. This seems unlikely due to the fact that they mislocalize when endocytosis is inhibited in AP-1 mutants (Figure 6.4) and that a Tvp23 homolog is enriched on AP-1 vesicles in mammalian cells (Hirst et al., 2012). Another possibility is that Tvp23 and Stv1 are only partially dependent on AP-1 for their late Golgi localization. Certain late Golgi proteins, such as Kex2 and Vps10, seem to maintain their steady-state localization by cycling through the PVE (Cooper and Stevens, 1996; Seaman et al., 1998). Thus, it is possible that late Golgi proteins can utilize both pathways with different efficiencies to maintain their steady-state Golgi localization. Finally, the most likely explanation is that an intra-Golgi recycling pathway still operates even in the absence of AP-1. Ent5 is a highly conserved epsin-like protein

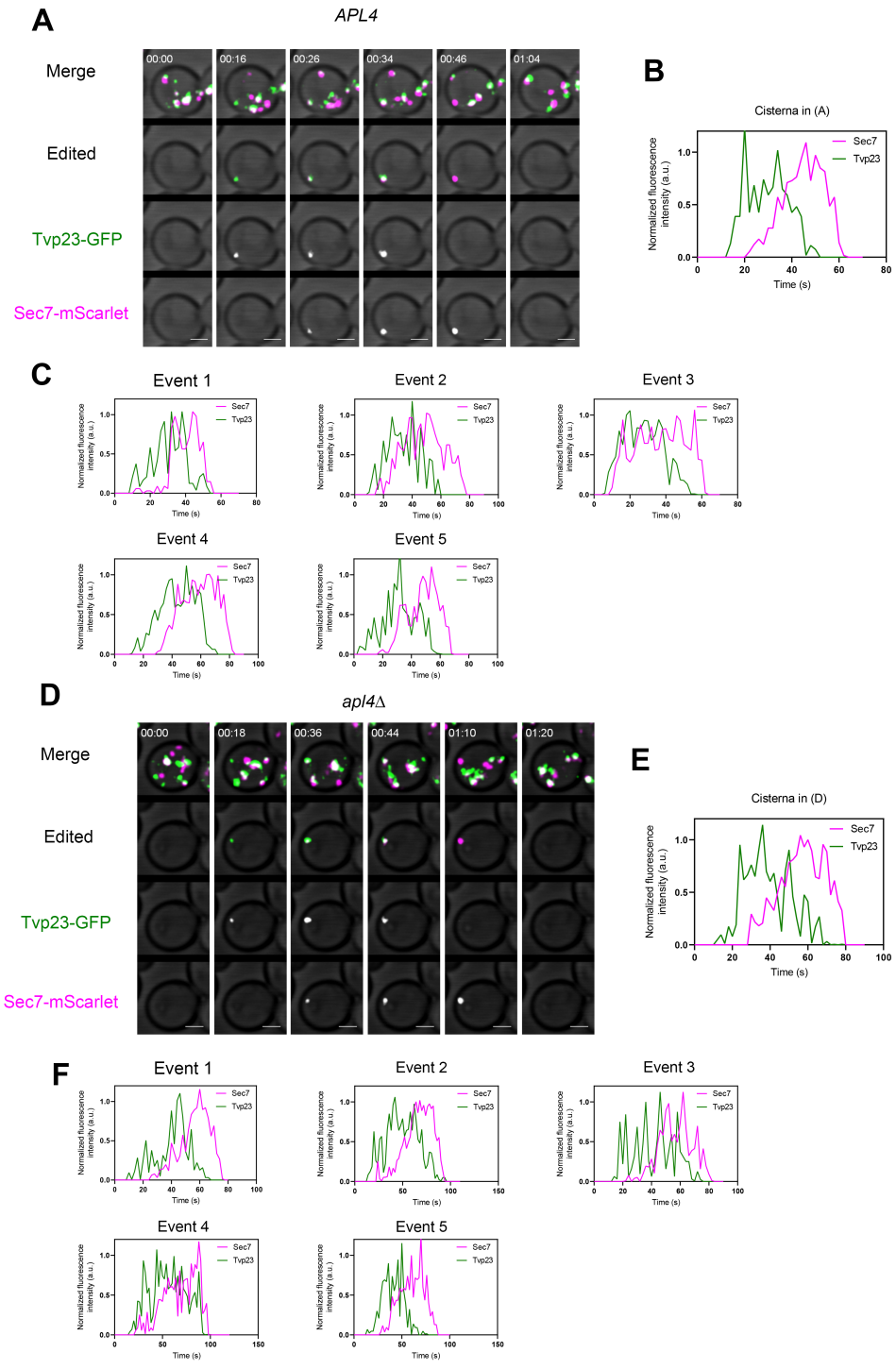

Figure 6.7: **Kinetics of putative AP-1 cargo Tvp23 in wild type and AP-1 mutant cells. (A-F)** were performed identically to Figure 6.6 but cells expressed Tvp23-GFP rather than GFP-Drs2.

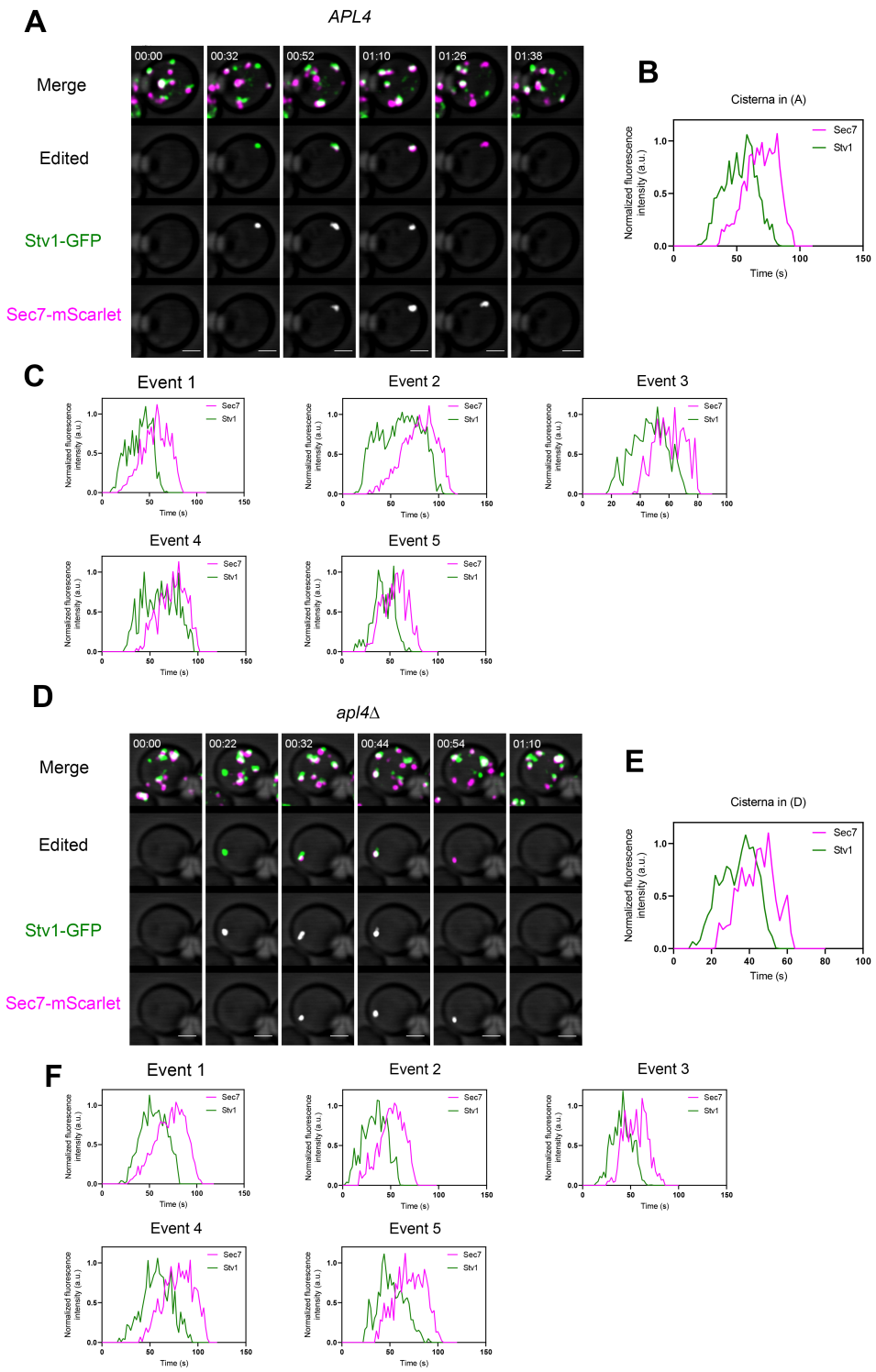

Figure 6.8: **Kinetics of putative AP-1 cargo Stv1 in wild type and AP-1 mutant cells. (A-F)** were performed identically to Figure 6.6 but cells expressed Stv1-GFP rather than GFP-Drs2.

that localizes to the TGN and display genetic interactions with Ggas, AP-1, and clathrin (Duncan et al., 2003; Costaguta et al., 2006; Copic et al., 2007). In certain circumstances Ent5 is capable of compensating for AP-1 mutants though the exact mechanism by which this occurs is unknown. Another epsin-like protein, Ent4, may also play a role though little is known of its function (Deng et al., 2009). Therefore, examining kinetics of putative AP-1 cargoes in AP-1 and Ent5 double mutants is a critical next step.

Based on these and previous results, I suggest a model in which the steady-state localization of late Golgi proteins is mediated by three distinct pathways. First, a subset of resident Golgi proteins cycle between the Golgi and late endosome. Transport from the Golgi is mediated by the Gga clathrin adaptors and retrieval is mediated by the retromer complex (Figure 6.9). Another subset of late Golgi proteins recycles within the Golgi via AP-1/Ent5 (Figure 6.9). AP-1 and Ent5 may have distinct cargo clients and cooperate to form clathrin coated vesicles at the late Golgi. For example, AP-1 likely specifically recognizes Mnn1 which would explain why intra-Golgi secretory cargo recycling is completely blocked in an AP-1 mutant (Figure 6.1). Finally, endocytosis can also retrieve leaked late Golgi proteins from the plasma membrane. In AP-1/Ent5 mutants, the endocytic retrieval route becomes essential for Golgi maturation (Figure 6.9). Future experiments will be dedicated to dissecting the mechanism by which these processes are organized.

Materials and methods

Yeast growth and transformation

The parental haploid *S. cerevisiae* strain was JK9-3da (*leu2-3,112 ura3-52 rme1 trp1 his4*; Heitman et al., 1991). Yeast cells were grown in baffled flasks with shaking at 23°C in nonfluorescent minimal glucose dropout medium (NSD; Bevis et al., 2002) or in rich glucose medium (YPD) supplemented with adenine and uracil. Unless otherwise indicated, cells were grown and imaged in unbuffered NSD.

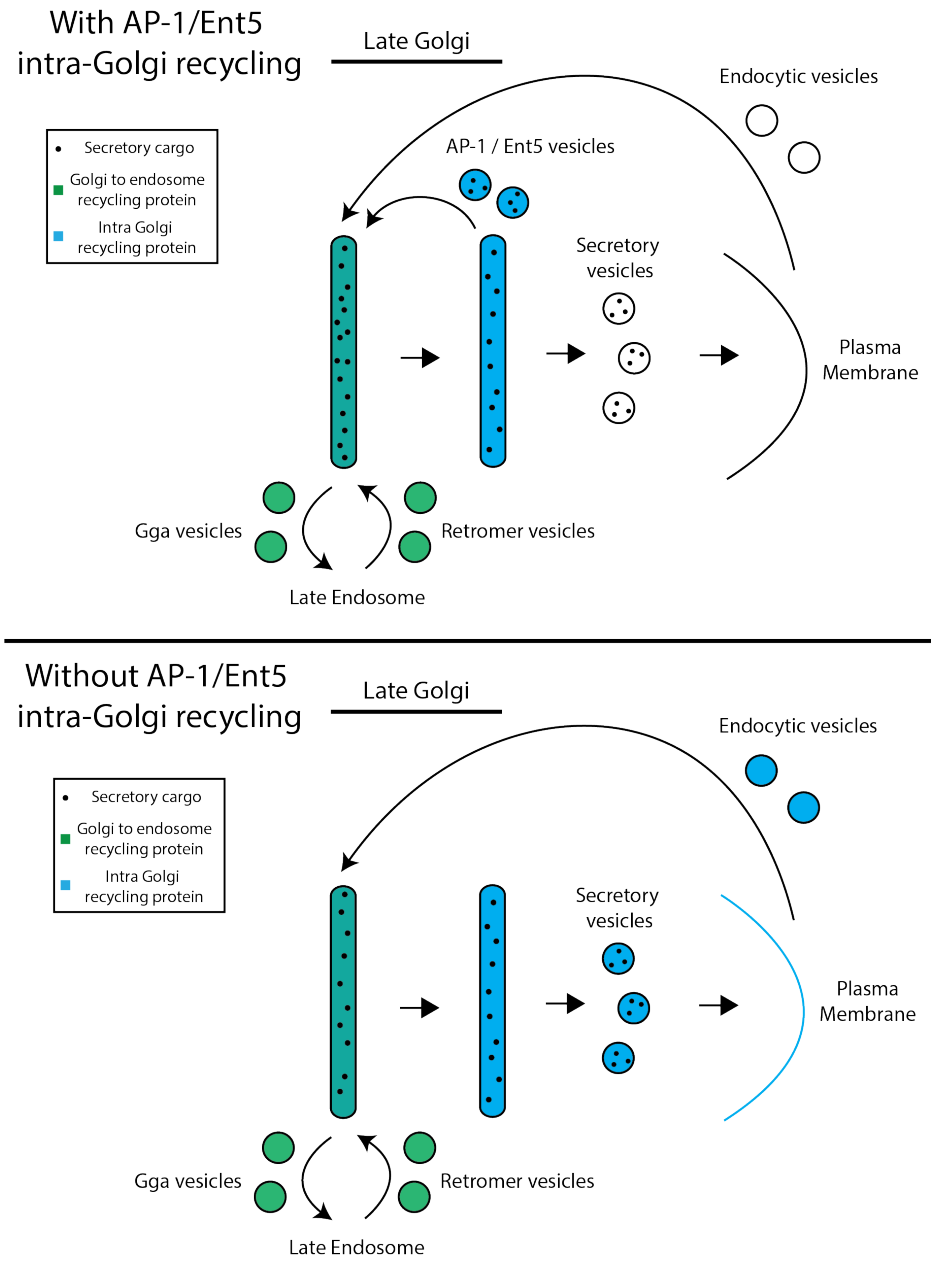

Figure 6.9: **Model of protein recycling at the Late Golgi.** In wild type cells, at the early-to-late Golgi transition AP-1/Ent5 vesicles carrying secretory cargo and resident Golgi enzymes, retromer mediated vesicles from the late endosome carrying Golgi to endosome recycling proteins, and endocytic vesicles begin to fuse. Gga vesicles destined for the late endosome begin to form. As the cisterna matures it begins to produce AP-1/Ent5 vesicles. Terminal maturation results in the formation of secretory vesicles bound for the plasma membrane. In AP-1/Ent5 mutants, Golgi to PVE traffic is unaffected but late Golgi proteins leak into secretory vesicles that fuse at the plasma membrane. Late Golgi proteins are then incorporated into endocytic vesicles which fuse with maturing Golgi cisternae.

The *vps10-104* mutation was generated via pop-in/pop-out mutagenesis as previously described (Fitzgerald and Glick, 2014). Deletion of the *PDR1*, *PDR3*, *APL4*, and *MNN1* genes was accomplished by replacement with a G418, nourseothricin, hygromycin or hygromycin resistance cassette from pFA6a-kanMX6, pAG25, or pAG32, respectively (Wach et al., 1994; Goldstein and McCusker, 1999).

Yeast cells were transformed with an amplified fragment and selected for resistance to the appropriate antibiotic.

Native yeast proteins were tagged by gene replacement using the pop-in/pop-out method to maintain endogenous expression levels. Secretory cargo proteins were expressed using a *TRP1* integrating vector with the strong constitutive *TPI1* promoter and the *CYC1* terminator (Fitzgerald and Glick, 2014). To ensure similar expression of secretory cargo proteins between strains, single-copy integrants were confirmed by PCR using primers
5'-GTGTACTTTGCAGTTATGACGCCAGATGG-3' and
5'-AGTCAACCCCCTGCGATGTATATTTTCCTG-3'.

Fluorescence microscopy

For live-cell fluorescence imaging, yeast strains were grown in NSD (pH ~4.0 for experiments employing the secretory cargo, pH 5.5 for all others) and were imaged at room temperature (23°C). Where indicated, SLF was diluted from a 100-mM stock in ethanol (Cayman Chemical; 10007974) to a final concentration of 100 µM. For static live-cell imaging, cells were attached to a concanavalin A–coated coverglass-bottom dish containing NSD (Losev et al., 2006) on a Leica SP8 or SP5 confocal microscope equipped with a 1.4 NA/63× oil objective, using a 60–80-nm pixel size, a 0.25–0.30-µm Z-step interval, and 20–30 optical sections. Z-stacks were captured at intervals of 2 s.

To inhibit endocytosis cells were incubated with 100uM CK-666 (Sigma - SML0006) diluted from a 50mM stock in DMSO. FM4-64FX was added directly to cells at a concentration of 0.8uM from a 1mM stock in DMSO.

Static images were converted to 16-bit and average projected (Hammond and Glick, 2000), then range-adjusted to the minimum and maximum pixel values in ImageJ (National Institutes of Health). Movies were deconvolved with Huygens Essential (Scientific Volume Imaging) using the classic maximum likelihood estimation algorithm (Day et al., 2017). Movies were converted to hyperstacks and average projected, then range-adjusted to maximize contrast in ImageJ. Custom ImageJ plugins were used to generate montages of time series, select individual structures and remove background structures, convert edited montages to hyperstacks, and measure fluorescence intensities (Day et al., 2016). Spot tracking was performed using the TrackMate plugin for Fiji.

HaloTag labeling

To visualize proteins fused to HaloTag, the JF_{646} ligand, kindly provided by Luke Lavis (Janelia Research Campus, Ashburn, VA), was added to 0.5 ml of culture medium to a final concentration of 1 µm from a 1-mM stock in DMSO. The medium was cleared of any precipitate by spinning at 17,000 g (13,000 rpm) in a microcentrifuge for 1 min. Then the cleared medium containing the JF_{646} ligand was added to 0.5 ml of yeast culture, and the cells were incubated with shaking at 23°C for 30 min. Excess dye was removed by filtration through and washing on a 0.22-µm syringe filter (Millipore; SLGV004SL). The washed cells were resuspended in NSD and adhered to a concanavalin A–coated coverglass-bottom dish. movies were captured immediately with an SP8 confocal microscope.

CHAPTER 7

DISCUSSION AND FUTURE DIRECTIONS

Golgi maturation was first directly visualized nearly fifteen years ago in landmark papers from the Glick and Nakano labs. Since that time, however, key predictions of the cisternal maturation model have remained untested. One key prediction of the cisternal maturation model is that secretory cargo remains within the cisternal lumen during maturation. By tracking a regulatable fluorescent secretory cargo during cisternal maturation, I was able to unambiguously verify that secretory cargo remains within a cisterna through the early-to-late Golgi transition (Casler et al., 2019). This work also led to an unexpected discovery, however, that some secretory cargo can be recycled within the Golgi in a manner that depends on the AP-1 adaptor complex. This exciting finding provides a new layer of complexity to cisternal maturation that could explain several key observations in the literature that are at odds with the classical cisternal maturation model. If AP-1 dependent recycling of secretory cargo is conserved, it could explain the non-linear export of secretory cargoes observed in mammalian cells (Patterson et al., 2009). Further, it could explain apparent transport of secretory cargo between Golgi stacks in fused cells (Pellet et al., 2013). Thus, my work has uncovered an unexpected pathway for the intra-Golgi recycling of secretory cargoes that may be a broadly conserved facet of cisternal maturation. My work has also highlighted gaps in the understanding of protein recycling within the Golgi. The driving force behind cisternal maturation is the continued recycling of resident Golgi proteins, however, these pathways are poorly characterized. COPI dependent recycling of early Golgi resident proteins is essential for maturation but exactly how these proteins are recognized and whether multiple COPI recycling pathways operate is unknown. More obviously, protein recycling at the late Golgi is very poorly characterized. AP-1 seems to be crucial for the recycling of secretory cargo and a subset of Golgi enzymes but is likely only part of the story. Therefore, a critical test of the cisternal maturation model will be to rigorously define the trafficking pathways operating

at each stage of maturation. The following sections will discuss potential avenues to better characterize Golgi recycling pathways.

Dissecting protein recycling in the Golgi

COPI

Currently, the best characterized Golgi recycling pathway is COPI dependent retrograde transport at the early Golgi. There are several crucial open questions regarding COPI recycling, however. First, do functionally distinct types of COPI vesicles exist? Morphological studies showed that depending on their location in the Golgi stack COPI vesicles have different lumenal densities (Donohoe et al., 2007). Further, there is some evidence of early Golgi proteins that do not recycle through the ER, implying that an intra-Golgi recycling pathway exists at the early Golgi (Levine et al., 2000). Budding yeast provides a unique opportunity to test the existence of two functionally distinct COPI recycling pathways. First, sets of Golgi proteins that recycle through the ER or within the Golgi can be differentiated using conditional inactivation of COPII. The localization of fluorescently tagged early Golgi proteins can be observed before and after COPII inactivation. Proteins that recycle through the ER will be trapped within the ER while proteins that recycle within the Golgi will not, providing a simple phenotypic readout for which pathway a protein follows. Once distinct sets of recycling proteins have been identified, photobleaching studies of maturing Golgi cisternae can be used to further examine recycling of these proteins. Do Golgi cisternae continuously produce vesicles or is vesicle production limited to certain stages of maturation? To test this, a protein that recycles within the Golgi could be tagged with two distinct fluorescent proteins. One fluorescent protein could be photobleached while the other remains unaltered as a means to track the bleached cisterna. Recovery of fluorescence of the bleached protein would indicate that recycling occurs throughout cisternal maturation while a lack of recovery would indicate that recycling occurs at specific times. Another open question is what types of adaptors exist to enhance cargo incorporation into COPI vesicles? This question could

be addressed by biotin proximity labeling experiments. Known recycling proteins could be tagged with a biotin ligase, which biotinylates proteins within very close distances, followed by pulldowns and mass spectrometry analysis of the biotinylated proteins to identify binding partners. While technically challenging this technique has already been employed to great effect to identify protein linkers between vesicles and tethers (Shin et al., 2017).

AP-1 / Clathrin

A bigger unanswered question is how proteins at the late Golgi maintain their steady-state localizations. Several trafficking pathways coincide at the late Golgi. Transport from the endocytic pathway, endosomal network, and intra-Golgi recycling likely all play a significant role in maintaining resident late Golgi protein localization. All of these pathways utilize clathrin coats with unique adaptors. There has yet to be a clear dissection of these vesicle populations, particularly in yeast. Recent work in mammalian cells offers a potential avenue to dissect these trafficking pathways. Relocalization of vesicle tethers is sufficient to capture specific vesicle populations (Wong and Munro, 2014). Thus, a promising approach is to artificially relocalize tethers normally present at the late Golgi and identify proteins that are enriched in the captured vesicle populations. The most likely candidates are the Imh1 and Sgm1 tethers and the COG and GARP tethering complexes; all of which have been implicated in capturing vesicles at the late Golgi (Yu and Hughson, 2010). Once the vesicle/tether network has been dissected it should be possible to perform similar experiments described for COPI above to uncover specific cargoes and the mechanisms of recycling.

My work has revealed that a secretory cargo can be recycled within the Golgi; however, whether this is a broadly conserved phenomenon is unknown. The recycling of secretory cargo is an exciting possibility to explain several observations in mammalian cells (see Chapter 3 discussion). Thus, a crucial next step will be to test if secretory cargo recycling exists in other organisms. Advances in genome editing in higher eukaryotes permits working with both gene deletions and conditional protein depletion. Thus, it should be possible to probe

the effect of removing AP-1 and/or the Ent5 homolog EpsinR on secretory cargo trafficking in other organisms. If secretory cargo recycling occurs in mammalian cells then disrupting the recycling pathway should alter the Golgi export kinetics of secretory cargoes. Mammalian cells also offer the opportunity to track native cargoes using tools such as the Retention Using Streptavidin Hooks (RUSH) system (Boncompain et al., 2012). If secretory cargo recycling proves to be a broadly conserved phenomenon, it opens many questions about the mechanisms of cargo selection and the functional purpose of the recycling pathway. A particularly attractive hypothesis is that secretory cargo recycling serves as a quality control mechanism. Cells could maintain secretory cargo within the Golgi until posttranslational modifications are complete and improperly folded or modified proteins can be removed.

A need for quantitative mathematical modeling of protein recycling

Advances in methodology and requirements from peer reviewers and editors has facilitated the rigorous reporting of quantitative biological results. While this trend is useful for highlighting the range and reproducibility of phenotypes it also has the advantage of generating data sets that can be used for mathematical modeling. Many aspects of membrane trafficking cannot be dissected with current experimental techniques. It is possible, however, to mathematically model these processes in an attempt to understand the feasibility of various models and inform future experiments. Modeling not only provides predictive constraints based on physical parameters but it also stimulates rigorous thought about the underlying assumptions that govern the model (for a thought provoking dissection of modeling in biological systems see Gunawaradena, 2014).

One area that is ripe for a comprehensive modeling study is protein recycling in the Golgi. The Golgi is a highly dynamic organelle that receives extensive vesicular input whilst simultaneously producing vesicles. To maintain homeostasis the balance of import versus export must be regulated. Currently the speed and resolution of microscopy limits our ability to accurately detect and track entire vesicle populations within living cells. Certain parameters,

including the size of different vesicles and size/number of Golgi membranes, have already been reported, however (Donohoe et al., 2007). Further, dynamic information about the Golgi lifetime of coat and adaptor proteins have been reported here and in previous work (Papanikou et al., 2015; Day et al., 2018; Casler et al., 2019, Casler and Glick 2020). There are also many reports describing the rate of cargo transport through the Golgi (Patterson et al., 2008; Chen et al., 2017; Casler et al., 2019). Thus, there is a wealth of data available to begin creating quantitative models of the physical constraints of Golgi vesicular trafficking. The cisternal maturation model postulates that retrograde vesicular trafficking is the primary determinant of resident Golgi protein localization. Mathematical models could put physical constraints on the feasibility of these retrograde trafficking pathways. What is the rate of vesicular flux required to replicate the observed distributions of Golgi proteins? Can the kinetic signatures of Golgi proteins be accounted for by the known Golgi recycling pathways? Does homotypic fusion of Golgi cisternae play a role in maturation? While unlikely to provide any definitive answers to these questions modeling may reveal significant gaps in our understanding Golgi protein recycling.

Coordinating protein sorting at the late Golgi

It has been assumed that all cargoes transit to the latest stage of the Golgi where they are simultaneously segregated and packaged into distinct carrier types. My work in yeast, however, has revealed that different classes of Golgi cargoes can exit the Golgi at different kinetic stages of cisternal maturation. This result is not directly contradictory to previous models, both vacuolar and secretory cargoes are sorted from what we have termed the late Golgi, but provides an extra layer of complexity that may aid in the fidelity of cargo sorting.

An attractive hypothesis is that different trafficking pathways are turned on and off in a linear manner during Golgi trafficking. A newly activated pathway could recruit the components required for the next pathway to begin which in turn shuts down the first pathway, thus creating a logical circuit that linearly progresses a cisterna through the maturation

process. Greg Payne's group published some of the first evidence that this type of circuitry may exist. They demonstrated that the Gga and AP-1 clathrin adaptors are sequentially recruited to the late Golgi (Daboussi et al., 2012; Daboussi et al., 2017). Importantly, disrupting Gga recruitment delayed the recruitment of AP-1 (Daboussi et al., 2012; Daboussi et al., 2017). They found that Ggas physically interact with and help recruit Pik1 (the yeast PI(4)P kinase) to the late Golgi, a role which is conserved in mammalian cells. Pik1 generates a pool of PI(4)P which is then involved in the recruitment of the AP-1 adaptor complex (Daboussi et al., 2012; Daboussi et al., 2017). Thus, the Gga pathway operating upstream of AP-1 is essential to the proper recruitment and activation of AP-1. This evidence agrees with my observations that vacuolar cargoes begin exiting the Golgi as the Ggas arrive and AP-1 dependent recycling of secretory cargoes occurs at a later kinetic stage. The sequential recruitment of adaptors may be fundamental to controlling the linearity of Golgi trafficking. A thrilling idea for future work would be to extend this analysis to dissecting the transition from the early to late Golgi. Perhaps components of the COPI intra-Golgi recycling machinery are required to begin recruiting components (or remove an inhibitor of recruitment) of the late Golgi trafficking machinery.

While this analysis has primarily focused on yeast, these ideas could potentially apply to mammalian systems as well. Although there is still no conclusive evidence that cisternal maturation is the primary mechanism of Golgi function in mammalian cells, several studies have published results that resemble my results from yeast. For example, Juan Bonifacino's lab has described the physical segregation of different classes of Golgi cargoes prior to their exit from the Golgi ribbon (Chen et al., 2017). In organisms that display stacked Golgi structures, different stages of cisternal maturation would be represented spatially by their distance from the *cis*-most cisternae (See Figure 4.16B). Thus, the physical segregation of endolysosomal cargoes in mammalian cells is strikingly similar to the kinetic segregation I have seen in yeast. Other groups have reported distinct localizations of adaptor proteins

at the TGN, which could reflect similar principles to the kinetic organization seen in yeast (Huang et al., 2019).

Concluding Remarks

Despite over one hundred years of research, our understanding of the Golgi apparatus remains incomplete. Now is an exciting time for Golgi research, however. New technologies are being created at rapid rates that facilitate complex experiments that were previously impossible. In this work I have engineered a tool to study the trafficking of cargo molecules traversing the Golgi in living cells. This technology was used to test fundamental predictions of the cisternal maturation model of Golgi function. The results are mostly congruent with the classical cisternal maturation model but offer new and exciting observations that may clarify confusing results in the literature. Further, this technology can be applied to the study of cargo trafficking in diverse model organisms - thus facilitating comparative studies to better our understanding of Golgi trafficking. To conclude, this work has generated a tool to study protein trafficking through the Golgi, made fundamental contributions to our understanding of the behavior of cargo molecules as they traverse the Golgi, and laid the foundation for future research to probe the molecular mechanisms of cargo trafficking and their evolutionary conservation.

REFERENCES

Adell, M.A.Y., Migliano, S.M. , Upadhyayula, S. , Bykov, Y.S., Sprenger, S. , Pakdel, M., Vogel, G.F., Jih, G. Skillern, W., Behrouzi, R., Babst, M., Schmidt, O., Hess M.W.,Briggs, J.A.G., Kirchhausen, T., and Teis, D. (2017). Recruitment dynamics of ESCRT-III and Vps4 to endosomes and implications for reverse membrane budding. eLife. 6:e31652.

Adolf, F. M., Rhiel, B., Hessling, Q., Gao, A., Hellwig, J., Béthune, Wieland, F.T. Proteomic Profiling of Mammalian COPII and COPI Vesicles. Cell Rep., 26 (2019), pp. 250-265.e5.

Amberg, D. C., Burke, D. J., and Strathern, J. N. (2006). Yeast colony PCR. Cold Spring Harbor Protocols, 1, prot4170.

Appenzeller-Herzog, C., B. Nyfeler, P. Burkhard, I. Santamaria, C. Lopez-Otin, and H.P. Hauri. (2005). Carbohydrate and conformation-dependent cargo capture for ER-exit. Mol. Biol. Cell. 16:1258–1267.

Arlt, H., Auffarth, K., Kurre, R., Lisse, D., Piehler, J., and Ungermann, C. (2015). Spatiotemporal dynamics of membrane remodeling and fusion proteins during endocytic transport. Mol. Biol. Cell. 26:1357–1370.

Armes, N., and Fried, M. (1996). Surfeit locus gene homologs are widely distributed in invertebrate genomes. Molecular and Cellular Biology, 16(10), 5591–5596.

Armstrong, J. A., and Schulz, J. R. (2008). Agarose gel electrophoresis. Current Protocols Essential Laboratory Techniques, 00, 7.2.1–7.2.20.

Avaro, S., Belgareh-Touze, N., Sibella-Arguelles, C., Volland, C. Haguenauer-Tsapis, R. Mutants defective in secretory/vacuolar pathways in the EUROFAN collection of yeast disruptants. Yeast 19, 351–371 (2002).

Balderhaar, H.J., and Ungermann C. (2013). CORVET and HOPS tethering complexes – coordinators of endosome and lysosome fusion. J. Cell Sci. 126:1307-1316.

Banerjee S and Kane PM (2017) Direct interaction of the Golgi V-ATPase a-subunit isoform with PI(4)P drives localization of Golgi V-ATPases in yeast. Mol. Biol. Cell 28(19):2518-2530.

Bannykh, S. I., Rowe, T., and Balch, W. E. (1996). The organization of endoplasmic reticulum export complexes. Journal of Cell Biology, 135(1), 19–35.

Bard, F., and Malhotra, V. (2006). The formation of TGN-to-plasma-membrane transport carriers. Annu Rev Cell Dev Biol 22, 439-455.

Barfield, R.M., Fromme, J.C., and Schekman, R. (2009). The exomer coat complex transports Fus1p to the plasma membrane via a novel plasma membrane sorting signal in yeast.

Mol. Biol. Cell. 20:4985–4996.

Barlowe, C., and Helenius, A. (2016). Cargo capture and bulk flow in the early secretory pathway. Annu. Rev. Cell Dev. Biol. 32:197–222.

Barlowe, C. K., and Miller, E. A. (2013). Secretory protein biogenesis and traffic in the early secretory pathway. Genetics, 193, 383–410.

Barrero, J.J., Papanikou, E., Casler, J.C., Day, K.J., and Glick, B.S. (2016). An improved reversibly dimerizing mutant of the FK506-binding protein FKBP. Cell. Logist. 6:e1204848.

Barrero, J.J., Casler, J.C., Valero, F., Ferrer, P., and Glick, B.S. (2018). An improved secretion signal enhances the secretion of model proteins from *Pichia pastoris*. Microb. Cell Fact. 17:161.

Becker, B., Bölinger, B., and Melkonian, M. (1995). Anterograde transport of algal scales through the Golgi complex is not mediated by vesicles. Trends Cell Biol. 5, 305–307.

Bevis, B.J., Hammond, A.T., Reinke, C.A., and Glick, B.S. (2002). De novo formation of transitional ER sites and Golgi structures in *Pichia pastoris*. Nat. Cell Biol. 4:750–756.

Beznoussenko, G.V., Parashuraman S., Rizzo, R., Polishchuk, R., Martella, O., Di Giandomenico, D., Fusella, A., Spaar, A., Sallese, M., Capestrano, M.G., et al. (2014). Transport of soluble proteins through the Golgi occurs by diffusion via continuities across cisternae. eLife. 3:e02009.

Beznoussenko, G.V., Ragnini-Wilson, A., Wilson, C., and Mironov, A.A. (2016). Three-dimensional and immune electron microscopic analysis of the secretory pathway in *Saccharomyces cerevisiae*. Histochem. Cell Biol. 146: 515–527.

Black, M.W., and Pelham H.R. (2000). A selective transport route from Golgi to late endosomes that requires the yeast GGA proteins. J. Cell Biol. 151:587-600.

Boncompain, G., and Perez, F. (2013). Fluorescence based analysis of trafficking in mammalian cells. Methods in Cell Biology, 118, 179–194.

Boncompain, G., Divoux, S., Gareil, N., de Forges, H., Lescure, A., Latreche, L., Mercanti, V., Jollivet, F., Raposo, G., and Perez, F. (2012). Synchronization of secretory protein traffic in populations of cells. Nat. Methods. 9:493–498.

Bonfanti, L., Mironov Jr,. A.A., Martinez-Menarguez, J.A., Martella, O., Fu'sella, A., Baldassarre, M., Buccione, R., Geuze, H.J., Mironov, A.A., and Luini, A. (1998). Procollagen traverses the Golgi stack without leaving the lumen of cisternae: evidence for cisternal maturation. Cell. 95: 993–1003.

Bowers, K., and Stevens, T.H. (2005). Protein transport from the late Golgi to the vacuole in the yeast *Saccharomyces cerevisiae*. Biochim. Biophys. Acta. 1744:438-454.

Brigance, W.T., Barlowe, C., and Graham, T.R. (2000). Organization of the yeast Golgi complex into at least four functionally distinct compartments. Mol. Biol. Cell. 11:171–182.

Bright, N.A., Davis, L.J., and Luzio, J.P., (2016). Endolysosomes are the principal intracellular sites of acid hydrolase activity. Curr. Biol. 26:2233-2245.

Bright, N.A., Gratian, M.J., and Luzio J.P. (2005). Endocytic delivery to lysosomes mediated by concurrent fusion and kissing events in living cells. Curr. Biol. 15:360-365.

Bykov YS, Schaffer, M., Dodonova, S.O., Albert, S., Plitzko, J.M., Baumeister, W., Engel, B.D., Briggs, J.A. The structure of the COPI coat determined within the cell. (2017). eLife, 6, Article e32493.

Canty, E. G. and Kadler, K. E. Procollagen trafficking, processing and fibrillogenesis. (2005). J. Cell Sci. 118, 1341-1353.

Capitani M, Sallese M. The KDEL receptor: new functions for an old protein. (2009). FEBS Lett 583:3863–3871.

Casler, J.C., and Glick, B.S. (2019). Visualizing secretory cargo transport in budding yeast. Curr. Protoc. Cell Biol. 83(1): e80.

Casler, J.C., Papanikou E., Barrero J.J., and Glick B.S. (2019). Maturation-driven transport and AP-1–dependent recycling of a secretory cargo in the Golgi. J Cell Biol 218 (5): 1582–1601.

Casler, J.C., and Glick, B.S. (2020). A microscopy-based kinetic analysis of yeast vacuolar protein sorting. eLife. 2020;9:e56844.

Castillon, G.A., Watanabe, R., Taylor, M., Schwabe, T.M., and Riezman, H. (2009). Concentration of GPI-anchored proteins upon ER exit in yeast. Traffic. 10:186–200.

Cereghino, J.L., E.G. Marcusson, and S.D. Emr. 1995. The cytoplasmic tail domain of the vacuolar protein sorting receptor Vps10p and a subset of VPS gene products regulate receptor stability, function, and localization. Mol. Biol. Cell. 6:1089-1102.

Cetera M., Lewellyn L., and Horne-Badovinac S. Cultivation and Live Imaging of Drosophila Ovaries. In: Bratu DP, McNeil GP, editors. Drosophila Oogenesis, Methods in Molecular Biology. Springer New York; New York, NY: 2016. pp. 215–226.

Chen, Y., Gershlick, D.C., Park, S.Y., and Bonifacino, J.S. (2017). Segregation in the Golgi complex precedes export of endolysosomal proteins in distinct transport carriers. J. Cell Biol.

216:4141–4151.

Cheung, P. Y., Limouse, C., Mabuchi, H. and Pfeffer, S.R. (2015). Protein flexibility is required for vesicle tethering at the Golgi. eLife 4, e12790.

Chi, R.J., J. Liu, M. West, J. Wang, G. Odorizzi, and C.G. Burd. 2014. Fission of SNX-BAR-coated endosomal retrograde transport carriers is promoted by the dynamin-related protein Vps1. J. Cell Biol. 204:793-806.

Chilcoat, N.D., Melia, S.M., Haddad, A., and Turkewitz, A.P. (1996). Granule lattic protein 1 (Grl1p), an acidic, calcium-binding protein in *Tetrahymena thermophila* dense-core secretory granules, influences granule size, shape, content organization, and release but not protein sorting or condensation. J. Cell Biol. 135, 1775-1787.

Conibear, E., and Stevens, T.H. (1998). Multiple sorting pathways between the late Golgi and the vacuole in yeast. Biochim. Biophys. Acta. 1404:211-230.

Cooper, A.A., and Stevens, T.H. (1996). Vps10p cycles between the late-Golgi and pre-vacuolar compartments in its function as the sorting receptor for multiple yeast vacuolar hydrolases. J. Cell Biol. 133, 529–541.

Coorey, N.V.C., Matthews, J.H., Bellows, D.S., and Atkinson, P.H. (2015). Pleiotropic drug-resistance attenuated genomic library improves elucidation of drug mechanisms. Mol. Biosyst. 11:3129–3136.

Copic A., Starr T.L., and Schekman R. (2007). Ent3p and Ent5p exhibit cargo specific functions in trafficking proteins between the trans-Golgi network and the endosomes in yeast. Mol Biol Cell 18, 1803–1815.

Costaguta G., Duncan M.C., Fernandez G.E., Huang G.H., Payne G.S. (2006). Distinct roles for TGN/endosome epsin-like adaptors Ent3p and Ent5p. Mol Biol Cell 17, 3907–3920.

Cowles, C.R., Odorizzi, G., Payne, G.S., and Emr S.D. (1997). The AP-3 adaptor complex is essential for cargo-selective transport to the yeast vacuole. Cell. 91:109-118.

Cox, J.S., and Walter, P. (1996). A novel mechanism for regulating activity of a transcription factor that controls the unfolded protein response. Cell. 87:391–404.

D'Angelo, G., Capasso, S., Sticco, L., and Russo, D. (2013). Glycosphingolipids: synthesis and functions. FEBS J. 280, 6338–6353.

Daboussi, L., Costaguta, G., Ghukasyan, R., and Payne G.S. (2017). Conserved role for Gga proteins in phosphatidylinositol 4-kinase localization to the trans-Golgi network. Proc. Natl Acad. Sci. USA. 114:3433-3438.

Daboussi, L., Costaguta G., and Payne, G.S. (2012). Phosphoinositide-mediated clathrin adaptor progression at the trans-Golgi network. Nat. Cell Biol. 14:239–248.

Dancourt, J., and Barlowe, C. (2010). Protein sorting receptors in the early secretory pathway. Annu. Rev. Biochem. 79:777–802.

Day, K.J., Staehelin, L.A. and Glick, B.S. (2013). A three-stage model of Golgi structure and function. Histochem. Cell Biol. 140:239–249.

Day, K.J., Papanikou, E., and Glick, B.S. (2016). 4D confocal imaging of yeast organelles. Methods Mol. Biol. 1496:1–11.

Day, K.J., La Rivière, P.J., Chandler, T., Bindokas, V.P., Ferrier, N.J., and Glick, B.S. (2017). Improved deconvolution of very weak confocal signals. F1000 Res. 6:787.

Day, K.J., Casler J.C., and Glick, B.S. (2018). Budding yeast has a minimal endomembrane system. Dev. Cell. 44:56–72.e4.

De Matteis, M.A., and Luini, A. (2008). Exiting the Golgi complex. Nat. Rev. Mol. Cell Biol. 9:273–284.

De Matteis, M.A., Wilson, C., D'Angelo, G. Phosphatidylinositol-4-phosphate: the Golgi and beyond. BioEssays News Rev. Mol. Cell. Dev. Biol., 35 (2013), pp. 612-622.

de Saint-Jean, M. et al. Osh4p exchanges sterols for phosphatidylinositol 4-phosphate between lipid bilayers. J. Cell Biol. 195, 965–978 (2011) .

Dell'Angelica, E.C., R. Puertollano, C. Mullins, R.C. Aguilar, J.D. Vargas, L.M. Hartnell, and J.S. Bonifacino. 2000. GGAs: a family of ADP ribosylation factor-binding proteins related to adaptors and associated with the Golgi complex. J. Cell Biol. 149:81-94.

Deng Y., Guo Y., Watson H., Au W.C., Shakoury-Elizeh M., Basrai M.A., Bonifacino J.S., Philpott C.C. (2009). Gga2 mediates sequential ubiquitin-independent and ubiquitin-dependent steps in the trafficking of ARN1 from the trans-golgi network to the vacuole. J Biol Chem 284: 23830–23841.

De Nobel, J.G., Klis, F.M., Munnik, T., Priem, J., and van den Ende, H. (1990). An assay of relative cell wall porosity in *Saccharomyces cerevisiae*, *Kluyveromyces lactis* and *Schizosaccharomyces pombe*. Yeast. 6:483–490.

Dell'Angelica, E.C., Puertollano, R., Mullins, C., Aguilar, R.C., Vargas, J.D., Hartnell, L.M., and Bonifacino, J.S. (2000). GGAs: a family of ADP ribosylation factor-binding proteins related to adaptors and associated with the Golgi complex. J. Cell Biol. 149:81-94.

Di Paolo, G. and De Camilli, P. (2006). Phosphoinositides in cell regulation and membrane

dynamics. Nature 443, 651–657.

Donohoe, B.S., Kang, B.H., and Staehelin, L.A. (2007). Identification and characterization of COPIa- and COPIb-type vesicle classes associated with plant and algal Golgi. Proc Natl Acad Sci USA 104, 163-168.

Di Santo, R., Aboulhouda, S., and Weinberg, D.E. (2016). The fail-safe mechanism of post-transcriptional silencing of unspliced HAC1 mRNA. eLife. 5: e20069.

Duden, R., and Schekman, R. (1997). Insights into Golgi function through mutants in yeast and animal cells. In Berger E.G., and Roth, J. (Eds.), The Golgi apparatus (pp. 219–246). Basel:Birkhauser Verlag.

Duncan M.C., Costaguta G., Payne G.S. (2003). Yeast epsin-related proteins required for Golgi-endosome traffic define a gamma-adaptin ear-binding motif. Nat Cell Biol 5, 77–81.

Dunlop, M.H., Ernst, A.M., Schroeder, L.K., Toomre, D.K., Lavieu,G., and Rothman, J.E. (2017). Land-locked mammalian Golgi reveals cargo transport between stable cisternae. Nat. Commun. 8:432.

Dunphy, W.G., and Rothman, J.E. (1985). Compartmental organization of the Golgi stack. Cell. 42:13–21.

Emr, S., Glick, B.S., Linstedt, A.D., Lippincott-Schwartz, J., Luini, A., Malhotra, V., Marsh, B.J., Nakano, A., Pfeffer, S.R., Rabouille, C., et al. (2009). Journeys through the Golgi - taking stock in a new era. J. Cell Biol. 187: 449–453.

Endrizzi, J.A., Breddam, K., and Remington, S.J. (1994). 2.8-Å structure of yeast serine carboxypeptidase. Biochemistry. 33:11106-11120.

Faini, M., Beck, R., Wieland, F.T., and Briggs, J.A. (2013). Vesicle coats: structure, function, and general principles of assembly. Trends Cell Biol 23, 279-288.

Farquhar, M.G., and Palade, G.E. (1981). The Golgi apparatus (complex) - (1954-1981) - from artifact to center stage. J Cell Biol 91, 77s-103s.

Feyder, S., De Craene, J.O., Bär, S., Bertazzi, D.L., and Friant, S. (2015). Membrane trafficking in the yeast *Saccharomyces cerevisiae* model. Int. J. Mol. Sci. 16:1509-1525.

Field, C., and Schekman, R. (1980). Localized secretion of acid phosphatase reflects the pattern of cell surface growth in *Saccharomyces cerevisiae*. J. Cell Biol. 86:123–128.

Finger, F.P., and Novick, P. (1998). Spatial regulation of exocytosis: lessons from yeast. J. Cell Biol. 142:609–612.

Fitzgerald, I., and Glick, B.S. (2014). Secretion of a foreign protein from budding yeasts is enhanced by cotranslational translocation and by suppression of vacuolar targeting. Microb. Cell Fact. 13:125.

Furukawa, N., and Mima, J. (2014). Multiple and distinct strategies of yeast SNAREs to confer the specificity of membrane fusion. Sci Rep 4, 4277.

Galat, A. (2008). Functional drift of sequence attributes in the FK506-binding proteins (FKBPs). J. Chem. Inf. Model. 48:1118–1130.

Gallagher, S.R. (2012). One-dimensional SDS gel electrophoresis of proteins. Current Protocols in Molecular Biology, 97, 10.2A.1–10.2A.44.

Gallagher, S.R., Winston, S.E., Fuller, S.A., and Hurrell, J G. (2008). Immunoblotting and immunodetection. Current Protocols in Molecular Biology, 83, 10.8.1–10.8.28.

Gaynor, E.C., and Emr, S.D. (1997). COPI-independent anterograde transport: cargo-selective ER to Golgi protein transport in yeast COPI mutants. J. Cell Biol. 136:789–802.

Gietz, R.D., and Woods, R.A. (2002). Transformation of yeast by lithium acetate/single stranded carrier DNA/polyethylene glycol method. Methods in Enzymology, 350, 87–96.

Glick, B.S., and Luini, A. (2011). Models for Golgi traffic: a critical assessment. Cold Spring Harb. Perspect. Biol. 3:a005215.

Glick, B.S., and Nakano, A. (2009). Membrane traffic within the Golgi apparatus. Annu. Rev. Cell Dev. Biol. 25:113–132.

Glick, B.S. (2014). Integrated self-organization of transitional ER and early Golgi compartments. BioEssays, 36(2), 129–133.

Goldstein, A.L., and McCusker J.H. (1999). Three new dominant drug resistance cassettes for gene disruption in *Saccharomyces cerevisiae*. Yeast. 15: 1541–1553.

Golgi, C. (1898). Intorno alla struttura delle cellule nervose. Bollettino della Società Medico-Chirurgica di Pavia. 13 (1): 316.

Graham, T.R., Seeger, M., Payne, G.S., MacKay, V.L., and Emr, S.D. (1994). Clathrin-dependent localization of α-1,3 mannosyltransferase to the Golgi complex of *Saccharomyces cerevisiae*. J. Cell Biol. 127:667-678.

Griffiths, G., and Simons, K. (1986). The *trans* Golgi network: sorting at the exit site of the Golgi complex. Science. 234:438-443.

Grimm, J.B., English, B.P., Chen, J., Slaughter, J.P., Zhang, Z., Revyakin, A., Patel,

R.,Macklin, J.J., Normanno, D., Singer, R.H., et al. (2015). A general method to improve fluorophores for live-cell and single-molecule microscopy. Nat. Methods. 12:244–250.

Gueldener, U., J. Heinisch, G.J. Koehler, D. Voss, and J.H. Hegemann. 2002. A second set of loxP marker cassettes for Cre-mediated multiple gene knockouts in budding yeast. Nucl. Acids Res. 30:e23.

Gunawardena, J. Models in biology: 'accurate descriptions of our pathetic thinking'. BMC Biol 12, 29 (2014).

Guo, Y., Zanetti, G., and Schekman, R. (2013). A novel GTP-binding protein adaptor protein complex responsible for export of Vangl2 from the trans Golgi network. eLife. 2:e00160.

Gut, A., Kappeler, F., Hyka, N., Balda, M.S., Hauri, H.P., and Matter, K. (1998). Carbohydrate-mediated Golgi to cell surface transport and apical targeting of membrane proteins. EMBO J. 17:1919–1929.

Harris, S.L., and Waters, M.G. (1996). Localization of a yeast early Golgi mannosyltransferase, och1p, involves retrograde transport. J. Cell Biol. 132, 985–998.

Hammond, A.T., and Glick, B.S. (2000). Raising the speed limits for 4D fluorescence microscopy. Traffic. 1:935–940.

Hecht, K.A., O"Donnell, A.F., and Brodsky, J.L. (2014). The proteolytic landscape of the yeast vacuole. Cell. Logist. 4:e28023.

Han K. An efficient DDAB-mediated transfection of Drosophila S2 cells. Nucleic Acids Res. 1996;24(21):4362–4363. Heitman, J., Movva, N.R., Hiestand, P.C., and Hall, M.N. (1991). FK 506-binding protein proline rotamase is a target for the immunosuppressive agent FK 506 in *Saccharomyces cerevisiae*. Proc. Natl. Acad. Sci. USA. 88: 1948–1952.

Henne, W.M., Buchkovich, N.J., and Emr, S.D. (2011). The ESCRT pathway. Dev. Cell. 21:77-91.

Hetrick B., Han, M.S., Helgeson, L.A., Nolen, B.J. (2013). Small molecules CK-666 and CK-869 inhibit actin-related protein 2/3 complex by blocking an activating conformational change. Chem. Biol., 20, pp. 701-712

Hinners, I., and Tooze, S.A. (2003). Changing directions: clathrin-mediated transport between the Golgi and endosomes. J. Cell Sci. 116:763-771.

Hirschberg, K., Miller, C.M., Ellenberg, J., Presley, J.F., Siggia, E.D., Phair, R.D., and Lippincott-Schwartz, J. (1998). Kinetic analysis of secretory protein traffic and characterization of Golgi to plasma membrane transport intermediates in living cells. J. Cell Biol. 143, 1485-1503.

Hirst, J., Lindsay, M.R., and Robinson, M.S. (2001). GGAs: roles of the different domains and comparison with AP-1 and clathrin. Mol. Biol. Cell. 12:3573-3588.

Hirst, J., Lui, W.W.Y., Bright, N.A., Totty, N., Seaman, M.N.J., and Robinson, M.S. (2000). A family of proteins with -adaptin and VHS domains that facilitate trafficking between the TGN and the vacuole/lysosome. J. Cell Biol. 149:67-79.

Hirst, J., Borner, G.H., Antrobus, R., Peden, A.A., Hodson, N.A., Sahlender, D.A., and Robinson, M.S. (2012). Distinct and overlapping roles for AP-1 and GGAs revealed by the "knocksideways" system. Curr. Biol. 22:1711–1716.

Holt, D.A., Luengo, J.I., Yamashita, D.S., Oh, H.J., Konialian, A.L., Yen, H.K., Rozamus, L.W., Brandt, M., Bossard, M.J., Levy, M.A, et al. (1993). Design, synthesis, and kinetic evaluation of high-affinity FKBP ligands and the X-ray crystal structures of their complexes with FKBP12. J. Am. Chem. Soc. 115:9925–9938.

Huang, Y., Ma, T., Lau, P.K., Wang, J., Zhao, T., Du, S., Loy, M.M.T., and Guo, Y. (2019). Visualization of Protein Sorting at the *Trans*-Golgi Network and Endosomes Through Super-Resolution Imaging. Front Cell Dev Biol. 7:181.

Hutagalung, A.H., and Novick, P.J. (2011). Role of Rab GTPases in membrane traffic and cell physiology. Physiol Rev 91, 119-149.

Ishii, M., Suda, Y., Kurokawa, K., and Nakano, A. (2016). COPI is essential for Golgi cisternal maturation and dynamics. J. Cell Sci. 129:3251–3261.

Jacobs, C.W., Adams, A.E.M., Szaniszlo, P.J., and Pringle, J.R. (1988). Functions of microtubules in the *Saccharomyces cerevisiae* cell cycle. J. Cell Biol. 107: 1409–1426.

Jahn, R., and Scheller, R.H. (2006). SNAREs–engines for membrane fusion. Nat Rev Mol Cell Biol 7, 631-643.

Johnson, L.M., Bankaitis, V.A., and Emr, S.D. (1987). Distinct sequence determinants direct intracellular sorting and modification of a yeast vacuolar protease. Cell. 48:875-885.

Johnson, N., and Glick, B.S. 2019. 4D microscopy of yeast. J. Vis. Exp.

Jørgensen, M.U., Emr, S.D., and Winther, J.R. (1999). Ligand recognition and domain structure of Vps10p, a vacuolar protein sorting receptor in *Saccharomyces cerevisiae*. Eur. J. Biochem. 260:461–469.

Kaiser, C.A., Gimeno, R.E., and Shaywitz, D.A. (1997). Protein secretion, membrane biogenesis, and endocytosis. In The Molecular and Cellular Biology of the Yeast *Saccharomyces*. Vol. 3. J.R. Pringle, J.R. Broach, and E.W. Jones, editors. Cold Spring Harbor Laboratory

Press. 91-227.

Katzmann, D.J., M. Babst, and S.D. Emr. 2001. Ubiquitin-dependent sorting into the multivesicular body pathway requires the function of a conserved endosomal protein sorting complex, ESCRT-I. Cell. 106:145-155.

Kaur, H., Sparvoli, D., Osakada, H., Iwamoto, M., Haraguchi, T., and Turkewitz, A.P. (2017). An endosomal syntaxin and the AP-3 complex are required for formation and maturation of candidate lysosome-related secretory organelles (mucocysts) in *Tetrahymena thermophila*. Mol. Biol. Cell 28, 1551-1564.

Kim, J.J., Lipatova, Z., Majumdar, U., and Segev, N. (2016). Regulation of Golgi cisternal progression by Ypt/Rab GTPases. Dev. Cell. 36:440–452.

Kirchhausen, T. Clathrin. (2000). Annu. Rev. Biochem. 69, 699–727.

Kornfeld, R., and Kornfeld, S. (1985). Assembly of asparagine-linked oligosaccharides. Annu. Rev. Biochem. 54:631–664.

Koval, M., Harley, J.E., Hick, E., and Steinberg, T.H. (1997). Connexin46 is retained as monomers in a trans-Golgi compartment of osteoblastic cells. J. Cell Biol. 137:847–857.

Kunz, J., Schneider, U., Deuter-Reinhard, M., Movva, N.R., and Hall, M.N. (1993). Target of rapamycin in yeast, TOR2, is an essential phosphatidylinositol kinase homolog required for G1 progression. Cell. 73:585-596.

Kurokawa, K., Ishii, M., Suda, Y., Ichihara, A., and Nakano, A. (2013). Live cell visualization of Golgi membrane dynamics by super-resolution confocal live imaging microscopy. Methods Cell Biol. 118:235-242.

Kurokawa, K., Okamoto, M., and Nakano, A. (2014). Contact of *cis*-Golgi with ER exit sites executes cargo capture and delivery from the ER. Nat. Commun. 5:3653.

Kurokawa, K., Osakada, O., Kodijani, T., Waga, M., Suda, Y., Asakawa, H., Haraguchi, T., and Nakano, A. (2019). Visualization of secretory cargo transport within the Golgi apparatus. J. Cell Biol.

Ladinsky, M.S., Mastronarde, D.N., McIntosh, J.R., Howell, K.E., and Staehelin, L.A. (1999). Golgi structure in three dimensions: functional insights from the normal rat kidney cell. J. Cell Biol. 144:1135-1149.

LaMontagne, E.D., and Heese, A. (2017). *Trans*-Golgi network/early endosome: A central sorting station for cargo proteins in plant immunity. Curr. Opin. Plant Biol. 40: 114–121.

Lavieu, G., Zheng, H., and Rothman, J.E. (2013). Stapled Golgi cisternae remain in place

as cargo passes through the stack. eLife. 2:e00558.

Leloup N, Lössl, P., Meijer, D.H., Brennich, M., Heck, A.J.R., Thies-Weesie, D.M.E., Janssen, B.J.C. (2017). Low pH-induced conformational change and dimerization of sortilin triggers endocytosed ligand release. Nat. Commun., 8, p. 1708.

Lerner D. W., McCoy D., Isabella A. J., Mahowald A. P., Gerlach G. F., Chaudhry T. A. and Horne-Badovinac S. (2013). A Rab10-dependent mechanism for polarized basement membrane secretion during organ morphogenesis. Dev. Cell 24, 159-168.

Levi, S.K., Bhattacharyya,D., Strack, R.L., Austin II, J.R.I., and Glick, B.S. (2010). The yeast GRASP Grh1 colocalizes with COPII and is dispensable for organizing the secretory pathway. Traffic. 11:1168–1179.

Levine, T.P., Wiggins, C.A., Munro, S. Inositol phosphorylceramide synthase is located in the Golgi apparatus of *Saccharomyces cerevisiae*. (2000). Mol. Biol. Cell, 11, pp. 2267-2281.

Lin, C.H., MacGurn, J.A., Chu, T., Stefan, C.J., and Emr, S.D. (2008). Arrestin-related ubiquitin-ligase adaptors regulate endocytosis and protein turnover at the cell surface. Cell. 135:714-725

Lippincott-Schwartz, J., Roberts, T.H., and Hirschberg, K. (2000). Secretory protein trafficking and organelle dynamics in living cells. Annu. Rev. Cell Dev. Biol. 16:557-589.

Liu K., Surendhran K., Nothwehr S.F., Graham T.R. (2008). P4-ATPase requirement for AP-1/clathrin function in protein transport from the *trans*-Golgi network and early endosomes. Mol. Biol. Cell 19:3526–35.

Llinares, E., Barry, A.O., and André, B. (2015). The AP-3 adaptor complex mediates sorting of yeast and mammalian PQ-loop-family basic amino acid transporters to the vacuolar/lysosomal membrane. Sci. Rep. 5:16665.

Lord, C., Ferro-Novick, S., and Miller E.A. (2013). The highly conserved COPII coat complex sorts cargo from the endoplasmic reticulum and targets it to the Golgi. Cold Spring Harb. Perspect. Biol. 5:a013367.

Losev, E., Reinke, C.A., Jellen, J., Strongin, D.E., Bevis, B.J., and Glick, B.S. (2006). Golgi maturation visualized in living yeast. Nature. 441:1002–1006.

Ma, M., and Burd, C.G. (2020). Retrograde trafficking and plasma membrane recycling pathways of the budding yeast *Saccharomyces cerevisiae*. Traffic. 21:45-59.

MacDonald, C., Buchkovich, N.J., Stringer, D.K., Emr, S.D., and Piper, R.C. (2012). Cargo ubiquitination is essential for multivesicular body intralumenal vesicle formation. 13:331- 338.

Makarow, M. (1988). Secretion of invertase in mitotic yeast cells. EMBO J. 7: 1475–1482.

Maley, F., Trimble, R.B., Tarentino, A.L., and Plummer Jr., T.H. (1989). Characterization of glycoproteins and their associated oligosaccharides through the use of endoglycosidases. Anal. Biochem. 180:195–204.

Malsam J., Satoh, A., Pelletier, L., and Warren, G. (2005). Golgin tethers define subpopulations of COPI vesicles. Science, 307, pp. 1095-1098.

Malsam J., Kreye S., and Sollner T.H. (2008). Membrane fusion: SNAREs and regulation. Cell Mol Life Sci 65, 2814–2832.

Marcusson, E.G., Horazdovsky, B.F., Lin Cereghino, J., Gharakhanian, E., and Emr, S.D. (1994). The sorting receptor for yeast vacuolar carboxypeptidase Y is encoded by the *VPS10* gene. Cell. 77:579-586.

Markgraf, D.F., F. Ahnert, H. Arlt, M. Mari, K. Peplowska, N. Epp, J. Griffith, F. Reggiori, and C. Ungermann. 2009. The CORVET subunit Vps8 cooperates with the Rab5 homolog Vps21 to induce clustering of late endosomal compartments. Mol. Biol. Cell. 20:5276-5289.

Matsuura-Tokita, K., Takeuchi, M., Ichihara, A., Mikuriya, K., and Nakano, A. (2006). Live imaging of yeast Golgi cisternal maturation. Nature. 441: 1007–1010.

McDonold, C.M., and Fromme, J.C. (2014). Four GTPases differentially regulate the Sec7 Arf-GEF to direct traffic at the *trans*-Golgi network. Dev. Cell. 30:759-767.

McNatt, M.W., McKittrick, I., West, M., and Odorizzi, G. (2007). Direct binding to Rsp5 mediates ubiquitin-independent sorting of Sna3 via the multivesicular body pathway. Mol. Biol. Cell. 18:697-706.

Menant, A., Barbey, R., and Thomas, D. (2006). Substrate-mediated remodeling of methioning transport by multiple ubiquitin-dependent mechanisms in yeast cells. EMBO J. 25:4436- 4447.

Miller, E.A., Beilharz, T.H., Malkus, P.N., Lee, M.C., Hamamoto, S., Orci, L., and Schekman, R. (2003). Multiple cargo binding sites on the COPII subunit Sec24p ensure capture of diverse membrane proteins into transport vesicles. Cell 114, 497-509.

Mironov, A.A., Weidman, P., and Luini, A. (1997). Variations on the intracellular transport theme: maturing cisternae and trafficking tubules. J Cell Biol 138, 481-484.

Mironov, A.A., Beznoussenko, G.V., Nicoziani, P., Martella, O., Trucco, A., Kweon, H.S., Di Giandomenico, D., Polishchuk, R.S., Fusella, A., Lupetti, P., et al. (2001). Small cargo proteins and large aggregates can traverse the Golgi by a common mechanism without leaving the lumen of cisternae. J. Cell Biol. 155:1225–1238.

Mitrovic, S., Ben-Tekaya, H., Koegler, E., Gruenberg, J., and Hauri, H.P. (2008). The cargo receptors Surf4, endoplasmic reticulum-Golgi intermediate compartment (ERGIC)-53, and p25 are required to maintain the architecture of ERGIC and Golgi. Mol. Biol. Cell. 19:1976–1990.

Mogelsvang, S., Marsh, B.J., Ladinsky, M.S., and Howell, K.E. (2004). Predicting function from structure: 3D structure studies of the mammalian Golgi complex. Traffic. 5:338-345.

Moscovici, M., Chien, W.Y., Abdelgawad, M., and Sun, Y.. (2010). Electrical power free, low dead volume, pressure-driven pumping for microfluidic applications. Biomicrofluidics. 4:46501.

Munro S. (2001). What can yeast tell us about N-linked glycosylation in the Golgi apparatus? FEBS Lett 498: 223–227.

Myers, M.D., and Payne, G.S. (2013). Clathrin, adaptors and disease: insights from the yeast *Saccharomyces cerevisiae*. Front. Biosci. 18:862–891.

Nam, A.S., Yin, Y. , von Marschall, Z., and Fisher, L.W. (2014). Efficient trafficking of acidic proteins out of the endoplasmic reticulum involves a conserved amino terminal IleProVal (IPV)-like tripeptide motif. Connect. Tissue Res. 55(Suppl 1):138–141.

Ng, D.T., Brown, J.D., and Walter, P. (1996). Signal sequences specify the targeting route to the endoplasmic reticulum membrane. J. Cell Biol. 134: 269–278.

Nilsson, T., Slusarewicz, P., Hoe, M. H., and Warren, G. (1993). Kin recognition. A model for the retention of Golgi enzymes. FEBS Lett. 330, 1–4.

Nishimura, K., Fukagawa, T., Takisawa, H., Kakimoto, T., and Kanemaki, M. (2009). An auxin-based degron system for the rapid depletion of proteins in nonplant cells. Nature Methods, 6(12), 917–922.

Novick, P., Field, C., and Schekman, R. (1980). Identification of 23 complementation groups required for post-translational events in the yeast secretory pathway. Cell. 21:205-215.

Nusblat A.D., Bright L.J., Turkewitz A.P.. 2012. Conservation and innovation in Tetrahymena membrane traffic: proteins, lipids, and compartments. Methods Cell Biol. 109:141–175.

Odorizzi, G., Cowles, C.R. and Emr, S.D. (1998). The AP-3 complex: a coat of many colors. Trends Cell Biol. 8:282-288.

Ohmuro-Matsuyama, Y., and Yamaji, H. (2018). Modifications of a signal sequence for antibody secretion from insect cells. Cytotechnology 70, 891-898.

Okamoto, M., Kurokawa, K., Matsuura-Tokita, K., Saito, C., Hirata, R. and Nakano, A. (2012). High-curvature domains of the ER are important for the organization of ER exit sites in *Saccharomyces cerevisiae*. J. Cell Sci. 125: 3412–3420.

Orci, L., Ravazzola, M., Volchuk, A., Engel, T., Gmachl, M., Amherdt, M., Perrelet, A., Sollner, T.H., and Rothman, J.E. (2000). Anterograde flow of cargo across the Golgi stack potentially mediated via bidirectional "percolating" COPI vesicles. Proc. Natl. Acad. Sci. USA. 97:10400–10405.

Otte, S., and Barlowe, C. (2004). Sorting signals can direct receptor-mediated export of soluble proteins into COPII vesicles. Nat. Cell Biol. 6:1189–1194.

Paetzel, M., Karla, A., Strynadka, N.C., and Dalbey, R.E. (2002). Signal peptidases. Chem. Rev. 102:4549–4580.

Pantazopoulou, A., and Glick, B.S. (2019). Membrane traffic pathways define the transitions in Golgi maturation. Front. Cell Dev. Biol.

Papanikou, E., and Glick, B.S. (2014). Golgi compartmentation and identity. Curr. Opin. Cell Biol. 29:74–81.

Papanikou, E., Day, K.J., Austin II, J., and Glick, B.S. (2015). COPI selectively drives maturation of the early Golgi. eLife. 4:e13232.

Patterson, G.H., Hirschberg, K., Polishchuk, R.S., Gerlich, D., Phair, R.D., and Lippincott-Schwartz, J. (2008). Transport through the Golgi apparatus by rapid partitioning within a two-phase membrane system. Cell. 133: 1055–1067.

Pelham, H.R.B. Insights from yeast endosomes.(2002) Curr. Opin. Cell Biol. 14:454-462.

Pellett, P.A., Dietrich, F., Bewersdorf, J., Rothman, J.E., and Lavieu, G. (2013). Inter-Golgi transport mediated by COPI-containing vesicles carrying small cargoes. eLife. 2:e01296.

Pfeffer, S.R. (2010). How the Golgi works: a cisternal progenitor model. Proc. Natl. Acad. Sci. USA. 107:19614–19618.

Piper, R.C, Bryant, N.J, Stevens, T.H. (1997). The membrane protein alkaline phosphatase is delivered to the vacuole by a route that is distinct from the VPS-dependent pathway. J. Cell Biol., 138, pp. 531-545.

Polishchuk, R.S., Polishchuk, E.V., Marra, P., Alberti, S., Buccione, R., Luini, A., and Mironov, A.A. (2000). Correlative light-electron microscopy reveals the tubular-saccular ultrastructure of carriers operating between the Golgi apparatus and plasma membrane. J.

Cell Biol. 148, 45-58.

Presley, J.F., Cole, N.B., Schroer, T.A., Hirschberg, K., Zaal, K.J.M., and Lippincott-Schwartz, J. (1997). ER-to-Golgi transport visualized in living cells. Nature. 389:81–85.

Preuss, D., Mulholland, J., Franzusoff, A., Segev, N., and Botstein, D. (1992). Characterization of the *Saccharomyces* Golgi complex through the cell cycle by immunoelectron microscopy. Mol. Biol. Cell. 3:789–803.

Prinz, W.A., Toulmay, A. and Balla, T. The functional universe of membrane contact sites. Nat Rev Mol Cell Biol 21, 7–24 (2020).

Rabouille, C., Hui, N., Hunte, F., Kieckbusch, R., Berger, E. G., Warren, G., et al. (1995). Mapping the distribution of Golgi enzymes involved in the construction of complex oligosaccharides. J. Cell Sci. 108, 1617–1627.

Rivera, V.M., Wang, X., Wardwell, S., Courage, N.L., Volchuk, A., Keenan, T., Holt, D. A., Gilman, M., Orci, L., Cerasoli Jr., F., et al. (2000). Regulation of protein secretion through controlled aggregation in the endoplasmic reticulum. Science. 287:826–830.

Rivera-Molina, F.E., and Novick, P.J. (2009). A Rab GAP cascade defines the boundary between two Rab GTPases on the secretory pathway. Proc. Natl. Acad. Sci. USA. 106:14408–14413.

Robinson J.S., Klionsky D.J., Banta L.M., Emr S.D. (1998). Protein sorting in *Saccharomyces cerevisiae*: isolation of mutants defective in the delivery and processing of multiple vacuolar hydrolases. Mol Cell Biol. 1988;8:4936–4948.

Rockwell, N.C., Krysan, D.J., Komiyama, T., and Fuller, R.S. (2002). Precursor processing by Kex2/furin proteases. Chem. Rev. 102:4525–4548.

Rogers, B., Decottignies, A., Kolaczkowski, M., Carvajal, E., Balzi, E., and Goffeau, A. (2001). The pleiotropic drug ABC transporters from *Saccharomyces cerevisiae*. J. Mol. Microbiol. Biotechnol. 3:207–214.

Rollins, C.T., Rivera, V.M., Woolfson, D.N., Keenan, T., Hatada, M., Adams, S.E., Andrade, L.J., Yaeger, D., van Schravendijk, M.R., Holt, D.A., et al. 2000. A ligand-reversible dimerization system for controlling protein-protein interactions. Proc. Natl. Acad. Sci. USA. 97:7096–7101.

Rossanese, O.W., Soderholm, J., Bevis, B.J., Sears, I.B., O'Connor, J., Williamson, E.K., and Glick, B.S. (1999). Golgi structure correlates with transitional endoplasmic reticulum organization in *Pichia pastoris* and *Saccharomyces cerevisiae*. J. Cell Biol. 145:69–81.

Rothman, J. H., Yamashiro, C. T., Kane, P. M., and Stevens, T. H. (1989). Protein tar-

geting to the yeast vacuole. Trends in Biochemical Sciences, 14, 347–350.

Rothstein, R. (1991). Targeting, disruption, replacement, and allele rescue: Integrative DNA transformation in yeast. Methods in Enzymology, 194, 281–301.

Saegusa, K., Sato, M., Morooka, N., Hara, T., and Sato, K. (2018). SFT-4/Surf4 control ER export of soluble cargo proteins and participate in ER exit site organization. J. Cell Biol. 217:2073–2085.

Saffi, G.T., and R.J. Botelho. 2019. Lysosome fission: planning for an exit. Trends Cell Biol. 29:635-646.

Sato, K., and Nakano, A. (2002). Emp47p and its close homolog Emp46p have a tyrosine-containing endoplasmic reticulum exit signal and function in glycoprotein secretion in *Saccharomyces cerevisiae*. Mol. Biol. Cell. 13: 2518–2532.

Scales, S.J., Pepperkok, R., and Kreis, T.E. (1997). Visualization of ER-to-Golgi transport in living cells reveals a sequential mode of action for COPII and COPI. Cell 90, 1137-1148.

Schindelin, J., Arganda-Carreras, I., Frise, E., Kaynig, V., Longair, M., Pietzsch, T., Preibisch, S., Rueden, C., Saalfeld, S., Schmid, B., Tinevez, J.Y., White, D.J., Hartenstein, V., Eliceiri, K., Tomancak, P., and Cardona, A. (2012). Fiji: an open-source platform for biological-image analysis. Nat. Methods 9, 676-682.

Schneider, C.A., Rasband, W.S., and Eliceiri, K.W. (2012). NIH Image to ImageJ: 25 years of image analysis. Nat. Methods. 9:671-675.

Seaman, M.N., McCaffery, J.M., and Emr, S.D. (1998). A membrane coat complex essential for endosome-to-Golgi retrograde transport in yeast. J. Cell Biol. 142, 665–681.

Schüller, C., Mamnun, Y.M., Wolfger, H., Rockwell, N., Thorner, J., and Kuchler, K. (2007). Membrane-active compounds activate the transcription factors Pdr1 and Pdr3 connecting pleiotropic drug resistance and membrane lipid homeostasis in *Saccharomyces cerevisiae*. Mol. Biol. Cell. 18:4932–4944.

Shakoury-Elizeh, M., Protchenko, O., Berger, A., Cox, J., Gable, K., Dunn, T.M., Prinz, W.A., Bard, M., and Philpott, C.C. (2010). Metabolic response to iron deficiency in *Saccharomyces cerevisiae*. J. Biol. Chem. 285:14823–14833.

Shang, Y., Song, X., Bowen, J., Corstanje, R., Gao, Y., Gaertig, J., and Gorovsky, M.A. (2002). A robust inducible-repressible promoter greatly facilitates gene knockouts, conditional expression, and overexpression of homologous and heterologous genes in Tetrahymena thermophila. Proc. Natl. Acad. Sci. USA 99, 3734-3739.

Shin J.J.H, Gillingham A.K., Begum F., Chadwick J., Munro S. (2017). TBC1D23 is a

bridging factor for endosomal vesicle capture by golgins at the trans-Golgi. Nat Cell Biol. 2017;19(12):1424-1432.

Spang, A. (2008). The life cycle of a transport vesicle. Cell Mol Life Sci 65, 2781-2789.

Spang, A. (2015). The road not taken: less traveled roads from the TGN to the plasma membrane. Membranes (Basel). 5:84–98.

Sparvoli D, Richardson E, Osakada H, Lan X, Iwamoto M, Bowman GR, Kontur C, Bourland WA, Lynn DH, Pritchard JK, Haraguchi T, Dacks JB, and Turkewitz AP. (2018). Remodeling the Specificity of an endosomal CORVET tether underlies formation of regulated secretory vesicles in the ciliate tetrahymena thermophila. Curr Biol 28, 697–710.e13.

Stevens, T., Esmon, B., and Schekman, R. (1982). Early stages in the yeast secretory pathway are required for transport of carboxypeptidase Y to the vacuole. Cell. 30:439-448.

Storrie, B., White, J., Röttger, S., Stelzer, E.H.K., Suganuma, T., and Nilsson, T. (1998). Recycling of Golgi-resident glycosyltransferases through the ER reveals a novel pathway and provides an explanation for nocodazole-induced Golgi scattering. J. Cell Biol. 143, 1505-1521.

Strack, R.L., Strongin, D.E., Bhattacharyya, D., Tao, W., Berman, A., Broxmeyer, H.E., Keenan, R.J., and Glick, B.S. (2008). A noncytotoxic DsRed variant for whole-cell labeling. Nat. Methods. 5:955–957.

Strack, R.L., Bhattacharyya, D., Glick, B.S., and Keenan, R.J. (2009a). Noncytotoxic orange and red/green derivatives of DsRed-Express2 for whole-cell labeling. BMC Biotechnol. 9:32.

Strack, R.L., Hein, B., Bhattacharyya, D., Hell, S.W., Keenan, R.J., and Glick, B.S. (2009b). A rapidly maturing far-red derivative of DsRed-Express2 for whole-cell labeling. Biochemistry. 48:8279–8281.

Strack, R.L., Keenan, R J., and Glick, B.S. (2011). Noncytotoxic DsRed derivatives for whole-cell labeling. Methods in Molecular Biology, 699, 355–370.

Suda, Y., Kurokawa, K., Hirata, R., and Nakano, A. (2013). Rab GAP cascade regulates dynamics of Ypt6 in the Golgi traffic. Proc. Natl. Acad. Sci. USA. 110:18976-18981.

Szul, T., and Sztul, E. (2011). COPII and COPI traffic at the ER-Golgi interface. Physiology 26, 348-364.

Thomas, L.L., and Fromme, J.C. (2020). Extensive GTPase crosstalk regulates Golgi trafficking and maturation. Curr. Opin. Cell Biol. 65:1-7.

Tang, H., Wang, S., Wang, J., Song, M. et al., N-hypermannose glycosylation disruption enhances recombinant protein production by regulating secretory pathway and cell wall in-

tegrity in *Saccharomyces cerevisiae*. Sci. Rep. 2016, 6, 1– 13.

Tie, H.C., Mahajan, D., Chen, B., Cheng, L., VanDongen, A.M., and Lu, L. (2016). A novel imaging method for quantitative Golgi localization reveals differential intra-Golgi trafficking of secretory cargoes. Mol. Biol. Cell. 27: 848–861.

Tojima, T., Suda, Y., Ishii, M., Kurokawa, K., and Nakano, A. (2019). Spatiotemporal dissection of the *trans*-Golgi network in budding yeast. J. Cell Sci. 132: jcs231159.

Toomre, D., Keller, P., White, J., Olivo, J.C., and Simons, K. (1999). Dual-color visualization of trans-Golgi network to plasma membrane traffic along microtubules in living cells. J. Cell Sci. 112, 21-33.

Toshima, J.Y., Nishinoaki, S., Sato, Y., Yamamoto, W., Furukawa, D., Siekhaus, D.E., Sawaguchi, A., and Toshima, J. (2014). Bifurcation of the endocytic pathway into Rab5-dependent and -independent transport to the vacuole. Nat. Commun. 5:3498.

Traub L.M., and Bonifacino J.S. (2013). Cargo recognition in clathrin-mediated endocytosis. Cold Spring Harb Perspect Biol 5: a016790.

Trimble, R.B., Maley, F., and Chu, F.K. (1983). Glycoprotein biosynthesis in yeast. protein conformation affects processing of high mannose oligosaccharides on carboxypeptidase Y and invertase. J. Biol. Chem. 258:2562–2567.

Trucco, A., Polishchuk, R.S., Martella, O., Di Pentima, A., Fusella, A., Di Giandomenico, D., San Pietro, E., Beznoussenko, G.V., Polishchuk, E.V., Baldassarre, M., et al. 2004. Secretory traffic triggers the formation of tubular continuities across Golgi sub-compartments. Nat. Cell Biol. 6: 1071–1081.

Tsui, M.M., and Banfield, D.K. (2000). Yeast Golgi SNARE interactions are promiscuous. J Cell Sci 113 (Pt 1), 145-152.

Valdivia, R.H., Baggott, D., Chuang, J.S., and Schekman, R.W. (2002). The yeast clathrin adaptor protein complex 1 is required for the efficient retention of a subset of late Golgi membrane proteins. Dev. Cell. 2:283–294.

Velasco, A., Hendricks, L., Moremen, K.W., Tulsiani, D.R.P., Touster, O., and Farquhar, M.G. (1993). Cell type-dependent variations in the subcellular distribution of α-mannosidase I and II. J. Cell Biol. 122, 39–51.

Valls, L.A., Hunter, C.P., Rothman, J.H., and Stevens, T.H. (1987). Protein sorting in yeast: the localization determinant of yeast vacuolar carboxypeptidase Y resides in the propeptide. Cell. 48:887-897.

Valls, L.A., Winther J.R., and Stevens, T.H. (1990). Yeast carboxypeptidase Y vacuolar

targeting signal is defined by four propeptide amino acids. J. Cell Biol. 111:361-368.

Vancha, A.R., Govindaraju, S., Parsa, K.V.L., Jasti, M., González-García, M., and Ballestero, R.P. (2004). Use of polyethyleneimine polymer in cell culture as attachment factor and lipofection enhancer. BMC Biotechnol. 4, 23.

Vater, C.A., Raymond, C.K., Ekena, K., Howald-Stevenson, I., and Stevens, T.H. (1992). The VPS1 protein, a homolog of dynamin required for vacuolar protein sorting in *Saccharomyces cerevisiae*, is a GTPase with two functionally separable domains. J. Cell Biol. 119:773–786.

Vida, T.A., Huyer, G,. and Emr, S.D. (1993). Yeast vacuolar proenzymes are sorted in the late Golgi complex and transported to the vacuole via a prevacuolar endosome-like compartment. J. Cell Biol. 121:1245-1256.

von Blume, J., Alleaume, A.M., Kienzle, C., Carreras-Sureda, A., Valverde, M., and Malhotra, V. (2012). Cab45 is required for Ca2+-dependent secretory cargo sorting at the *trans*-Golgi network. J. Cell Biol. 199:1057–1066.

Vowels, J.J. and Payne, G.S. (1998). A dileucine-like sorting signal directs transport into an AP-3-dependent, clathrin-independent pathway to the yeast vacuole. EMBO J. 17, 2482–2493.

Wach, A., Brachat, A., Pohlmann, R., and Philippsen, P. (1994). New heterologous modules for classical or PCR-based gene disruptions in *Saccharomyces cerevisiae*. Yeast. 10:1793–1808.

Wang, Y.J., Wang, J., Sun, H.Q., Martinez, M., Sun, Y.X., Macia, E.,Kirchhausen, T., Albanesi, J.P., Roth, M.G., and Yin, H.L. (2003). Phosphatidylinositol 4 phosphate regulates targeting of clathrin adaptor AP-1 complexes to the Golgi. Cell 114, 299–310.

Wang, C.W., Hamamoto, S., Orci, L. and Schekman, R. (2006). Exomer: A coat complex for transport of select membrane proteins from the trans-Golgi network to the plasma membrane in yeast. J. Cell Biol. 174, 973 – 983.

Whitfield, S.T., Burston, H.E., Bean, B.D., Raghuram, N., Maldonado-Baez, L., Davey, M., Wendland, B., and Conibear, E. (2016). The alternate AP-1 adaptor subunit Apm2 interacts with the Mil1 regulatory protein and confers differential cargo sorting. Mol. Biol. Cell. 27:588–598.

Willer, M., Forte, G.M., and Stirling, C.J. (2008). Sec61p is required for ERAD-L: genetic dissection of the translocation and ERAD-L functions of Sec61P using novel derivatives of CPY. J. Biol. Chem. 283:33883–33888.

Wood C.S., Schmitz K.R., Bessman N.J., Setty T.G., Ferguson K.M., and Burd C.G. (2009). PtdIns4P recognition by Vps74/GOLPH3 links PtdIns 4-kinase signaling to retrograde Golgi trafficking. J Cell Biol 187: 967–975.

Wooding, S., and H.R.B. Pelham. 1998. The dynamics of Golgi protein traffic visualized in living yeast cells. Mol. Biol. Cell. 9:2667-2680.

Wong, M. and Munro, S. Membrane trafficking. (2014). The specificity of vesicle traffic to the Golgi is encoded in the golgin coiled-coil proteins. Science 346, 1256898.

Wong, M., Gillingham, A.K. and Munro, S. (2017). The golgin coiled-coil proteins capture different types of transport carriers via distinct N-terminal motifs. BMC Biol. 15, 3.

Wooding, S., and Pelham, H.R.B. (1998). The dynamics of Golgi protein traffic visualized in living yeast cells. Mol. Biol. Cell. 9:2667–2680.

Wu, H., Ng, B.S., and Thibault, G. (2014). Endoplasmic reticulum stress response in yeast and humans. Biosci. Rep. 34:e00118.

Yin, Y., Garcia, M.R., Novak, A.J., Saunders, A.M., Ank, R.S., Nam, A.S., and Fisher, L.W. (2018). Surf4 (Erv29p) binds amino-terminal tripeptide motifs of soluble cargo proteins with different affinities, enabling prioritization of their exit from the endoplasmic reticulum. PLoS Biol. 16:e2005140.

Yu, I.M., and Hughson, F.M. (2010). Tethering factors as organizers of intracellular vesicular traffic. Annu Rev Cell Dev Biol 26, 137-156.

Zhdankina, O., Strand, N.L., Redmond, J.M., and Boman, A.L. (2001). Yeast GGA proteins interact with GTP-bound Arf and facilitate transport through the Golgi. Yeast. 18:1-18.

Zhou W., Chang J., Wang X., Savelieff M.G., Zhao Y., Ke S., Ye B. GM130 is required for compartmental organization of dendritic golgi outposts. Curr. Biol., 24 (2014), pp. 1227-1233

Zhou W., Chang J., Wang Xin., Savelieff M.G., Zhao Y., Ke S., and Ye B. GM130 Is Required for Compartmental Organization of Dendritic Golgi Outposts. Current Biology, Volume 24, Issue 11, 2014, Pages 1227-1233.

APPENDIX A

REMOVAL OF PUTATIVE GOLGI TETHERS DOES NOT OBVIOUSLY ALTER THE ORGANIZATION OF ERES-GOLGI UNITS IN *PICHIA PASTORIS*

A crucial, unanswered question is how sites of protein export at the ER, ER exit sites (ERES), are generated and maintained. ERES are ribosome-free ER domains, present in all eukaryotes, that act as sites of COPII coated vesicle formation (Bannykh et al., 1996). COPII vesicles carry cargo from the ER to the Golgi (Barlowe and Miller 2013). The mechanism by which COPII vesicle formation is constrained to ERES is still debated. Interestingly, ERES are often found in close proximity to Golgi cisternae. One possibility is that ERES and Golgi stacks form as an integrated unit by the action of tethering proteins that link nascent COPII vesicles to Golgi membranes (Glick 2014). In this scenario, removal of the tethers should disrupt ERES-Golgi associations. To test this hypothesis I used the budding yeast *Pichia pastoris*, which contains a few large ERES that always associate with the *cis* face of a stacked Golgi (Levi et al., 2010). Deletion of putative, non-essential Golgi tethers Grh1, Coy1, or Rud3 caused no obvious change in the association of early Golgi with ERES (Figure A.1). To remove essential tethers I optimized auxin-inducible degradation for use in *Pichia pastoris*. Auxin-inducible degradation allows for rapid, reversible depletion of tagged proteins upon addition of the plant hormone auxin (Nishimura et al., 2009). Addition of auxin to a strain expressing the F-box transport inhibitor response 1 (TIR1) protein and Uso1-3xAID severely impaired growth (Figure A.2). Depletion of Uso1 caused no obvious change in ERES-Golgi association (Figure A.3). Interestingly, depletion of Uso1 did cause a redistribution of the early Golgi marker Vrg4 (Figure A.3). The normal punctate Vrg4 pattern was replaced with a diffuse localization which potentially represents ER-localized Vrg4. Therefore, Uso1 is dispensible for the organization ERES-Golgi units but is required for the localization of some Golgi enzymes. One possibility is that ERES-Golgi tethering

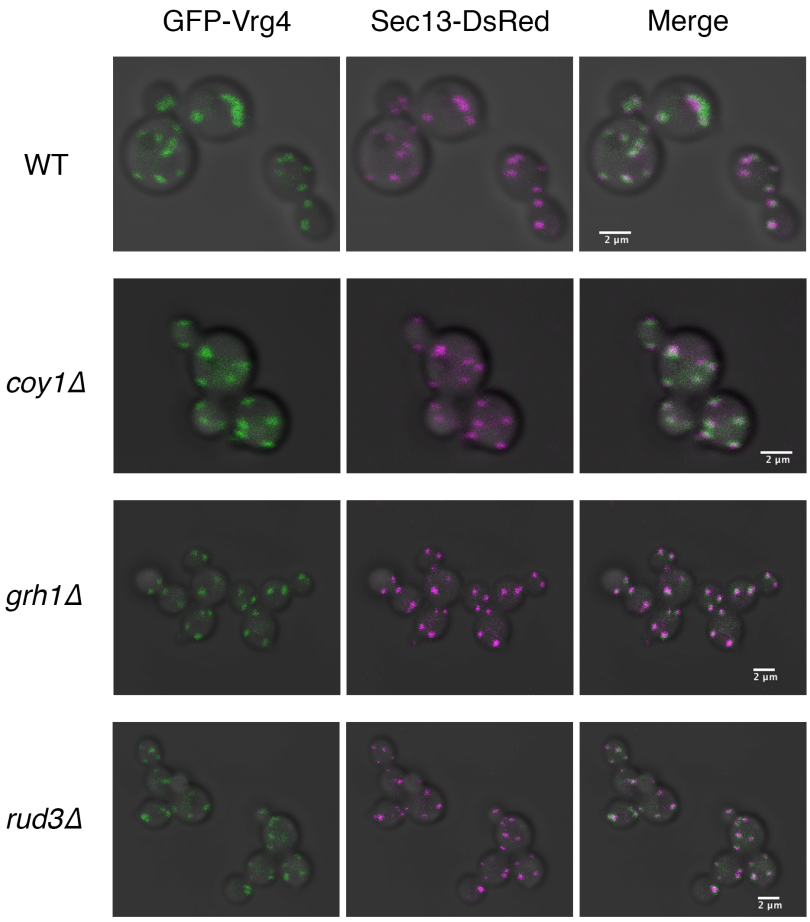

Figure A.1: **Deletion of potential ER-Golgi tethers has no effect on the organization of ERES-Golgi units in *Pichia pastoris*.** *Pichia* strains expressing Sec13-dsRed (ERES marker) and GFP-Vrg4 (early Golgi marker) containing deletions of the indicated putative tethers were grown to mid-log phase in NSD and imaged on a Leica SP5 confocal microscope. Note that in all conditions the ERES and Golgi markers remain in close proximity to one another. Scale bars 2μm.

interactions are redundant and disruption of the interaction will require removal of multiple tethers.

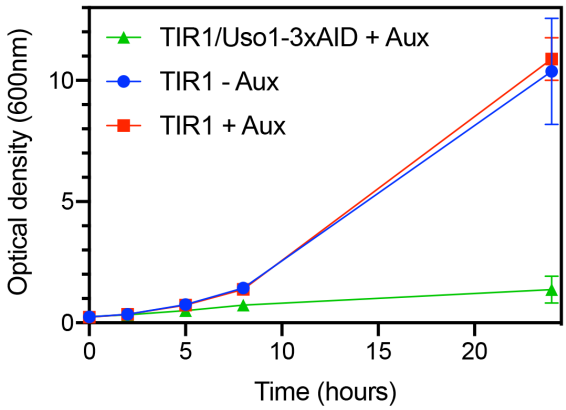

Figure A.2: **Growth inhibition by auxin-inducible degradation of Uso1.** A wild type *Pichia pastoris* strain, a strain expressing TIR1, and a strain expressing TIR1 and Uso1-3xAID were grown overnight in rich media, diluted to an OD_{600} of 0.2, treated with 500μM indole-3-acetic-acid (a natural auxin, IAA), and grown at 30°C. The OD_{600} was measured at the indicated timepoints. Yeast growth immediately halted upon addition of auxin only when Uso1 contained the 3xAID tag.

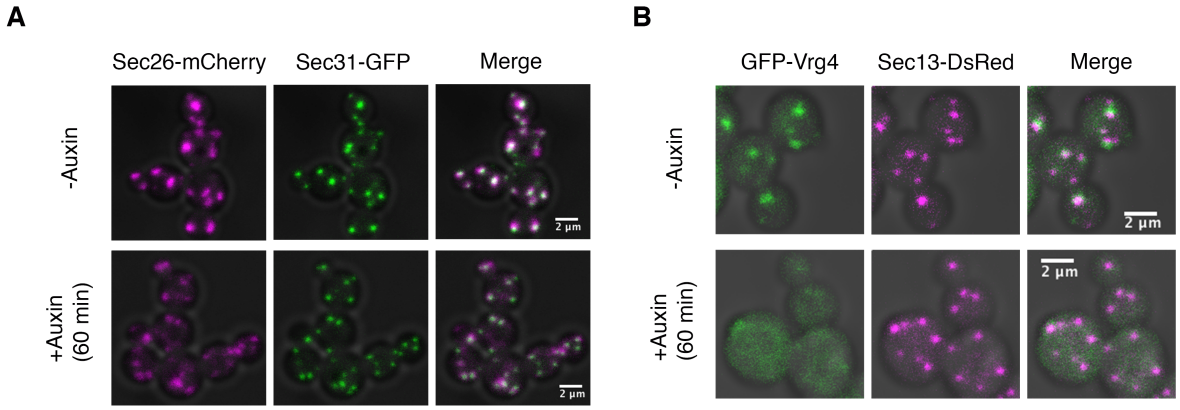

Figure A.3: **Uso1 depletion does not disrupt ERES-Golgi units but does cause a re-distribution of a resident Golgi enzyme. (A)** A *Pichia* strain expressing Sec26-mCherry (early Golgi marker), Sec31-GFP (ERES marker), and Uso1-3xAID was grown to mid-log phase, treated with 500μM IAA, and imaged on a Leica SP5 confocal microscope. **(B)** Cells were grown and treated as in (A) except they expressed the early Golgi marker GFP-Vrg4 and the ERES marker Sec13-DsRed. Note the loss of GFP-Vrg4 punctate fluorescence after auxin treatment. Scale bars 2μm.

APPENDIX B

ASPARAGINE-LINKED GLYCOSYLATION AFFECTS VACUOLAR TARGETING

Most proteins moving through the secretory pathway are subject to significant posttranslational modification within the Golgi apparatus. One of the most prevalent modifications is the addition and trimming of glycans. Secreted proteins and vacuolar proteins alike are subject to asparagine-linked glycosylation (N-glycosylation). Interstingly, despite interacting with the same glycosylation machinery secreted and vacuolar proteins typically display different glycosylation profiles (Avaro et al., 2002). CPY, a vacuolar hydrolase, contains four N-linked glycosylation sites but the glycosylation profile is not nearly as extensive as that of secreted protein invertase (Avaro et al., 2002). During our analysis of vacuolar protein sorting (Chapter 4) we sought to probe how N-linked glycosylation may relate to vacuolar targeting. To test this, I constructed a series *S. cerevisiae* strains expressing non-aggregating variants of ESCargo either containing or lacking N-linked glycosylation sites and probed steady state vacuolar targeting. As seen previously, a small amount of the glycosylatable cargo accumulates in the vacuole which can be suppressed by deletion of *VPS10* (Figure B.1, Figure 4.1). Surprisingly, ESCargo variants that lacked a glycosylation motif resulted in a drastic increase in the amount of cargo fluorescence in the vacuole (Figure B.1). Importantly, these ESCargo variants do not contain any known vacuolar targeting motif and would be expected to behave as secretory cargoes. This increase was affected but not completely abrogated by removal of Vps10 (Figure B.1). Thus, the presence of N-glycans affects the accumulation of a fluorescent cargo in the vacuole in a manner not entirely dependent on Vps10. Of note, this experiment does not rule out the possibility that the lack of N-glycans enhances protein stability or protects the molecule from proteolytic degradation in the vacuole, however. Additionally, more experimentation is needed to determine if this is a phenomenon applicable to any cargo moving through the secretory pathway.

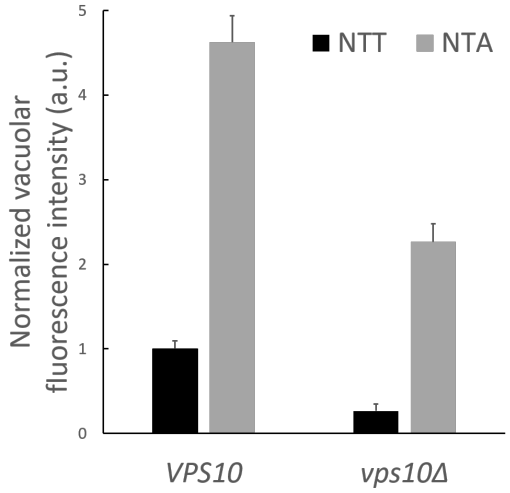

Figure B.1: **Presence of N-glycans affects vacuolar targeting.** *S. cerevisiae* strains expressing non-aggregating ESCargo variants either containing (NTT) or lacking (NTA) an N-linked glycosylation site and the vacuolar marker Vph1-GFP in either *VPS10* or *vps10*Δ backgrounds were grown to mid-log phase in minimal media, adhered to a confocal dish, and imaged on a Leica SP5 confocal microscope. The Vph1-GFP signal was used to generate a mask and quantify the amount of cargo signal within the vacuole. Values were normalized to the *VPS10* expressing the ESCargo variant containing a glycosylation site. Error bars represent SEM. Data points taken from at least 69 cells per condition.

Why might the presence of N-glycans affect vacuolar targeting? One possibility is that the association of cargoes with the glycosylation machinery prevents sorting into vacuole targeted vesicles. This could be accomplished either by kinetic association of the cargo molecules with the glycosylation machinery itself or due to physical properties unique to heavily glycosylated proteins. Previously I have shown that N-glycosylation directs cargoes for intra-Golgi recycling (see Chapter 3 or Casler et al., 2019). Therefore, glycosylation could serve as a means to enhance the residence time of cargo within the Golgi - ensuring proper modification and allowing cargo additional chances to interact with the appropriate receptors. Vacuolar cargoes, which are sorted out of the Golgi earlier than secretory cargoes (See Chapter 4 or Casler and Glick 2020), encounter transport receptors and are exported from the Golgi near the midpoint of cisternal maturation - resulting in a lower residence time in the Golgi and a less robust glycosylation profile. Cargoes lacking glycosylation sites would not be subjected

to this quality control mechanism and could leak into both vacuole targeted and secretory vesicles. Interestingly, deletion of enzymes within the N-linked glycosylation pathway has been shown to enhance the secretion of foreign proteins (Tang et al., 2016). It would be interesting to see if vacuolar protein targeting is increased in these genetic backgrounds as well.